


Title	Modified screen printed electrodes for electrochemical sensing applications in food and beverage analysis
Author(s)	Duffy, Gerard
Publication date	2017
Original citation	Duffy, G. 2017. Modified screen printed electrodes for electrochemical sensing applications in food and beverage analysis. PhD Thesis, University College Cork.
Type of publication	Doctoral thesis
Rights	© 2017, Gerard Duffy. http://creativecommons.org/licenses/by-nc-nd/3.0/ 
Embargo information	No embargo required
Item downloaded from	http://hdl.handle.net/10468/4629

Downloaded on 2018-08-23T20:34:26Z

Modified Screen Printed Electrodes for Electrochemical Sensing Applications in Food and Beverage Analysis

Gerard Duffy

BA (MOD)

111223831



NATIONAL UNIVERSITY OF IRELAND, CORK

FACULTY OF SCIENCE

DEPARTMENT OF CHEMISTRY

TYNDALL NATIONAL INSTITUTE

**Thesis submitted for the degree of
Doctor of Philosophy**

January 2017

Head of Department: Prof Justin Holmes

Supervisor: Dr Eric Moore

Research supported by the Integrated Nanoscience Platform for Ireland
(INSPIRE)

Contents

List of Figures	vii
Abstract	xvi
Abbreviations	xviii
Acknowledgements	xxiii
1 Introduction	1
1.1 Electrochemical Sensors For Food Analysis	2
1.2 Thesis Aims and Objectives	3
1.2.1 Chapter 1	3
1.2.2 Chapter 2	4
1.2.3 Chapter 3	4
1.2.4 Chapter 4	4
1.2.5 Chapter 5	4
1.3 Biological and Chemical Sensors	5
1.4 Biosensor classification	6
1.4.1 Transducers	6
1.4.1.1 Optical	7
1.4.1.2 Mass/Acoustic	7
1.4.1.3 Electrochemical	8
1.4.2 Biological Recognition Elements	8
1.4.2.1 Enzymes	8
1.4.2.2 DNA	8
1.4.2.3 Whole Cells	9
1.4.2.4 Molecularly Imprinted Polymers	9
1.4.2.5 Aptamers	9
1.4.2.6 Antibodies	10
1.5 Enzyme Linked Immunosorbent Assay	12
1.5.1 Direct ELISA	13
1.5.2 Indirect ELISA	13
1.5.3 Sandwich ELISA	13
1.5.4 Competitive ELISA	14
1.5.5 Displacement ELISA	14
1.5.6 Photometry and Beer-Lambert Law	15
1.5.7 Enzyme Substrate Reactions	16
1.6 Electrochemical Immunosensors	17
1.6.1 Antibody/Antigen Immobilisation	19
1.6.2 Non-specific binding	21
1.7 Electrochemistry Fundamentals	22
1.7.1 The Electrochemical Cell	22
1.7.2 Electrode/Solution Interface - Double Layer Models	23
1.7.3 Mass Transport	24
1.7.3.1 Diffusion	24
1.7.3.2 Migration	25
1.7.3.3 Convection	25

1.7.3.4	Nernst Planck Equation	25
1.8	Electrochemical Techniques	26
1.8.1	Cyclic Voltammetry	26
1.8.2	Square Wave Voltammetry	29
1.9	Chemically Modified Electrode Surfaces	30
1.9.1	Carbon Nanostructures	30
1.9.2	Electrochemistry of sp ² Carbon	32
1.9.2.1	Thin Layer Effects	34
1.9.2.2	Determining the Influence of Thin Layer Effects	35
1.9.2.3	Inner and Outer Sphere Redox Probes	36
1.10	Other Materials for Electrochemical Sensing	37
1.10.1	Boron Doped Diamond	37
1.10.2	Self Assembled Monolayers	38
1.10.3	Metallic nanoparticles	39
1.10.4	Polymers	39
1.10.5	Magnetic beads	40
1.11	Physical Characterisation Techniques	40
1.11.1	SEM	40
1.11.2	X-ray photoelectron spectroscopy (XPS)	41
1.11.3	Raman Spectroscopy	42
1.12	Target Analytes	43
1.12.1	Mycotoxins	43
1.12.2	Caffeine	45
1.13	Sample Preparation	46
1.14	Statistical Analysis	47
1.14.1	Fitting Immunoassay data	47
1.14.2	Limit of Detection	48
1.14.3	Sensitivity	49
1.14.4	f-test and p-test	49
1.14.5	ANOVA analysis	50
References	51

2	Detection of Mouse IgG at Pretreated and Nanostructured Screen Printed Electrodes	65
2.1	Objectives and Novelty	66
2.2	Introduction	66
2.2.1	Screen Printed Electrodes	66
2.2.2	Model Electrochemical Immunosensors	68
2.2.3	Screen Printed Carbon Pretreatment	68
2.2.4	Nanocarbon modified electrode based Electrochemical Immunosensors for IgG Detection	69
2.3	Materials and Methods	69
2.3.1	Reagents	69
2.3.2	Buffer Preparation	70
2.3.3	Screen Printed Electrodes	70
2.3.4	Electrode Modifications	71

2.3.5	Electrode Pretreatment	71
2.3.6	Cyclic Voltammetry	72
2.3.7	Amperometry	73
2.3.8	Open Circuit Potential	73
2.3.9	XPS (TCD)	73
2.3.10	SEM	73
2.3.11	Contact Angle	74
2.3.12	ELISA	74
2.3.12.1	Capture ELISA	75
2.3.12.2	Competitive ELISA	76
2.3.13	Electrochemical Immunoassay	76
2.3.13.1	Electrochemical Capture Assay	77
2.3.13.2	Electrochemical Competitive Assay	78
2.4	Results and Discussion (Part 1) - Characterisation of Electrochemically pretreated graphite electrodes	79
2.4.1	Thin Layer Effects	79
2.4.2	Electrochemical Characterisation at Pretreated Electrodes - Ferri/Ferrocyanide	81
2.4.3	Electrochemical Characterisation at Pretreated Electrodes - Hexaammine Ruthenium (III) Chloride	82
2.4.4	Scan Rate Studies	84
2.4.4.1	Scan Rate Studies - Hexaammine Ruthenium (III) Chloride	85
2.4.4.2	Scan Rate Studies - Ferri/Ferrocyanide	86
2.4.5	Amperometric Detection of p-aminophenol	88
2.5	X-ray Photon Spectroscopy (XPS)	90
2.5.1	Scanning Electron Microscopy (SEM)	91
2.5.2	Contact Angle Measurements	93
2.5.3	Reference Electrode	94
2.6	Part 2 - Immunoassay Development	96
2.6.1	Capture ELISA	96
2.6.2	Competitive ELISA	97
2.6.3	Control Assays	99
2.6.4	Electrochemical Capture Assay	100
2.6.5	Electrochemical Competitive Assay	103
2.7	Part 3 - Development of Electrochemical Immunosensor at Nanocarbon modified Electrodes	104
2.7.1	Optimisation of Nanomaterial Concentration and Solvent	104
2.7.2	Electrode Characterisation	108
2.7.2.1	SEM	108
2.7.3	Contact Angle	109
2.7.4	Thin Layer Effects	110
2.7.5	Electrochemical Characterisation - Ferri/Ferrocyanide	112
2.7.5.1	Scan Rate Studies - Ferri/Ferrocyanide	113
2.7.6	Electrochemical Characterisation - Hexaamine Ruthenium (III) Chloride	114

2.7.6.1	Scan rate studies - Hexaamine Ruthenium (III) Chloride	115
2.7.7	Amperometric p-aminophenol detection	117
2.7.8	Electrochemical Immunoassay at MWCNT/Nafion electrode	118
2.7.9	Summary of Results and Control Assays	120
2.8	Conclusions and Future Prospects	122
	References	123
3	Electrochemical Immunosensor for Deoxynivalenol Detection	128
3.1	Objectives and Novelty	129
3.2	Introduction	129
3.3	Methods of Deoxynivalenol Detection	131
3.3.1	Fast Screening methodologies	131
3.3.1.1	Optical Biosensor techniques	131
3.3.1.2	Immunoassay techniques	132
3.3.2	Chromotography based methods	133
3.3.3	Screen Printed Electrodes for Mycotoxin Detection	133
3.4	Materials and Methods	134
3.4.1	Instrumentation	134
3.4.2	Reagents	134
3.4.3	Electrode preparation	134
3.4.4	Anti-DON IgG/Anti-mouse IgG binding study (Direct Capture Assay)	134
3.4.5	Chessboard ELISA	135
3.4.6	AP Labelled Anti-mouse IgG Optimisation (Indirect Capture Assay)	136
3.4.7	Indirect Competitive ELISA	137
3.4.8	Coating Conjugate Optimisation - Indirect Capture Assay	138
3.4.9	Detecting Antibody Optimisation - Indirect Capture Assay	138
3.4.10	Blocking Study - Indirect Capture Assay	139
3.4.11	Indirect Competitive Electrochemical Immunoassay	139
3.5	Results and Discussion Part 1 - ELISA	140
3.5.1	Anti-DON/Anti-mouse IgG binding - Direct Capture Assay	140
3.5.2	Chessboard Titration	141
3.5.3	Anti-mouse IgG Optimisation	142
3.5.4	Competitive ELISA	143
3.6	Results and Discussion Part 2 - Electrochemical Immunoassay	144
3.6.1	Assay component solution	145
3.6.2	Coating Conjugate Optimisation	146
3.6.3	Detecting Antibody Optimisation	146
3.6.4	Blocking Study	147
3.6.5	AP labelled anti-mouse optimisation	148
3.6.6	Indirect Competitive Immunosensor	149
3.7	Conclusions and Future Work	151
	References	152

4	Electrochemical Detection of Caffeine	155
4.1	Objectives and Novelty	156
4.2	Introduction	156
4.2.1	Nafion modified electrodes	158
4.2.2	Screen Printed Graphene Electrodes	159
4.3	Materials and Methods	160
4.3.1	Reagents	160
4.3.2	Electrochemical measurements	160
4.3.3	Modification of Electrodes with Nafion	161
4.3.4	Effect of pH and Supporting Electrolyte	161
4.3.5	Real Sample Analysis	161
4.3.6	Raman Spectroscopy	161
4.3.7	SEM	161
4.3.8	Contact Angle	162
4.4	Results and Discussion	162
4.4.1	Influence of pH and Supporting Electrolyte	162
4.4.2	Nafion Modified electrodes	165
4.4.3	Electrochemically Pretreated Electrodes	167
4.4.4	SEM	168
4.4.4.1	Pretreated Electrode	168
4.4.4.2	Nafion modified electrode	168
4.4.5	Contact Angle	169
4.4.6	Electrochemical Characterisation	169
4.4.6.1	Ferri/ferrocyanide	170
4.4.6.2	Hexamine Ruthenium (III) Chloride	172
4.4.7	Cleaning Study	175
4.4.8	Effect of scan rate	177
4.5	Optimisation of SVW parameters	179
4.6	Analytical Characteristics of Developed Sensors	181
4.6.1	Pretreated Electrode	181
4.6.2	Nafion modified electrode	182
4.7	Sensor Storage	184
4.8	Interference Analysis	185
4.9	Real Sample Analysis	187
4.10	Part 2 - Caffeine Detection at Screen Printed Graphene	188
4.10.1	Electrochemical Characterisation	188
4.10.1.1	Scan Rate Studies	190
4.10.2	SEM	192
4.10.3	Raman Spectroscopy	193
4.10.4	Caffeine Detection at Screen Printed Graphene	195
4.10.5	Influence of pH	195
4.10.6	Electrochemical Detection of Caffeine	196
4.11	Conclusions	197
	References	199
5	Conclusions and Future Prospects	204

5.1	Conclusions and Future Prospects	205
5.1.1	New Carbon Nanostructures	205
5.1.2	Paper Based Analytical Devices	206
5.1.3	Advanced Instrumentation	206
5.1.4	Lab on a Chip/MicroTotal Analysis Systems	207
	References	209
A	XPS	212
B	Thin Layer Effects	215
B.1	Ferri/Ferrocyanide	215
B.2	Ruthenium (III) Chloride	217
C	Publications	219
C.1	Journal Publications	219
C.2	Oral Presentations	219
C.3	Poster Presentations	220

List of Figures

1.1	Schematic of sample screening with an Electrochemical Sensor	2
1.2	Outline of chapter structure within the thesis	5
1.3	Biosensor classification based on analyte, biological recognition element and transducer	6
1.4	Schematic of typical antibody IgG structure showing constant and variable regions as well as connecting disulphide bond . . .	11
1.5	Direct capture (left), Indirect capture (centre) and sandwich (right) ELISA assays	12
1.6	Direct competitive (left) and Indirect competitive ELISA formats	14
1.7	Displacement ELISA format	15
1.8	Multiskan Ex Plate Reader measurement principle (reproduced from the operating manual)	16
1.9	AP/pNPP substrate reaction	16
1.10	Schematic of typical electrochemical immunosensor utilising a sandwich assay approach. Also shown are some of the various materials and modifications used in this type of sensor development including self assembled monolayers, gold nanoparticles, graphene and carbon nanotubes.	18
1.11	AP/pAPP substrate reaction	18
1.12	Antibody Immobilisation	19
1.13	Strategies for antibody immobilisation [49]	20
1.14	Conjugation of proteins to carboxylated CNTs using EDC in the presence or absence of sulfo-NHS	21
1.15	3 Electrode Electrochemical Cell	23
1.16	Grahame Electrical Double Layer Model	24
1.17	Cyclic Voltammetry Waveform	26
1.18	Typical Cyclic Voltammogram	26
1.19	Potential wave form for Square Wave Voltammetry	29
1.20	Typical Square Wave Voltammogram	30
1.21	Graphene as the fundamental 2D building block for a range of different carbon nanostructures including buckyballs (C ₆₀), carbon nanotubes and graphite [58]	31
1.22	Schematic of the microstructure of graphite showing discrete regions which contain edge sites. [66]	34
1.23	Schematic of diffusion at a carbon nanotube modified electrode surface showing highlighting the contribution of both semi-infinite diffusion and thin layer diffusion of analyte within the carbon nanotube matrix. [75]	35
1.24	Inner and Outer Sphere Redox probes at carbon electrodes[77]	37
1.25	SEM of as-grown microcrystalline boron doped diamond [80] .	38
1.26	SEM of reduced graphene oxide/gold nanoparticle composite used for ascorbic acid, dopamine and uric acid detection [97] .	41
1.27	Raman Spectroscopy of graphene and graphite [101]	43
1.28	Chemically structures of some multiclass mycotoxins [110] . . .	44

1.29	Proposed mechanism for caffeine oxidation [126]	46
1.30	Limit of detection for a linear calibration curve	49
1.31	Limit of detection for an indirect competitive immunoassay	49
2.1	Sheet of commercial Kanichi Limited screen printed carbon electrodes as purchased. Each individual sensor consists of a graphite working and counter electrode as well as Ag/AgCl reference electrode.	71
2.2	Set up for electrochemical measurements showing a screen printed electrode connected to a Palmsens electrode connector inside a Faraday cage.	72
2.3	Dataphysics contact angle instrument	74
2.4	Laminar Flow Hood with ELISA plate	74
2.5	Photograph of the Multiskan Ex Photometer used in all ELISA experiments	75
2.6	Typical amperometric immunoassay measurement response in which 25 mg/mL pAPP is added to a stirred solution containing an alkaline phosphatase labelled antibody in DEA buffer pH 9.5	77
2.7	Typical graph of log peak current vs log of scan rate for a pretreated SPE in 1 mM ferri/ferrocyanide. All other graphs are displayed in the appendix of this thesis.	80
2.8	Comparison of different pretreatment procedures. Cyclic voltammograms were carried out at a scan rate of 100 mV s ⁻¹ in 1 mM [Fe(CN) ₆] ^{3-/4-}	81
2.9	Comparison of different pretreatment procedures. Cyclic voltammograms were carried out at a scan rate of 100 mV s ⁻¹ in 1 mM hexamine ruthenium (III) chloride	83
2.10	CV in PBS pretreated with 1 mM hexamine ruthenium (III) chloride in PBS pH 7.4 at a scan rate of 100 mV/s	84
2.11	CVs at 20, 40, 60, 80, 100, 120, 140, 160, 180, 200 mV/s at pretreated electrodes in hexamine ruthenium (III) chloride	85
2.12	CVs at 20, 40, 60, 80, 100, 120, 140, 160, 180, 200 mV/s at each pretreated electrode in hexamine ruthenium (III) chloride	86
2.13	CVs of 1 mM Ferri/ferrocyanide at an untreated SPE at varying scan rates of 20, 40, 60, 80, 100, 120, 140, 160, 180, 200 mV/s	86
2.14	CVs of 1 mM Ferri/ferrocyanide at electrochemically pretreated SPEs at varying scan rates of 20, 40, 60, 80, 100, 120, 140, 160, 180, 200 mV/s	87
2.15	CVs of 1 mM Ferri/ferrocyanide at an SPE pretreated with PBS at varying scan rates of 20, 40, 60, 80, 100, 120, 140, 160, 180, 200 mV/s	88
2.16	Standard addition of 5mM stock solution of pAP to DEA buffer pH 9.5 under stirred conditions at bare and electrochemically pretreated electrodes	89
2.17	Calibration curve for p-aminophenol at concentrations of 10, 20, 30, 40, 50, 60 μM	89

2.18 Scanning Electron Micrographs of untreated (A,B), Na ₂ CO ₃ (C,D), H ₂ SO ₄ (E,F), NaOH (G,H), PBS Anodic (I,J), PBS CV (K,L)	92
2.19 Contact Angle (degrees) at pretreated electrodes resultant from 2 μL of water being dispensed on the working electrode surface	94
2.20 Comparison of on chip and external reference electrode at bare screen printed electrode. CV carried out at a scan rate of 100 mV s ⁻¹ in 1 mM [Fe(CN) ₆] ^{3-/4-}	95
2.21 Open Circuit Potential (OCP) measurement for 5 hours in 1 M KCl	95
2.22 Schematic of Capture assay for mouse IgG whereby IgG binds to AP labelled anti-mouse IgG	96
2.23 Capture assay varying mouse IgG concentration from 1 mg/mL to 13 x 10 ⁶ mg/mL with a fixed AP labelled anti-mouse dilution of 1/30,000. R ² = 0.9932, n = 3.	97
2.24 Schematic of a competitive assay with immobilised IgG competing with free IgG to bind to AP labelled anti-mouse IgG	97
2.25 Competitive ELISA with coating IgG concentration of 0.04 mg/mL. R ² = 0.9965, n = 3.	98
2.26 Competitive ELISAs with coating IgG concentration of 0.008 mg/mL and two different competition step times - 60 mins and 90 mins. n = 3.	99
2.27 Competitive assay for 0.002 mg/mL IgG - absorbances for full assay for assay missing one step of the protocol	100
2.28 Electrochemical capture assay varying coating antibody concentration from 1 mg/mL to 0.000013 mg/mL. R ² = 0.6771, n = 3.	101
2.29 Optimisation of AP labelled anti-mouse IgG concentration	102
2.30 Electrochemical capture assay for mouse IgG using an AP labelled anti-mouse dilution of 1/1000. R ² = 0.971	102
2.31 Competitive Electrochemical Immunoassay with a coating antibody concentration of 0.2 mg/mL exhibiting low dose hook effect	103
2.32 Finalised competitive Electrochemical Immunoassay for Mouse IgG detection at an electrochemically pretreated screen printed electrode with a coating antibody concentration of 0.04 mg/mL and competition incubation time of 90 minutes. R ² = 0.9608, n = 3.	103
2.33 RGO solutions at concentrations of 0.05, 0.1, 0.3, 0.5 and 1 mg/mL (left to right) in 1:1 water/DMF	105
2.34 MWCNT solutions at concentrations of 0.05, 0.1, 0.3, 0.5 and 1 mg/ml (left to right) in 1:1 water/DMF	105
2.35 CV of 500 μM p-aminophenol in a supporting electrolyte of 0.1 M DEA buffer with a scan rate of 100 mV/s at graphite and MWCNT modified electrodes of the following concentrations: 0.05, 0.1, 0.3, 0.5 and 1 mg/mL	106
2.36 Peak anodic current from CV of MWCNT modified electrodes of varying concentration (from Fig. 2.32)	106

2.37 CV of 500 μM p-aminophenol in a supporting electrolyte of 0.1 M DEA buffer at graphite and RGO modified electrodes of the following concentrations: 0.05, 0.1, 0.3, 0.5 and 1 mg/mL . . .	107
2.38 Peak anodic current from CV from RGO modified electrodes of varying concentration (from Fig. 2.37)	107
2.39 MWCNT/Nafion and RGO/Nafion solutions of 1 mg/mL in 0.5 % Nafion before and after sonication	108
2.40 SEM of modified electrodes at nanocarbon modified electrodes. MWCNT (A,B) MWCNT/Nafion (C,D) RGO (E,F) RGO/Nafion (G,H)	109
2.41 Contact angle droplets at nanocarbon modified electrodes . . .	110
2.42 Log I_A vs Log v at a MWCNT modified electrode. The graphs for the other electrodes are contained in the appendix	111
2.43 CVs of nanocarbon modified electrodes in 100 μM $[\text{Fe}(\text{CN})_6]^{3-/4-}$ in 1 M KCl at a scan rate of 100 mV/s.	112
2.44 CVs at scan rates of 20 - 200 mV/s in 1 mM $[\text{Fe}(\text{CN})_6]^{3-/4-}$ (1 M KCl supporting electrolyte) at nanocarbon modified electrodes.	114
2.45 CVs of 1 mM Hexamine Ruthenium (III) Chloride in 50 mM PBS pH 7.4 at nanocarbon modified electrodes.	115
2.46 CVs at scan rates of 20 - 200 mV/s in 1 mM Hexamine Ruthenium (III) Chloride	116
2.47 Standard addition of 10 μL of 5 mM stock solution of pAP to DEA buffer pH 9.5 under stirred conditions at bare and nanocarbon modified electrodes	117
2.48 Calibration curve for p-aminophenol detection at nanocarbon modified electrodes - concentrations of 10, 20, 30, 40, 50, 60 μM	118
2.49 Hydrodynamic amperograms for a range of mouse IgG concentrations at a MWCNT/Nafion electrode. After a period of 200 seconds 50 μL of pAPP (25 mg/mL) was added to a stirred solution of 4950 μL DEA buffer, pH 9.5. A fixed potential of 0.28 mV was used.	119
2.50 Competitive electrochemical immunoassay for mouse IgG at a MWCNT/Nafion electrode with parameters optimised in section 2 of this chapter for a pre-anodised electrode - coating antibody concentration: 0.04 mg/mL, competition incubation time: 90 mins, $R^2 = 0.9286$ and $n = 3$	119
2.51 Competitive electrochemical immunoassay at untreated electrode. $R^2 = 0.954$, $n = 3$	120
2.52 Competitive electrochemical immunoassay at pre-anodised electrode using covalent attachment. $R^2 = 0.976$, $n = 3$	121
3.1 Chemical Structure of Deoxynivalenol	130
3.2 Healthy (left) and fusarium infected maize (right) [4]	130
3.3 Schematic of chessboard titration	136

3.4	Schematic of indirect capture assay showing binding DON-BSA immobilised onto a surface with a anti-DON antibody and subsequent binding to anti-mouse AP labelled.	137
3.5	Steps involved in the preparation of immunosensor for DON detection	140
3.6	Direct capture assay for anti-DON/anti-mouse IgG revealing saturation at an anti-DON IgG concentration of 0.2 mg/mL. An AP labelled anti-mouse IgG dilution of 1/30,000 was used. . . .	141
3.7	Chessboard titration results in which DON-BSA and anti-DON IgG concentrations were varied simultaneously with a maximum absorbance at a DON-BSA concentration of 1/10 and an anti-DON IgG concentration of 0.04 mg/mL.	142
3.8	Indirect capture assay were AP labelled anti-mouse IgG concentration is varied with DON-BSA and anti-DON IgG concentrations of 1/100 and 0.04 mg/mL respectively. n = 3. .	143
3.9	Indirect Competitive ELISA for DON with optimised DON-BSA, anti-DON IgG and AP labelled anti-mouse IgG of 1/100, 0.04 mg/mL and 1/16,000 respectively. $R^2 = 0.9975$, n = 3.	144
3.10	Optimisation of assay component solution	145
3.11	Optimisation of DON-BSA coating conjugate using an indirect capture capture assay with a fixed anti-DON IgG concentration of 0.04 mg/mL and a 1/1000 dilution of AP labelled anti-mouse IgG. Saturation was achieved at a DON-BSA concentration of 0.04 mg/mL. n = 3.	146
3.12	Optimisation of anti-DON IgG concentration using an indirect capture assay with DON-BSA concentration of 0.04 mg/mL, AP labelled anti-mouse IgG dilution of 1/1000. Current saturation occurred at 0.008 mg/mL. n = 3.	147
3.13	An indirect capture assay with DON-BSA concentration of 0.04 mg/mL, AP labelled anti-mouse IgG dilution of 1/1000 and anti-DON IgG concentration of 0.008 mg/mL. 4 different blocking solutions were compared - 1 % BSA, 2 % BSA, 1 % BSA and 2 % BSA. n = 3.	148
3.14	An indirect capture assay with DON-BSA concentration of 0.04 mg/mL and anti-DON IgG concentration of 0.008 mg/mL. 3 different concentrations of AP labelled anti-mouse were compared - 1/750, 1/500 and 1/100. n = 3.	149
3.15	Hydrodynamic amperograms for a range of DON concentrations at a MWCNT/Nafion electrode. After a period of 200 seconds 100 μ L of pAPP (25 mg/mL) was added to a stirred solution of 4900 μ L DEA buffer, pH 9.5. A fixed potential of 0.28 mV was used.	150

3.16	Indirect competitive electrochemical immunoassay for DON with optimised experimental conditions of DON-BSA concentration of 0.04 mg/mL, AP labelled anti-mouse IgG dilution of 1/100 and anti-DON IgG concentration of 0.008 mg/mL. 1 % casein was used as a blocking solution. $R^2 = 0.9679$, $n = 3$	150
4.1	Chemical structure of caffeine	157
4.2	Variation of pH as a function of peak potential of cyclic voltammetry measurements with a scan rate of 100 mV/s in 200 μ M caffeine (Britton-Robinson supporting electrolyte. $R^2 = 0.8485$, $n = 3$.)	163
4.3	Variation of pH as a function of peak current of cyclic voltammetry measurements with a scan rate of 100 mV/s in 200 μ M caffeine (Britton-Robinson supporting electrolyte).	163
4.4	Cyclic voltammograms of 200 μ M caffeine in different acidic media at a scan rate of 100 mV/s with a bare graphite SPE. . .	164
4.5	Comparison of peak current from cyclic voltammetry measurements of 200 μ M caffeine in a 0.1 M solutions of a range of acidic media.	164
4.6	Cyclic Voltammograms of 1 mM ferri/ferrocyanide in 1M KCl at electrodes modified with 0.1 %, 0.2 % and 0.3 % Nafion concentrations.	166
4.7	Cyclic Voltammograms of 200 μ M caffeine at electrodes with 0.1 %, 0.2 % and 0.3 % Nafion concentrations	166
4.8	Cyclic Voltammograms of 200 μ M caffeine in 0.1 M H_3PO_4 at bare graphite and electrochemically pretreated graphite electrodes	167
4.9	Scanning Electron Micrographs of electrochemically pretreated electrodes	168
4.10	Scanning Electron Micrographs of Untreated (above) and Nafion modified (below) graphite working electrodes	169
4.11	Contact angle droplets at both Nafion modified and pretreated electrodes showing the hydrophilic nature of the pretreated electrode in comparison to the bare SPE.	169
4.12	Cyclic voltammograms at an electrochemically pretreated electrode at scan rates of 20, 40, 60, 80, 100, 120, 140, 160, 180 and 200 mV/s in 1 mM $[Fe(CN)_6]^{3-/4-}$ in 1M KCl	170
4.13	Graph of peak anodic and cathodic peak current vs square root of scan rate from the electrochemically pretreated electrode . .	171
4.14	Cyclic voltammograms at a Nafion modified electrode at scan rates of 20, 40, 60, 80, 100, 120, 140, 160, 180 and 200 mV/s in 1 mM $[Fe(CN)_6]^{3-/4-}$ in 1M KCl	171
4.15	Graph of peak anodic and cathodic peak current vs square root of scan rate from the Nafion modified electrode	172

4.16 Cyclic voltammograms at an electrochemically pretreated electrode at scan rates of 20, 40, 60, 80, 100, 120, 140, 160, 180 and 200 mV/s in 1 mM hexamine ruthenium (III) chloride in 0.1 M PBS	173
4.17 Graph of peak anodic and cathodic peak current vs square root of scan rate from the electrochemically pretreated electrode . .	173
4.18 Cyclic voltammograms at a Nafion modified electrode at scan rates of 20, 40, 60, 80, 100, 120, 140, 160, 180 and 200 mV/s in 1 mM hexamine ruthenium (III) chloride in 0.1 M PBS . . .	174
4.19 Graph of peak anodic and cathodic peak current vs square root of scan rate from the Nafion modified electrode	174
4.20 Cyclic Voltammogram in blank 0.1 M phosphoric acid subsequent to measurement in 200 μ M caffeine solution	175
4.21 Consecutive CV measurements in 200 μ M caffeine solution with cleaning step between each measurement	176
4.22 CVs at a Nafion modified electrode in the presence of 200 μ M caffeine at a range of scan rates	177
4.23 Variation of peak current with square root of scan rate at Nafion modified electrode in 200 μ M caffeine	178
4.24 Variation of peak current with square root of scan rate at n=Nafion modified electrode in 200 μ M caffeine	178
4.25 Variation of peak current with square root of scan rate at Nafion modified electrode in 200 μ M caffeine	179
4.26 Variation of SWV frequency at fixed amplitude of 30 mV in 200 μ M caffeine solution (diluted in 0.1 M H ₃ PO ₄).	180
4.27 Variation of SWV amplitude at fixed frequency of 20 Hz in 200 μ M caffeine solution (diluted in 0.1 M H ₃ PO ₄).	180
4.28 Linear sweep voltammograms at electrochemically pretreated screen printed electrode at varying caffeine concentrations - 10 μ M, 14 μ M, 20 μ M, 30 μ M, 50 μ M, 70 μ M, 89 μ M, 109 μ M, 128 μ M, 148 μ M	181
4.29 Calibration curve of electrochemically pretreated electrode for caffeine detection showing two linear regions. The lower region has an R ² value of 0.9648 while the upper region has an R ² value of 0.9839. n = 3.	182
4.30 Square voltammograms at Nafion modified screen printed electrode at varying caffeine concentrations - 10 μ M, 30 μ M, 50 μ M, 70 μ M, 89 μ M, 109 μ M, 128 μ M and 148 μ M	183
4.31 Calibration curve of Nafion modified electrode for caffeine detection at a Nafion modified electrode in a 0.1 M H ₃ PO ₄ supporting electrolyte.	183
4.32 Nafion sensor signal for 100 μ M caffeine at 4 degrees celcius and room temperature	184
4.33 Pretreated sensor signal for 100 μ M caffeine at 4 degrees celcius and room temperature	185

4.34	Linear sweep voltammogram of 100 μM caffeine in the presence of 100 μM glucose and 100 μM sucrose at electrochemically pretreated electrode	186
4.35	Square voltammogram of 100 μM caffeine in the presence of 100 μM glucose and 100 μM sucrose at Nafion modified electrode	186
4.36	Linear Sweep voltammogram in 1/10 dilution of Red Bull at an electrochemically pretreated electrode	187
4.37	Square voltammogram in 1/10 dilution of Red Bull at a Nafion modified electrode	188
4.38	Cyclic voltammograms at bare SPE and GSPE in 1 mM hexaamine ruthenium (III) chloride with a supporting electrolyte of 0.1 M PBS buffer at a scan rate of 100 mV/s.	189
4.39	Cyclic voltammograms at bare SPE and GSPE in 1 mM ferri/ferrocyanide with a supporting electrolyte of 1 M KCl at a scan rate of 100 mV/s.	189
4.40	Cyclic voltammograms at a screen printed graphene electrode at scan rates of 20, 40, 60, 80, 100, 120, 140, 160, 180 and 200 mV/s in 1 mM $[\text{Fe}(\text{CN})_6]^{3-/4-}$ in 1M KCl	190
4.41	Graph of peak anodic and cathodic peak current vs square root of scan rate from a screen printed graphene electrode	191
4.42	Cyclic voltammograms at a screen printed graphene electrode at scan rates of 20, 40, 60, 80, 100, 120, 140, 160, 180 and 200 mV/s in 1 mM hexaamine ruthenium (III) chloride in 0.1M PBS	191
4.43	Graph of peak anodic and cathodic peak current vs square root of scan rate from a screen printed graphene electrode	192
4.44	Scanning Electron Micrographs of screen printed graphene working electrodes at magnifications of 5000x (top left), 2500 (top right) 1000x (bottom left) and 500x (bottom right)	193
4.45	Raman spectra for bare SPE and GSPEs	194
4.46	D and G bands at bare SPE and GSPEs	195
4.47	Variation of pH as a function of peak potential of cyclic voltammetry measurements with a scan rate of 100 mV/s in 200 μM caffeine (Britton-Robinson supporting electrolyte) at a graphene SPE. $R^2 = 0.8959$, $n = 3$	195
4.48	Variation of pH as a function of peak current of cyclic voltammetry measurements with a scan rate of 100 mV/s in 200 μM caffeine (Britton-Robinson supporting electrolyte) at a graphene SPE.	196
4.49	CVs at bare SPE and GSPE in the presence of 200 μM caffeine	197
5.1	Structure of carbon nanohorns (a) and TEM image (b) [1]	205
5.2	Integrated smart phone/electrochemical sensors [13]	207
5.3	Lab on a Chip for Integrated Multiplex Immunoassay [16]	208
A.1	XPS spectra of untreated and electrochemically pretreated electrodes.	212
A.2	XPS spectra for bare and pre-treated electrodes	213

A.3 XPS spectra for electrochemically pretreated graphite electrodes and graphene SPEs.	214
--	-----

Abstract

Electrochemical sensor technology has the potential to revolutionise analytical measurements in food analysis by providing a cheap, easy to use and portable alternative to traditional chromatography and mass spectrometry based techniques. In this thesis two such sensors are developed - one for the detection of caffeine and other for the detection of the mycotoxin, deoxynivalenol. These sensors are developed from both a food safety and quality control point of view. The majority of sensor development has been for the medical point of care sector, however apart from blood glucose sensing, commercial successes have been limited. Regulatory barriers are not as significant in the food industry compared to the medical industry and hence, real world applications should be more feasible.

Chapter 1 provides a general introduction to sensor technology for food analysis with an emphasis on electrochemical transducers and modified electrodes in particular. Background theory is outlined for both fundamental electrochemistry and immunoassay development and previously published work in electrochemical sensors for food analysis is summarised. In Chapter 2 a number of electrochemical pretreatment techniques are compared with multiwall carbon nanotubes (MWCNT) and reduced graphene oxide (RGO) modified screen printed electrodes in the development of an electrochemical immunosensor for mouse IgG detection. It was found that a MWCNT/Nafion modified electrode had the most promising analytical characteristics with an LOD of 0.2 ppm, IC₅₀ value of 0.3 ppm, linear range of 0.04 - 2.7 ppm and R² value of 0.9286. Subsequent to the optimisation of an electrode material for this model analyte (mouse IgG), an electrochemical immunosensor for deoxynivalenol was developed in Chapter 3. Firstly, an ELISA protocol was developed with a LOD of 0.534 ppm and linear range of 0.9 - 53 ppm, followed by the transfer of this protocol onto the MWCNT/Nafion electrode. A limit of detection of 0.95 ppm and IC₅₀ value of 2 ppm were found. These values are promising considering that the EU maximum residue limit (MRL) for DON in wheat samples is 1.75 ppm. However, the developed sensor was unable to detect DON in wheat samples suggesting that a more sophisticated sample pretreatment method would need to be investigated.

In Chapter 4, a number of different approaches for electrochemical caffeine detection are investigated namely electrochemically pretreated, nafion

modified and screen printed graphene electrodes. It was found that the nafion modified electrode was the most suitable in energy drinks samples. This sensor had a LOD of 8 μM and linear range of 10 - 128 μM . Finally, in Chapter 5 some suggestions are given to future directions for electrochemical sensor development.

Abbreviations

- **APTS** 2,2'-azino-bis(3-ethylbenzothiazoline-6-sulphonic acid
- **AP** Alkaline Phosphatase
- **AA** Ascorbic Acid
- **Ag/AgCl** Silver/Silver Chloride
- **AOAC** Association of Analytical Communities
- **BDD** Boron doped diamond
- **BPPG** Basal plane pyrolytic graphite
- **BSA** Bovine Serum Albumin
- **C_H** Constant Heavy
- **C_L** Constant Light
- **CV** Cyclic Voltammtry
- **DA** Dopamine
- **DNA** Deoxyribonucleic Acid
- **DON** Deoxynivalenol
- **DPV** Differential Pulse Voltammetry
- **ELISA** Enzyme Linked Immunosorbent Assay
- **ECIS** Electric cell substrate impedance sensing
- **EDC** 1-Ethyl-3-(3-dimethylaminopropyl)carbodimide
- **EU** European Union
- **EPPG** Edge plane pyrolytic graphite
- **ELIME** Enzyme-Linked-Immunochemical-Electrochemical
- **FPIA** Fluorescence polarization immunoassay
- **GC** Glassy Carbon
- **GC-FID** Gas Chromatography-Flame Ionisation Detection
- **GC-EC** Gas Chromatography-Electron Capture

- **GC-MS** Gas Chromatography-Mass Spectrometry
- **AuNP** Gold Nanoparticle
- **HPLC-UV** High Performance Liquid Chromatography-Ultra Violet
- **HPLC-FI** High Performance Liquid Chromatography-Fluorescence
- **IgG/E/A/M** Immunoglobulin G/E/A/M
- **LOD** Limit of Detection
- **LR** Linear Range
- **LFD** Lateral Flow Dipstick
- **MIP** Molecularly Imprinted Polymer
- **MUA** 11-mercaptoundecanoic acid
- **MPA** 3-mercaptopropionic acid
- **MWCNT** Multi-walled carbon nanotubes
- **NHS** N-hydroxysulfosuccinimide
- **OD** Optical Density
- **PBS** Phosphate Buffered Saline
- **pAPP** para aminophenyl phosphate
- **pNPP** para nitrophenyl phosphate
- **PEDOT** Poly(3,4-ethylenedioxythiophene)
- **PANI** polyaniline
- **PPy** polypyrrole
- **QCM** Quartz Crystal Microbalance
- **SAM** Self Assembled Monolayer
- **SEM** Scanning Electron Microscopy
- **SPR** Surface Plasmon Resonance
- **SPE** Screen Printed Electrode
- **SWCNT** Single-walled carbon nanotubes
- **SWV** Square Wave Voltammetry

- **TEM** Transmission Electron Microscopy
- **TMB** Tetramethylbenzidine
- **TM** Transverse magnetic
- **UA** Uric Acid
- **V_H** Variable Heavy
- **V_L** Variable Light
- **XPS** X-ray photoelectron Spectroscopy

I, Gerard Duffy, certify that this thesis is my own work and I have not obtained a degree in this university or elsewhere on the basis of the work submitted in this thesis.

Gerard Duffy

For my parents

Acknowledgements

Firstly, I would like to thank my supervisor Dr Eric Moore who gave me the opportunity to work in his lab - in particular his understanding and support when I took time off books at the end of my second year. I would also like to express my thanks to everyone in the Sensing and Separation group, past and present - Eileen, Michelle, Una, Walter, Niall, Shauna, Lisa, Yingeng, Xi and Shifa who over the years turned from colleagues into friends.

Another big thank you to all the new friends that I've made in Cork outside the lab especially Barry, Patrick, Jack, Dave, Ian and Eric. A special thank you is also in order for Laura for her patience, understanding and support.

To Stephen, Colm, James, Conor, Niall C and Niall M thanks for the friendship, the craic, the chat and the laughs. To David, James, Rachel, Therese, Evan, Anna, Mary and Matthew, thank you for having me to stay on various weekends and always providing perspective.

Finally, my deepest thanks to my parents, to whom this thesis is dedicated. In particular when things were tough a supporting voice at the end of the phone was always there. Without them I simply wouldn't have been able to finish this thesis. For that and so much more I'm eternally grateful.

*Getting started, keeping going, getting started again - in art and in life, it
seems to me this is the essential rhythm not only of achievement but of survival*
Seamus Heaney

Chapter 1

Introduction

1.1 Electrochemical Sensors For Food Analysis

The need to ensure food safety, quality and standards is of great concern to both the food industry and the consumer. At present, the majority of the necessary analysis is carried out at the end of the production process using a range of separation methods in conjunction with common chromatographic techniques such as GC-FID, GD-EC, GC-MS, HPLC-UV, HPLC-Fl and HPLC-MS [1]. This approach has a number of limitations. Firstly, as the analysis is carried out at the end of the process, contaminated batches of product can go through an expensive production process before any concerns are raised. Secondly, these methods of analysis are time consuming, require highly trained personnel and are expensive, especially considering the high volume of samples required to be analysed. Electrochemical sensors offer a possible alternative to this approach, by allowing for a screening step before the production process is fully complete. This would mean a smaller number of samples would be required to be analysed by the more expensive chromatographic techniques as outlined in Fig. 1.1.

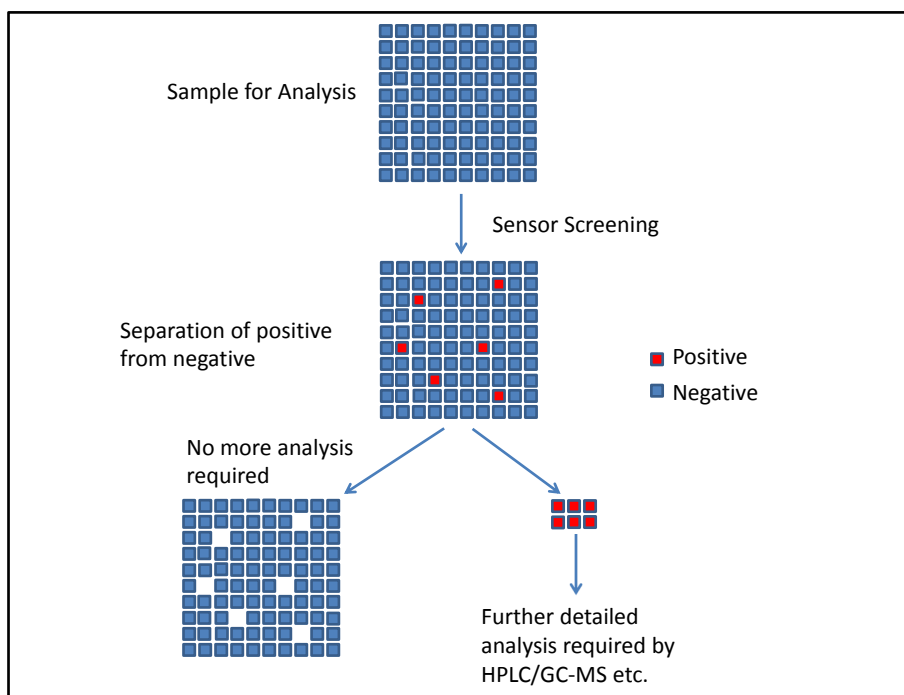


Figure 1.1: Schematic of sample screening with an Electrochemical Sensor

Futhermore, contamination can occur at the production, packaging, transport or storage stages of food production [2]. With this in mind, sensor technology offers the possibility of providing quick on site analysis with real time

information. However, biosensors in general have failed to gain much traction in the food analysis. The reasons suggested for this include the conservative nature of the market, the high cost of commercial biosensors in a small profit margin field and the tendency of biosensors companies to focus their products on pharmaceutical applications [3]. However, this could be about to change due to the ever increasing guidelines outlined by the European Food Safety Authority, a number of high profile food safety and authenticity scandals and the renewed focus of sensor based researchers on food analysis applications [4, 5]

1.2 Thesis Aims and Objectives

The aim of this thesis was to develop electrochemical sensors for the detection of the mycotoxin deoxynivalenol (DON) and for the psychoactive substance caffeine in food and food-related products. These analytes require monitoring from both a food safety and quality perspective. In the case of caffeine the concern of food companies is mostly from a food quality and standards point of view despite the fact that high doses of caffeine are harmful to human health. On the other hand, DON detection is approached very much from a food safety perspective as illness from mycotoxin contamination is a significant risk. The detection of these analytes is currently carried out by traditional chromatographic and bioassay techniques which are costly, time consuming and require skilled personnel to carry out the analysis [2] The sensors developed in this thesis have the potential to offer a low cost, portable and time efficient solution to these issues. An outline of the thesis structure is given in Fig. 1.2.

1.2.1 Chapter 1

In the subsequent sections of chapter 1 a general introduction is given to biosensors and electroanalysis. Attention is given to recent advances in electrochemical immunosensors as well as electrode modification strategies for immunosensors and for electrochemical sensors in general. In particular, the sp^2 family of carbon electrodes, namely graphite, graphene, graphene oxide and carbon nanotubes are discussed in detail as they are used extensively in this thesis. Finally, the latest electrochemical sensors from the literature for mycotoxin and caffeine detection are outlined.

1.2.2 Chapter 2

Chapter 2 is concerned with the evaluation of electrode materials for electrochemical immunosensor applications. Two approaches are investigated with mouse IgG used as a model analyte. Firstly, a number of previously reported electrochemical pretreatment approaches are compared using a range of characterisation techniques with the most promising pretreatment being used to develop an immunosensor. Secondly, reduced graphene oxide and carboxylic acid functionalised multiwalled carbon nanotubes are compared in a similar manner.

1.2.3 Chapter 3

In Chapter 3 an electrochemical immunosensor for deoxynivalenol detection is developed using a carboxylic acid functionalised multiwalled carbon nanotube/Nafion modified screen printed electrode. This electrode was deemed to be the most promising for immunosensor applications from the studies carried out in Chapter 2.

1.2.4 Chapter 4

In Chapter 4 the development of an electrochemical sensor for caffeine detection is outlined. As caffeine is electrochemically active, a biological recognition element isn't required. Again, an electrochemical pretreatment approach is undertaken, on this occasion in comparison to a Nafion modified screen printed graphite electrode. The developed sensor is used to determine caffeine concentrations in energy drinks.

1.2.5 Chapter 5

At the end of each of the experimental chapters (2,3 and 4) specific details are given which could be explored for the improvement of the developed sensors. In chapter 5 however, a broader outline is given to potential future developments in the field. In particular, emphasis is given to the discussion of integrated analysis systems which the sensors developed in thesis could be

used in conjunction with. This should provide ideas for the next stage of this research.

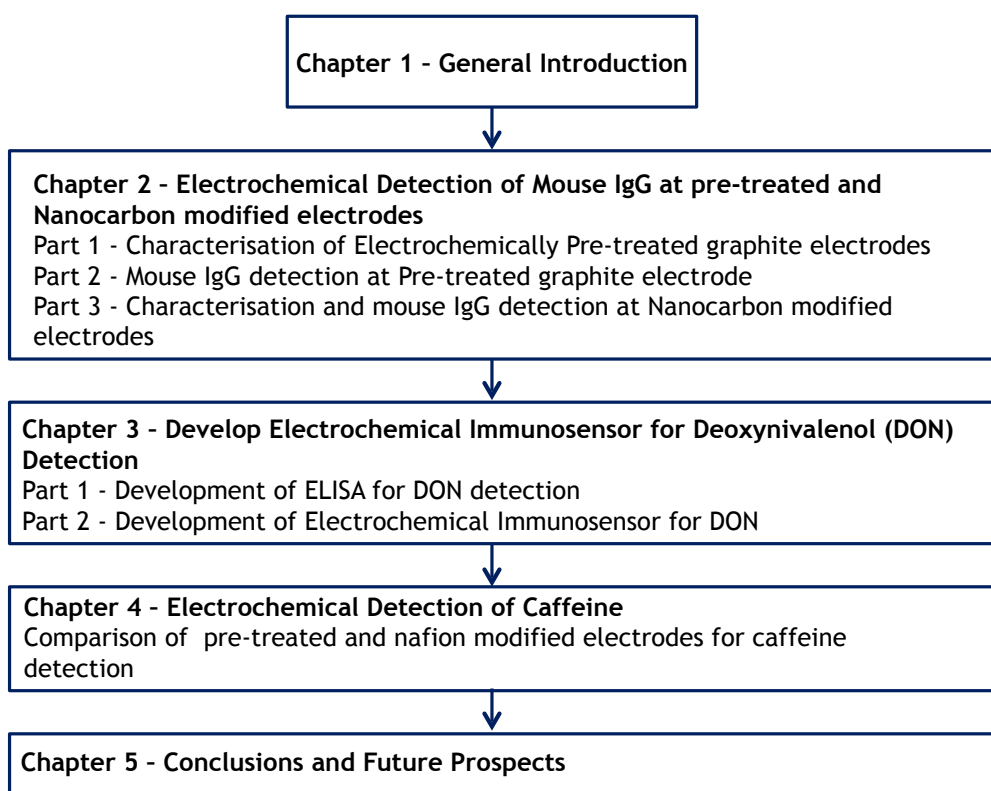


Figure 1.2: Outline of chapter structure within the thesis

1.3 Biological and Chemical Sensors

A chemical sensor can be defined as a device that transforms a variety of chemical information into an analytically useful signal [6]. These devices contain two key components, a chemical recognition system and a physio-chemical transducer. If the recognition system contains a biological element, the sensor is known as a biosensor. Biosensors can in turn be defined either by their recognition element, or by the physio chemical transducer that is used to produce an analytical signal. The different forms of biosensor are summarised in Fig. 1.3. The central motivation for the development of biosensor technology is in the replacement of or as a compliment to traditional, laborious analytical techniques. These new devices should be portable and easy

to use allowing fast results for home, hospital or industrial use.

The first biosensor was reported by Clark and Lyons - a blood glucose sensor which was used to monitor patients during cardiovascular surgery [7]. The glucose sensor has been a major commercial success story with home use devices accounting for 80 % of the entire biosensor market[8]. Despite the fact that research focus and commercial successes have been in the medical sector, biological and chemical sensors are now beginning to be developed in a wider range of fields such as pharmaceutical analysis, environmental monitoring and food analysis [9, 10, 3]. Food analysis is a particularly promising field as the regulatory requirements bring a product to market are less than in other fields. The development of sensor technology for this area is the focus of this thesis.

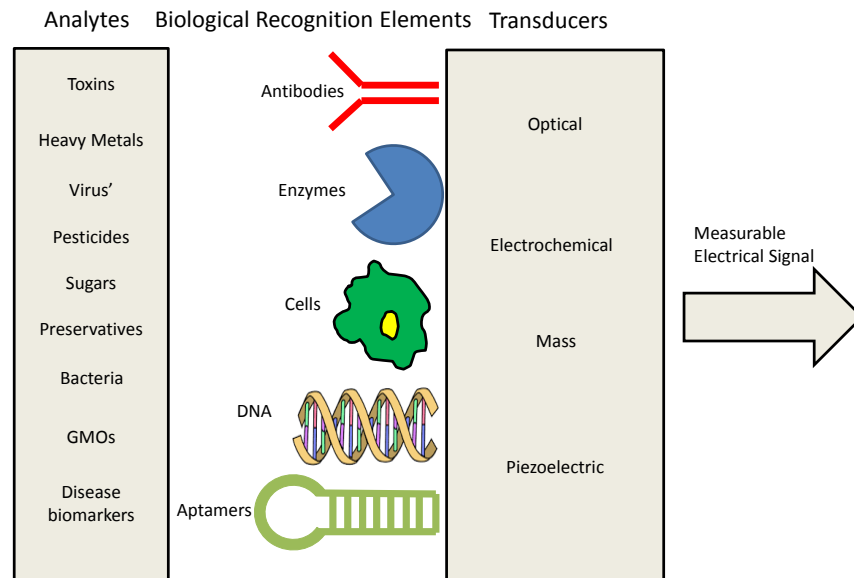


Figure 1.3: Biosensor classification based on analyte, biological recognition element and transducer

1.4 Biosensor classification

1.4.1 Transducers

The transducer element of a sensor transfers the signal produced by the biochemical reaction into an electrically readable output. For example, in

the case of electrochemical sensors, the electrode itself is the transducer. In the following subsections a number of different transducers used in biosensor design are discussed.

1.4.1.1 Optical

Surface Plasmon Resonance (SPR) is a phenomenon which occurs when transverse magnetic (TM) polarized photons incident on a metal dielectric surface oscillate at the same frequency as the valence electrons of the metal. The surface wave (plasmon) produced is then sensitive to changes in the refractive index near the metal surface [11]. Biochemical changes such as the antigen-antibody interaction within the plasmon field can result in changes to the plasmon resonance which is detected as a change in the refractive index. Hence, biochemical detection can occur.

The use of fibre optics is another strategy for optical based biosensor development. Fibre optic biosensors all contain the following elements: a light source, and optical transmission medium such as a fibre or wave guide, a biological recognition element, optical probes for transduction and an optical detection system [12]. The advantages of this type of sensor include the ability for label free detection, isolation from electromagnetic interference, compact design, accuracy and low cost [13]. However, challenges still exist in the miniaturisation of the sensors as well as how to increase the stability of the immobilised biocomponent.

1.4.1.2 Mass/Acoustic

A quartz crystal microbalance (QCM) consists of a quartz disk combined with electrical contacts [14]. The QCM is piezoelectric i.e. the application of an external electric field can induce an internal mechanical stress. This basic device can be converted into a biosensor with the immobilisation of a biological component. There is a linear relationship between the oscillating frequency of the piezoelectric crystal and the mass variation on its surface. This change in mass occurs when the analyte interacts with the biospecific agent immobilised on the crystal surface which leads to a sensitive form of detection [15].

1.4.1.3 Electrochemical

Electrochemical transducers rely on the generation of an electrochemically active compound that can be oxidised or reduced, or through the change in the surface properties of electrodes that can be detected electrochemically. The main advantage of electrochemical transducers is the possibility that these transducers have for miniaturisation and portability. This is particularly important for in-field, medical, environmental or food analysis. The main advances in this area has been through the development of novel electrode materials that have allowed sensitive and selective determination of a wide range of analytes [16, 17]. Electrochemical sensors are the focus of this thesis and hence are discussed in detail throughout the rest of this chapter.

1.4.2 Biological Recognition Elements

It is also the case that biosensors can be classified in terms of the biological recognition element used as outlined in the following sections.

1.4.2.1 Enzymes

The majority of enzyme based biosensors have been developed for the detection of glucose through the use of the enzyme glucose oxidase [18]. Much of the research in this area has been in the connection of the redox centre of the enzyme with an electrode surface through the use of mediators such as ferrocene and benzoquinone [19]. These mediators allow an increase in the rate of electron transfer which ultimately leads to lower limits of detection. However, recent advances in the detection of glucose have showed that non-enzymatic approaches are also viable [20].

1.4.2.2 DNA

Single stranded DNA, when immobilised onto a sensor surface, can be used to detect its complimentary strand in a sample. The two strands then form a hybrid on the surface which can be detected by a range of different transducers - electrochemical, optical, gravimetric and SPR [21]. In a similar way to immunosensors, DNA biosensors often use a labelling step which can be

photometric, enzymic or electroactive [22]. Much of the recent advances in the area have come in the area of integrated devices; so called 'lab on a chip' devices [23]. These sensors could have applications in determining food authenticity, particularly in light of recent food fraud scandals.

1.4.2.3 Whole Cells

Living cells are a versatile recognition element used in biosensors for drug screening, clinical diagnostics, food analysis and environmental monitoring [24]. One particularly popular technique has been the use of electrical cell substrate impedance sensing (ECIS) which allows the label free monitoring of cell attachment and spreading of cells on electrode surfaces [25, 26]. ECIS has been also applied to cytotoxicity monitoring in environmental samples [27].

1.4.2.4 Molecularly Imprinted Polymers

Molecularly imprinted polymers (MIP) are an example of synthetic molecules that can be used in biosensor applications. The synthesis of MIPs follows three main steps. Firstly, functional monomers attach to the analyte of interest through reversible or non-covalent bonding [28]. Secondly, a polymerisation process occurs through a range of strategies which allows the formation of a polymer/functional monomer/analyte matrix [29]. Finally, the analyte is removed revealing a polymer with specific recognition sites for the analyte in question. The MIP can then be deposited onto the sensing surface of choice. One of the key advantages of MIPs is their robustness and low cost of production. Due to the regulatory barriers being much lower for the food industry, Uzun et. al have suggested that the first commercial biosensor using MIPs could well be for food analysis applications [29].

1.4.2.5 Aptamers

A new class of biological recognition element known as aptamers are attracting interest as a possible rival for antibodies in biosensor applications [30, 31, 32]. Aptamers are synthetic nucleic acid probes that have the ability to bind to small molecules, thus performing the same role as antibodies. However, they also offer some significant advantages such as not requiring animals for their

production. The production of aptamers *in vitro* allows them to be engineered to bind to a specific region of the target and also avoids the complication associated with antibodies of identifying endogenous proteins as opposed to the intended target. One of the most significant advantages that aptamers have in comparison to antibodies is their stability at ambient temperatures which is particularly important for sensor storage and transport. Ochratoxin A has proved to be a popular analyte for the use of aptamers, even justifying a review article in the area [33]. Electrochemical aptasensors have also been developed for a range of other food related analytes such as fumonisin B1 [34], tetracyclines [35], aflatoxin M1 [36] and kanamycin [37] amongst others.

1.4.2.6 Antibodies

Antibodies can be defined as proteins produced by an organism that are used to counteract a specific antigen. They come in five main classes, IgG, IgA, IgM, IgD and IgE. The most basic form of antibody consists of two light and two heavy chains held together by noncovalent and disulphide bonds. The heavy chain of the antibody determines which class it belongs to. The IgG, IgE and IgD forms consist of the basic IgG structure with two light and heavy chains. In contrast, IgA molecules can consist of a singlet, doublet or triplet of this basic structure whilst IgM molecules are pentameric in structure.

In Fig. 1.4 you can see the structure of an IgG antibody. This type of antibody has four polypeptide chains, two heavy chains, and two light chains linked by disulphide bonds. Both the heavy and light chains have variable regions (V_H and V_L) which are responsible for antigen binding.

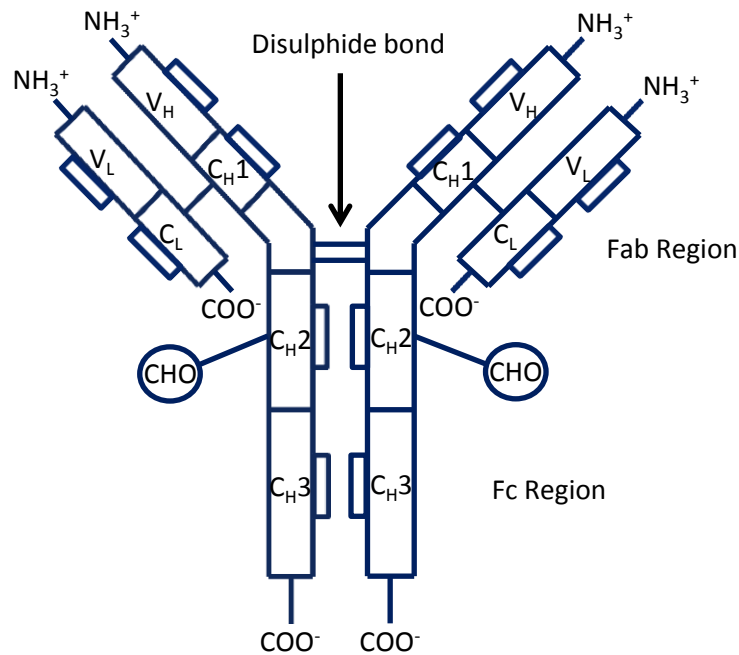


Figure 1.4: Schematic of typical antibody IgG structure showing constant and variable regions as well as connecting disulphide bond

Antibodies can also be divided into two different class types, depending on how they are produced. Antibodies produced from multiple B-lymphocyte lines are known as polyclonal antibodies, whereas antibodies that are produced from the clones of a single B-lymphocyte [38]. The advantages and disadvantages of using these types of antibodies are outlined in Table 1.1

Table 1.1: Monoclonal vs Polyclonal Antibodies

Monoclonal Antibodies	Polyclonal Antibodies
High cost to prepare	Cheaper to prepare
Same affinities	Different affinities
Monospecific antibody	Cannot be reproduced
Detects only one epitope	Recognises multiple epitopes
Efficient for binding of antigens within a mixture of related molecules	Not useful for probing specific domains of antigens

Furthermore, in terms of bioassay development, primary antibodies are defined as those antibodies that target the species of interest in an assay. In contrast, secondary antibodies are targeted towards the primary antibody by binding of their Fab domain to the Fc domain of the primary antibody. This allows for great

flexibility in ELISA experiments (see following sections) by enabling labelling of secondary antibodies which can be used with a range of different primary antibodies. Hence, the specific binding of an enzyme to a primary antibody is often not required.

1.5 Enzyme Linked Immunosorbent Assay

Enzyme linked immunosorbent assay (ELISA) is a common immunoassay technique that has become, since its establishment in the early 1970s [39, 40], a fundamental tool in the analytical sciences with wide ranging applications. The basis of the ELISA procedure is the high specificity and affinity that an antibody has for an antigen which allows binding of the antigen whilst in the presence of hundreds of other substances. A range of different ELISA formats are possible, some of which are shown in Fig. 1.5. The choice of ELISA format is dependent on the requirements of the assay and the reagents available. For example, in the case of small molecule detection, the competitive assay is most appropriate. These experimental formats are outlined in detail in subsequent sections.

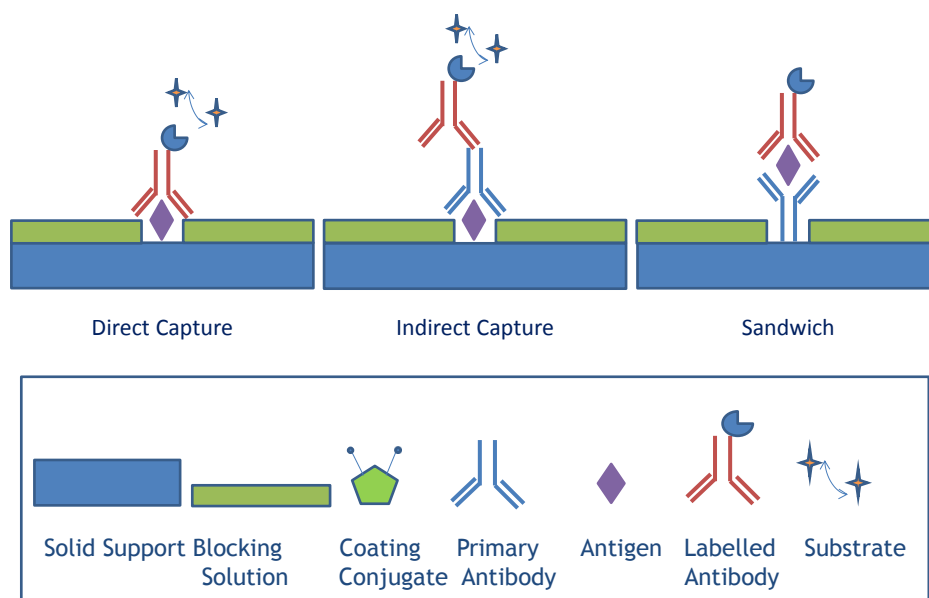


Figure 1.5: Direct capture (left), Indirect capture (centre) and sandwich (right) ELISA assays

1.5.1 Direct ELISA

In the direct ELISA format an antigen or antibody is immobilised directly onto the solid support [41]. The next step involves blocking all vacant sites on the surface followed by the binding of the enzyme labelled antibody to the antigen. Any unbound compounds are then washed away using a washing buffer which leaves only the antigen-antibody conjugate on the surface of the microtitre well. Finally, an enzyme substrate is added which the enzyme converts into a detectable product. The intensity of the signal produced is directly proportional to the amount of antibody (or antigen in the case of an antigen capture assay) captured. This intensity is measured using an absorbance plate reader, which measures absorbances at the appropriate wavelength for the enzyme used.

1.5.2 Indirect ELISA

Indirect ELISA makes use of enzyme labelled secondary antibodies which bind to the detecting antibody as opposed to an enzyme labelled primary antibody in the case of the direct ELISA format. Secondary antibodies bind specifically to their primary antibody counterpart in a similar way to the antibody-antigen binding. In the same procedure as the direct assay, a primary antibody-antigen complex is developed in the microtitre well. At this stage of the process, an enzyme labelled secondary antibody is introduced which binds with its primary conjugate. The enzyme substrate then indicates the concentration of the antibody, also using an absorbance plate reader. The indirect system offers the advantage that a wide range of antisera can be investigated for binding to a particular antigen using a single antispecies conjugate [42]. This offers fantastic versatility in antispecies conjugates of which there are thousands commercially available.

1.5.3 Sandwich ELISA

In a sandwich assay, as indicated in Fig. 1.5 above, the antigen to be detected is sandwiched between two antibodies. The primary antibody's secondary antibody is then attached (with enzyme label) and the same detection routine is carried out. The advantage of the sandwich assay is increased sensitivity in comparison to the direct and indirect approaches [43].

1.5.4 Competitive ELISA

In a competitive ELISA (Fig. 1.6), the analyte to be detected competes with a labeled antibody in order to bind to a primary antibody that has been attached onto the well surface. In this format, there is an inverse relationship between analyte concentration and absorbance signal due to the fact that the greater the amount of labeled antibodies that attach to the coating conjugate, the less analyte is present in the sample. Competitive assays are generally used for the detection of small molecule analytes as only one antigen binding site is required in contrast to the sites needed in a sandwich assay [44].

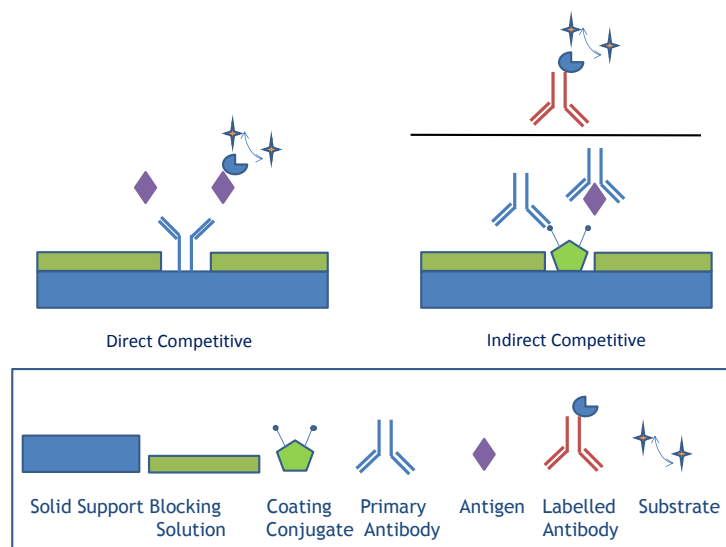


Figure 1.6: Direct competitive (left) and Indirect competitive ELISA formats

1.5.5 Displacement ELISA

A displacement assay (Fig. 1.7) has a similar set of steps to the indirect competitive assay. However, instead of a competition step between antibody and antigen, the labelled secondary antibody is allowed to bind to the primary antibody uninhibited. Then in the final step of the assay, the analyte is added which displaces the coating conjugate/primary/secondary antibody complex that has formed on the plate. Hence, a high concentration of analyte leads to a low signal. The advantage of this type of assay is that the analyte can be added at the very end of the assay allowing the plate to be prepared and stored in advance. However, it also entails an extra incubation step which increases overall assay time.

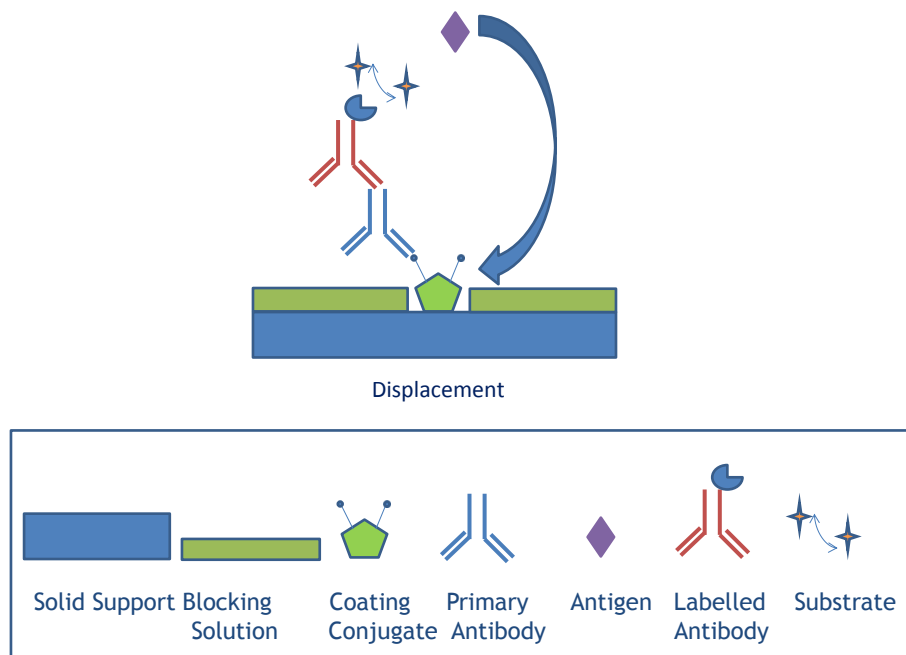


Figure 1.7: Displacement ELISA format

1.5.6 Photometry and Beer-Lambert Law

Photometry is a method used to measure the amount of light that a chemical sample adsorbs as light passes through it. It is the measurement principle upon which all ELISA experiments are based. Each compound adsorbs light over a range of wavelengths and the amount adsorbed is related to the concentration of the sample as described by the Beer-Lambert law:

$$Absorbance = \epsilon lc \quad (1.1)$$

where the absorbance is defined as follows:

$$Absorbance = -\text{Log}_{10} \frac{I}{I_0} \quad (1.2)$$

and ϵ is the molar attenuation, c is the concentration and l is the path length of the beam of light through the sample.

A schematic representation of the measurement principle of the photometer is given in Fig. 1.8. Firstly, a quartz tungsten halogen lamp (1) produces light

which is chopped by the chopper wheel to minimise electronic noise (2). The light then passes through the condenser lens (3) before part of the visible light is reflected by a translucent mirror (4) which evens out the spectral density. An appropriate wavelength is then selected using an interference filter (6). An optical fibre bundle (7) then refracts the light into eight equal parallel beams and deflects the beam upwards where it is focused using lenses (8). Finally the intensity of the light is measured using a photocell detector (9).

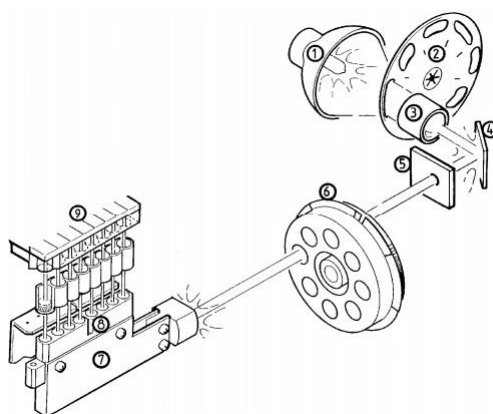


Figure 1.8: Multiskan Ex Plate Reader measurement principle (reproduced from the operating manual)

1.5.7 Enzyme Substrate Reactions

The two most commonly used enzymes in ELISA are alkaline phosphatase and horseradish peroxidase. In the case of alkaline phosphatase, p-nitrophenol phosphate (pNPP) is the most commonly used substrate and is used to produce p-nitrophenol. The specific reaction is described in Fig 1.9. The intensity of the yellow colour is representative of the concentration of the analyte present.



Figure 1.9: AP/pNPP substrate reaction

1.6 Electrochemical Immunosensors

Electrochemical immunosensors, in a similar way to ELISA measurements, also rely on the ability of antibodies to detect specific antigens. However, in contrast to ELISA the signal is detected via an electrochemical signal as opposed to a colour change. This is achieved by using an enzyme substrate that, when reacting with an enzyme labelled secondary antibody, produces a product that can be oxidised or reduced with the application of a fixed voltage. In the case of alkaline phosphatase labelled secondary antibodies, para aminophenyl phosphate (pAPP) (see Fig 1.11) is commonly used and tetramethylbenzidine/hydrogen peroxide (TMB/H₂O₂) is used for horseradish peroxidase labelled secondary antibodies. TMB/HRP has the advantage of being able to be used for both optical and electrochemical assays. Electrochemical immunosensors have a number of significant advantages over ELISA including their small size, low cost and portability. Another advantage, particularly in food samples, is the fact that there are significantly less electrochemical interferences in food matrices as opposed to optical interferences.

A schematic of a sandwich assay based electrochemical immunosensor is shown in Fig. 1.10 which outlines some of the various strategies that have been used in this type of sensor development in recent years. These include the type of electrode material used - most commonly glassy carbon, screen printed carbon, polycrystalline gold, screen printed gold and boron doped diamond. Also shown is a number of electrode modification techniques that have been used to increase electrode surface area, allowing for greater antibody immobilisation. These include nanomaterials such as gold nanoparticles, carbon nanotubes and graphene as well as the use of self assembled monolayers which enable well oriented antibody immobilisation. Finally, Fig 1.10 also describes the use of an external magnet which can be used with magnetic particles coated with antibodies for successful immobilisation.

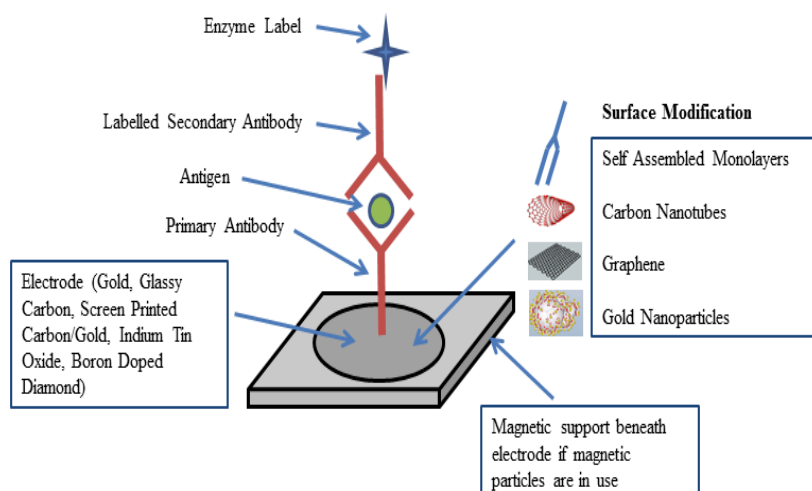


Figure 1.10: Schematic of typical electrochemical immunosensor utilizing a sandwich assay approach. Also shown are some of the various materials and modifications used in this type of sensor development including self assembled monolayers, gold nanoparticles, graphene and carbon nanotubes.

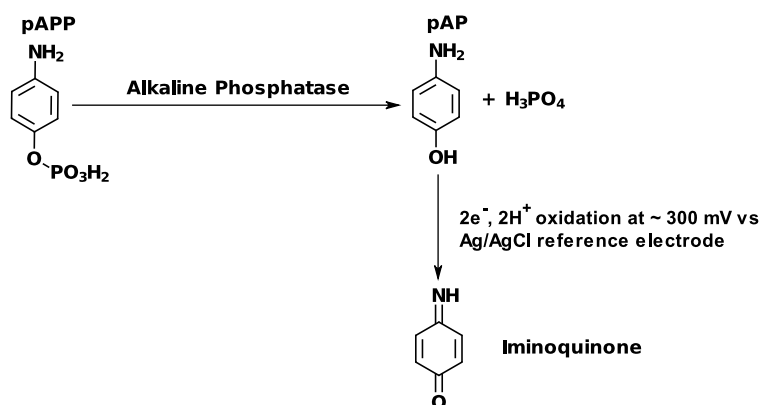


Figure 1.11: AP/pAPP substrate reaction

Despite the fact that electrochemical immunosensor development adopts similar steps to the development of an optical assay, the translation of the ELISA assay to an electrochemical format is not straightforward. The reason for that is the ELISA the measurement step occurs in a homogeneous solution whereas for an electrochemical immunosensor the measurement step occurs at the electrode/solution interface [45]. Hence, the immobilisation of any biological entities onto the the electrode can necessarily change the measurement signal.

However, it is this very change in measurement signal that has allowed the development of another class of electrochemical immunosensors which do not require antibody labelling. Instead electrochemical impedance spectroscopy is used in order to measure the change of surface impedance on the electrode surface, upon the creation of an antibody/antigen immunocomplex [46]. Label free approaches provide the advantage of reducing the number of assay steps required which in turn reduces assay time.

1.6.1 Antibody/Antigen Immobilisation

A key factor in the design of any immunosensor is the successful immobilisation of antibodies onto the sensor surface. The antibodies should be evenly distributed, well aligned and stable on the surface [47]. Fig. 1.12 describes some possible antibody positions on the sensor and the resulting activity of the antibody. Evidently, only properly aligned antibodies will enable successful antibody/antigen binding events.

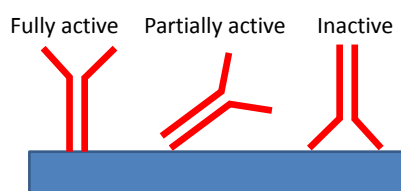


Figure 1.12: Antibody Immobilisation

In the case of electrochemical immunosensors, a number of methods have been used to try and achieve successful immobilisation. The simplest of these is passive adsorption of the antibody onto the electrode surface. This involves the incubation of the antibody (often in a carbonate buffer of pH 9.6) at room temperature, 37 degrees celcius or for longer periods at 4 degrees celcius. The drawback of this approach is the random orientation of the antibodies on the surface. Despite this drawback, it has proved to be a popular technique and has been used in several studies particularly when using screen printed electrodes [48].

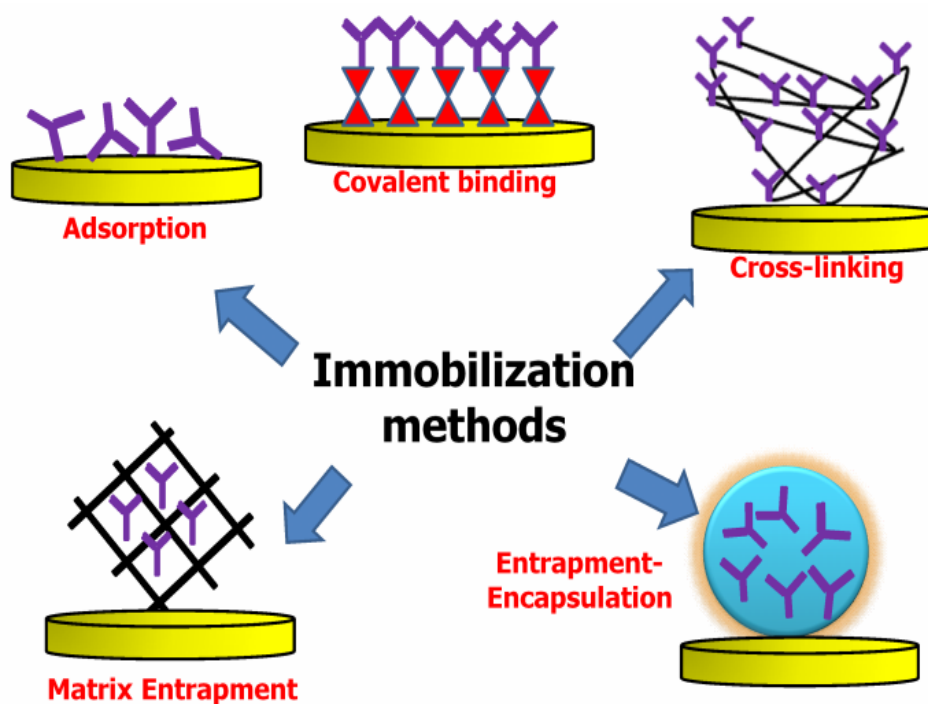


Figure 1.13: Strategies for antibody immobilisation [49]

Another option for antibody immobilisation is through covalent attachment. The cross linker 1-Ethyl-3-(3-dimethylaminopropyl)carbodiimide (EDC) in conjunction with Sulfo-NHS (N-hydroxysulfosuccinimide) is often used for this type of attachment. This approach allows for a more well oriented antibody which can remain active on the surface. Fig.1.14 shows how EDC/NHS chemistry can be used for the immobilisation of proteins (antibodies in the case of an electrochemical immunosensor) onto a carboxylic acid functionalised carbon nanotube. Firstly, EDC reacts with the carboxylic groups on the nanotube surface, producing an o-acylisourea intermediate. Without the use of NHS (upper mechanism in Fig 1.14), this intermediate is very unstable and susceptible to hydrolysis. Inclusion of NHS allows of a more stable NHS ester which binds to primary amines that are present on an antibody. As indicated in Fig 1.13 other approaches include matrix entrapment, cross-linking and entrapment encapsulation can also be used.

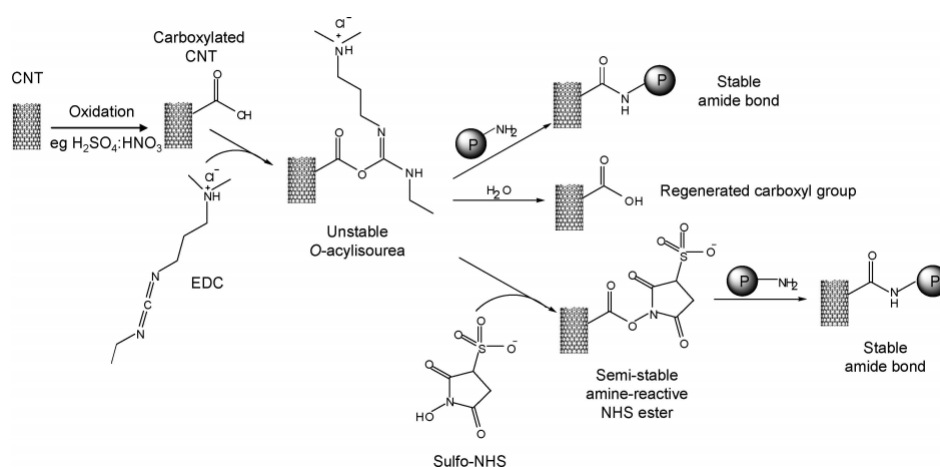


Figure 1.14: Conjugation of proteins to carboxylated CNTs using EDC in the presence or absence of sulfo-NHS

1.6.2 Non-specific binding

A common problem in immunoassays is the issue of non-specific binding, in which binding events occur other than the designed antibody/analyte or antibody/antibody interactions. Most commonly these occur between secondary antibodies and either the ELISA plate well or sensor surface. A number of strategies are used to prevent this unwanted binding. Firstly, after immobilisation of the antibody or antigen onto the substrate, a blocking step is carried out in which a protein that binds to the substrate, but not to any of the constituents of the assay, is added to block binding sites on the surface. Common choices of this protein include bovine serum albumin (BSA), casein and non-fat dried milk. Often the approach in immunosensor design is to compare these blocking agents to determine which provide the best signal to noise ratios [50].

1.7 Electrochemistry Fundamentals

1.7.1 The Electrochemical Cell

Electrochemical cells can be divided into two main classes. Galvanic (or voltaic) cells derive electrical energy from spontaneous reactions and are the basis upon which batteries work. In contrast, electrolytic cells require an external voltage in order to drive a chemical reaction. Every electrochemical cell contains an anode and cathode where oxidation and reduction occur respectively as well as an electrolyte which allows the flow of ions between anode and cathode.

The current that flows in an electrochemical cell is of two main forms: Faradaic and non-Faradaic. Faradaic current occurs due to either oxidation or reduction reactions. In contrast non-Faradaic or capacitive current is due to the electrode double layer (discussed below). To achieve high signal to noise ratios in an electrochemical sensor it is necessary to minimise this capacitive current where possible.

In Fig. 1.15 a typical electrochemical cell set up containing working, reference and counter electrodes can be seen. The choice of working electrode is key in the design of any electrochemical experiment. For sensing applications the electrode should be chemically inert, provide a wide potential window, low capacitive background currents and fast electron transfer kinetics. Popular choices of working electrode include glassy carbon, polycrystalline gold, screen printed carbon, carbon paste and boron doped diamond. The purpose of the reference electrode is to provide a fixed potential against which the potential at the working electrode can be measured. It should be placed as close as possible to the working electrode in order to avoid iR drop (the voltage associated with the solution). Its purpose is to provide a stable potential against which the potential at the working electrode is measured. Common choices of reference electrode include the silver/silver chloride electrode and saturated calomel electrode. The function of the counter (auxiliary) electrode is to supply the current required by the working electrode without limiting the measured response of the cell. As the counter electrode should not influence the measured data, it should therefore be larger than the working electrode.

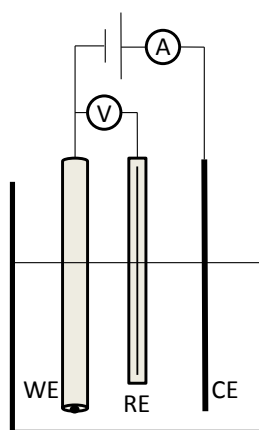


Figure 1.15: 3 Electrode Electrochemical Cell

1.7.2 Electrode/Solution Interface - Double Layer Models

When an electrode is placed in solution, the charges on the surface attract opposite charges from the solution creating a double layer as found in a capacitor. This concept was first described by Helmholtz in the 19th century. The model predicted a double layer capacitance that was constant and independent of ion concentration and electrode potential. However, this contradicted experiment which shows that the double layer capacitance is dependent on both quantities. An improved model was then suggested by Gouy and Chapman which introduced a diffuse double layer which took into account the thermal motion of ions in solution. This model suggested that the oppositely charged ion concentration in solution was greatest at the electrode surface but decreased away from the surface until a homogeneous solution of cations and anions exists in the bulk solution.

Stern provided a further improvement on the model by taking into account the size of the ions in solution and combining the features of the Helmholtz and Gouy-Chapman models. Grahame then proposed (Fig. 1.16) that if some ions lost their solvation shell it would be possible to penetrate the Stern layer and be adsorbed onto the electrode surface. Further developments in the understanding of the electric double layer are ongoing [51].

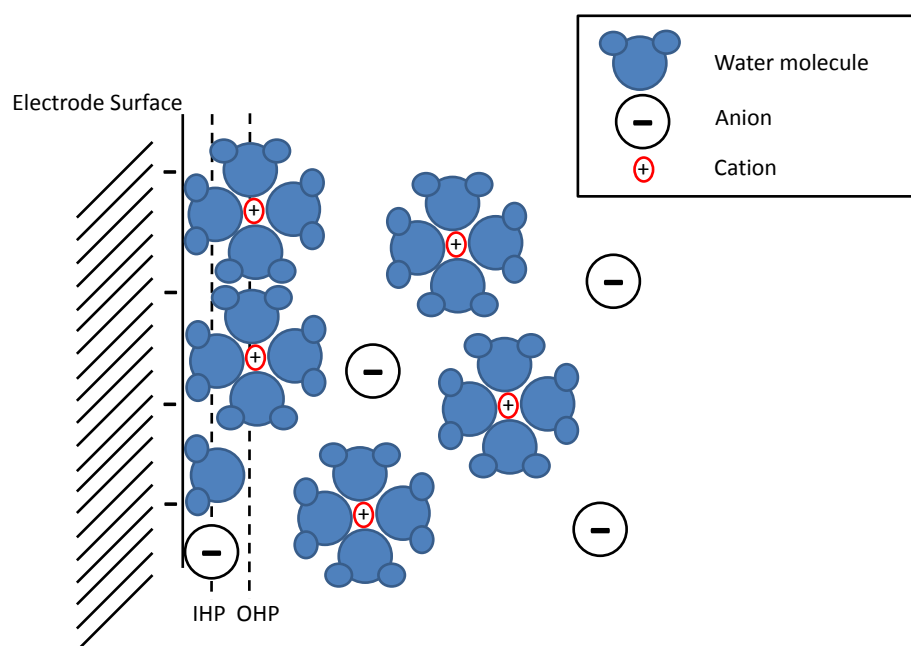


Figure 1.16: Grahame Electrical Double Layer Model

1.7.3 Mass Transport

1.7.3.1 Diffusion

Diffusion is the movement of a species due to a concentration gradient [52]. In electrochemical measurements, it is often the case that the concentration is different in the bulk solution as opposed to the electrode surface and hence diffusion plays a role. This difference in concentration is due to the fact that at the electrode surface a reaction is taking place which converts the starting material to product. So, there is a concentration profile where the concentration of O and R are a function of distance from the electrode surface. This can be up to 10^{-2} cm thick [52]. In an unstirred solution, when undertaking cyclic voltammetry or chronoamperometric measurements for example, diffusion is the main contributor to mass transport.

Diffusion is governed by Fick's laws, stated below for one dimension. Fick's first law shows how diffusion will take place from high to low concentrations. Fick's second law is then a statement about the concentration then varies with time. In the case of macro electrodes diffusion can be entirely accounted for in one dimension only (perpendicular to the electrode surface). However, in the case

of micro and nano electrodes radial diffusion also plays a significant role.

Fick's first law:

$$J = -D \frac{dc}{dx} \quad (1.3)$$

Fick's second law:

$$\frac{\partial c}{\partial t} = D \frac{\partial^2 c}{\partial x^2} \quad (1.4)$$

1.7.3.2 Migration

Migration is the movement of a charged species due to a potential gradient and accounts for the completion of the circuit through the solution between the electrodes [52]. In general it is not a form of mass transport for the electroactive species in solution as the charge is passed through an excess of supporting electrolyte.

1.7.3.3 Convection

Convection is the movement of a species due to mechanical forces, such as the stirring of the solution or the rotation of the electrode [52]. Unwanted or natural convection can occur due to vibration, which can be minimised by using a Faraday cage. However, forced convection can also be of use in electrochemical measurements allowing higher current densities to be achieved. It is generally introduced through the use of either a magnetic stirrer bar or a rotating electrode.

1.7.3.4 Nernst Planck Equation

These three forms of mass transport can be described in a single expression known as the Nernst Planck Equation:

$$\frac{\partial c}{\partial t} = \nabla \left[D \nabla c - uc + \frac{Dze}{k_B T} c (\nabla \phi + \frac{\partial A}{\partial t}) \right] \quad (1.5)$$

where c = concentration, D = diffusion coefficient, u = relative velocity of the observer, z = valence of ionic species, e = charge on the electron, k_B =

Boltzmann constant and φ = concentration per unit mol.

1.8 Electrochemical Techniques

In the following sections an introduction is given to the experimental techniques that are used throughout this thesis.

1.8.1 Cyclic Voltammetry

In a cyclic voltammetry experiment the potential is swept linearly between the reference and working electrode. The voltage is increased linearly (Fig 1.17) until it reaches a specified value (V_1), at which point the voltage is reversed until the value reaches the initial voltage (V_0). The current is then measured between the working and counter electrode which is plotted against the applied voltages to produce the cyclic voltammogram. A typical cyclic voltammogram for a one electron process can be seen in Fig. 1.18 below.

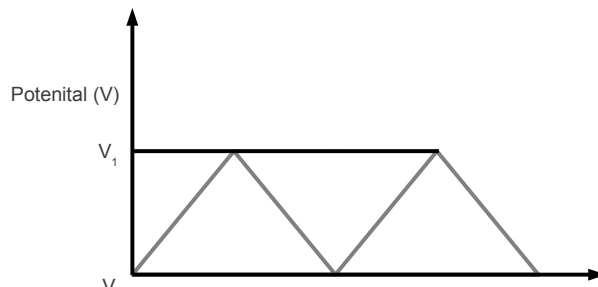


Figure 1.17: Cyclic Voltammetry Waveform

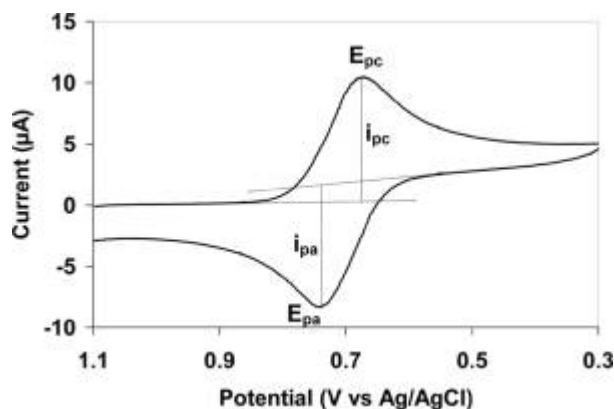


Figure 1.18: Typical Cyclic Voltammogram

In order to understand the shape of this voltammogram, consider a redox reaction:



The voltage is linearly increased as indicated in Fig 1.16 above. At a certain point it becomes energetically favourable for electrons to be transferred from the electrode to the solution, which causes a sharp increase in the current. The current then falls off as the concentration of the oxidant becomes depleted at the electrode surface. This trend continues until the voltage reaches a specified value (V_1), at which point the potential is decreased at the same scan rate. The reverse process now occurs, as the reductant becomes oxidised which causes anodic current to flow (electrons flow into the electrode from the solution). This continues until the reductant is depleted, at which point the system returns to its initial state, completing the cyclic voltammogram seen below.

A more in depth understanding of the processes involved in cyclic voltammetry may be gained by considering the Nernst equation as well as the concentration profiles of the oxidant and reductant at the electrode surface:

$$E = E^{0'} + \frac{RT}{nF} \ln \frac{C_0}{C_R} \quad (1.8)$$

E = applied potential

$E^{0'}$ = redox potential of the couple

C_0 = surface concentration of the oxidant

C_R = surface concentration of the reductant

n = number of electrons involved in the process

T = absolute temperature

R = universal gas constant = $8.31 \text{ JK}^{-1} \text{ mol}^{-1}$

F = Faraday constant = $9.65 \times 10^4 \text{ C mol}^{-1}$

Now, consider the ratio of C_0 to C_R by simple manipulation of the Nernst equation:

$$\frac{C_0}{C_R} = \text{Exp} \left(\frac{nF(E - E^{0'})}{RT} \right) \quad (1.9)$$

By applying a certain potential, the concentrations C_0 and C_R are forced to maintain a certain ratio. For example, as the potential is scanned positively, the concentration of C_0 is increased in order to satisfy the equation.

It is necessary also to consider concentrations profiles of the oxidant and reductant in order to further understand the shape of the cyclic voltammogram. Fick's first law states that the flux of a species in solution through a plane parallel to an perfectly flat electrode surface of infinite dimensions at the electrode surface ($x=0$) is given by [52]:

$$\text{Flux} = -D \left(\frac{dc}{dx} \right)_{x=0} \quad (1.10)$$

D = the diffusion coefficient of the species

c = concentration of the species at the electrode surface

Next, we can use Faradays law to relate the charge q required to convert N moles of the species to its relevant product, involving the transfer of n electrons [52]:

$$q = \int_0^t i dt \quad (1.11)$$

$$\therefore i = nF \frac{dN}{dt} \quad (1.12)$$

Also, if it's noted that

$$\frac{dN}{dt} = A \times \text{Flux} \quad (1.13)$$

$$\Rightarrow i = -FAD \left(\frac{dc}{dx} \right)_{x=0} \quad (1.14)$$

Hence, the current is proportional to the rate of change of the species concentration, or equivalently it's proportional to the slope of the concentration profile of the species of interest. So, in a cyclic voltammogram the

current can be determined by analysing the slope of the corresponding concentration-distance profile.

The peak current (i_p) of the cyclic voltammogram is then given by the Randles-Sevcik equation, which at 298K is given by:

$$i_p = (2.69 \times 10^5) n^{\frac{3}{2}} A D^{\frac{1}{2}} C v^{\frac{1}{2}} \quad (1.15)$$

Where n is the electron stoichiometry, A is the electrode area, D is the diffusion coefficient, C is the concentration of the species in question and v is the scan rate. The Randles-Sevcik can be derived from Fick's second law of diffusion using the appropriate boundary conditions.

1.8.2 Square Wave Voltammetry

The waveform of square wave voltammetry as seen in Fig. 1.19 is a combination of a square wave imposed onto a potential staircase where ΔE_p is the square wave amplitude, ΔE_s is the staircase height, t_p is the pulse time and t_s is the cycle period. The advantage of SWV and other pulse techniques is that it allows the removal of background capacitive current. Hence, limits of detection of 10^{-8} M are achievable.

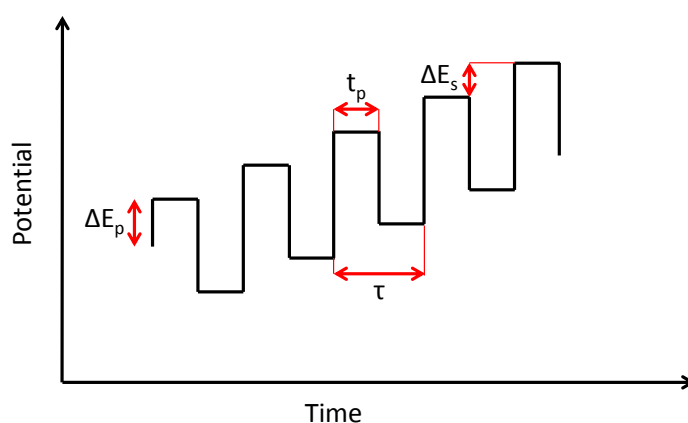


Figure 1.19: Potential wave form for Square Wave Voltammetry

The difference in current between the end of the forward and reverse scans is plotted against the staircase potential as seen in Fig. 1.20 below

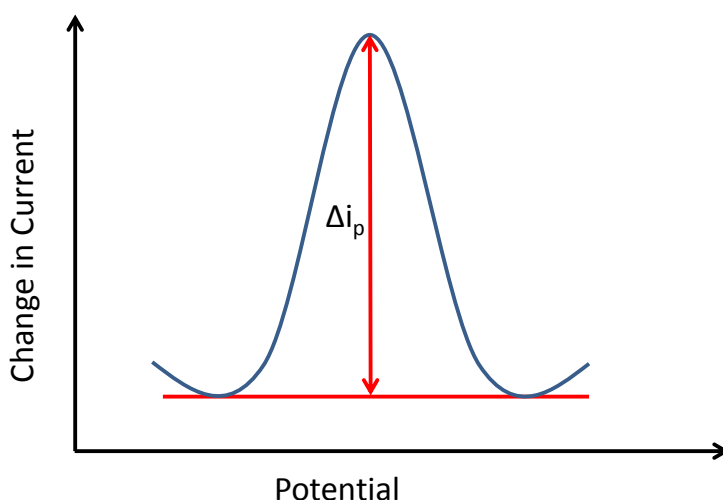


Figure 1.20: Typical Square Wave Voltammogram

1.9 Chemically Modified Electrode Surfaces

It is often the case that the surface of the working electrode is modified in order to improve the electroanalytical characteristics of the electrode. In this section some of the recent developments in electrode modifications are discussed. Particular attention is paid to carbon nanomaterials.

1.9.1 Carbon Nanostructures

Carbon nanotubes and graphene (Fig. 1.21) have garnered a tremendous amount of interest from the scientific community and beyond since their discoveries in 1991 and 2004 respectively [53, 54]. This is due to their extraordinary electrical and mechanical properties [55, 56]. These properties, as well as their large surface to volume ratio, have been exploited extensively in electrochemical sensors. In 1996, Britto et. al reported for the first time the modification of a glassy carbon electrode with carbon nanotubes in order to improve sensor performance in the detection of dopamine [57]. This was followed by a plethora of papers using carbon nanotubes in a range of different sensing devices [16]. Similarly, in the aftermath of the discovery of graphene, a range of studies were reported which showed improved sensor performance attributed to the use of this material [17].

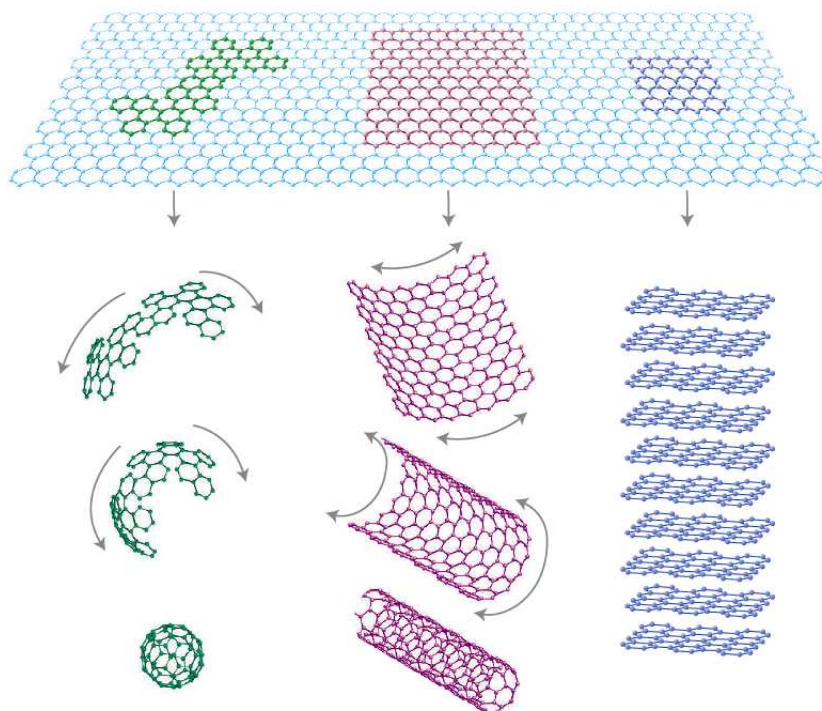


Figure 1.21: Graphene as the fundamental 2D building block for a range of different carbon nanostructures including buckyballs (C_{60}), carbon nanotubes and graphite [58]

The motivation for the use of both carbon nanotubes and graphene has often been explained as offering superior electrocatalytic effects over conventional electrode materials such as glassy carbon and graphite. However, there has also been a suggestion that the benefits of using these materials might be somewhat overstated [59, 60]. This highlights the need to accompany any claim of enhanced electroanalytical performance resulting from carbon nanostructures with the appropriate controls. For example, it has been suggested that the electroactive sites of carbon nanotubes exist at the edge sites of the structure and don't offer superior electrocatalytic activity when compared to edge plane pyrolytic graphite [59, 60]. Similarly, defects in the basal plane and edge planes have been shown to be areas of electrochemical activity in graphene.

Graphene oxide has also been used extensively in electrochemical sensors in recent years. It's popularity has soared since the discovery of graphene, however, this material has been known to exist for over a century. As early as 1859, Brodie was able to show that graphite could be oxidised through the use of potassium chlorate in fuming nitric acid [61]. This method was improved upon by Staudenmaier by adding the chlorate in small amounts over the course of the reaction which allowed the procedure to be performed practically in a

single reaction vessel [62]. The method that is currently used for graphite oxidation was then developed by Hummers and Offeman in the 1950s [63]. In this method graphite is reacted with potassium permanganate and concentrated sulphuric acid [64].

However, despite some reservations carbon nanomaterials continue to play a significant role in sensor development today. One reason for this is that graphene and carbon nanotubes can now be functionalised to allow enhanced binding of biomolecules. For example, shortened single walled carbon nanotubes have been deposited on electrode surfaces creating a so called nanotube forest which allow the immobilisation of antibodies for immunosensor applications [65].

1.9.2 Electrochemistry of sp^2 Carbon

In this thesis, screen printed graphite, graphene, reduced graphene oxide and multiwalled carbon nanotube electrodes are used. These sp^2 carbon based electrodes are amongst the most commonly used in electroanalysis today. Despite their popularity, and the fact they have been in use for centuries (see timeline below), the fundamental electrochemical properties of these materials is still an ongoing research topic. In particular, the role played by the edge plane versus the basal plane has been explored extensively in recent years (illustrated in Fig. 1.22). Two opposing schools of thought have emerged.

The most prevalent theory is that the electrochemical activity occurs exclusively at edge plane sites and that the basal plane is practically inert [59, 66, 67]. This insight emerged from work on carbon nanotubes which brought into question the electrocatalytic properties of nanotubes as first reported by Britto and co-workers and further developed by Wang et. al in the early 2000s [57, 16]. Control experiments in which basal plane pyrolytic graphite (BPPG) electrodes were modified with graphite powder as well as carbon nanotubes showed that both modifications produced a similar electrocatalytic effect [68]. The same group followed this paper with a comparison of multiwalled carbon nanotube modified electrodes and edge plane pyrolytic graphite electrodes (EPPG) [69].

TIMELINE 1: *Electrochemistry of sp^2 carbon electrodes*

- 19th Century ● Humphry Davy uses graphite electrodes in the production of alkali metals
- 1960s ● First description of carbon nanotubes
- 1985 ● Sir Harry Kroto discovers C_{60}
- 1991 ● Seminal publication by Iijima on carbon nanotubes
- 1996 ● Britto et. al describe first carbon nanotube modified electrode for electroanalysis
- 2004 ● Geim and Novoselov produce graphene for the first time from the mechanical exfoliation of graphite
- 2005/2006 ● Compton and Banks show that the edge sites of graphite to be the sites of electrochemical activity
- 2014-2016 ● Unwin and co-workers contradict work of Compton and Banks

Cyclic voltammetry results showed that the electron transfer kinetics were very similar for both electrodes. It was therefore concluded that the reactive sites of carbon nanotubes occur at the ends of nanotubes. Furthermore, it was argued that any electrochemical activity observed from BPPG electrodes was due solely to defects in plane which exposed edge plane sites. Fig 1.20 shows the proposed microscopic structure of BPPG electrode comprising of discrete regions with edges which account for the electrodes electroactivity. This explanation for the electrocatalytic properties of carbon nanotubes was then extended to graphene electrodes in which its electrochemistry could be explained again through defect density [70, 71, 72]. This reasoning is now the textbook explanation for electrochemistry at carbon electrodes [51].

However, recent results by Unwin and co-workers may require a re-think of this accepted viewpoint. Voltammetry conducted at freshly cleaved BPPG electrodes suggests that there is in fact little difference between the electrochemical activity of the basal plane and edge plane [73]. This will no doubt be explored further in the coming years.

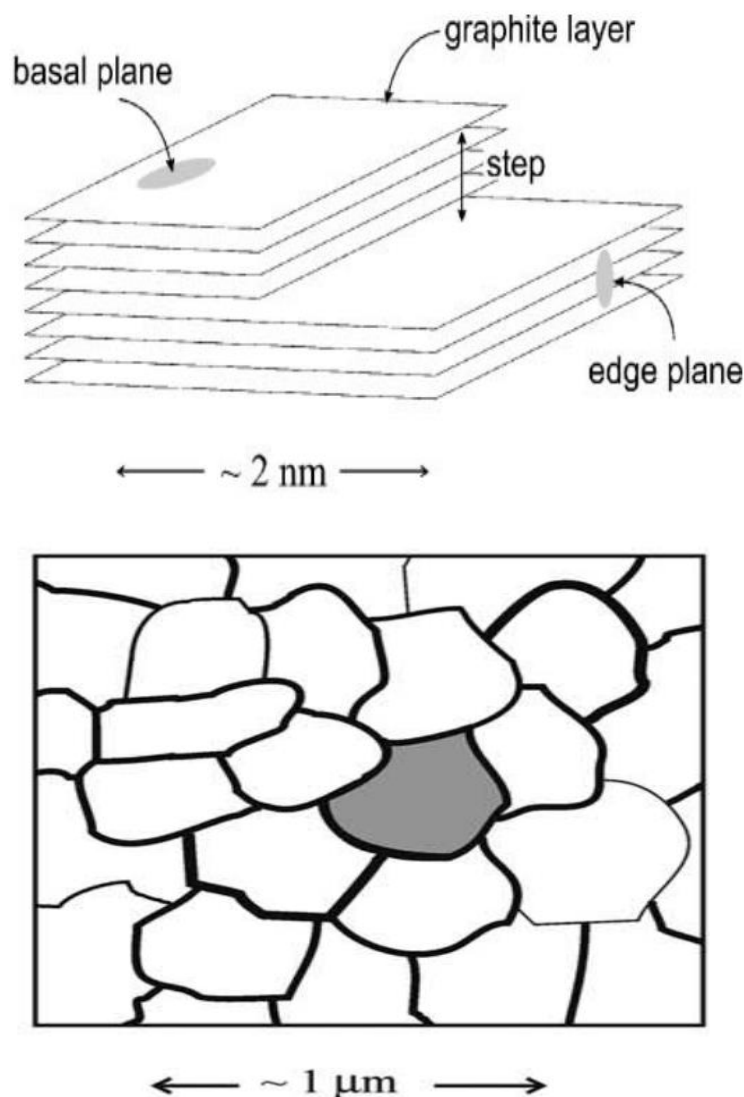


Figure 1.22: Schematic of the microstructure of graphite showing discrete regions which contain edge sites. [66]

1.9.2.1 Thin Layer Effects

Work on carbon nanotube modified electrodes has revealed that thin layer effects due to trapping of the electroactive species in the porous structure of the carbon nanotube network can have a considerable effect on its electrochemical characteristics (Fig. 1.23) [74, 75, 76]. Differentiating between purely semi-infinite diffusion and a contribution of thin layers can be done by graphing the \log_{10} of peak current versus \log_{10} of scan rate. A slope of around 0.5 indicates semi-infinite diffusion whereas a slope closer to 1 indicates thin layer effects. The justification for this is explained in the following paragraphs

by considering the Randles-Sevcik equation which applies to purely diffusional, electrochemically reversible behaviour and the contrasting thin layer effects.

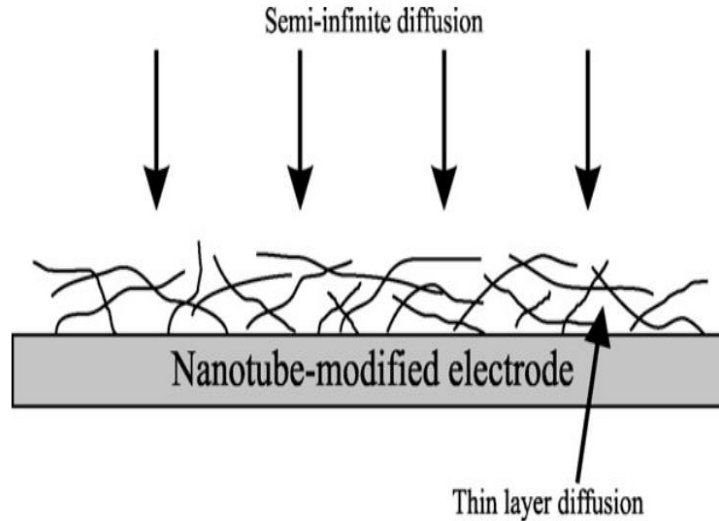


Figure 1.23: Schematic of diffusion at a carbon nanotube modified electrode surface showing highlighting the contribution of both semi-infinite diffusion and thin layer diffusion of analyte within the carbon nanotube matrix. [75]

1.9.2.2 Determining the Influence of Thin Layer Effects

The Randles Sevcik equation is given by:

$$i_p = (2.69 \times 10^5) n^{\frac{3}{2}} A D^{\frac{1}{2}} C v^{\frac{1}{2}} \quad (1.16)$$

If we let

$$(2.69 \times 10^5) n^{\frac{3}{2}} A D^{\frac{1}{2}} C = \chi \quad (1.17)$$

then the Randles Sevcik equation can be written as:

$$i_p = \chi v^{\frac{1}{2}} \quad (1.18)$$

Taking the \log_{10} of both sides of the equation:

$$\log_{10} i_p = \log_{10} [\chi v^{\frac{1}{2}}] \quad (1.19)$$

Then, if we note that $\log(AB) = \log(A+B)$, the equation can be written as

$$\log_{10}i_p = \log_{10}v^{\frac{1}{2}} + \log_{10}\chi \quad (1.20)$$

By using the fact that $\log(x^y) = y\log(x)$ we find that

$$\log_{10}i_p = \frac{1}{2}v + \log_{10}\chi \quad (1.21)$$

Hence, a graph of $\log_{10}i_p$ vs $\log_{10}v$ should have a slope of 1/2 for diffusion limited processes obeying the Randles Sevcik equation.

Next we can consider the peak current for an n electron, reversible surface bound process:

$$I_p = \frac{n^2 F^2}{4RT} \nu A \Gamma \quad (1.22)$$

By taking the \log_{10} of both sides and following a similar process as described for the Randles-Sevcik equation the following expression is found:

$$\log_{10}i_p = v + \log_{10}n^2 F^2 A \Gamma [(4RT)^{-1}] \quad (1.23)$$

Hence, in this case, graphing $\log_{10}i_p$ vs $\log_{10}v$ will give a slope of 1 indicating that thin layer effects dominate the voltammetric response.

1.9.2.3 Inner and Outer Sphere Redox Probes

Throughout this thesis, inner and outer sphere redox probes are used to characterise various electrode materials. In the case of the outer sphere process, the reaction centre is considered to occur in the outer Helmholtz plane and doesn't penetrate the layer of solvation molecules that are adsorbed onto the electrode surface. In contrast, the inner sphere process occurs through a common ligand¹ and are strongly surface dependent [51]. In this thesis, ruthenium (III) chloride is the outer sphere redox probe that is used. The ferri/ferrocyanide redox couple is used to investigate surface effects. This redox

¹a ligand is an ion or molecule attached to a metal atom by coordinate bonding

probe is described as a weakly interacting outer sphere probe according to McCreery in Fig 1.24 below.

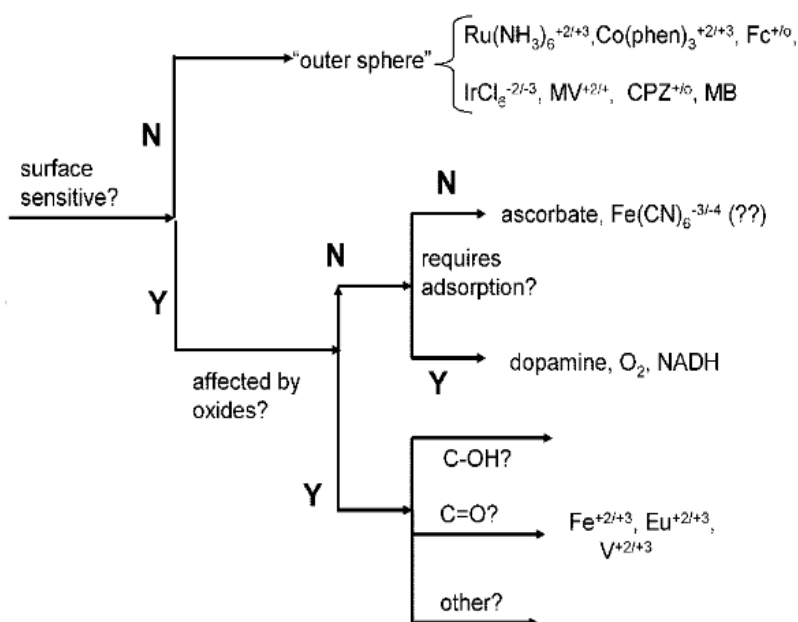


Figure 1.24: Inner and Outer Sphere Redox probes at carbon electrodes[77]

1.10 Other Materials for Electrochemical Sensing

In the following sections, some other electrode materials and modifications are introduced. They are discussed from both a fundamental electrochemistry and immunosensor development point of view. Although dealt with separately here it is acknowledged that these materials are often used in conjunction with one another in biosensor development.

1.10.1 Boron Doped Diamond

Boron doped diamond (BDD) is an sp^3 hybridised electrode material that has a number of attractive properties for electrochemical sensor development, most notably a very high overpotential for both oxygen and hydrogen evolution [78]. This allows for a wide potential window enabling detection of analytes that oxidise at high potentials and would otherwise be masked by background currents. An example of this was the detection of the quorum sensing molecules PQS and HHQ at potentials of around 1.2 V and 1.5 V vs a Ag/AgCl reference

electrode with a limit of detection of 1 nM for PQS [79]. These molecules are indicative of *Pseudomonas aeruginosa* and could be potentially used for environmental or point of care applications. An SEM image of a BDD electrode is shown in Fig. 1.25.

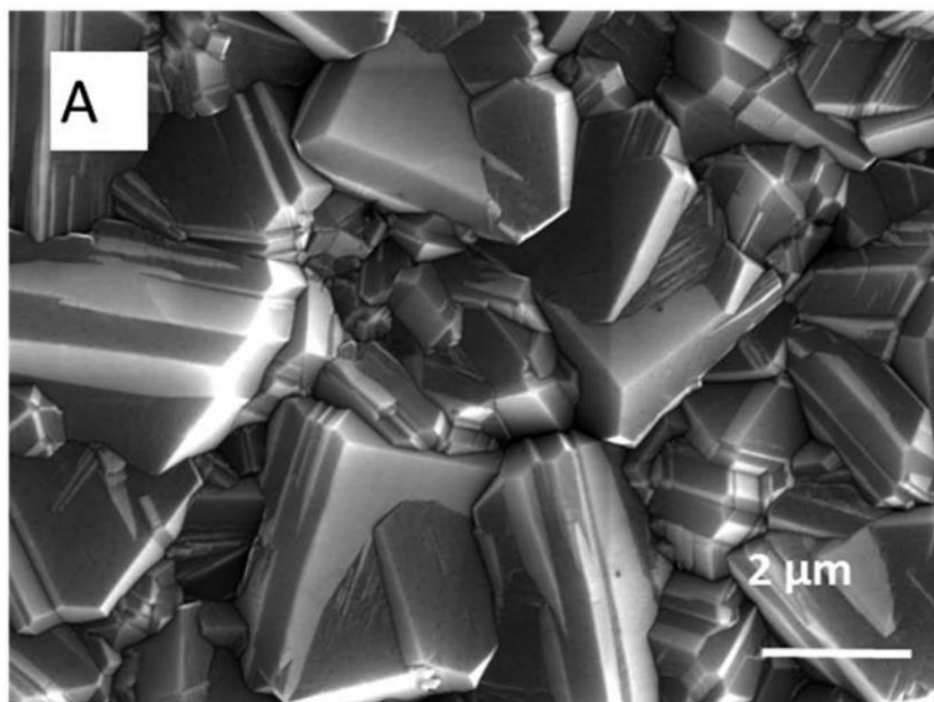


Figure 1.25: SEM of as-grown microcrystalline boron doped diamond [80]

BDD electrodes have also been used in immunosensor applications for IgG detection [81]. The electrode was modified with *o*-aminobenzoic acid allowing carbonyl groups to be formed on the electrode for antibody immobilisation. The BDD electrode had a 10 times lower LOD than the GC electrode used in the study. However, this is one of the few examples of this type of application.

1.10.2 Self Assembled Monolayers

Self assembled monolayers have attracted a considerable amount of interest in the design of electrochemical immunosensors due to their ability to allow well orientated attachment of antibodies onto electrode surfaces [82]. Despite the fact that there are a range of different SAMs that can be formed on electrode surfaces, the majority of research has focused on thiol based SAMs on gold electrodes. The reason for this is that thiols form an exceptionally strong bond on gold surfaces [83]. However, the exact nature of this

interaction is still not fully understood [84] [85]. Both long chain thiols such as 11-mercaptoundecanoic acid (MUA) and short chain thiols such as 3-mercaptopropionic acid (MPA) have been used in biosensor applications. The popularity of SAMs owes much to the ease with which electrode surfaces can be modified by the relevant SAM. The electrode is simply immersed in a dilute solution of the compound for an optimised period of time, allowing the self assembled monolayer to form. It is interesting to note that di-thiolated SAMs [86] which have the potential to offer a more stable scaffold for antibody immobilisation and also to provide superior antibody spacing have not received much interest in the detection of food borne pathogens.

1.10.3 Metallic nanoparticles

Nanoparticles are generally defined as particles of size 1 nm to 100 nm whose properties differ from those of the bulk material [87]. They have gained a significant amount of interest in biosensor applications due to their unique electronic, optical and electrocatalytic properties [88]. 5 different ways in which nanoparticles are used in electrochemical biosensors include biomolecule immobilisation; catalysis of electrochemical reactions; enhancement of electron transfer; biomolecule labelling and acting as a reactant [89]. For example, amperometric enzyme biosensors utilised nanoparticle modified electrode surfaces by helping to establish electrical contact between the redox protein and the electrode material [90].

1.10.4 Polymers

Conducting polymers have been used in electrochemical immunosensor technology due to their rapid electron transfer and sensitivity, specificity and biocompatibility [91]. They are characterised by their extended pi orbital system which allows electron transfer along the back bone of the polymer [92]. Two of the most well investigated polymers for the immobilisation of biomolecules are polypyrrole (PPy) and polyaniline (PANI). PANI has the advantage of excellent stability and processability, however, unlike PPy cannot be deposited onto electrode surfaces from neutral pH solutions [91]. Poly(3,4-ethylenedioxythiophene) (PEDOT) has also been used extensively in biosensor applications [93].

1.10.5 Magnetic beads

Magnetic beads have been used in electrochemical immunosensors for antibody immobilisation; separation and transport [65]. Their popularity can be attributed to their high surface area, chemical and physical stability, low toxicity and biocompatibility [94]. A strategy commonly employed is to allow the coating antibody to react with the magnetic beads prior to immobilisation onto the electrode surface with the aid of an external magnet. DropSens now provide a custom made external magnet to be used with their screen printed electrodes for exactly this purpose. This approach has the added advantage of not involving the electrode in the entire immunological chain which can lead to its passivation [45]. It is often the case that streptavidin coated beads are used which allow very strong binding to a biotinylated antibody.

1.11 Physical Characterisation Techniques

In this thesis a number of characterisation techniques were used to physically describe and investigate the electrodes and the various modifications used. This work was carried out by the following people:

- Scanning Electron Microscopy (SEM) - Vince Lodge, Nanoscale Characterisation Laboratory, Tyndall National Institute
- X-ray Photoelectron Spectroscopy (XPS) - Dr Cian Cummins (under the supervision of Professor Mick Morris), CRANN & AMBER, Trinity College Dublin
- Raman Spectroscopy - Dr Mircea Mondreanu, Tyndall National Institute

In this section a brief introduction is given to each technique in the context of sensor development.

1.11.1 SEM

SEM has now become an indispensable tool for the electroanalytical chemist by allowing nanoscale imaging of electrode surfaces. These images provide confirmation of any proposed electrode modification and also help in explaining the origin of the electrochemical characteristics of the electrode. For example

in Fig. 1.26 an SEM image of a AuNP/graphene composite for the detection of AA, DA and UA is shown, confirming that AUNPs have indeed been successfully deposited onto the graphene surface.

SEM measurements are based on analysing the interaction between high energy, accelerated electrons and the sample in question. This approach overcomes the limitations of optical microscopy (diffraction barrier) which is only able to distinguish between two objects that are half the wavelength of light used apart. As the optical spectrum is 400-700 nm, features < 200 nm are unable to be distinguished. In contrast, electron wavelength for an acceleration voltage of 100 keV is 0.037 Å allowing images to be produced on the nanoscale [95]. The electron beams are produced most commonly by either tungsten hairpin or lanthanum hexaboride filaments through thermionic emission which are then focussed on the sample using electromagnetic condenser lenses [96]. The electrons, after coming in contact with the sample will produce secondary, Auger², and backscattered electrons as well as x-rays. Electrons will also pass through the sample (which can be used in transmission electron microscopy (TEM)).

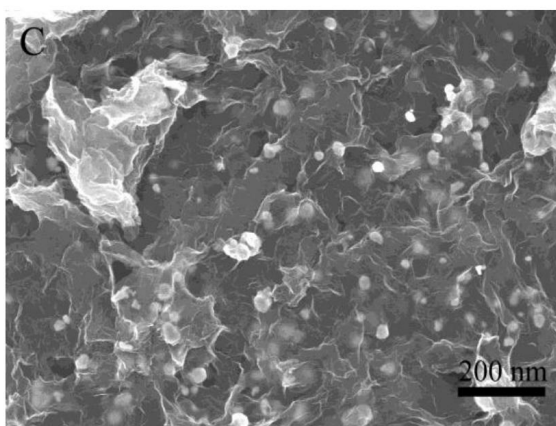


Figure 1.26: SEM of reduced graphene oxide/gold nanoparticle composite used for ascorbic acid, dopamine and uric acid detection [97]

1.11.2 X-ray photoelectron spectroscopy (XPS)

XPS is a surface sensitive technique which allows precise elemental analysis of sample surfaces. Electrochemistry is concerned with the electrode/solution interface and hence electrode surface composition has a major impact on

²beam electrons can core electrons in the sample which then transfer energy to another electron which is emitted, the so called Auger electrons

observed results. In particular XPS has been used on carbon based electrodes by studying how oxygen content on the electrode surface can have both positive and detrimental effects of electrochemical performance [98, 99].

The measurement principle of XPS is based on the photoelectric effect, first explained by Einstein during his *annus mirabilis*, 1905. Previously, it had been observed that electrons are emitted from metals when radiation (light) is shone onto the metal but that the intensity of the light does not correlate with the emission rate of the electrons as predicted by classical electromagnetic theory. Instead, by considering light as quantised discrete packets of energy (photons), the emission rate of electrons is dependent of the frequency of the incoming photons which depends on energy, via the Planck relation, $E = hf$. So, only photons with a frequency or energy greater than that of the work function of the metal will result in electron emission.

The high frequency radiation used in XPS, as the name suggests, comes from x-rays whose energy is much greater than the work function of the sample. The energy of the emitted electrons can then be used to determine the electronic states of atoms, molecules and solids. X-rays penetrate relatively deeply into the sample but most of the electrons from deeper in the solid are inelastically scattered producing a broad structure at higher binding energies [95]. The sharp peaks at lower energies are due to electron emission nearer the surface and hence XPS is a surface characterisation technique.

1.11.3 Raman Spectroscopy

Raman spectroscopy has emerged as a key technique in the characterisation of the sp^2 carbon materials (see Fig. 1.27) [100, 101, 102, 103, 104]. In this thesis it was used in the characterisation of screen printed graphene electrodes (Chapter 4) to confirm a lack of graphene behaviour. Raman spectroscopy is a vibrational spectroscopy technique based on the phenomenon of inelastic scattering of radiation by a solid, liquid or gas [105]. This is in contrast to more commonly observed elastic Rayleigh scattering. Only 10^6 - 10^8 photons are scattered inelastically, so Raman scattering is considered an inherently weak process [106].

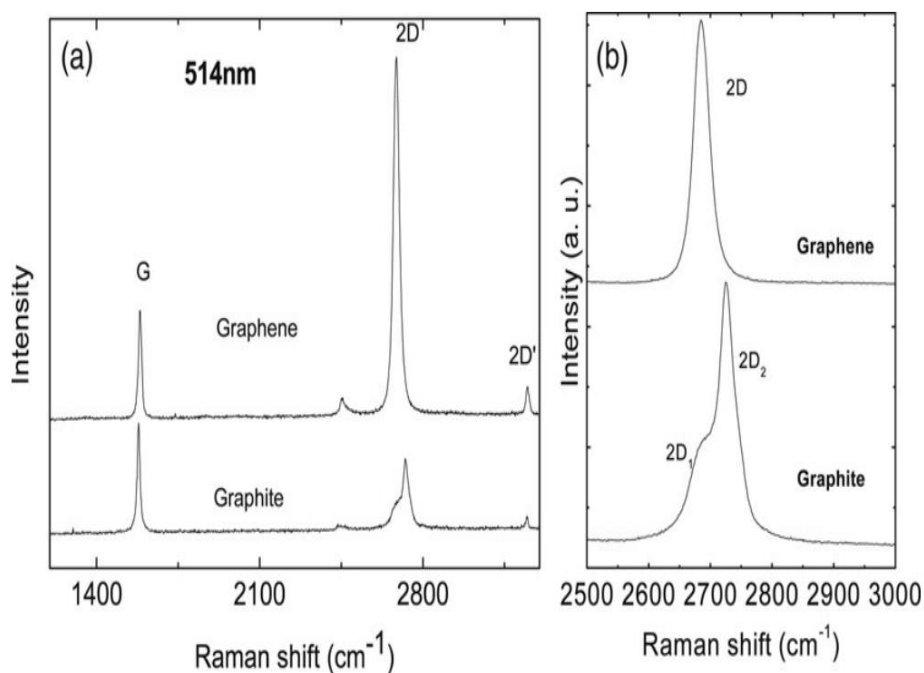


Figure 1.27: Raman Spectroscopy of graphene and graphite [101]

1.12 Target Analytes

This thesis is concerned with the detection of two analytes namely deoxynivalenol (a B-tricothecene mycotoxin) and caffeine (a methylxanthine). In this section a brief introduction is given to mycotoxin and methylxanthine detection. Specific information relating to deoxynivalenol and caffeine detection is given at the start of chapters 3 and 4 respectively.

1.12.1 Mycotoxins

Mycotoxins are toxic secondary metabolites produced by various different fungi the chemical structures are shown in Fig. 1.28. A relationship between mycotoxins and ill-health has been suspected for centuries and modern studies have revealed that high mycotoxin content in food leads to mutagenicity, teratogenicity and carcinogenicity [107][108]. This is a pressing concern in food safety when it is considered that 25 to 50% of the crops harvested worldwide are estimated to be contaminated with mycotoxins [109]. This estimate rises to 80% in tropical regions. Hence the European Union has strict

rules on the maximum levels of mycotoxins in various foodstuffs as outlined in Commission Regulation (EC) No 1886/2006.

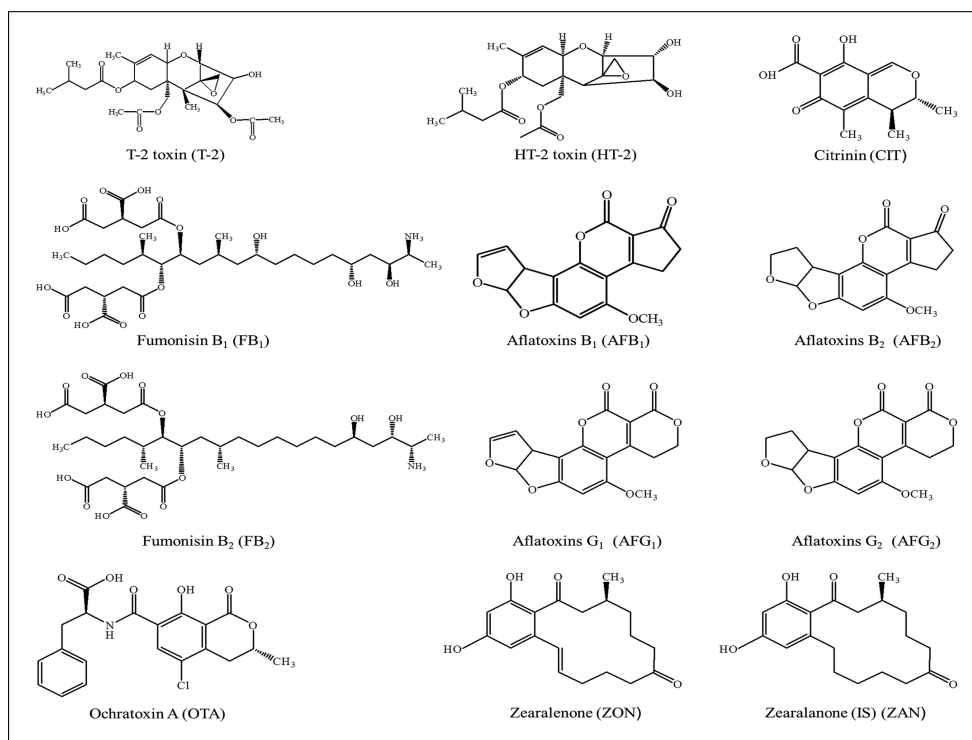


Figure 1.28: Chemically structures of some multiclass mycotoxins [110]

Mycotoxins are small molecules with a small number of binding sites for antibodies. Hence, sandwich based assays where the antigen is sandwiched between a primary and labelled secondary antibody are not suitable for mycotoxin detection due to the requirement for two distinct binding sites. Instead competitive assays are typically used. Much of this research has been concerned with the detection of aflatoxin B1 and aflatoxin M1. Aflatoxin B1 is produced by strains of both *Aspergillus flavus* and *Aspergillus parasiticus* found in grain products. Upon ingestion of these contaminated grains lactating animals produce aflatoxin M1 which is present in their milk. However, there is no direct correlation between aflatoxin B1 and M1, so tests are required for both stages of the food chain. It is also important to note that maximum residue levels allowable are dependent on the sample being analysed. For example, the maximum allowable concentrations of deoxynivalenol in wheat, breakfast cereal and baby food are 1750 $\mu\text{/kg}$, 500 $\mu\text{/kg}$ and 200 $\mu\text{/kg}$ respectively. Hence, a more cost effective but less sensitive sensor would be suitable for wheat samples compared to baby food samples.

Table 1.2: Recent Developments in Electrochemical Immunosensors for Mycotoxin Detection in Food Samples

Analyte	Sensor modification	Electrode Material	Electrochemical Method	LOD	Real Sample	Ref.
OTA A	AuNP labelled antigen	SPCE	DPV	0.1 ng/ml	Wheat	[111]
OTA A	Pre concentration with magnetic nanoparticles modified with amine groups	GCE	SWV	0.02 μg^{-1}	Wine grapes	[112]
AFB1	Graphene/conducting polymer/gold nanoparticle/ionic liquid composite film	gold	Cyclic Voltammetry	1fM	Peanut, Milk, Rice, Flour, Soybeans	[113]
Zearalenone	Magnetic beads as antibody support	GCE	Amperometric	0.4 $\mu\text{g/L}$	Infant foods	[114]
Aflatoxin M1	Magnetic nanoparticles coated with antibodies	SPCE	Chronoamperometry	0.01 ppb	Milk	[115]
Zearalenone	MWCNT modified electrode	GCE	Amperometric	0.77 ppb	Corn	[116]
Fumonisin	Untreated electrode surface	SPGE	Chronoamperometry	5 $\mu\text{g/L}$	corn	[117]
Zearalenone	Magnetic beads coupled to protein G for immobilisation of antibodies	SPCE	Amperometric	0.007 $\mu\text{g/L}$	Baby Food	[118]
AFM1	Electrochemical microplate	SPCE	Intermittent Pulse Amperometry	1 pg/mL	Milk	[119]
AFM1	Unmodified electrode	SPCE	Amperometric	39 ng/l	Milk	[120]
AFB1	Magnetic beads as immobilisation support	SPCE	DPV	0.6 ng/mL	Corn	[121]
AFB1	AChE inhibition on Prussian Blue modified electrodes	SPCE	Amperometric	2 ppb	Olive Oil	[122]
AFB1	Magnetic beads modified with CoFe_2O_4 nanoparticles as the core and Prussian Blue NP doped silica as the shell	ITO	DPV	6 pg/mL	Red Paprika	[123]
AFB1	Reduced graphene oxide/polypyrrole/pyrrolepropylic acid	GCE	Impedimetric	10 fg/mL	Corn	[124]
FB1,FB2,FB3	Magnetic beads coupled to protein G for immobilisation of antibodies	SPCE	Amperometric	0.33 $\mu\text{g/L}$	Beer	[125]

1.12.2 Caffeine

Caffeine is a psychoactive substance that is a constituent of tea, coffee, soft drinks, energy drinks as well as a range of pharmaceutical formulations. Regular monitoring of caffeine levels in these products is a necessity for both food and pharmaceutical companies from both a quality control and food safety standpoint.

Unlike the mycotoxins discussed in the previous section caffeine is electrochemically active. Hence, no biological recognition element is required

for detection. Instead direct voltammetry can be used for caffeine detection with the mechanism below describing the overall 4 electron, 4 proton oxidation mechanism (Fig. 1.29).

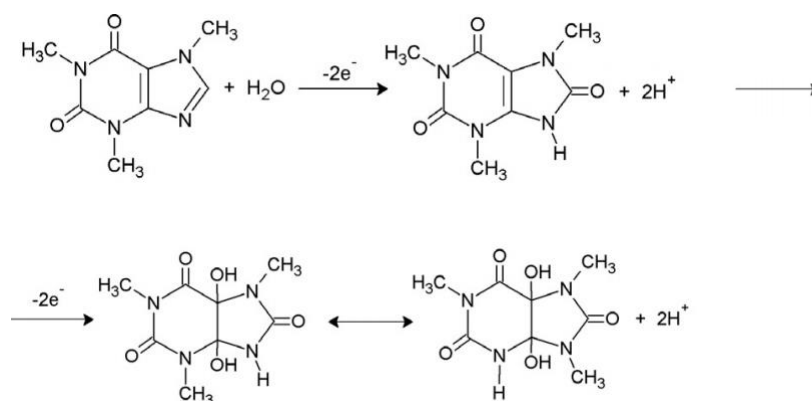


Figure 1.29: Proposed mechanism for caffeine oxidation [126]

Chapter 4 of this thesis is concerned with caffeine detection at pretreated and nafion modified electrodes. Further discussion of the literature of caffeine is discussed in the introduction of that chapter.

1.13 Sample Preparation

Sample preparation is necessary for most types of food samples in order to isolate the analyte from its matrix and allow it to be analysed in a liquid form. A range of methods exist for analyte extraction including liquid-liquid extraction, microwave assisted solvent extraction, ultrasonication extraction, accelerated solvent extraction, supercritical fluid extraction, membrane extraction and solid phase extraction [127]. The main issue with solvent extraction is the need to use large amounts of solvent and the length of time required to complete the procedure [128]. Hence, solid phase extraction has become a popular technique and recent advances have used molecularly imprinted polymers and

carbon nanotubes in these extraction devices.

For liquid samples, the sample preparation tends not to be as laborious. For example, in the case of milk, centrifugation of the sample separates it into layers of fat, cream and skimmed milk which removes interferences that may be present in the fats [129]. An alternative approach is to use dried milk and simply dissolve it in water prior to spiking with the antigen of interest [130].

Meat samples provide a greater technical challenge. An example of this was outlined by Yang et. al who developed an electrochemical immunosensor for the detection of clenbuterol in pork samples [131]. Prior to analysis with their biosensor, the pork samples were first broken down, homogenised using HClO_4 , ultrasonicated for 20 mins and heated to 80 degrees celcius for 30 minutes. This was followed by 5 minutes of centrifugation after the sample had cooled, adjustment to pH 10 and extraction using ethyl acetate.

In biosensor development this has proved to be one of the main stumbling blocks in producing commercially available devices. The strategies mentioned above are all “off chip“. In other words, they are performed prior to introduction onto the device which is an obvious issue for on-site analysis.

1.14 Statistical Analysis

1.14.1 Fitting Immunoassay data

In this thesis a 4 parameter logistic model is used to fit all immunoassay data. This is done using the GraphPad Prism software. The equation for the model is:

$$y = d + \frac{a - d}{1 + (x/c)^b} \quad (1.24)$$

y = the response x = concentration a = lower asymptote d = upper asymptote
c = point of inflection - model EC50 value

The bend points, which determine the linear range of the graph can be described as follows :

$$y_{\text{bend lower}} = \frac{a - d}{1 + 1/k} + d \quad (1.25)$$

$$y_{bend\ higher} = \frac{a - d}{1 + k} + d \quad (1.26)$$

where $k = 4.6805$

The corresponding x values (concentrations) are then given by:

$$x_{bend\ higher/lower} = c \left(\frac{a - y_{bend\ higher/lower}}{y_{bend\ higher/lower} - d} \right)^{1/b} \quad (1.27)$$

This is one of the few mathematically rigorous methods of determining the linear range of immunoassay data [132]. It is commonplace for the linear range to be described without any explanation as to how the values were determined. As such, when comparing the linear ranges reported in the literature it must be noted that these are most likely only very approximate ranges.

1.14.2 Limit of Detection

The International Union of Pure and Applied Chemistry define the limit of detection (LOD) as follows:

$$LOD = \frac{k s_b}{m} \quad (1.28)$$

A calibration curve is plotted using the signal for a range of concentrations, including a blank sample. The value of k is taken to be 3 which equates to a confidence limit of 99.86% that a measured sample is greater than or equal to 3 times the average of the blank signal plus 3 times the standard deviation of the blank signal [133]. Graphical representations are outlined in Fig. 1.30 and 1.31.

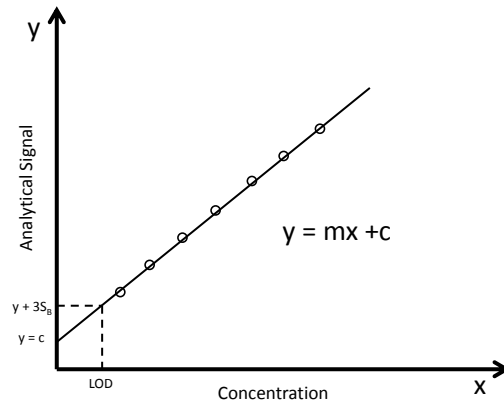


Figure 1.30: Limit of detection for a linear calibration curve

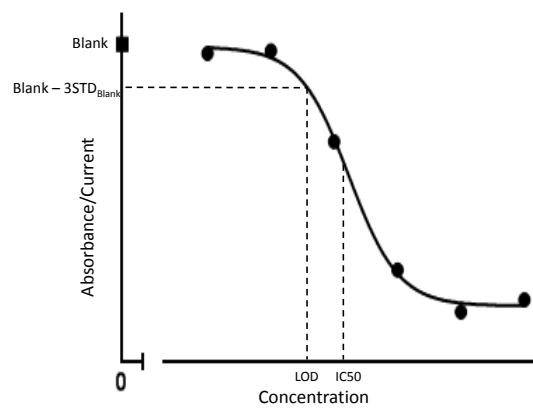


Figure 1.31: Limit of detection for an indirect competitive immunoassay

1.14.3 Sensitivity

The sensitivity of a linear calibration curve is given by the slope of the line (m), where the equation of the line is given by:

$$y = mx + c \quad (1.29)$$

and c is intercept of the line with the line.

1.14.4 f-test and p-test

The purpose of both the f-test and t-test is to test the null hypothesis (H_0 - the analytical method is not subject to systematic error. The f test compares the

standard deviations of two sets of data to see if they are significantly different. If $F > F_{\text{Critical}}$ then H_0 is rejected. Conversely, if $F < F_{\text{Critical}}$ then H_0 is accepted and there is no significant variation between the methods.

Once it has been established whether there is a significant variation of in the standard deviations of the data, a t-test can then be performed to see if there is a significant difference between the two data sets. If $t_{\text{stat}} > t_{\text{Critical}}$, then H_0 is rejected and the two means differ. Then, if $t_{\text{stat}} < t_{\text{Critical}}$ H_0 is accepted and the two means have no significant differences.

1.14.5 ANOVA analysis

ANOVA analysis extends significance testing to more than two sets of data. It indicates whether the variation in variances or means is due to the controlled factor or from random error. Single factor ANOVA is used when comparing several sets of observations. On the other hand, two factor ANOVA takes into account two experimental variables.

References

- [1] Francesco Ricci, Giulia Volpe, Laura Micheli, and Giuseppe Palleschi. A review on novel developments and applications of immunosensors in food analysis. *Analytica Chimica Acta*, 605(2):111–129, December 2007.
- [2] Marinella Farre and Damia Barcelo. Analysis of emerging contaminants in food. *Trac-Trends in Analytical Chemistry*, 43:240–253, February 2013.
- [3] T. F. McGrath, C. T. Elliott, and T. L. Fodey. Biosensors for the analysis of microbiological and chemical contaminants in food. *Analytical and Bioanalytical Chemistry*, 403(1):75–92, April 2012.
- [4] Shahrooz Rahmati, Nurhidayatullaili Muhd Julkapli, Wageeh A. Yehye, and Wan Jefrey Basirun. Identification of meat origin in food products—A review. *Food Control*, 68:379–390, October 2016.
- [5] Lucian Rotariu, Florence Lagarde, Nicole Jaffrezic-Renault, and Camelia Bala. Electrochemical biosensors for fast detection of food contaminants – trends and perspective. *TrAC Trends in Analytical Chemistry*, 79:80–87, May 2016.
- [6] A. Hulanicki, S. Glab, and F. Ingman. Chemical Sensors Definitions and Classification. *Pure and Applied Chemistry*, 63(9):1247–1250, September 1991.
- [7] Lc Clark and C. Lyons. Electrode Systems for Continuous Monitoring in Cardiovascular Surgery. *Annals of the New York Academy of Sciences*, 102(1):29–&, 1962.
- [8] Anthony G. A. Aggidis, Jeffrey D. Newman, and George A. Aggidis. Investigating pipeline and state of the art blood glucose biosensors to formulate next steps. *Biosensors and Bioelectronics*, 74:243–262, December 2015.
- [9] D. H. Yu, B. Blankert, J. C. Vire, and J. M. Kauffmann. Biosensors in drug discovery and drug analysis. *Analytical Letters*, 38(11):1687–1701, 2005.
- [10] Sara Rodriguez-Mozaz, Maria J. Lopez de Alda, and Damia Barcelo. Biosensors as useful tools for environmental analysis and monitoring. *Analytical and Bioanalytical Chemistry*, 386(4):1025–1041, October 2006.

- [11] Ibrahim Abdulhalim, Mohammad Zourob, and Akhlesh Lakhtakia. Surface Plasmon Resonance for Biosensing: A Mini-Review. *Electromagnetics*, 28(3):214–242, April 2008.
- [12] K. Narsaiah, Shyam Narayan Jha, Rishi Bhardwaj, Rajiv Sharma, and Ramesh Kumar. Optical biosensors for food quality and safety assurance—a review. *Journal of Food Science and Technology*, 49(4):383–406, August 2012.
- [13] Angela Leung, P. Mohana Shankar, and Raj Mutharasan. A review of fiber-optic biosensors. *Sensors and Actuators B: Chemical*, 125(2):688–703, August 2007.
- [14] C. K. O’Sullivan and G. G. Guilbault. Commercial quartz crystal microbalances – theory and applications. *Biosensors and Bioelectronics*, 14(8–9):663–670, December 1999.
- [15] Zhihong Shen, Mingchuan Huang, Caide Xiao, Yun Zhang, Xiangqun Zeng, and Peng G. Wang. Nonlabeled Quartz Crystal Microbalance Biosensor for Bacterial Detection Using Carbohydrate and Lectin Recognitions. *Analytical Chemistry*, 79(6):2312–2319, March 2007.
- [16] Joseph Wang. Carbon-Nanotube Based Electrochemical Biosensors: A Review. *Electroanalysis*, 17(1):7–14, 2005.
- [17] Yuyan Shao, Jun Wang, Hong Wu, Jun Liu, Ilhan A. Aksay, and Yuehe Lin. Graphene Based Electrochemical Sensors and Biosensors: A Review. *Electroanalysis*, 22(10):1027–1036, May 2010.
- [18] J. Wang. Glucose biosensors: 40 years of advances and challenges. *Electroanalysis*, 13(12):983–988, #aug# 2001.
- [19] Asha Chaubey and B. D. Malhotra. Mediated biosensors. *Biosensors and Bioelectronics*, 17(6–7):441–456, June 2002.
- [20] Sejin Park, Hankil Boo, and Taek Dong Chung. Electrochemical non-enzymatic glucose sensors. *Analytica Chimica Acta*, 556(1):46–57, January 2006.
- [21] K. Kerman, M. Kobayashi, and E. Tamiya. Recent trends in electrochemical DNA biosensor technology. *Measurement Science & Technology*, 15(2):R1–R11, February 2004.
- [22] Brian R. Eggins. *Biosensors: an introduction*. Wiley-Teubner, July 1996.

- [23] Mònica Mir, Antoni Homs, and Josep Samitier. Integrated electrochemical DNA biosensors for lab-on-a-chip devices. *ELECTROPHORESIS*, 30(19):3386–3397, October 2009.
- [24] J. J. Pancrazio, J. P. Whelan, D. A. Borkholder, W. Ma, and D. A. Stenger. Development and Application of Cell-Based Biosensors. *Annals of Biomedical Engineering*, 27(6):697–711, November 1999.
- [25] Joachim Wegener, Charles R. Keese, and Ivar Giaever. Electric Cell–Substrate Impedance Sensing (ECIS) as a Noninvasive Means to Monitor the Kinetics of Cell Spreading to Artificial Surfaces. *Experimental Cell Research*, 259(1):158–166, August 2000.
- [26] Walter Messina, Michelle Fitzgerald, and Eric Moore. SEM and ECIS Investigation of Cells Cultured on Nanopillar Modified Interdigitated Impedance Electrodes for Analysis of Cell Growth and Cytotoxicity of Potential Anticancer Drugs. *Electroanalysis*, 28(9):2188–2195, September 2016.
- [27] Caide Xiao and John H. T. Luong. On-Line Monitoring of Cell Growth and Cytotoxicity Using Electric Cell-Substrate Impedance Sensing (ECIS). *Biotechnology Progress*, 19(3):1000–1005, January 2003.
- [28] Viviana Scognamiglio, Amina Antonacci, Maya D. Lambreva, Simona C. Litescu, and Giuseppina Rea. Synthetic biology and biomimetic chemistry as converging technologies fostering a new generation of smart biosensors. *Biosensors & Bioelectronics*, 74:1076–1086, December 2015.
- [29] Lokman Uzun and Anthony P. F. Turner. Molecularly-imprinted polymer sensors: realising their potential. *Biosensors & Bioelectronics*, 76:131–144, February 2016.
- [30] E. Luzzi, M. Minunni, S. Tombelli, and M. Mascini. New trends in affinity sensing: aptamers for ligand binding. *TrAC Trends in Analytical Chemistry*, 22(11):810–818, December 2003.
- [31] Sumedha D. Jayasena. Aptamers: An Emerging Class of Molecules That Rival Antibodies in Diagnostics. *Clinical Chemistry*, 45(9):1628–1650, September 1999.
- [32] Kejun Feng, Yan Kang, Jing-Jin Zhao, Ya-Li Liu, Jian-Hui Jiang, Guo-Li Shen, and Ru-Qin Yu. Electrochemical immunosensor with

- aptamer-based enzymatic amplification. *Analytical Biochemistry*, 378(1):38–42, July 2008.
- [33] Amina Rhouati, Cheng Yang, Akhtar Hayat, and Jean-Louis Marty. Aptamers: A Promising Tool for Ochratoxin A Detection in Food Analysis. *Toxins*, 5(11):1988–2008, November 2013.
- [34] Zhi-Yu Shi, Ya-Ting Zheng, Hao-Bo Zhang, Cheng-Hua He, Wen-Da Wu, and Hai-Bin Zhang. DNA Electrochemical Aptasensor for Detecting Fumonisin B-1 Based on Graphene and Thionine Nanocomposite. *Electroanalysis*, 27(5):1097–1103, May 2015.
- [35] Yoon-Jin Kim, Yeon Seok Kim, Javed H. Niazi, and Man Bock Gu. Electrochemical aptasensor for tetracycline detection. *Bioprocess and Biosystems Engineering*, 33(1):31–37, January 2010.
- [36] Binh Hai Nguyen, Lam Dai Tran, Quan Phuc Do, Huy Le Nguyen, Ngoc Huan Tran, and Phuc Xuan Nguyen. Label-free detection of aflatoxin M1 with electrochemical Fe₃O₄/polyaniline-based aptasensor. *Materials Science & Engineering C-Materials for Biological Applications*, 33(4):2229–2234, May 2013.
- [37] Xiaoli Qin, Wenjuan Guo, Huijing Yu, Juan Zhao, and Meishan Pei. A novel electrochemical aptasensor based on MWCNTs-BMIMPF₆ and amino functionalized graphene nanocomposite films for determination of kanamycin. *Analytical Methods*, 7(13):5419–5427, 2015.
- [38] Miroslav Pohanka. Monoclonal and polyclonal antibodies production - preparation of potent biorecognition element. *Journal of Applied Biomedicine*, 7(3):115–121, 2009.
- [39] E. Engvall and P. Perlmann. Enzyme-Linked Immunosorbent Assay (elisa) Quantitative Assay of Immunoglobulin-G. *Immunochemistry*, 8(9):871–&, 1971.
- [40] E. Engvall and P. Perlmann. Enzyme-Linked Immunosorbent Assay, Elisa .3. Quantitation of Specific Antibodies by Enzyme-Labeled Anti-Immunoglobulin in Antigen-Coated Tubes. *Journal of Immunology*, 109(1):129–&, 1972.
- [41] A. Voller, A. Bartlett, and D. E. Bidwell. Enzyme immunoassays with special reference to ELISA techniques. *Journal of Clinical Pathology*, 31(6):507–520, June 1978.

- [42] J. R. Crowther. The ELISA Guidebook, Second Edition. In *The ELISA Guidebook, Second Edition*, volume 516. Springer, 2009.
- [43] Chandra Kumar Dixit, Sandeep Kumar Vashist, Feidhlim T. O'Neill, Brian O'Reilly, Brian D. MacCraith, and Richard O'Kennedy. Development of a High Sensitivity Rapid Sandwich ELISA Procedure and Its Comparison with the Conventional Approach. *Analytical Chemistry*, 82(16):7049–7052, August 2010.
- [44] S. V. Reddy, D. Kiran Mayi, M. Uma Reddy, K. Thirumala-Devi, and D. V. R. Reddy. Aflatoxins B1 in different grades of chillies (*Capsicum annum* L.) in India as determined by indirect competitive-ELISA. *Food Additives & Contaminants*, 18(6):553–558, June 2001.
- [45] Francesco Ricci, Gianluca Adornetto, and Giuseppe Palleschi. A review of experimental aspects of electrochemical immunosensors. *Electrochimica Acta*, 84:74–83, December 2012.
- [46] Mamas I. Prodromidis. Impedimetric immunosensors—A review. *Electrochimica Acta*, 55(14):4227–4233, May 2010.
- [47] Bin Lu, Malcolm R. Smyth, and Richard O'Kennedy. Tutorial review. Oriented immobilization of antibodies and its applications in immunoassays and immunosensors. *Analyst*, 121(3):29R–32R, 1996.
- [48] K. A Fährnich, M Pravda, and G. G Guilbault. Disposable amperometric immunosensor for the detection of polycyclic aromatic hydrocarbons (PAHs) using screen-printed electrodes. *Biosensors and Bioelectronics*, 18(1):73–82, January 2003.
- [49] Blanca A. G. Rodriguez, Erika K. G. Trindade, Diego G. A. Cabral, Erika C. L. Soares, Cayo E. L. Menezes, Danielle C. M. Ferreira, Renata K. Mendes, and Rosa F. Dutra. Nanomaterials for advancing the health immunosensor. *Biosensors - Micro and Nanoscale Applications*, 2015.
- [50] Eric J. Moore, Mark P. Kreuzer, Miloslav Pravda, and George G. Guilbault. Development of a Rapid Single-Drop Analysis Biosensor for Screening of Phenanthrene in Water Samples. *Electroanalysis*, 16(20):1653–1659, October 2004.
- [51] R. G. Compton and C. E. Banks. *Understanding Voltammetry, 2nd Edition*. Imperial Coll Press, Covent Garden, 2011.

- [52] D. Pletcher. *Instrumental Methods in Electrochemistry*. Ellis Horwood, January 2001.
- [53] S. Iijima. Helical Microtubules of Graphitic Carbon. *Nature*, 354(6348):56–58, November 1991.
- [54] K. S. Novoselov, A. K. Geim, S. V. Morozov, D. Jiang, Y. Zhang, S. V. Dubonos, I. V. Grigorieva, and A. A. Firsov. Electric field effect in atomically thin carbon films. *Science*, 306(5696):666–669, October 2004.
- [55] Martin Knupfer. Electronic properties of carbon nanostructures. *Surface Science Reports*, 42(1–2):1–74, April 2001.
- [56] A. H. Castro Neto, F. Guinea, N. M. R. Peres, K. S. Novoselov, and A. K. Geim. The electronic properties of graphene. *Reviews of Modern Physics*, 81(1):109–162, January 2009.
- [57] P. J. Britto, K. S. V. Santhanam, and P. M. Ajayan. Carbon nanotube electrode for oxidation of dopamine. *Bioelectrochemistry and Bioenergetics*, 41(1):121–125, October 1996.
- [58] A. K. Geim and K. S. Novoselov. The rise of graphene. *Nature Materials*, 6(3):183–191, March 2007.
- [59] Craig E. Banks and Richard G. Compton. New electrodes for old: from carbon nanotubes to edge plane pyrolytic graphite. *The Analyst*, 131(1):15, 2006.
- [60] Dale A. C. Brownson, Lindsey J. Munro, Dimitrios K. Kampouris, and Craig E. Banks. Electrochemistry of graphene: not such a beneficial electrode material? *Rsc Advances*, 1(6):978–988, 2011.
- [61] B. C. Brodie. On the Atomic Weight of Graphite. *Philosophical Transactions of the Royal Society of London*, 149:249–259, January 1859.
- [62] L. Staudenmaier. Verfahren zur Darstellung der Graphitsäure. *Berichte der deutschen chemischen Gesellschaft*, 31(2):1481–1487, May 1898.
- [63] Ws Hummers and Re Offeman. Preparation of Graphitic Oxide. *Journal of the American Chemical Society*, 80(6):1339–1339, 1958.
- [64] Daniel R. Dreyer, Sungjin Park, Christopher W. Bielawski, and Rodney S.

- Ruoff. The chemistry of graphene oxide. *Chemical Society Reviews*, 39(1):228–240, 2010.
- [65] James F. Rusling. Nanomaterials-based electrochemical immunosensors for proteins. *The Chemical Record*, 12(1):164–176, 2012.
- [66] Craig E. Banks, Trevor J. Davies, Gregory G. Wildgoose, and Richard G. Compton. Electrocatalysis at graphite and carbon nanotube modified electrodes: edge-plane sites and tube ends are the reactive sites. *Chemical Communications*, 16(7):829–841, February 2005.
- [67] Trevor J. Davies, Michael E. Hyde, and Richard G. Compton. Nanotrench Arrays Reveal Insight into Graphite Electrochemistry. *Angewandte Chemie*, 117(32):5251–5256, August 2005.
- [68] R. R. Moore, C. E. Banks, and R. G. Compton. Basal plane pyrolytic graphite modified electrodes: Comparison of carbon nanotubes and graphite powder as electrocatalysts. *Analytical Chemistry*, 76(10):2677–2682, May 2004.
- [69] C. E. Banks, R. R. Moore, T. J. Davies, and R. G. Compton. Investigation of modified basal plane pyrolytic graphite electrodes: definitive evidence for the electrocatalytic properties of the ends of carbon nanotubes. *Chemical Communications*, 10(16):1804–1805, 2004.
- [70] Dale A. C. Brownson, Dimitrios K. Kampouris, and Craig E. Banks. Graphene electrochemistry: fundamental concepts through to prominent applications. *Chemical Society Reviews*, 41(21):6944–6976, 2012.
- [71] Dale A. C. Brownson and Craig E. Banks. Graphene electrochemistry: an overview of potential applications. *Analyst*, 135(11):2768–2778, 2010.
- [72] Adriano Ambrosi, Chun Kiang Chua, Alessandra Bonanni, and Martin Pumera. Electrochemistry of Graphene and Related Materials. *Chemical Reviews*, 114(14):7150–7188, July 2014.
- [73] Stanley C. S. Lai, Anisha N. Patel, Kim McKelvey, and Patrick R. Unwin. Definitive Evidence for Fast Electron Transfer at Pristine Basal Plane Graphite from High-Resolution Electrochemical Imaging. *Angewandte Chemie-International Edition*, 51(22):5405–5408, 2012.
- [74] Marcus J. Sims, Neil V. Rees, Edmund J. F. Dickinson, and Richard G. Compton. Effects of thin-layer diffusion in the electrochemical detection

- of nicotine on basal plane pyrolytic graphite (BPPG) electrodes modified with layers of multi-walled carbon nanotubes (MWCNT-BPPG). *Sensors and Actuators B: Chemical*, 144(1):153–158, January 2010.
- [75] Ian Streeter, Gregory G. Wildgoose, Lidong Shao, and Richard G. Compton. Cyclic voltammetry on electrode surfaces covered with porous layers: An analysis of electron transfer kinetics at single-walled carbon nanotube modified electrodes. *Sensors and Actuators B-Chemical*, 133(2):462–466, August 2008.
- [76] Gareth P. Keeley and Michael E. G. Lyons. The Effects of Thin Layer Diffusion at Glassy Carbon Electrodes Modified with Porous Films of Single-Walled Carbon Nanotubes. *International Journal of Electrochemical Science*, 4(6):794–809, June 2009.
- [77] Richard L. McCreery. Advanced Carbon Electrode Materials for Molecular Electrochemistry. *Chemical Reviews*, 108(7):2646–2687, July 2008.
- [78] John H. T. Luong, Keith B. Male, and Jeremy D. Glennon. Boron-doped diamond electrode: synthesis, characterization, functionalization and analytical applications. *Analyst*, 134(10):1965–1979, 2009.
- [79] Lin Zhou, Jeremy D. Glennon, John H. T. Luong, F. Jerry Reen, Fergal O’Gara, Christina McSweeney, and Gerard P. McGlacken. Detection of the Pseudomonas Quinolone Signal (PQS) by cyclic voltammetry and amperometry using a boron doped diamond electrode. *Chemical Communications*, 47(37):10347, 2011.
- [80] Julie V. Macpherson. A practical guide to using boron doped diamond in electrochemical research. *Physical Chemistry Chemical Physics*, 17(5):2935–2949, 2015.
- [81] Anchana Preechaworapun, Tribidasari A. Ivandini, Akane Suzuki, Akira Fujishima, Orawon Chailapakul, and Yasuaki Einaga. Development of amperometric immunosensor using boron-doped diamond with poly(o-aminobenzoic acid). *Analytical Chemistry*, 80(6):2077–2083, March 2008.
- [82] Azrilawani Ahmad and Eric Moore. Electrochemical immunosensor modified with self-assembled monolayer of 11-mercaptoundecanoic acid

- on gold electrodes for detection of benzo[a]pyrene in water. *The Analyst*, 137(24):5839, 2012.
- [83] Daniel Mandler and Shlomit Kraus-Ophir. Self-assembled monolayers (SAMs) for electrochemical sensing. *Journal of Solid State Electrochemistry*, 15(7-8):1535–1558, July 2011.
- [84] C. Vericat, M. E. Vela, G. Benitez, P. Carro, and R. C. Salvarezza. Self-assembled monolayers of thiols and dithiols on gold: new challenges for a well-known system. *Chemical Society Reviews*, 39(5):1805, 2010.
- [85] D. P. Woodruff. The interface structure of n-alkylthiolate self-assembled monolayers on coinage metal surfaces. *Physical Chemistry Chemical Physics*, 10(48):7211–7221, December 2008.
- [86] Alex Fragoso, Noemi Laboria, Daniel Latta, and Ciara K. O’Sullivan. Electron permeable self-assembled monolayers of dithiolated aromatic scaffolds on gold for biosensor applications. *Analytical Chemistry*, 80(7):2556–2563, April 2008.
- [87] Mélanie Auffan, Jérôme Rose, Jean-Yves Bottero, Gregory V. Lowry, Jean-Pierre Jolivet, and Mark R. Wiesner. Towards a definition of inorganic nanoparticles from an environmental, health and safety perspective. *Nature Nanotechnology*, 4(10):634–641, October 2009.
- [88] Eugenii Katz, Itamar Willner, and Joseph Wang. Electroanalytical and Bioelectroanalytical Systems Based on Metal and Semiconductor Nanoparticles. *Electroanalysis*, 16(1-2):19–44, 2004.
- [89] Xiliang Luo, Aoife Morrin, Anthony J. Killard, and Malcolm R. Smyth. Application of Nanoparticles in Electrochemical Sensors and Biosensors. *Electroanalysis*, 18(4):319–326, 2006.
- [90] M. L. Mena, P. Yáñez-Sedeño, and J. M. Pingarrón. A comparison of different strategies for the construction of amperometric enzyme biosensors using gold nanoparticle-modified electrodes. *Analytical Biochemistry*, 336(1):20–27, January 2005.
- [91] F. R. R. Teles and L. P. Fonseca. Applications of polymers for biomolecule immobilization in electrochemical biosensors. *Materials Science and Engineering: C*, 28(8):1530–1543, December 2008.
- [92] Md Aminur Rahman, Pankaj Kumar, Deog-Su Park, and Yoon-Bo

- Shim. *Electrochemical Sensors Based on Organic Conjugated Polymers. Sensors*, 8(1):118–141, January 2008.
- [93] Bansi D. Malhotra, Asha Chaubey, and S. P. Singh. Prospects of conducting polymers in biosensors. *Analytica Chimica Acta*, 578(1):59–74, September 2006.
- [94] Hideki Kuramitz. Magnetic microbead-based electrochemical immunoassays. *Analytical and Bioanalytical Chemistry*, 394(1):61–69, May 2009. WOS:000265035700009.
- [95] A. K. Cheetham and Peter Day. *Solid State Chemistry: Techniques*. Clarendon Press, 1988. Google-Books-ID: qW9m9k6KivwC.
- [96] K. D. Vernon-Parry. Scanning electron microscopy: an introduction. *III-Vs Review*, 13(4):40–44, July 2000.
- [97] Chunyan Wang, Fucheng Ye, Hongfu Wu, and Yong Qian. Depositing Au Nanoparticles onto Graphene Sheets for Simultaneous Electrochemical Detection Ascorbic Acid, Dopamine and Uric Acid. *International Journal of Electrochemical Science*, 8(2):2440–2448, February 2013.
- [98] C. H. Goeting, F. Marken, A. Gutierrez-Sosa, R. G. Compton, and J. S. Foord. Electrochemically induced surface modifications of boron-doped diamond electrodes: an X-ray photoelectron spectroscopy study. *Diamond and Related Materials*, 9(3-6):390–396, May 2000.
- [99] A. Dekanski, J. Stevanovic, R. Stevanovic, B. Z. Nikolic, and V. M. Jovanovic. Glassy carbon electrodes I. Characterization and electrochemical activation. *Carbon*, 39(8):1195–1205, 2001.
- [100] M. S. Dresselhaus, G. Dresselhaus, R. Saito, and A. Jorio. Raman spectroscopy of carbon nanotubes. *Physics Reports-Review Section of Physics Letters*, 409(2):47–99, March 2005.
- [101] Andrea C. Ferrari. Raman spectroscopy of graphene and graphite: Disorder, electron-phonon coupling, doping and nonadiabatic effects. *Solid State Communications*, 143(1-2):47–57, July 2007.
- [102] Konstantin N. Kudin, Bulent Ozbas, Hannes C. Schniepp, Robert K. Prud'homme, Ilhan A. Aksay, and Roberto Car. Raman spectra of graphite oxide and functionalized graphene sheets. *Nano Letters*, 8(1):36–41, January 2008.

- [103] L. M. Malard, M. A. Pimenta, G. Dresselhaus, and M. S. Dresselhaus. Raman spectroscopy in graphene. *Physics Reports-Review Section of Physics Letters*, 473(5-6):51–87, April 2009.
- [104] M. A. Pimenta, G. Dresselhaus, M. S. Dresselhaus, L. G. Cancado, A. Jorio, and R. Saito. Studying disorder in graphite-based systems by Raman spectroscopy. *Physical Chemistry Chemical Physics*, 9(11):1276–1291, 2007.
- [105] Evtim V. Efremov, Freek Ariese, and Cees Gooijer. Achievements in resonance Raman spectroscopy: Review of a technique with a distinct analytical chemistry potential. *Analytica Chimica Acta*, 606(2):119–134, January 2008.
- [106] Ewen Smith and Geoffrey Dent. *Modern Raman Spectroscopy: A Practical Approach*. John Wiley & Sons, March 2013. Google-Books-ID: M3jUr05d018C.
- [107] Y. Ueno. The Toxicology of Mycotoxins. *Crc Critical Reviews in Toxicology*, 14(2):99–132, 1985.
- [108] Ying Wang, Nan Liu, Baoan Ning, Ming Liu, Zhiqiang Lv, Zhiyong Sun, Yuan Peng, Cuicui Chen, Junwen Li, and Zhixian Gao. Simultaneous and rapid detection of six different mycotoxins using an immunochip. *Biosensors & Bioelectronics*, 34(1):44–50, April 2012.
- [109] U. Konietzny and R. Greiner. The application of PCR in the detection of mycotoxigenic fungi in foods. *Brazilian Journal of Microbiology*, 34(4):283–300, December 2003.
- [110] Hongmei Liu, Weijun Kong, Congmin Liu, Qiutao Liu, Yichen Hu, and Meihua Yang. Rapid analysis and identification of multi-class mycotoxins in *Morinda officinalis* by UFLC-ESI-MS/MS. *Rsc Advances*, 5(78):63561–63571, 2015.
- [111] Juan C. Vidal, Laura Bonel, Patricia Duato, and Juan R. Castillo. Improved electrochemical competitive immunosensor for ochratoxin A with a biotinylated monoclonal antibody capture probe and colloidal gold nanostructuring. *Analytical Methods*, 3(4):977, 2011.
- [112] Martín A. Fernández-Baldo, Franco A. Bertolino, Germán A. Messina, Maria I. Sanz, and Julio Raba. Modified magnetic nanoparticles in

- an electrochemical method for the ochratoxin A determination in *Vitis vinifera* red grapes tissues. *Talanta*, 83(2):651–657, December 2010.
- [113] Zhou Linting, Li Ruiyi, Li Zaijun, Xia Qianfang, Fang Yinjun, and Liu Junkang. An immunosensor for ultrasensitive detection of aflatoxin B1 with an enhanced electrochemical performance based on graphene/conducting polymer/gold nanoparticles/the ionic liquid composite film on modified gold electrode with electrodeposition. *Sensors and Actuators B: Chemical*, 174:359–365, November 2012.
- [114] Mirian Hervás, Miguel A. López, and Alberto Escarpa. Integrated electrokinetic magnetic bead-based electrochemical immunoassay on microfluidic chips for reliable control of permitted levels of zearalenone in infant foods. *The Analyst*, 136(10):2131, 2011.
- [115] Nathalie Paniel, Antonio Radoi, and Jean-Louis Marty. Development of an Electrochemical Biosensor for the Detection of Aflatoxin M1 in Milk. *Sensors*, 10(10):9439–9448, October 2010.
- [116] Nancy V. Panini, Franco A. Bertolino, Eloy Salinas, Germán A. Messina, and Julio Raba. Zearalenone determination in corn silage samples using an immunosensor in a continuous-flow/stopped-flow systems. *Biochemical Engineering Journal*, 51(1–2):7–13, August 2010.
- [117] Mohamad Kamal Abdul Kadir and Ibtisam E. Tothill. Development of an Electrochemical Immunosensor for Fumonisin Detection in Foods. *Toxins*, 2(4):382–398, April 2010.
- [118] Mirian Hervás, Miguel Ángel López, and Alberto Escarpa. Simplified calibration and analysis on screen-printed disposable platforms for electrochemical magnetic bead-based immunosensing of zearalenone in baby food samples. *Biosensors and Bioelectronics*, 25(7):1755–1760, March 2010.
- [119] D. Neagu, S. Perrino, L. Micheli, G. Palleschi, and D. Moscone. Aflatoxin M1 determination and stability study in milk samples using a screen-printed 96-well electrochemical microplate. *International Dairy Journal*, 19(12):753–758, December 2009.
- [120] Charlie O. Parker and Ibtisam E. Tothill. Development of an electrochemical immunosensor for aflatoxin M1 in milk with focus on

- matrix interference. *Biosensors and Bioelectronics*, 24(8):2452–2457, April 2009.
- [121] S. Piermarini, G. Volpe, L. Micheli, D. Moscone, and G. Palleschi. An ELIME-array for detection of aflatoxin B1 in corn samples. *Food Control*, 20(4):371–375, April 2009.
- [122] Ines Ben Rejeb, Fabiana Arduini, Adina Arvinte, Aziz Amine, Mohamed Gargouri, Laura Micheli, Camelia Bala, Danila Moscone, and Giuseppe Palleschi. Development of a bio-electrochemical assay for AFB1 detection in olive oil. *Biosensors and Bioelectronics*, 24(7):1962–1968, March 2009.
- [123] Dianping Tang, Zhaoyang Zhong, Reinhard Niessner, and Dietmar Knopp. Multifunctional magnetic bead-based electrochemical immunoassay for the detection of aflatoxin B1 in food. *The Analyst*, 134(8):1554, 2009.
- [124] Dan Wang, Weihua Hu, Yonghua Xiong, Yang Xu, and Chang Ming Li. Multifunctionalized reduced graphene oxide-doped polypyrrole/pyrrolepropylic acid nanocomposite impedimetric immunosensor to ultra-sensitively detect small molecular aflatoxin B1. *Biosensors and Bioelectronics*, 63:185–189, January 2015.
- [125] Adrián Jodra, Miguel Ángel López, and Alberto Escarpa. Disposable and reliable electrochemical magnetoimmunosensor for Fumonisin simplified determination in maize-based foodstuffs. *Biosensors and Bioelectronics*, 64:633–638, February 2015.
- [126] C. A. Martínez-Huitle, N. Suely Fernandes, S. Ferro, A. De Battisti, and M. A. Quiroz. Fabrication and application of Nafion®-modified boron-doped diamond electrode as sensor for detecting caffeine. *Diamond and Related Materials*, 19(10):1188–1193, October 2010.
- [127] Angelika Beyer and Marek Biziuk. Applications of sample preparation techniques in the analysis of pesticides and PCBs in food. *Food Chemistry*, 108(2):669–680, May 2008.
- [128] P. L. Buldini, L. Ricci, and J. L. Sharma. Recent applications of sample preparation techniques in food analysis. *Journal of Chromatography A*, 975(1):47–70, October 2002.
- [129] L. Micheli, R. Grecco, M. Badea, D. Moscone, and G. Palleschi. An electrochemical immunosensor for aflatoxin M1 determination in

- milk using screen-printed electrodes. *Biosensors & Bioelectronics*, 21(4):588–596, October 2005.
- [130] J. Homola, J. Dostalek, S. F. Chen, A. Rasooly, S. Y. Jiang, and S. S. Yee. Spectral surface plasmon resonance biosensor for detection of staphylococcal enterotoxin B in milk. *International Journal of Food Microbiology*, 75(1-2):61–69, May 2002.
- [131] Xin Yang, Feng Wu, Di-Zhao Chen, and Hong-Wei Lin. An electrochemical immunosensor for rapid determination of clenbuterol by using magnetic nanocomposites to modify screen printed carbon electrode based on competitive immunoassay mode. *Sensors and Actuators B-Chemical*, 192:529–535, March 2014.
- [132] J. L. Sebaugh and P. D. McCray. Defining the linear portion of a sigmoid-shaped curve: bend points. *Pharmaceutical Statistics*, 2(3):167–174, July 2003.
- [133] Gary L. Long and J. D. Winefordner. Limit of detection. A closer look at the IUPAC definition. *Analytical Chemistry*, 55(7):712A–724A, June 1983.

Chapter 2

Detection of Mouse IgG at Pretreated and Nanostructured Screen Printed Electrodes

2.1 Objectives and Novelty

The aim of this chapter was to develop a screen printed electrode for electrochemical immunosensor applications using mouse IgG as a model analyte. This optimised material would then be used for the detection of deoxynivalenol in chapter 3.

Two strategies were investigated. Firstly, a number of electrochemical pretreatments previously described in the literature were compared in order to establish the most effective electrode activation technique. Secondly, MWCNTs and RGO were compared with the same aim in mind. These materials were analysed using electrochemical and physical techniques which gave insight into the fundamental electrochemistry occurring at these modified surfaces. Then, a model immunosensor was constructed which investigated whether improved electrochemical activity translates to improved immunosensor performance. It was found that a MWCNT/Nafion modified electrode offered the lowest LOD for IgG detection (0.2×10^{-3} mg/mL) compared to the other modified electrodes trialled. Hence, this modification was then used in Chapter 3 for deoxynivalenol detection.

The study in this chapter presents the first time a systematic comparison has taken place between multiwalled carbon nanotube, reduced graphene oxide and electrochemically pretreated screen printed electrodes for alkaline phosphatase based electrochemical immunosensors. Although these materials have all previously been used for immunosensor applications this type of comparison provides useful insights for researchers using these modifications for future studies. This point is emphasised by Yang et. al who described this lack of comparative work - “... *there have been few head-to-head comparisons of the relative performance of CNTs and graphene in biosensing, and certainly none in completely optimized systems* ” [1].

2.2 Introduction

2.2.1 Screen Printed Electrodes

Screen printed electrodes are now commonly used in electroanalysis owing to their high conductivity, ease of fabrication, electrochemical activity and low cost

[2]. Platinum and gold screen printed electrodes are commercially available and have been successfully used in sensor applications but for the purposes of this thesis SPEs refer solely to carbon based electrodes. These electrodes have been used in the direct detection of electroactive compounds such as dopamine, the detection of heavy metals as well as for the construction of biosensors based on enzymes and antibodies [3, 4, 5, 6].

Another supposed advantage of SPEs is the lack of cleaning and polishing required prior to use, in contrast to other electrode types. Although polishing of the electrode may not be required, electrochemical pretreatment has been shown to improve the electrochemical characteristics of SPEs [7, 8, 9, 10] This improvement is achieved by either performing cyclic voltammograms in dilute acids or pre-anodising the electrode by applying a fixed potential for an optimised period of time. Charge transfer properties are said to be improved through an increase in oxygen functionalities, increase in effective surface area, exposure of edge plane sites and removal of the insulating polymeric binder [11]. However, attempts to distinguish between these effects are rarely discussed or investigated.

In recent years, work by Banks and Compton (discussed in Chapter 1), has brought a greater understanding to the fundamental properties of carbon based electrodes. Through studies on carbon nanotube electrodes it was shown that the end sites of carbon nanotubes are the dominant contributor to electrochemical activity. As carbon nanotubes can be considered as rolled up sheet(s) of graphene; and graphite is in turn a stacked layer of graphene sheets, this observation is important when considering a range of carbon based electrodes. As such the electrochemistry of SPEs can be solely described by their edge plane content:

$$I - E_{SPE} = \epsilon[I - E_{edge}]$$

where ϵ is described by Davies et. al as a complicated function which takes into the account relative sizes and areas of electrodes as well as non linear diffusion [12]. However, as discussed previously, this description of graphite electrochemistry has been disputed by recent work from the Unwin group who showed that the basal plane of graphite can also contribute to its electrochemical activity [13].

2.2.2 Model Electrochemical Immunosensors

In the development of new materials and methods for electrochemical immunosensor applications it is often the case that a model analyte is used. One such example is the use of a mouse or rabbit IgG which bind to commercially available enzyme conjugated anti-mouse or anti-rabbit antibodies. The advantage of this approach is the low cost of the reagents in use. For example, Moore et. al developed a single drop immunsensor protocol for rabbit IgG prior to applying the method to the detection of phenanthrene [14]. A similar approach was employed to assess the use of conducting polymers in immunosensor applications [15]. In both cases a competitive approach was employed whereby an antibody immobilised on the electrode surface competed with a free antibody in solution for binding sites on an enzyme labelled secondary antibody (also in solution). In a different approach, a sandwich assay was employed by Diaz-Gonzalez et. al for the detection of rabbit IgG by immobilising bio-tinylated anti-rabbit IgG onto a streptavidin coated screen printed electrode [16]. Rabbit IgG was then allowed to bind to the anti-rabbit IgG on the surface before alkaline phosphatase labelled anti-rabbit IgG facilitated electrochemical detection. In this chapter, the competitive assay approach of Moore et. al and Darain is used to compare pretreated and nanocarbon modified screen printed electrodes for mouse IgG detection.

2.2.3 Screen Printed Carbon Pretreatment

It has been shown over the last number of years that pretreatment of screen printed carbon and carbon paste electrodes has a significant impact on the electrode kinetics. Many of these techniques are based on the pre-anodisation of the electrode surface. For example, Wang et. al applied potentials ranging from 1.5V to 2V for short periods (30 s - 3 mins) to electrodes in a 0.05M phosphate buffer, pH 7.4 [7] which drastically decreased the peak separation in cyclic voltammetry measurements of acetaminophen and catechol. Dock et. al and Cui et. al also improved electrode performance by applying a 1.2 V potential for 5 minutes to the electrodes in saturated sodium carbonate solution [8, 9]. Another approach is to cycle the electrode in a weak acid in order to strip the surface of the electrode, removing any insulative material present [10]. This method enabled a 50% decrease in peak separations when investigating the ferri/ferrocyanide redox couple. A similar method was employed by Kadara et.

al who potential cycled the electrode in 0.1 M NaOH between -1.0 V and 1.0 V for 10 minutes [11].

2.2.4 Nanocarbon modified electrode based Electrochemical Immunosensors for IgG Detection

As discussed in Chapter 1, carbon nanomaterials have been used extensively in the design of electrochemical immunosensors, motivated by their electrocatalytic effects and large surface area. These approaches have been investigated in a small number of cases for IgG detection in model systems. Aziz et. al developed a sensor for mouse IgG that used an indium tin oxide electrode modified with carboxylated multiwalled carbon nanotubes and poly(ethylene glycol)-silane copolymer which achieved a very low limit of detection of 10 pg/mL [17]. Interesting work was also carried out by the Pumera group which compared a range of graphenes (graphite oxide, graphene oxide, thermally reduced graphene oxide, electrochemically reduced graphene oxide) for the detection of IgG using a label free impedance approach [18]. Thermally reduced graphene oxide was deemed to be the most effective of the materials studied. However, repeatability of their results doesn't appear to be satisfactory suggesting that this approach, whilst straightforward, would be susceptible to false positive and negative results. In this chapter similar comparisons are undertaken, However, in this case, an enzyme labelled immunosensor is investigated.

2.3 Materials and Methods

2.3.1 Reagents

Phosphate Buffer Saline (PBS) tablets, sulphuric acid, potassium chloride, sodium carbonate, sodium bicarbonate, sodium hydroxide, potassium hexa cyanoferrate (III), potassium hexa cyanoferrate (II) trihydrate, hexaammine ruthenium (III) chloride, mouse IgG, anti-mouse AP labelled, bovine serum albumin (BSA), trizma base, p-nitrophenol phosphate, diethanolamine were purchased from Sigma Aldrich (Dublin, Ireland). 50 mL 0.05 M PBS solution was obtained by dissolving 1 PBS tablet in 40 ml of nanopure water.

4-aminophenyl phosphate monosodium salt hydrate was purchased from Gold Biotechnology (St. Louis, USA). Carboxylic acid functionalised multi-walled carbon nanotubes (>8 % carboxylic acid functionalised, avg. diam. x L 9.5 nm x 1.5 μ m) and reduced graphene oxide (> 80 % carbon content) were purchased from Sigma Aldrich (Wicklow, Ireland).

2.3.2 Buffer Preparation

50 mM Carbonate/bicarbonate pH 9.5 buffer was prepared by making up equimolar solutions of sodium hydrogen carbon carbonate and sodium carbonate which were then mixed together until a pH 9.5 was achieved. 100 mL of 50 mM Tris-HCl solution (Tris buffer) was made by adding 0.605 grams of Trizma base to nanopure water and adjusting to pH 7.4 with 1 M HCl. Washing buffer consisted of 50 mM Tris buffer with the addition of 0.05 % Tween 20 solution. 100 mL of 0.1 M DEA buffer pH 9.5 containing 1 mM $MgCl_2$ was made by first adding 0.0203 grams of $MgCl_2$ to 100 mL of nanopure water. Next 962 μ L of water is removed from the container and is replaced with 962 μ L of DEA solution. The solution is then adjusted to pH 9.5 using 1 M HCl.

2.3.3 Screen Printed Electrodes

Screen Printed electrodes were purchased from Kanichi Research Limited (Manchester, UK). They consisted for a central graphite working electrode (area = 0.071 cm²), graphite counter electrode and Ag/AgCl paste reference electrode. In Fig 2.1, an array of electrodes as purchased is shown.

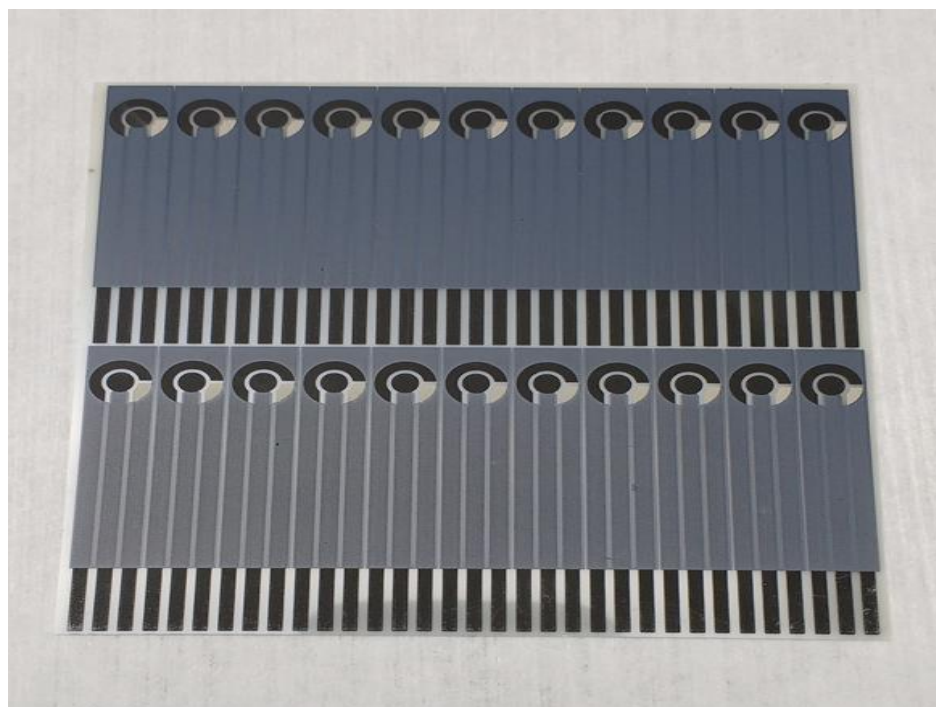


Figure 2.1: Sheet of commercial Kanichi Limited screen printed carbon electrodes as purchased. Each individual sensor consists of a graphite working and counter electrode as well as Ag/AgCl reference electrode.

2.3.4 Electrode Modifications

Initially, 2 mg/ml concentrations of RGO and MWCNTs were prepared in DMF and sonicated for at least 1 hour in a water bath or until stable solutions were obtained. These stock solutions were then diluted with nanopure water to give 0.05, 0.1, 0.3, 0.5 and 1 mg/ml solutions of RGO and MWCNT. 2 μ l of these solutions were then pipetted onto a bare working electrode and left to dry at room temperature. In order to prepare RGO/Nafion and MWCNT/Nafion solutions, 1 mg of either MWCNTs or RGO were prepared in 0.5 % Nafion solution which had in turn been prepared in 70 % ethanol. 0.5 μ l of these solutions were then pipetted onto a bare working electrode and left to dry at room temperature.

2.3.5 Electrode Pretreatment

A number of previously reported electrochemical pretreatment procedures were compared to evaluated to see which one had the largest impact on SPE

performance:

- The electrode was cycled in 0.2 M H₂SO₄ solution between 1.2 and 1.5 V [10]
- A 1.2 V potential was applied to the electrode for 5 mins in saturated Na₂CO₃ solution [9]
- The electrode was cycled between -1 V and 1V in 0.1 M NaOH solution [11]
- A 1.5 V potential was applied to the electrode for 2 minutes in 0.05 M PBS [7]
- The electrode was cycled between -0.5 V and 2 V in 0.05 M PBS - this pretreatment was not reported previously but used to investigate the impact of high potentials on the electrodes

2.3.6 Cyclic Voltammetry

Cyclic voltammetry measurements were carried out using a Palmsens portable potentiostat (Palmsens BV, the Netherlands) in a home made Faraday cage. When comparing electrodes at 100 mV/s three separate electrodes were used. For the scan rate studies, a single electrode was re-used for each scan rate.

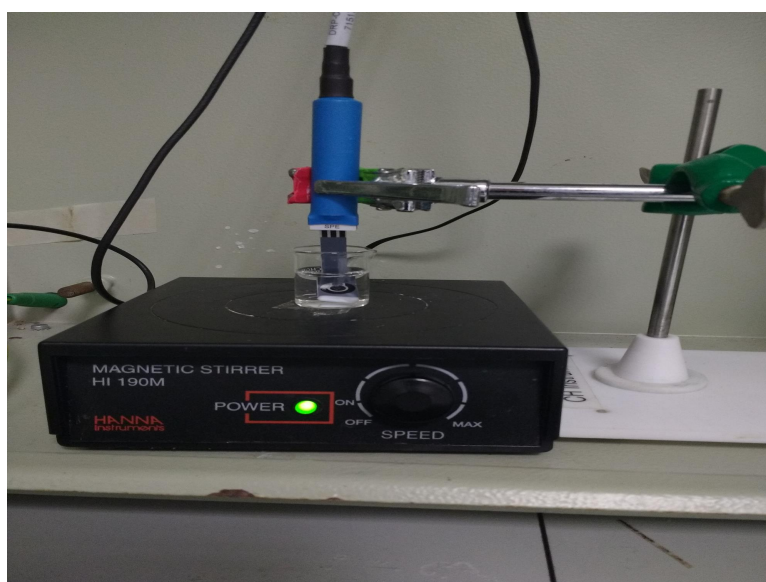


Figure 2.2: Set up for electrochemical measurements showing a screen printed electrode connected to a Palmsens electrode connector inside a Faraday cage.

2.3.7 Amperometry

Amperometric measurements were carried out using CHI 660B potentiostat (Austin, TX, USA) inside a commercial Faraday Cage (Metrohm Autolab BV, Kanaalweg, The Netherlands). For p-aminophenol detection, amperometric measurements were carried out in 0.1 M DEA buffer, pH 9.5. In the case of electrochemically pretreated electrodes, a wait time of 100 seconds was used prior to the addition of 10 μ l of 5 mM p-aminophenol (prepared in H₂SO₄) to 4990 μ l DEA buffer and 5 subsequent additions were carried out at 40 second intervals. For nanocarbon modified electrodes, an initial wait time of 200 seconds was used.

2.3.8 Open Circuit Potential

An open circuit potential experiment was carried out in which a two electrode set up was used with the 'on-chip' reference electrode connected to the working electrode cable and an external Ag/Ag/Cl reference used. A 1 M KCl solution was used. The measurement time was 5 hours.

2.3.9 XPS (TCD)

XPS measurements were performed under ultra-high vacuum conditions ($<5 \times 10^{-10}$ mbar) on a VG Scientific ECSAlab Mk II system using Al K α X-rays (1486.6 eV). The analyser pass energy was set to 200 eV for survey spectra recorded. An electron flood gun was used for charge compensation and the binding energy scale was referenced to the adventitious carbon 1s core-level at 284.8 eV.

2.3.10 SEM

SEM measurements were carried out on an FEI Quanta 650 SEM. A tilt angle of 45° was used for the bare and pretreated electrodes and a tilt angle of 0° was used for the nanocarbon modified electrodes. Acceleration voltages of either 10/20/30 kV were used.

2.3.11 Contact Angle

Contact Angle measurements were carried out using a Contact Angle System OCA (Dataphysics Instruments, GmbH, Filderstadt, Germany) (Fig. 2.3). Measurements were carried out in sessile drop mode using a volume of $2 \mu\text{L}$ and a flow rate of $4.9 \mu\text{L/s}$.

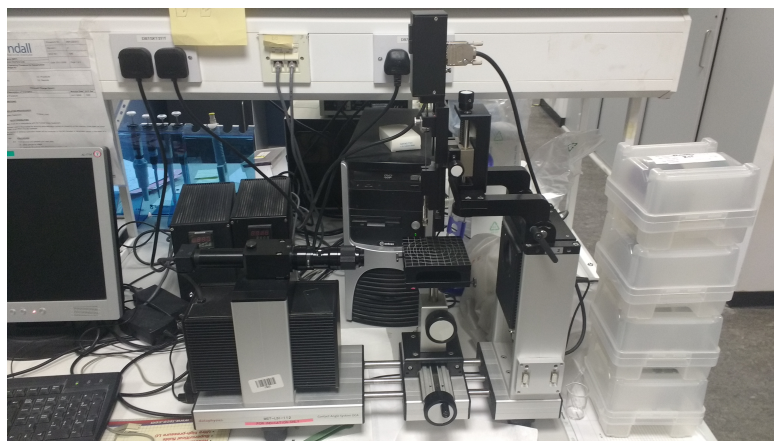


Figure 2.3: Dataphysics contact angle instrument

2.3.12 ELISA

All bioassay development experiments (both ELISA and on-chip electrochemical immunoassay) were carried out in a benchtop laminar flow hood (Fig. 2.4).

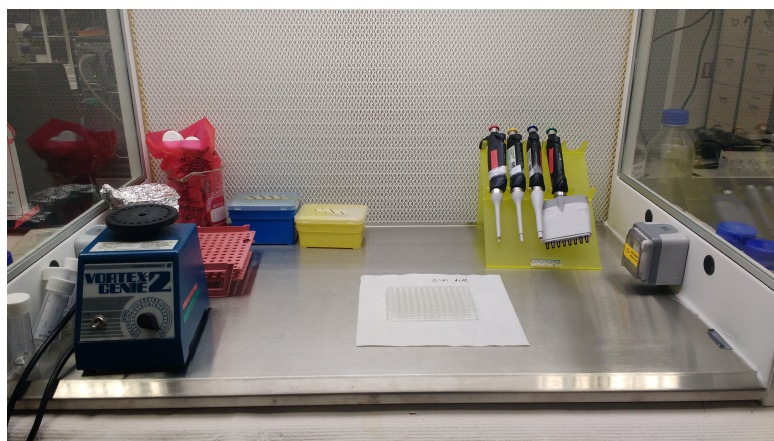


Figure 2.4: Laminar Flow Hood with ELISA plate

All ELISA measurements were carried out using a ThermoScientific Multiskan Ex photometer using a 405 nm filter (pictured in Fig. 2.5).



Figure 2.5: Photograph of the Multiskan Ex Photometer used in all ELISA experiments

2.3.12.1 Capture ELISA

- A 1/5 serial dilution of mouse IgG in carbonate buffer pH 9.5 was carried out from a 5 mg/ml stock solution
- 50 μL of each concentration was added to the wells in triplicate before the plate was covered and incubated at 37° C for 1 hour
- After incubation, the contents of the plate were discarded and 200 μL of washing buffer was added to each well (x3)
- 200 μL of blocking solution was added to each well and the plate was covered and incubated at 37° C for 1 hour
- Blocking solution was discarded and each well was washed with washing buffer (x3)
- 50 μL anti-mouse alkaline phosphatase labelled antibody (1/30,000 dilution) was added to each well and the plate was covered and incubated for 1 hour at 37° C
- After discarding the plate contents, 100 μL of pNPP solution (1 mg/mL) was added to each well and a further incubation at 37° C was carried out for 1 hour
- The plate was then analysed using the plate reader

2.3.12.2 Competitive ELISA

- 50 μL of a fixed concentration of mouse IgG was added to each well, covered and incubated at 37° C for 1 hour
- After incubation, the contents of the plate were discarded and 200 μL of washing buffer was added to each well (x3)
- 200 μL of blocking solution was added to each well and the plate was covered and incubated at 37° C for 1 hour
- A 1/5 serial dilution of mouse IgG was carried out and 25 μL of each concentration was mixed with 25 μL anti-mouse AP labelled (1/30,000 dilution) prior to addition to the plate and incubation at 37° C for 1 hour
- After incubation, the contents of the wells were discarded and washed with Tris-Tween-HCl (x3)
- After discarding the plate contents, 100 μL of pNPP solution (1 mg/mL) was added to each well and a further incubation at 37° C was carried out for 1 hour
- The plate was then analysed using the plate reader

2.3.13 Electrochemical Immunoassay

Electrochemical immunoassay measurements were carried out in a 5 mL glass beaker with a stirrer bar and external magnetic stirrer providing solution rotation. 50 μL of 25 mg/mL pAPP solution was added to 4950 μL of stirred DEA buffer for each measurement step. A typical response is shown in Fig 2.6.

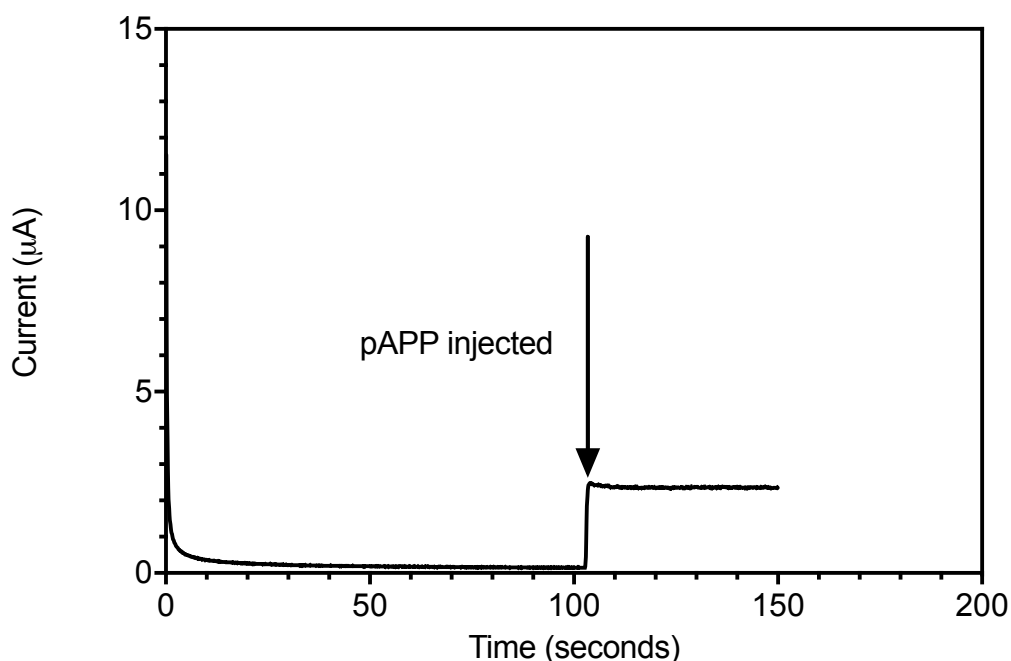


Figure 2.6: Typical amperometric immunoassay measurement response in which 25 mg/mL pAPP is added to a stirred solution containing an alkaline phosphatase labelled antibody in DEA buffer pH 9.5

2.3.13.1 Electrochemical Capture Assay

- All electrodes were activated by applied a fixed potential of 1.2 V for 5 mins
- A 1/5 serial dilution of mouse IgG was carried out in carbonate/bicarbonate buffer pH 9.5 and 5 μ L of each antibody dilution was added to the working electrode surface (n=3). The electrodes were incubated in sealed petri dishes at room temperature for 1 hour.
- The electrodes were then washed with 300 μ L of Tris-HCl solution pH 7.4 (x2) and 800 μ L of nanopure water to remove excess antibody solution. The electrodes were dried with nitrogen gas.
- 30 μ L of 2 % BSA in Tris-HCl pH 7.4 was pipetted onto the electrode surface and the electrodes were incubated at room temperature for 1 hour.
- The electrodes were then washed with 300 μ L of Tris-HCl solution pH 7.4 (x2) and 800 μ L of nanopure water to remove excess blocking solution. The electrodes were dried with nitrogen gas.

- 5 μL of a 1/1000 dilution of alkaline phosphatase labelled anti-mouse IgG was added to the working electrode surface and incubated for 1 hour at room temperature
- The electrodes were then washed with 300 μL of Tris-HCl solution pH 7.4 (x2) and 800 μL of nanopure water to remove excess unattached secondary antibodies. The electrodes were stored in DEA buffer and kept at 4° C prior to measurement.
- Measurement was carried out by adding 50 μL of 25 mg/mL pAPP solution to 4950 μL of stirred DEA buffer

2.3.13.2 Electrochemical Competitive Assay

- All electrodes were activated by applied a fixed potential of 1.2 V for 5 mins
- A 1/5 serial dilution of mouse IgG was carried out in carbonate/bicarbonate buffer pH 9.5 and 5 μL of each antibody dilution was added to the working electrode surface (n=3). The electrodes were incubated in sealed petri dishes at room temperature for 1 hour.
- The electrodes were then washed with 300 μL of Tris-HCl solution pH 7.4 (x2) and 800 μL of nanopure water to remove excess antibody solution. The electrodes were dried with nitrogen gas.
- 30 μL of 2 % BSA in Tris-HCl pH 7.4 was pipetted onto the electrode surface and the electrodes were incubated at room temperature for 1 hour.
- The electrodes were then washed with 300 μL of Tris-HCl solution pH 7.4 (x2) and 800 μL of nanopure water to remove excess blocking solution. The electrodes were dried with nitrogen gas.
- 5 μL of a 1/1000 dilution of alkaline phosphatase labelled anti-mouse IgG was added to the working electrode surface and incubated for 1 hour at room temperature
- The electrodes were then washed with 300 μL of Tris-HCl solution pH 7.4 (x2) and 800 μL of nanopure water to remove excess unattached secondary antibodies. The electrodes were stored in DEA buffer and kept at 4° C prior to measurement.

2.4 Results and Discussion (Part 1) - Characterisation of Electrochemically pretreated graphite electrodes

2.4.1 Thin Layer Effects

Work on carbon nanotube modified electrodes has revealed that thin layer effects due to trapping of the electroactive species in the porous structure of the carbon nanotube network can have a considerable effect on its electrochemical characteristics [19, 20, 21]. Differentiating between purely semi-infinite diffusion and the contribution of thin layers can be done by graphing the \log_{10} of peak current versus \log_{10} of scan rate from cyclic voltammetry measurements. A slope of around 0.5 indicates semi-infinite diffusion whereas a slope closer to 1 indicates thin layer effects. The justification for this is explained in Chapter 1 by considering the Randles-Sevcik which applies to purely diffusional, electrochemically reversible behaviour and the contrasting thin layer effects.

This analysis was carried out for each electrode pretreatment using both $[\text{Fe}(\text{CN})_6]^{3-/4-}$ and hexaammine ruthenium (III) chloride. Each graph shows a linear dependence between $\log_{10}i_p$ and $\log_{10}\nu$ (Fig 2.7). Analysis of the slope of each graph shows that more “ideal” diffusion only behaviour is observed for hexaammine ruthenium (III) chloride with slopes of around 0.55 for all the pretreatments bar the PBS CV treatment which had a slope of 0.6. This increase may suggest that thin layer effects are occurring and could explain the large capacitive currents observed. Values within 0.05 of 1/2 have been deemed to suggest purely diffusional behaviour and the absence of thin layer effects [22]. The lower slopes of around 0.4 observed for ferri/ferrocyanide also indicate an absence of thin layer effects but suggest that values such as electrochemical surface area could not as accurately be calculated as for hexaammine ruthenium (III) chloride.

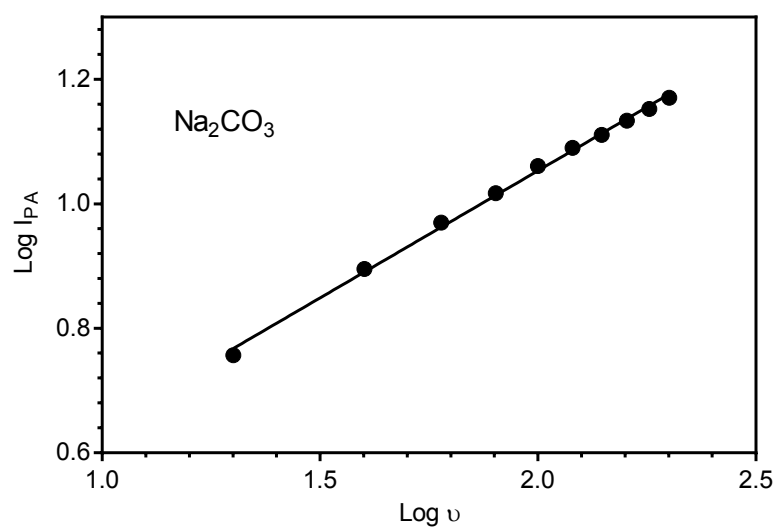


Figure 2.7: Typical graph of log peak current vs log of scan rate for a pretreated SPE in 1 mM ferri/ferrocyanide. All other graphs are displayed in the appendix of this thesis.

Table 2.1: Slopes of Log I_p vs Log v at electrochemically pretreated electrodes

	Slope (Log I_p vs Log v)	R^2
<u>Untreated</u>		
Ferri/ferrocyanide	0.297	0.9601
Hexaammine ruthenium (III) chloride	0.519	0.9991
<u>Na₂CO₃</u>		
Ferri/ferrocyanide	0.409	0.9976
Hexaammine ruthenium (III) chloride	0.543	0.9998
<u>H₂SO₄</u>		
Ferri/ferrocyanide	0.395	0.9966
Hexaammine ruthenium (III) chloride	0.557	0.9977
<u>NaOH</u>		
Ferri/ferrocyanide	0.409	0.9968
Hexaammine ruthenium (III) chloride	0.558	0.9991
<u>PBS Anodic</u>		
Ferri/ferrocyanide	0.407	0.9967
Hexaammine ruthenium (III) chloride	0.556	0.9982
<u>PBS CV</u>		
Ferri/ferrocyanide	0.3825	0.9943
Hexaammine ruthenium (III) chloride	0.600	0.995

2.4.2 Electrochemical Characterisation at Pretreated Electrodes - Ferri/Ferrocyanide

Each electrochemical pretreatment, as described in section 2.5.5, was carried out on the screen printed electrodes ($n=3$). The performance of which was then evaluated by cyclic voltammetry in 1 mM ferri/ferrocyanide with a 1 M KCl supporting electrolyte. It can be seen from Fig. 2.8 that all of the pretreatment procedures result in an increase of both anodic and cathodic current as well as a decrease in peak potential separation (ΔE). However, in the case of the CVs in phosphate buffer saline as a pretreatment there is also an increase in non-Faradaic background current. This type of behaviour is not advantageous for electrochemical sensing as high background currents leads to low signal to noise ratios and hence increased limits of detection.

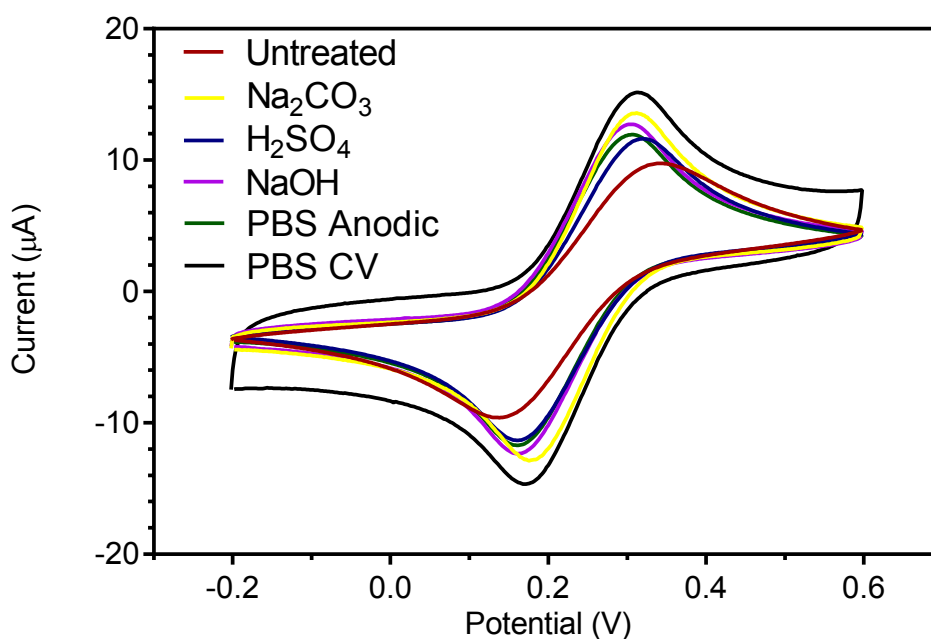


Figure 2.8: Comparison of different pretreatment procedures. Cyclic voltammograms were carried out at a scan rate of 100 mV s^{-1} in 1 mM $[\text{Fe}(\text{CN})_6]^{3-/4-}$.

Table 2.2: Peak potential separation and peak anodic current from CV measurements for different electrochemical pretreatments. n=3

Pretreatment	ΔE (mV)	I_{PA}
H ₂ SO ₄	145(\pm 8)	10.4 (\pm 0.6)
PBS Anodic	144 (\pm 11)	10.6 (\pm 0.9)
PBS CV	139 (\pm 7)	11.2 (\pm 0.7)
NaOH	137 (\pm 8)	11.6 (\pm 0.3)
Na ₂ CO ₃	131 (\pm 4)	12.3 (\pm 0.4)
Untreated	178 (\pm 9)	8.5 (\pm 0.1)

From Table 2.2, the Na₂CO₃ pretreatment resulted in the largest peak current of 12.3 μ A (\pm 0.4) and smallest ΔE of 131 mV (\pm 4) which are a considerable improvement compared to the untreated values of 8.5 μ A (\pm 0.1) and 178 mV (\pm 9) respectively. As shown in the previous section, graphs of Log I_A vs Log ν for ferri/ferrocyanide didn't produce a slope of 0.5. Hence, the Randles Sevcik equation wasn't used to calculate electrode surface areas etc.

2.4.3 Electrochemical Characterisation at Pretreated Electrodes - Hexaamine Ruthenium (III) Chloride

Next, the same pretreatments were evaluated using hexaamine ruthenium (III) chloride which is an ideal outer sphere redox probe. In contrast to ferricyanide, hexaamine ruthenium (III) chloride is independent of surface oxides (discussed more fully in Chapter 1). Hence, non-surface oxide effects could be evaluated. Fig. 2.9 (with data tabulated in Table 2.3) shows that in contrast to the previous section all pretreatments have a similar effect on the electrochemical behaviour of the SPEs apart from the PBS CV pretreatment. In fact, there is a slight increase in ΔE , in contrast to the decrease that was observed for ferri/ferrocyanide. As can be observed from Fig 2.9 and table 2.3, there is only a slight difference in oxidation peak current. Similarly to ferri/ferrocyanide, CV cycling in PBS completely distorts the voltammogram with large oxidation current and background non-Faradaic current.

As mentioned previously, the electrodes displayed more ideal behaviour for hexaamine ruthenium (III) chloride as opposed to ferricyanide. Hence, electrochemical surface areas and % roughness could be calculated from the

Randles-Sevcik equation. The surface area was determined by equating the slope of a graph of the anodic peak current vs square root of scan rate (the actual graphs are displayed in section 2.5.4.1) to $268,600n^{3/2}AD^{1/2}C$. Hence, the electrochemical surface area could be calculated. The diffusion coefficient used was $8.4 \times 10^{-6} \text{ cm}^2/\text{s}$ [23].

Table 2.3: Oxidation and Reduction peak separation at pretreated electrodes in hexamine ruthenium (III) chloride

Pretreatment	ΔE (mV)	I_{PA}	A_{R-S} (cm ²)	% Roughness Factor
H ₂ SO ₄	134 (± 1)	4.5 (± 0.3)	0.669	94.2
PBS Anodic	130 (± 1)	4.07 (± 0.03)	0.0707	98.8
PBS CV	234 (± 1)	5.3 (± 0.7)	0.1638	203.1
NaOH	135 (± 1)	4.63 (± 0.02)	0.0742	104.5
Na ₂ CO ₃	136 (± 1)	4.73 (± 0.04)	0.0749	105.4
Untreated	116 (± 1)	4.41 (± 0.05)	0.0633	89.1

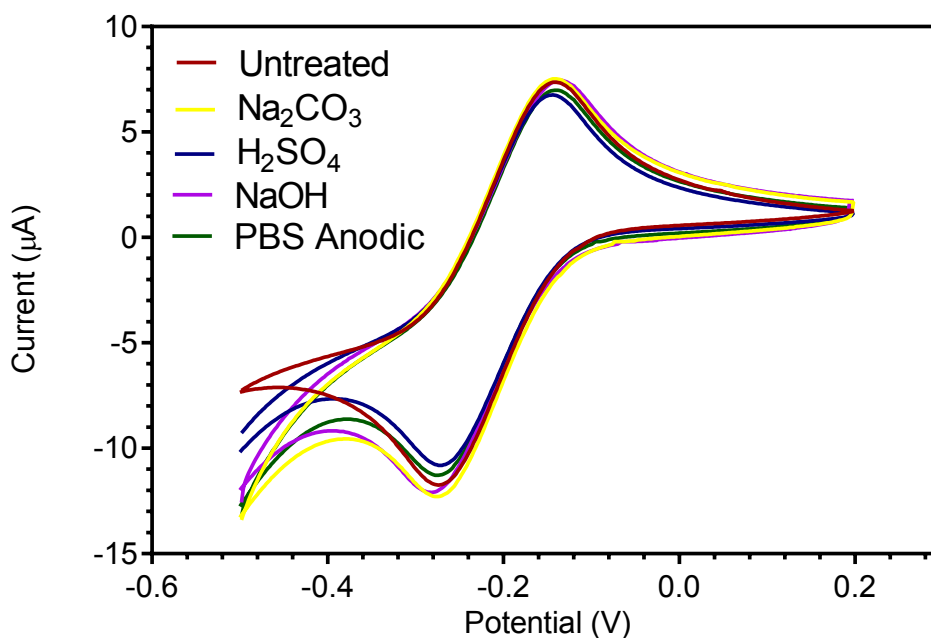


Figure 2.9: Comparison of different pretreatment procedures. Cyclic voltammograms were carried out at a scan rate of 100 mV s^{-1} in 1 mM hexamine ruthenium (III) chloride

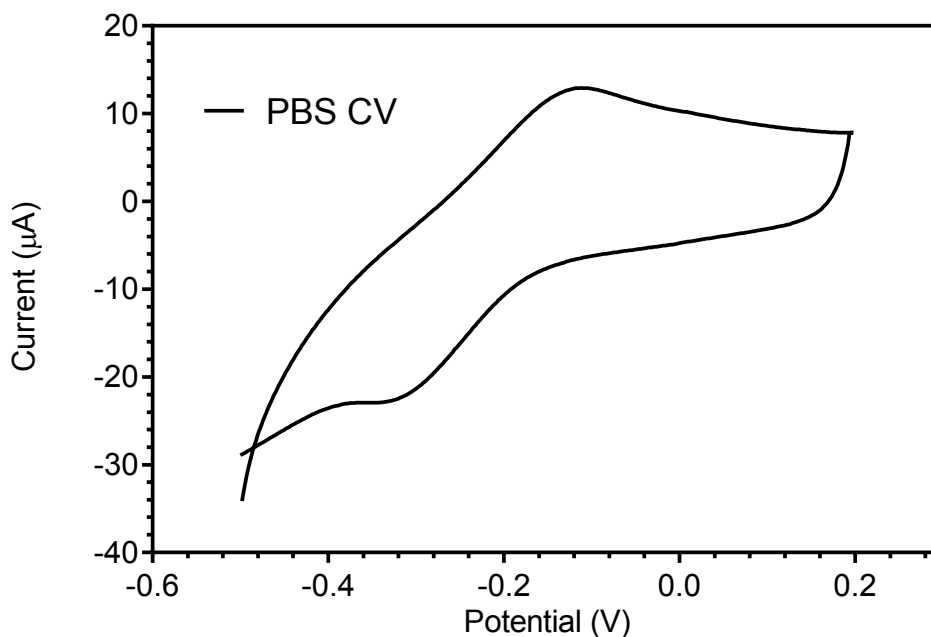


Figure 2.10: CV in PBS pretreated with 1 mM hexamine ruthenium (III) chloride in PBS pH 7.4 at a scan rate of 100 mV/s

2.4.4 Scan Rate Studies

Scan rate studies were carried out using both ferri/ferrocyanide and hexaammine ruthenium (III) chloride. Both showed a linear relationship between peak current and square root of scan rate indicating a diffusion limited response in all cases (Fig 2.11 and Fig 2.12) A shift in peak potential with increasing scan rate was also observed which is expected for a quasi reversible reaction. For a theoretically ideal 1 electron oxidation/reduction reaction this shift would not be observed. The individual results are displayed over the next two pages.

2.4.4.1 Scan Rate Studies - Hexaammine Ruthenium (III) Chloride

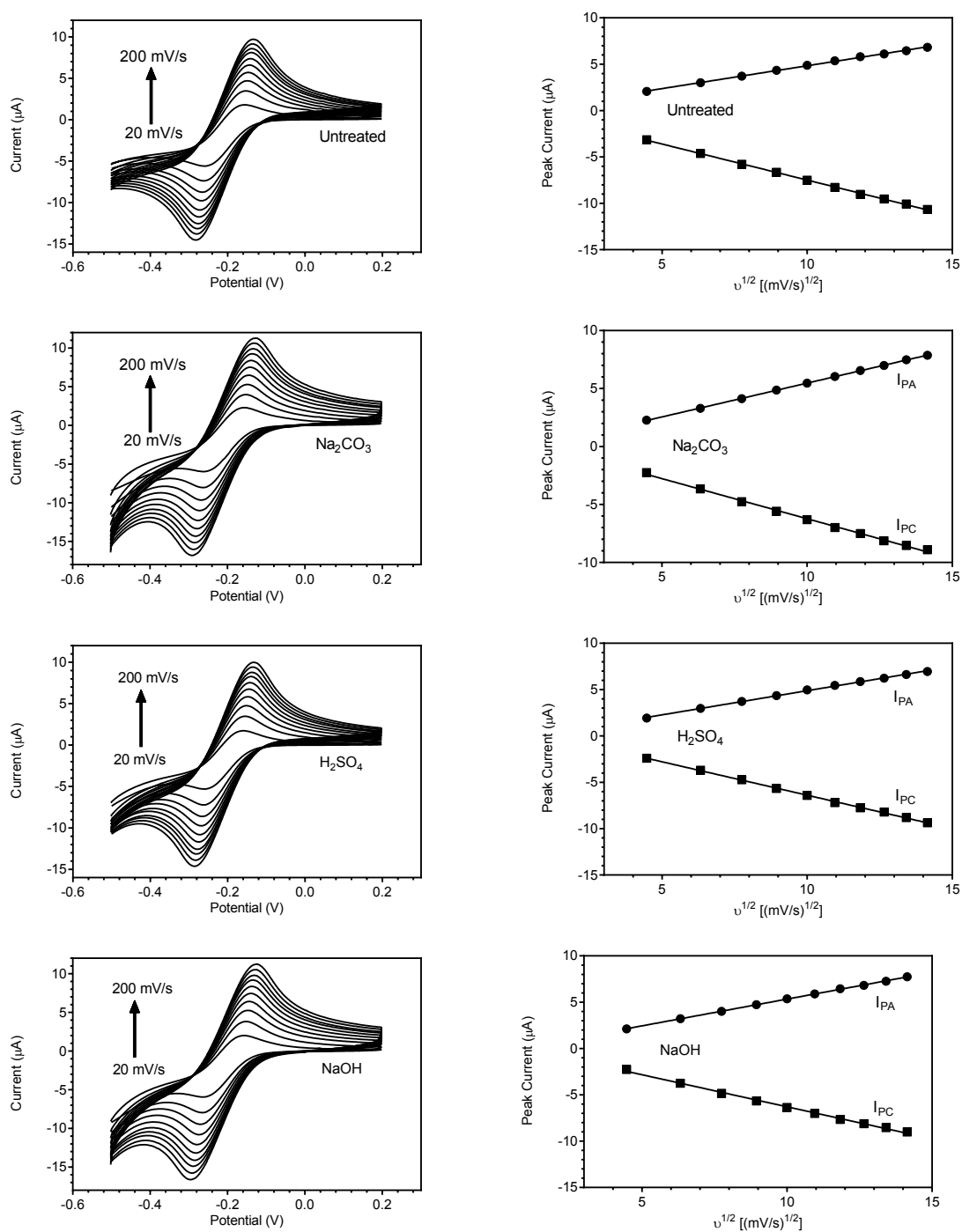


Figure 2.11: CVs at 20, 40, 60, 80, 100, 120, 140, 160, 180, 200 mV/s at pretreated electrodes in hexaammine ruthenium (III) chloride

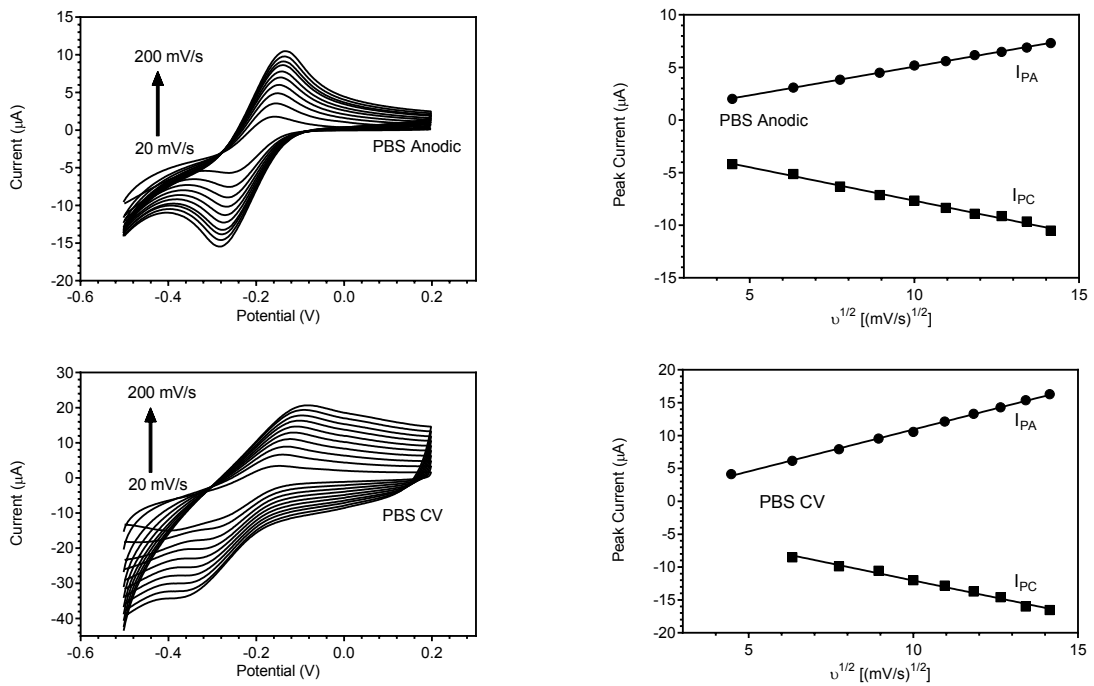


Figure 2.12: CVs at 20, 40, 60, 80, 100, 120, 140, 160, 180, 200 mV/s at each pretreated electrode in hexamine ruthenium (III) chloride

2.4.4.2 Scan Rate Studies - Ferri/Ferrocyanide

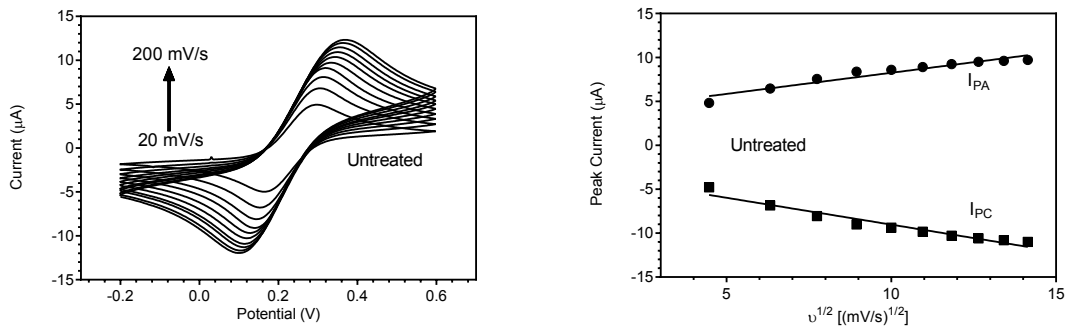


Figure 2.13: CVs of 1 mM Ferri/ferrocyanide at an untreated SPE at varying scan rates of 20, 40, 60, 80, 100, 120, 140, 160, 180, 200 mV/s

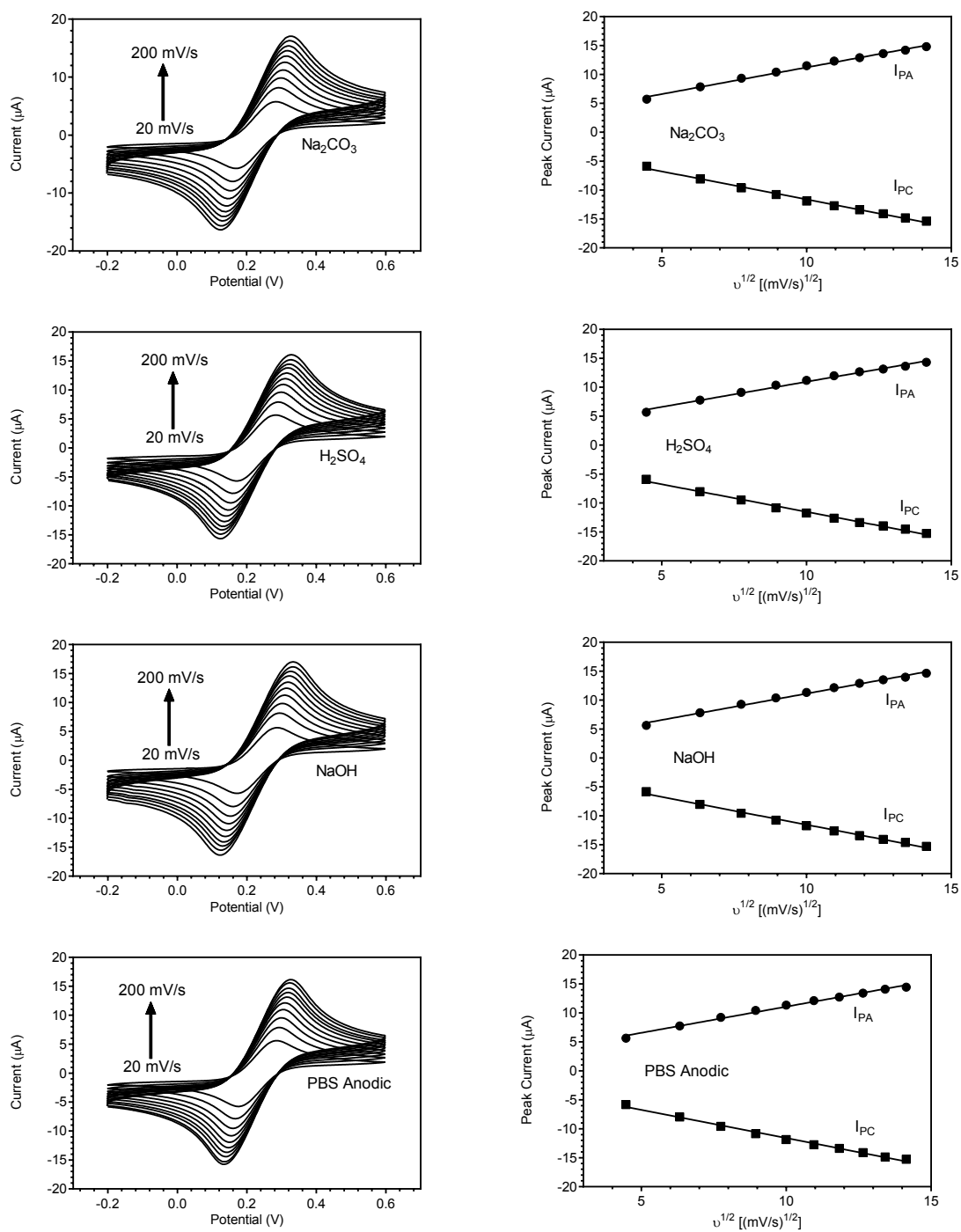


Figure 2.14: CVs of 1 mM Ferri/ferrocyanide at electrochemically pretreated SPEs at varying scan rates of 20, 40, 60, 80, 100, 120, 140, 160, 180, 200 mV/s

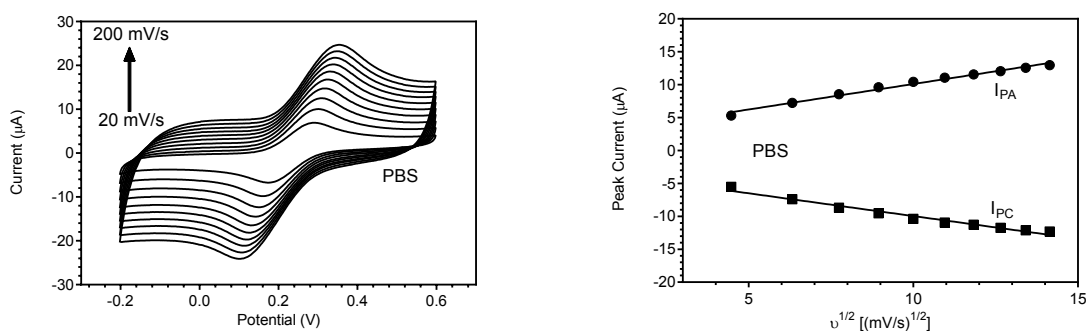


Figure 2.15: CVs of 1 mM Ferri/ferrocyanide at an SPE pretreated with PBS at varying scan rates of 20, 40, 60, 80, 100, 120, 140, 160, 180, 200 mV/s

2.4.5 Amperometric Detection of p-aminophenol

For electrochemical immunosensors utilising an alkaline phosphatase labelled secondary antibody, the electrochemically active compound p-aminophenol is produced from the enzyme reacting with a p-aminophenyl phosphate substrate. Hence, electrode materials that display a favourable response towards p-aminophenol should be promising for this type of immunosensor development. Hence, the pretreated electrodes were used to detect p-aminophenol amperometrically. This electrochemical technique is a common choice for immunosensor development. DEA buffer pH 9.5 was used as this is an optimal buffer system for the AP/pAPP reaction that will be used in subsequent sections of this thesis. 10 μ L additions of pAP were carried out at 20 second intervals as shown in Fig 2.16 at a fixed potential of 0.28 V. Normally a voltage of 0.3 V is used for p-aminophenol detection vs a Ag/AgCl but in this case 0.28 V is used due to the potential difference between the on chip and an external reference electrode (see section 2.6.3). It would appear indicate that the PBS anodic pretreatment provides the greatest improvement in analytical signal compared to the bare electrode.

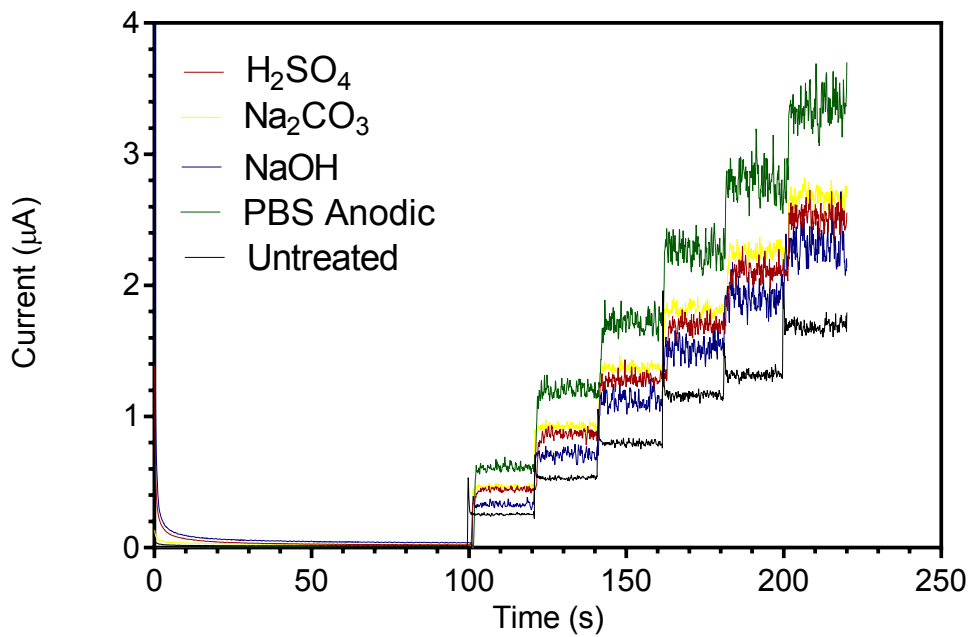


Figure 2.16: Standard addition of 5mM stock solution of pAP to DEA buffer pH 9.5 under stirred conditions at bare and electrochemically pretreated electrodes

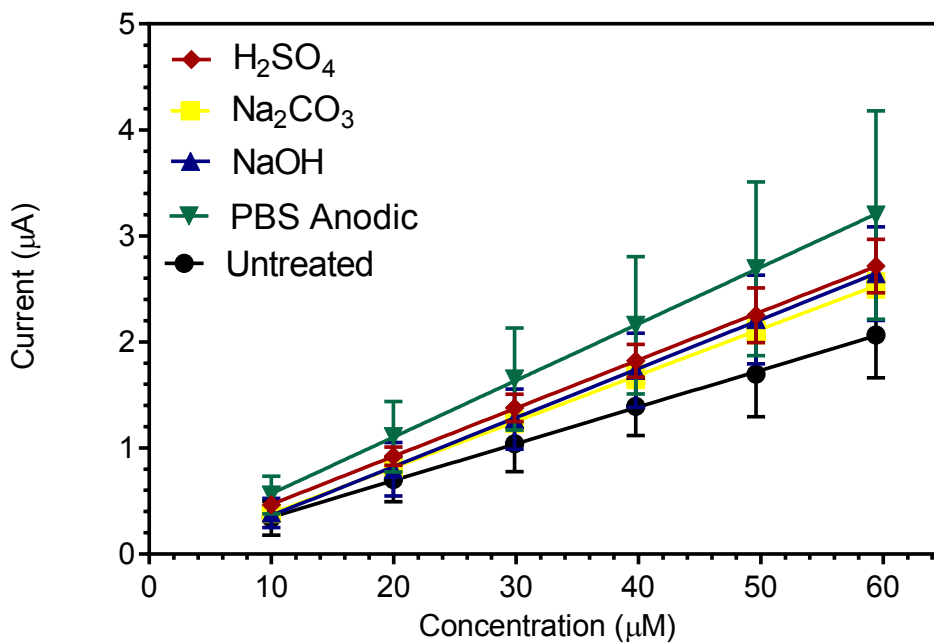


Figure 2.17: Calibration curve for p-aminophenol at concentrations of 10, 20, 30, 40, 50, 60 μM

This can be seen further confirmed by viewing the calibration curve (Fig. 2.17 above) and analysis of the calibration curve sensitivities (Table 2.4 below).

However, upon carrying out an ANOVA analysis on the calibration curve for each electrode a P value of 0.05748. In other words if the slopes were identical there is a 5.7 % chance of randomly choosing data points with slopes this different. Hence, there is no significant difference between all slopes/sensitivities.

Table 2.4: Sensitivity for amperometric p-aminophenol detection at pretreated electrodes

	Slope/Sensitivity ($\mu\text{A}/\mu\text{M}$)	R ²
H ₂ SO ₄	0.0454	0.0966
Na ₂ CO ₃	0.0435	0.9887
NaOH	0.0462	0.8927
PBS Anodic	0.0534	0.7497
Untreated	0.0346	0.8507

2.5 X-ray Photon Spectroscopy (XPS)

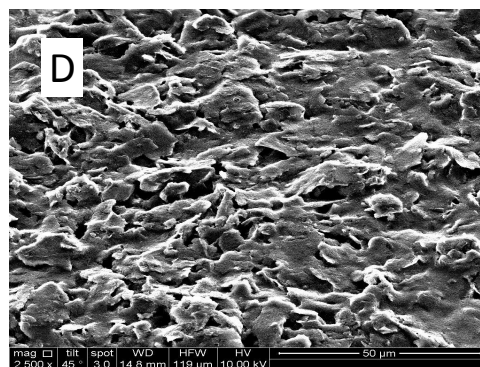
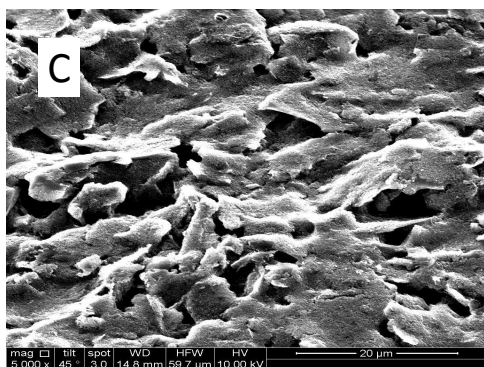
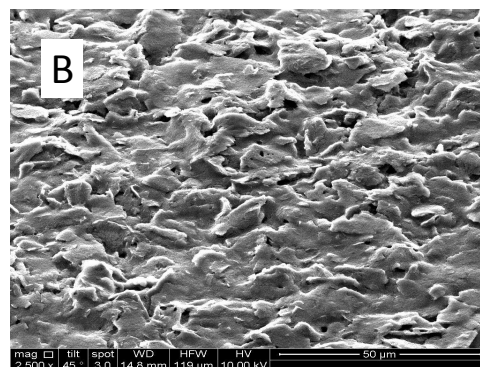
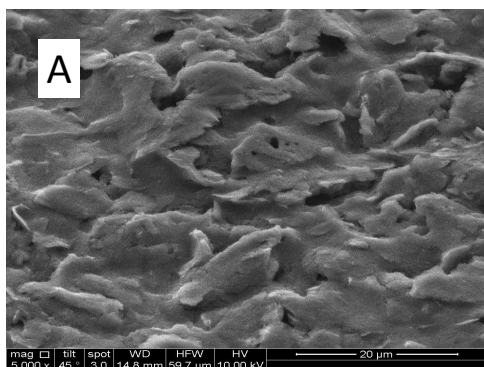
XPS measurements were carried out in order to further investigate the role of oxygen functionalities and polymeric binder in the electrochemical activity of pretreated SPEs. The XPS spectra for the bare and pretreated electrodes (shown in Appendix A), display characteristic binding energies for the C 1s peak at 285 eV, Cl 1s peak at 200 eV and O 1s peak at 520 eV. Unfortunately, it was not possible to de-convolute the C 1s peak to establish the exact nature of the oxygen functionalities created by the pretreatments as had been achieved in some other studies [24, 25]. This was due to the insensitivity of the instrumentation involved. Interestingly though, the dramatic drop in polymer binder (Cl content) was observed for the H₂SO₄ pretreatment.

Table 2.5: Atomic %s of carbon, oxygen and chlorine at the surface of pretreated SPEs

Pretreatment	C 1s At %	O 1s At %	Cl 2p At %
Untreated	80.65	11.16	8.2
Na ₂ CO ₃	81.85	6.68	11.47
H ₂ SO ₄	79.79	14.38	5.84
NaOH	77.84	11.11	11.05
PBS Anodic	81.15	11.22	7.63
PBS CV	79.33	10.99	9.68

2.5.1 Scanning Electron Microscopy (SEM)

SEM images were taken at both untreated and modified electrodes (Fig. 2.18). It is not obvious from the two magnifications used (5000x and 2500x) that there is any significant change in the surface morphology of the electrodes after pretreatment in comparison to the untreated electrode (A and B). This is in contrast to Cui et. al who suggested that SEM of Na₂CO₃ pre-anodised electrodes showed clear evidence of the removal of polymeric binder [9].



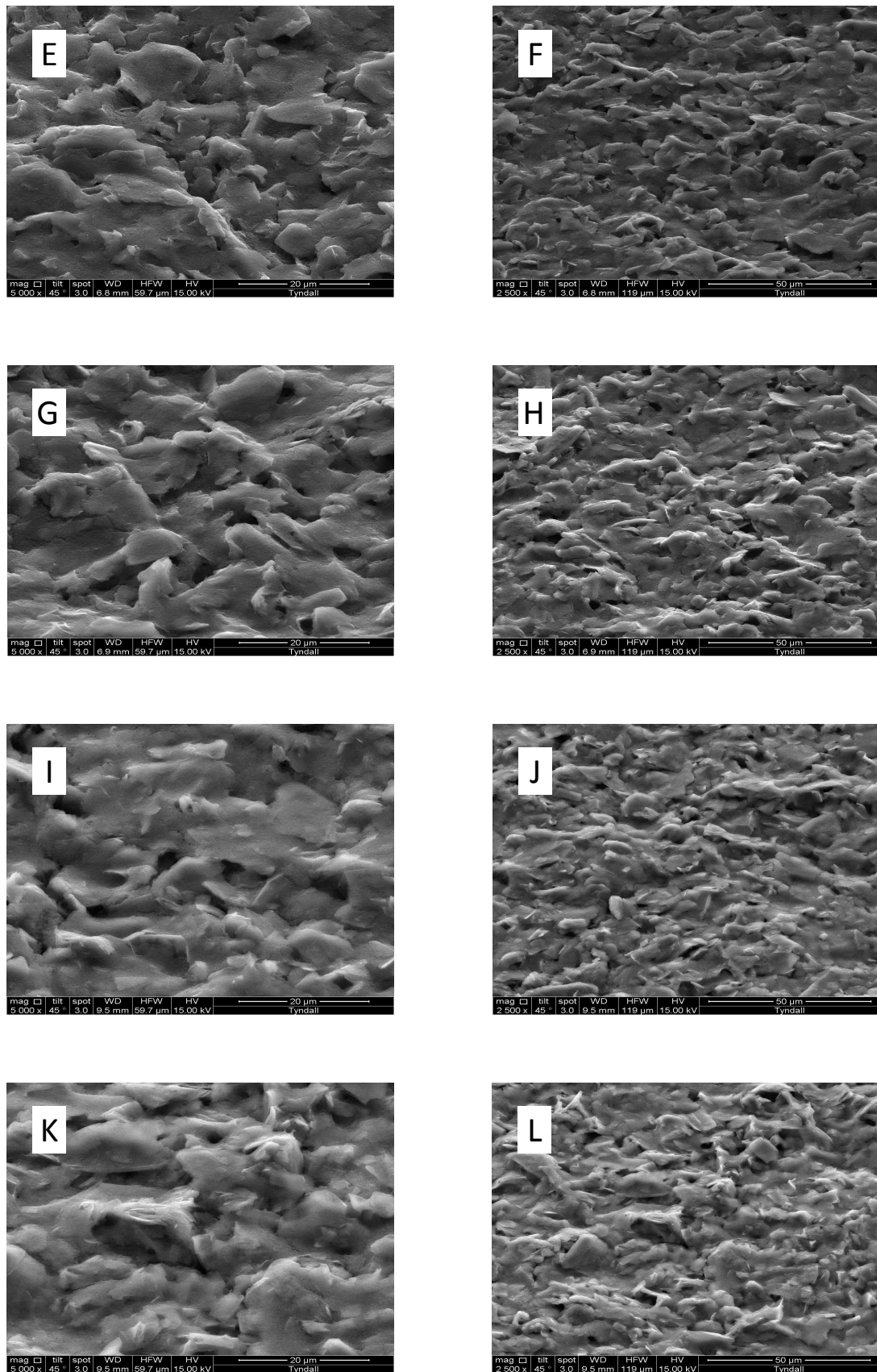
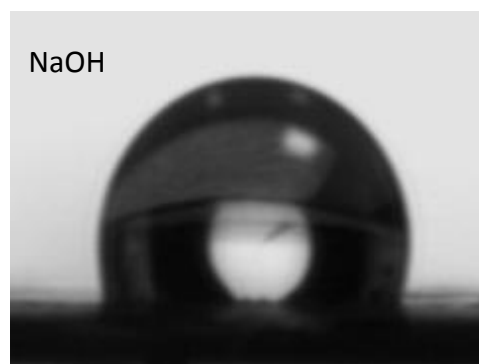
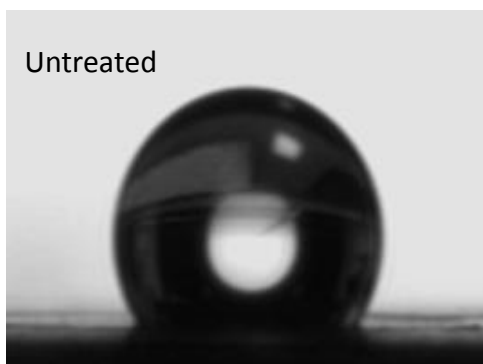


Figure 2.18: Scanning Electron Micrographs of untreated (A,B), Na_2CO_3 (C,D), H_2SO_4 (E,F), NaOH (G,H), PBS Anodic (I,J), PBS CV (K,L)

2.5.2 Contact Angle Measurements

Analysis of the hydrophilicity of the electrodes after each pretreatment was carried out using contact angle measurements. As seen from Fig. 2.19 and more accurately from table 2.6, the contact angle decreases at each pretreated electrode. This is most pronounced for the electrode pretreated by CV scans in PBS and least pronounced for the NaOH pretreatment. This suggests that the PBS treated electrode has the greatest surface roughness compared to the other electrodes. This is in agreement with the electrochemical measurements above. Oxygen functionalities can also have an impact on surface/water interactions. For example, it has been shown that freshly cleaved HOPG surfaces can display an increase of contact angle of 25° after 10 seconds of exposure to ambient air (from $64-90^\circ$) [26]. It has been reported extensively that the water contact angle for graphite is in the $75-95^\circ$ range [27, 28] Therefore, it would suggest that the larger contact angles observed at the bare screen printed electrode is due to the polymeric binder present in the graphite ink and also a contribution from ambient contamination in air.



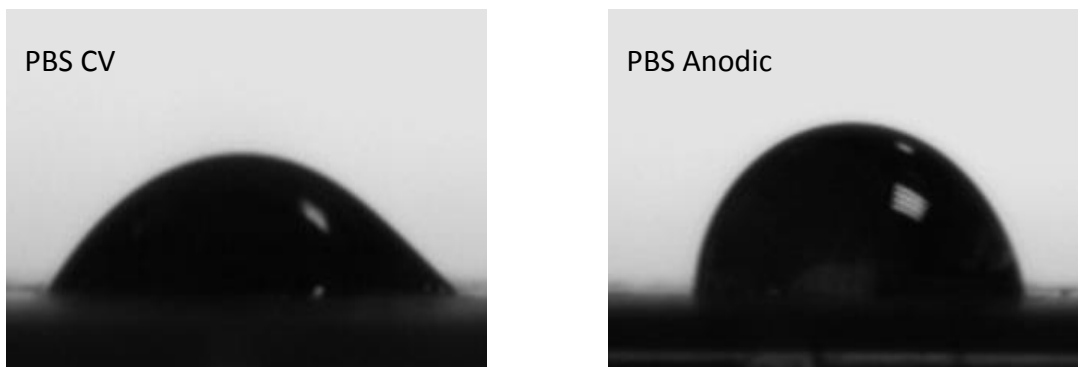


Figure 2.19: Contact Angle (degrees) at pretreated electrodes resultant from 2 μL of water being dispensed on the working electrode surface

Table 2.6: Contact angles at untreated and electrochemically pretreated electrodes

Electrode Pretreatment	Contact Angle
Untreated	130.05 ± 3.15
H_2SO_4	71.0 ± 0.8
NaOH	110.00 ± 3.64
Na_2CO_3	82.6 ± 2.7
PBS Anodic	81.45 ± 1.48
PBS CV	58.95 ± 12.35

2.5.3 Reference Electrode

The performance of the on-chip Ag/AgCl paste reference electrode was compared to a commercially available Ag/AgCl electrode. A difference of 0.2 V was observed in the measurement of the potential of oxidation of ferri/ferrocyanide redox couple can be seen in Fig. 2.20. The stability of the reference electrode was then examined through the use of open circuit potential measurements. After a settling of the potential after 1 hour, it remained stable for up to 5 hours (Fig. 2.21).

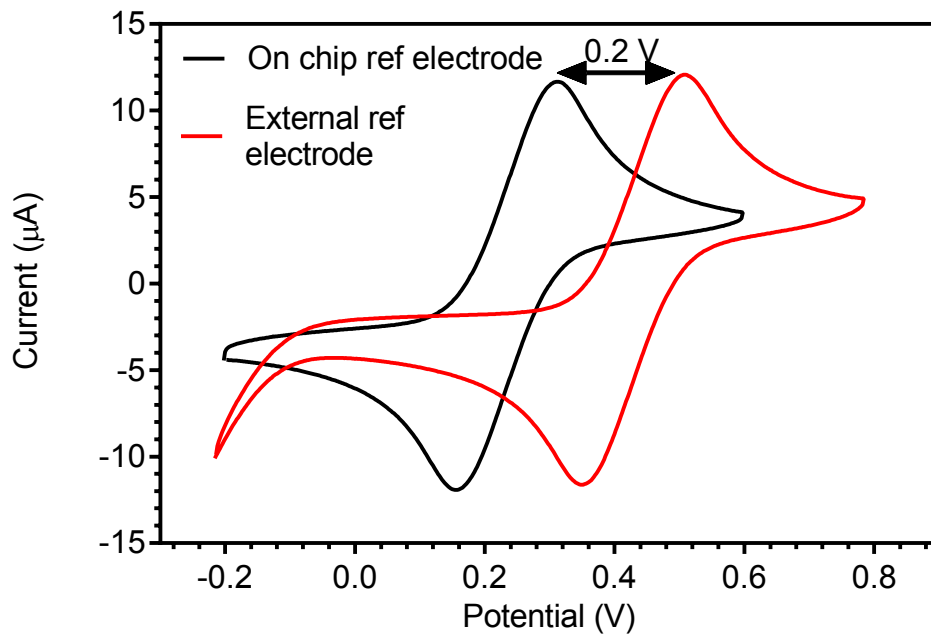


Figure 2.20: Comparison of on chip and external reference electrode at bare screen printed electrode. CV carried out at a scan rate of 100 mV s^{-1} in $1 \text{ mM } [\text{Fe}(\text{CN})_6]^{3-/4-}$

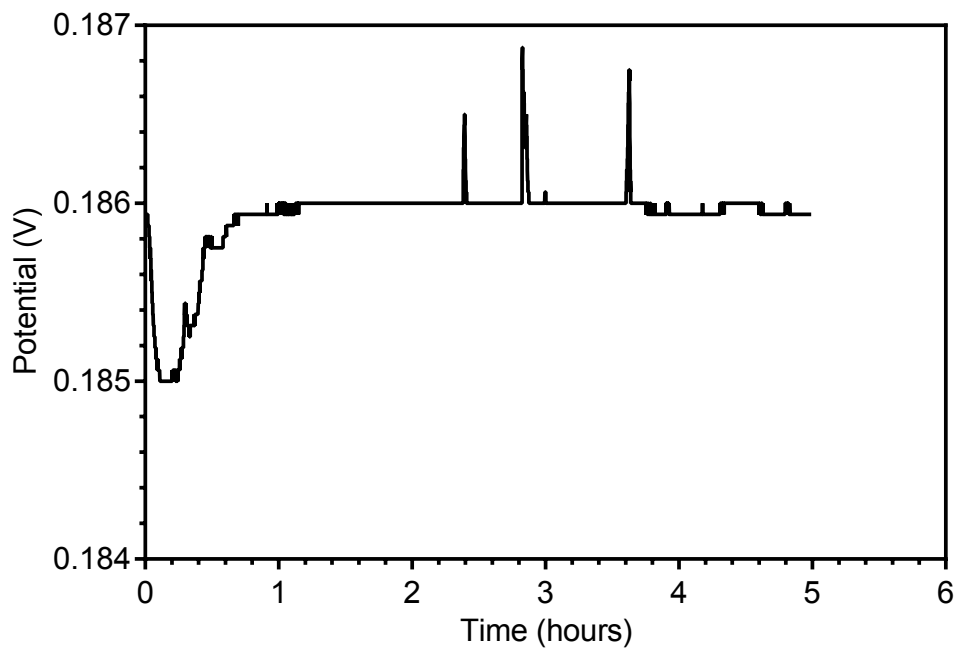


Figure 2.21: Open Circuit Potential (OCP) measurement for 5 hours in 1 M KCl

2.6 Part 2 - Immunoassay Development

In part two of this chapter, a competitive electrochemical immunosensor for mouse IgG is developed using a screen printed electrode pre-anodised in saturated Na_2CO_3 which showed the most promising electrochemical properties as outlined in part one. Firstly, an ELISA was developed and subsequently the method was then transferred to the pre-anodised electrode.

2.6.1 Capture ELISA

The first step in ELISA development was to carry out a capture assay in which a 1/5 serial dilution of primary IgG was added in triplicate to an ELISA plate, followed by washing, blocking measurement as described in section 2.4.12.1. The purpose of this assay was to establish a coating antibody concentration that could be used in the competitive assay and also to establish the affinity of the mouse IgG to the AP-labelled anti-mouse secondary antibody. A schematic for this assay is shown in Fig. 2.22.

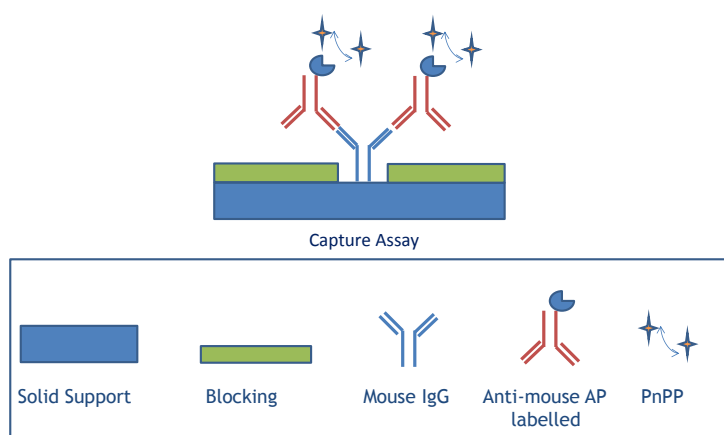


Figure 2.22: Schematic of Capture assay for mouse IgG whereby IgG binds to AP labelled anti-mouse IgG

It can be seen from Fig. 2.23 that saturation is achieved at a primary IgG concentration of around 0.04 mg/mL.

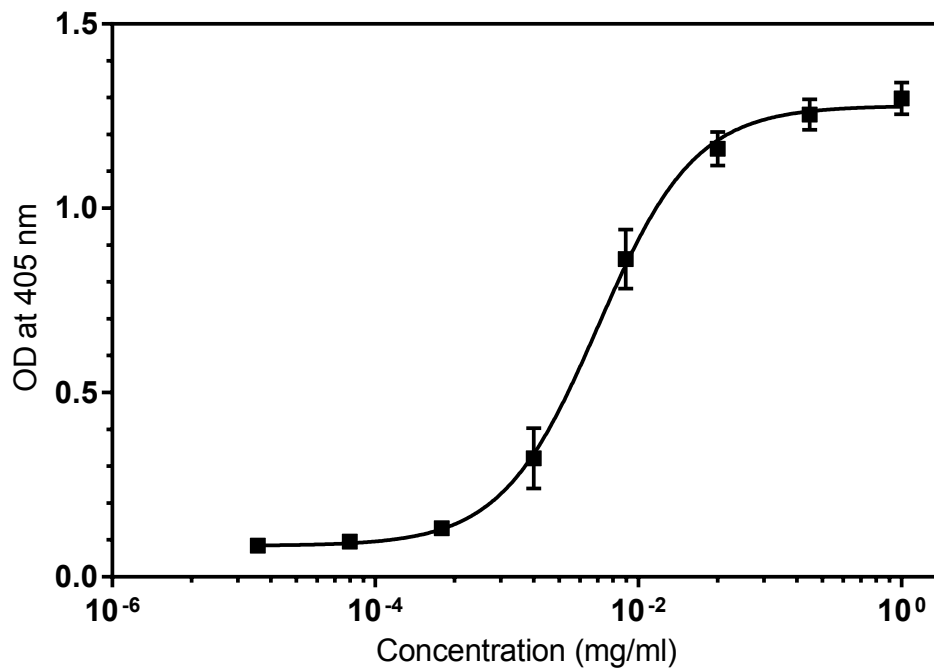


Figure 2.23: Capture assay varying mouse IgG concentration from 1 mg/mL to 13×10^6 mg/mL with a fixed AP labelled anti-mouse dilution of 1/30,000. $R^2 = 0.9932$, $n = 3$.

2.6.2 Competitive ELISA

Next, a competitive ELISA was carried out in which a fixed concentration of IgG on the surface of the plate and free IgG in solution (varying concentration) competed to bind with a fixed amount of enzyme labelled secondary antibody. This format, as seen in Fig. 2.24, is equivalent to that used by Kreuzer et. al for IgE detection in blood samples [29].

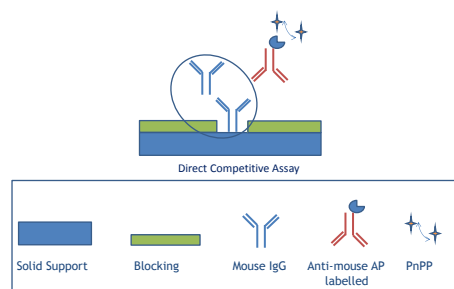


Figure 2.24: Schematic of a competitive assay with immobilised IgG competing with free IgG to bind to AP labelled anti-mouse IgG

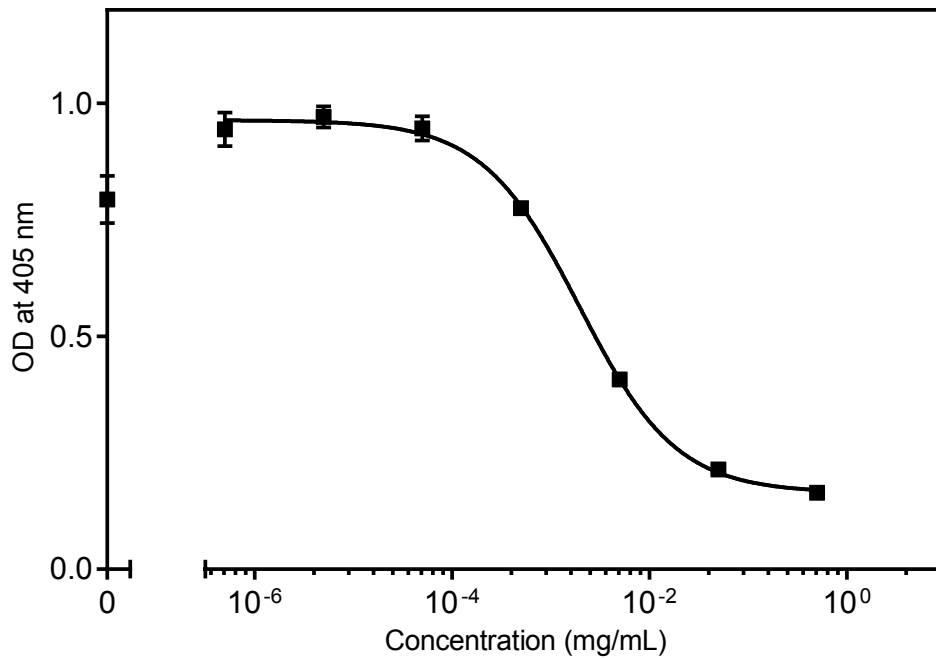


Figure 2.25: Competitive ELISA with coating IgG concentration of 0.04 mg/mL. $R^2 = 0.9965$, $n = 3$.

A fixed concentration of 0.04 mg/mL was used to coat the surface of the plate as this concentration gave a saturated coverage of IgG as described in the previous section. However, as can be seen in Fig. 2.25, the zero concentration gave an absorbance reading below that of the lower concentrations. This is tentatively attributed to the low dose hook effect which is occasionally seen in competitive assays [30, 31].

In order to deal with this issue Xu et. al recommend a number of possible solutions [31]. Two of these were investigated namely, decreasing the coating antibody concentration and increasing the time allowed in the assay for competition. Firstly, the coating antibody concentration was decreased to 0.008 mg/mL which from Fig. 2.26 can be seen to have a positive effect on removing the hook effect. However, a slight decrease in zero concentration still remains.

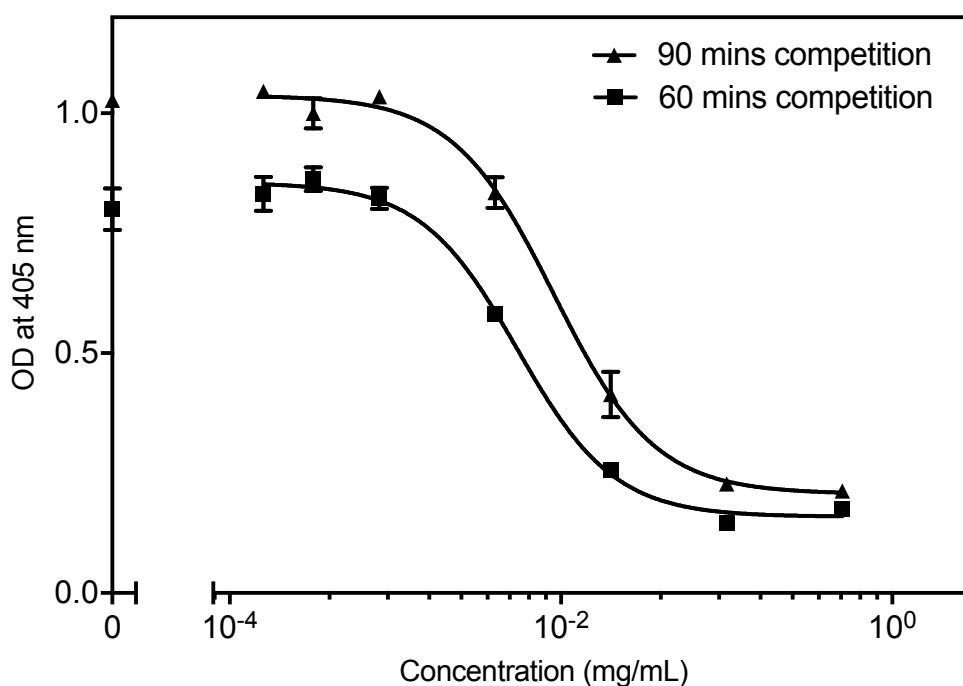


Figure 2.26: Competitive ELISAs with coating IgG concentration of 0.008 mg/mL and two different competition step times - 60 mins and 90 mins. $n = 3$.

Next, using this decreased coating antibody concentration, the assay competition time was increased from 60 mins to 90 mins. The combination of this change in assay time and decreased competition time fully eliminated this low dose hook effect as seen in Fig. 2.26. The analytical parameters for this finalised assay are given in the table below.

Table 2.7: Analytical Performance of Competitive Immunoassay for Mouse IgG Detection

LOD	IC50	Linear Range	R ²
0.75 ppm	9.079 ppm	3.071 - 26.83 ppm	0.9942

2.6.3 Control Assays

Finally, control assays were carried to fully quantify the role each step takes in the optimised protocol (Fig. 2.27). Unsurprisingly, without either the secondary antibody or pNPP substrate very low absorbance signals were produced, as without the enzyme or substrate no reaction leading to a colour change could

occur. Also, without the primary antibody there was very little binding of the secondary antibody to the surface of the plate meaning that the blocking solution of 1 % BSA was effective in preventing non-specific binding of the secondary antibody. The role of the blocking solution can be further seen in the assay carried out without BSA. The higher than normal absorbances indicate that the secondary antibody is binding to the plate, giving absorbances not related purely to mouse IgG concentration. Also, higher absorbances are seen in the situation in which washing buffer is not used as the free antibody which binds to the anti-mouse secondary antibody is not fully washed away after the competition step.

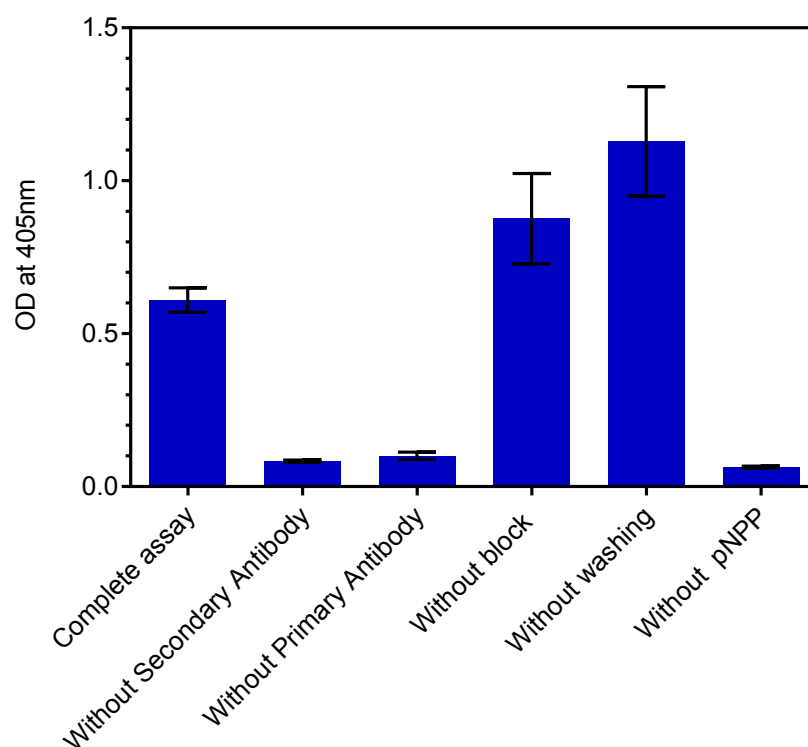


Figure 2.27: Competitive assay for 0.002 mg/mL IgG - absorbances for full assay for assay missing one step of the protocol

2.6.4 Electrochemical Capture Assay

After establishing an optimised ELISA procedure for mouse IgG detection, this method was then transferred to a pre-anodised screen printed electrode. Similar steps in assay optimisation were carried out as those described in the previous sections for optical detection. Firstly, a capture assay was carried

out using the same parameters as those used for the Capture ELISA, except incubations were carried out at room temperature as opposed to 37° C to avoid evaporation of the small volumes of liquid used.

It can be clearly seen from Fig. 2.28 that along with the poor reproducibility of the results, there is very little separation between the signal achieved for low and high IgG concentrations.

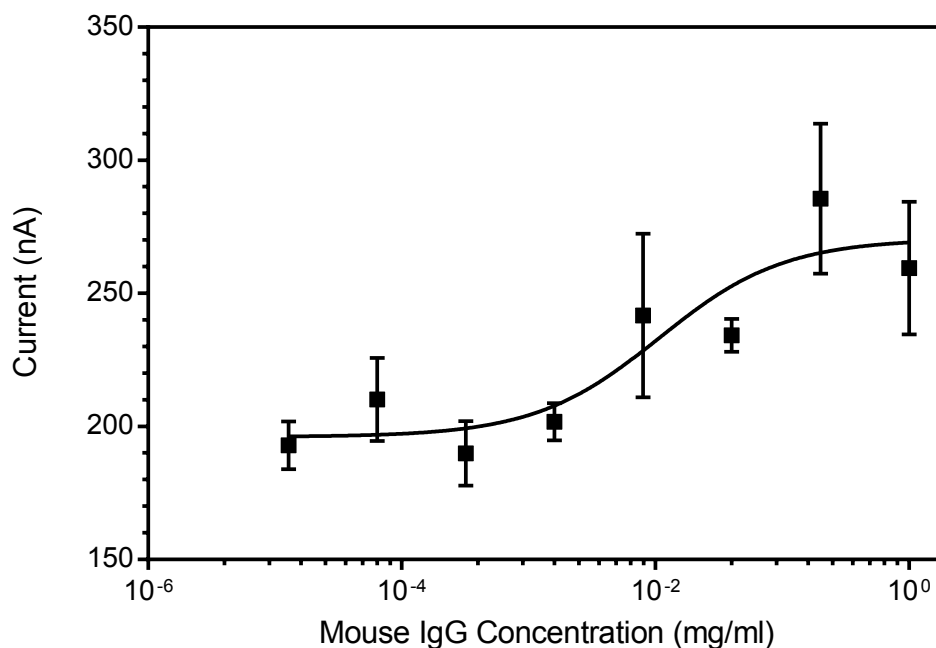


Figure 2.28: Electrochemical capture assay varying coating antibody concentration from 1 mg/mL to 0.000013 mg/mL. $R^2 = 0.6771$, $n = 3$.

Clearly, optimisation of the assay components was required. Hence, capture assays were performed using a fixed concentration of mouse IgG and varying secondary antibody dilution. Blank results were included (0 mouse IgG) to ensure that increased secondary antibody concentration didn't also lead to an increase in non-specific binding of the secondary antibody to the sensor surface. Fig. 2.29 shows that a dilution of 1/1000 anti-mouse IgG gave a large current signal without a significant amount of non specific binding and hence this dilution was used for all further assays.

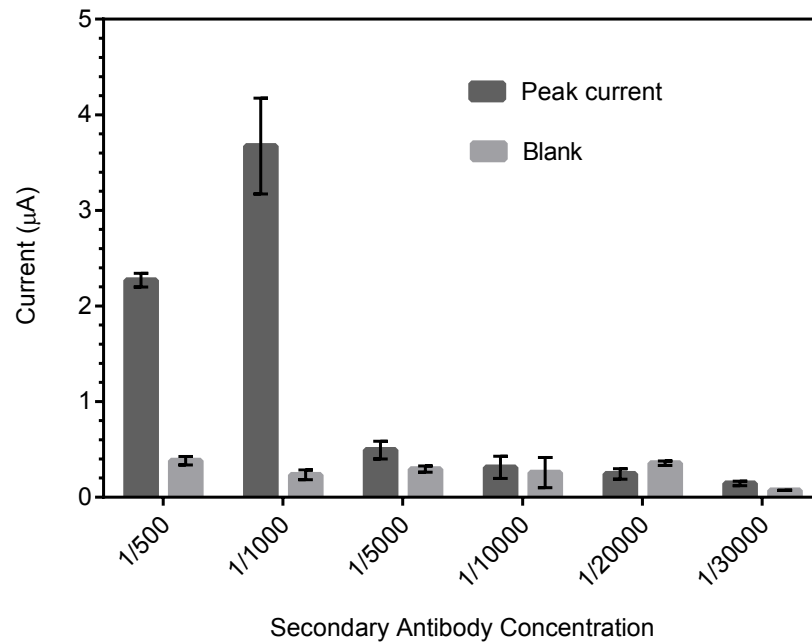


Figure 2.29: Optimisation of AP labelled anti-mouse IgG concentration

The capture assay was then repeated using the optimised secondary antibody concentration (Fig. 2.30) showing a significantly improved result with saturation being achieved at a concentration of 0.2 mg/mL IgG.

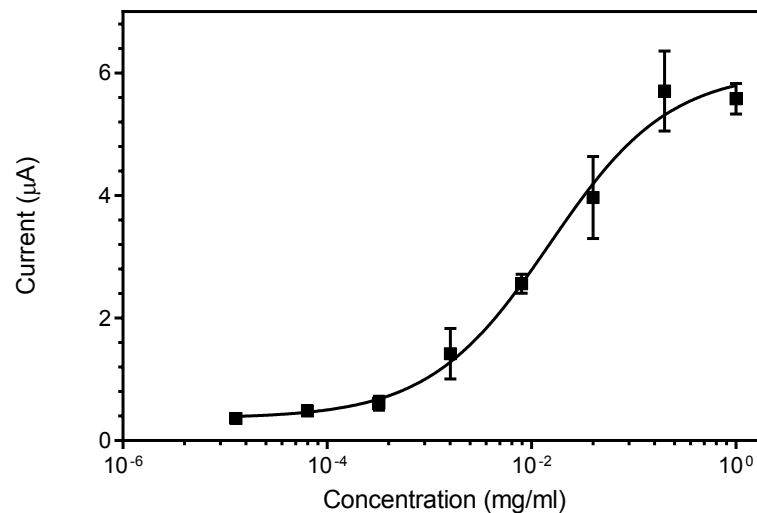


Figure 2.30: Electrochemical capture assay for mouse IgG using an AP labelled anti-mouse dilution of 1/1000. $R^2 = 0.971$

2.6.5 Electrochemical Competitive Assay

A competitive assay was then carried out using the coating antibody concentration of 0.2 mg/mL. Again low dose hook effect was observed (Fig. 2.31).

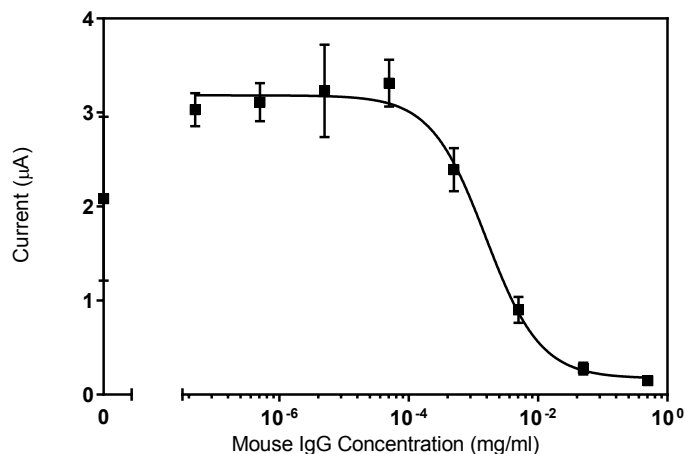


Figure 2.31: Competitive Electrochemical Immunoassay with a coating antibody concentration of 0.2 mg/mL exhibiting low dose hook effect

The same approach was taken to solving this issue as for competitive ELISA. So, competition incubation time was increased to 90 mins and the coating antibody concentration was decreased to 0.04 mg/mL. The results are seen in Fig. 2.32.

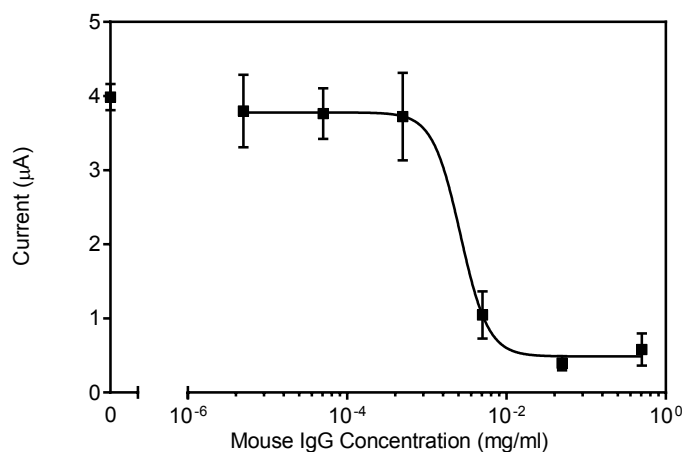


Figure 2.32: Finalised competitive Electrochemical Immunoassay for Mouse IgG detection at an electrochemically pretreated screen printed electrode with a coating antibody concentration of 0.04 mg/mL and competition incubation time of 90 minutes. $R^2 = 0.9608$, $n = 3$.

Table 2.8: Analytical Performance of Electrochemical Immunoassay

LOD	IC50	Linear Range	R ²
0.925 ppm	2.644 ppm	1.4 - 4.9 ppm	0.9608

2.7 Part 3 - Development of Electrochemical Immunosensor at Nanocarbon modified Electrodes

In this section, similar analysis is carried out to that undertaken in parts 1 and 2 of this chapter. However, in this part, carbon nanomaterial modified electrodes are used. In particular, multiwalled carbon nanotubes (MWCNTs) and reduced graphene oxide (RGO) are compared.

2.7.1 Optimisation of Nanomaterial Concentration and Solvent

The first step in optimising the nanomaterial modified electrodes was to choose a suitable nanomaterial concentration and solvent. Using a solvent of 1:1 DMF to water [32], a comparative study of various concentrations of RGO and COOH-MWCNTs was carried out after sonication for at least 1 hour. From an initial visual test as seen in Fig. 2.33 and Fig. 2.34, dispersion of the RGO sheets was more successful than that achieved for the MWCNTs, particularly in the case of concentrations of 1 mg/mL.

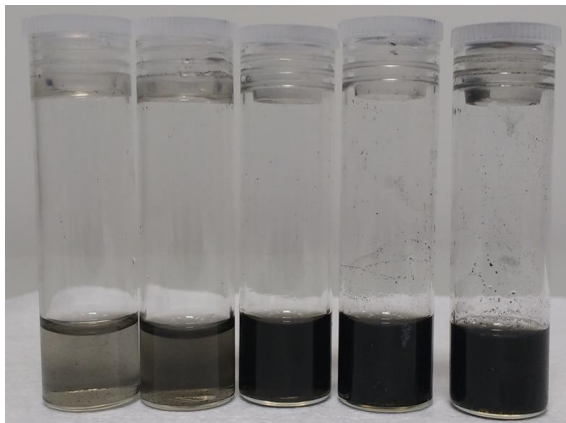


Figure 2.33: RGO solutions at concentrations of 0.05, 0.1, 0.3, 0.5 and 1 mg/mL (left to right) in 1:1 water/DMF



Figure 2.34: MWCNT solutions at concentrations of 0.05, 0.1, 0.3, 0.5 and 1 mg/ml (left to right) in 1:1 water/DMF

CVs were carried out at each concentration in 500 μM of p-aminophenol. From Fig. 2.35 it can be seen there is an increase in oxidation peak current with a corresponding increase in background non-Faradaic current.

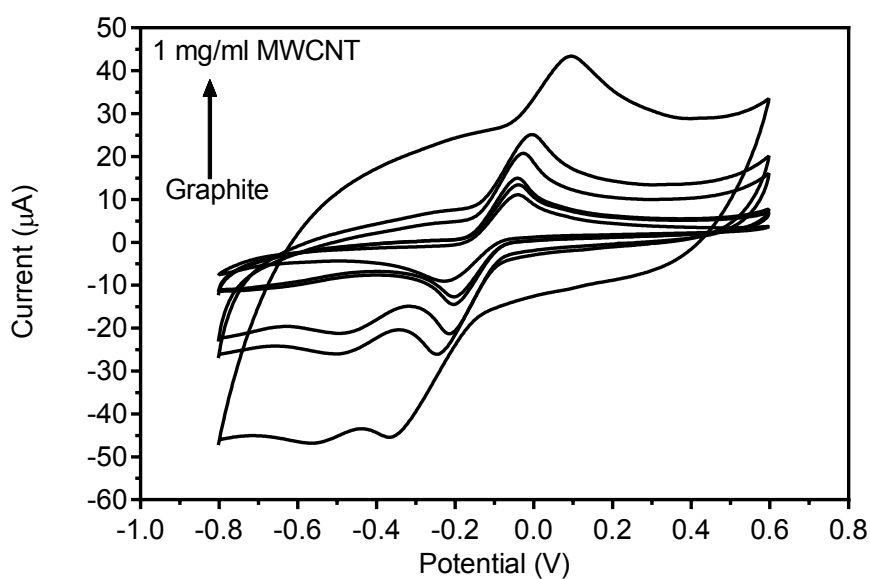


Figure 2.35: CV of 500 μM p-aminophenol in a supporting electrolyte of 0.1 M DEA buffer with a scan rate of 100 mV/s at graphite and MWCNT modified electrodes of the following concentrations: 0.05, 0.1, 0.3, 0.5 and 1 mg/mL

Despite the increase in background current, the overall net peak current still increases in a near linear fashion with increasing MWCNT concentration as seen in Fig. 2.36.

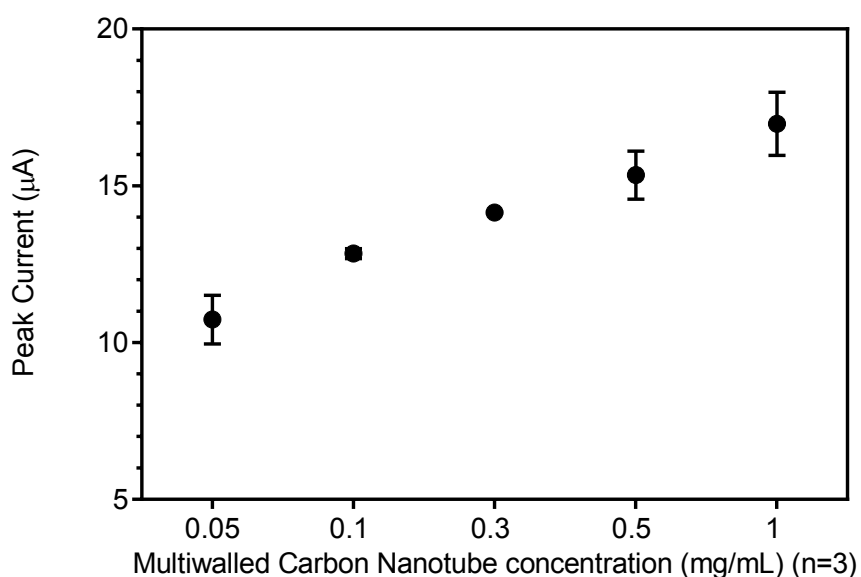


Figure 2.36: Peak anodic current from CV of MWCNT modified electrodes of varying concentration (from Fig. 2.32)

Similarly, an increase in RGO concentration corresponds to an increase in peak current (Figs. 2.37 and 2.38). Interestingly however, this increase doesn't produce a current value greater than that of graphite - despite the fact that graphite is the underlying substrate. This would indicate that the DMF/water solvent itself has a negative effect on the electrochemical characteristics of the electrodes.

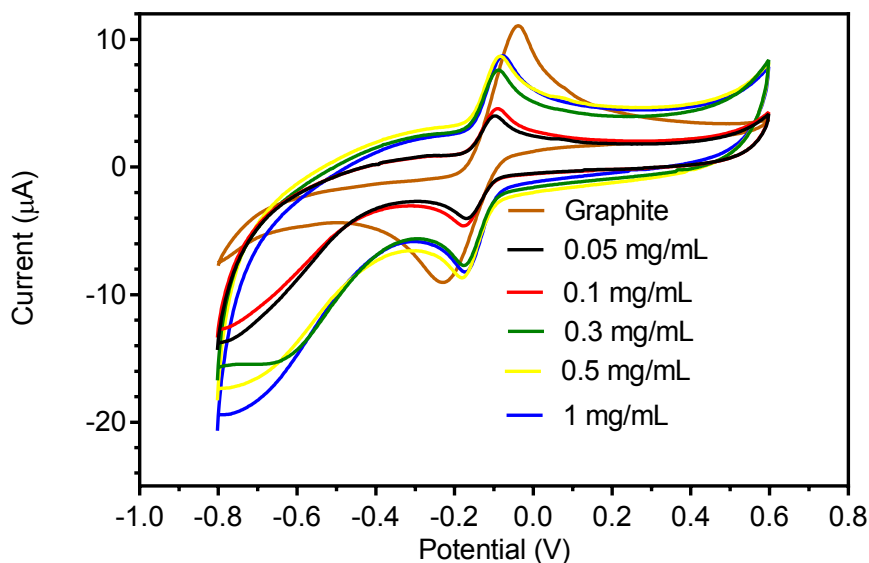


Figure 2.37: CV of 500 μM p-aminophenol in a supporting electrolyte of 0.1 M DEA buffer at graphite and RGO modified electrodes of the following concentrations: 0.05, 0.1, 0.3, 0.5 and 1 mg/mL

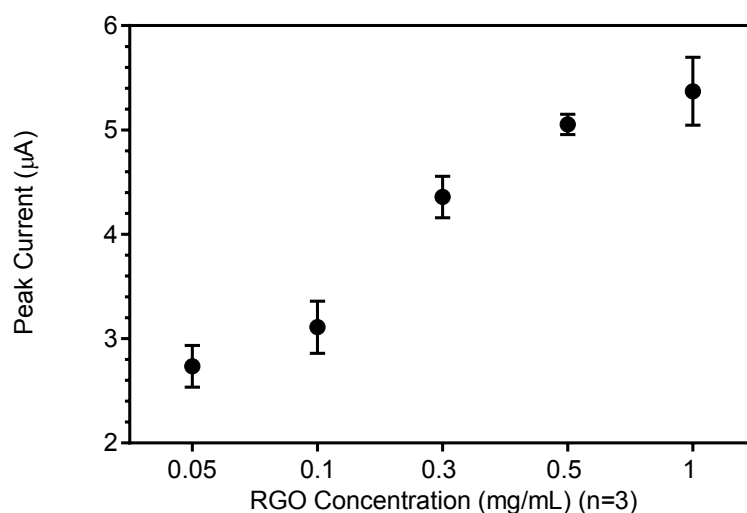


Figure 2.38: Peak anodic current from CV from RGO modified electrodes of varying concentration (from Fig. 2.37)

From these electrochemical measurements it was deemed that 1 mg/mL was an optimal concentration of both RGO and MWCNT. Prior to further comparison, these concentrations were then dispersed in Nafion to see the effect of a different solvent. From Fig. 2.39 it is evident that Nafion improves the dispersion of the nanotubes in agreement with the work of Wang [33].

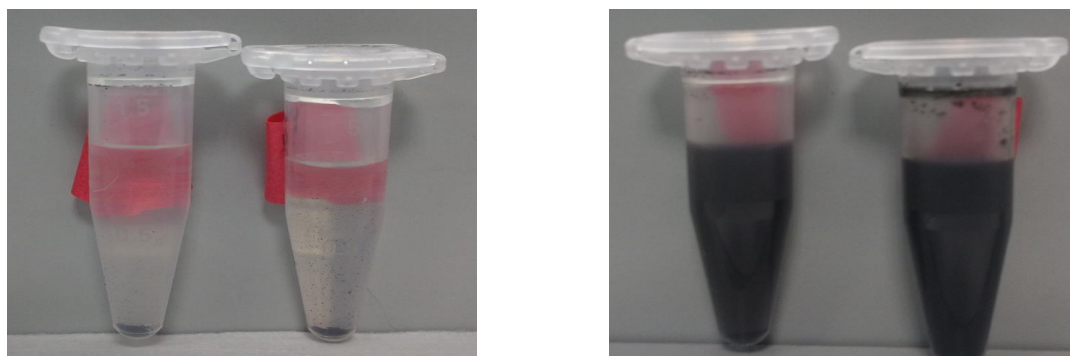
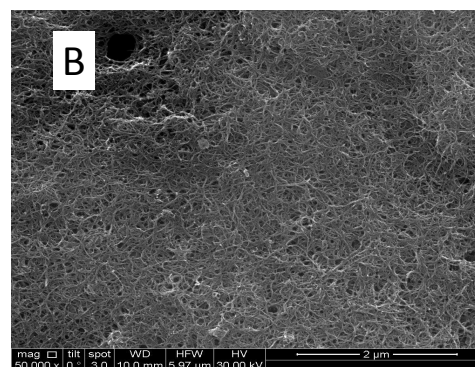
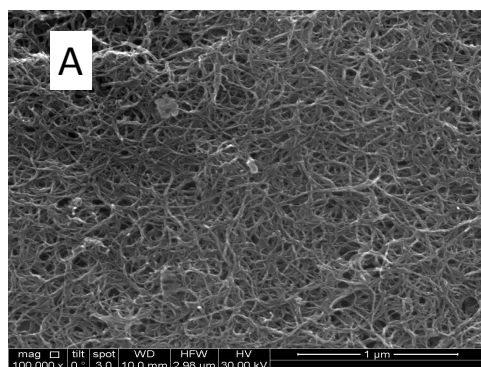


Figure 2.39: MWCNT/Nafion and RGO/Nafion solutions of 1 mg/mL in 0.5 % Nafion before and after sonication

2.7.2 Electrode Characterisation

2.7.2.1 SEM

SEM measurements revealed that in the case of both solvents (DMF/water and Nafion), MWCNTs completely covered the electrode surface. However, this was not the case for RGO. Images E-H in Fig. 2.40. show that RGO only partially covers the electrode. This suggests that any electrochemical behaviour at these electrodes can be attributed to a mixture of graphite and RGO characteristics. In particular, at the RGO/Nafion electrode only small amounts of the dropcast material (highlighted in the red boxes) appeared to have attached to the graphite substrate.



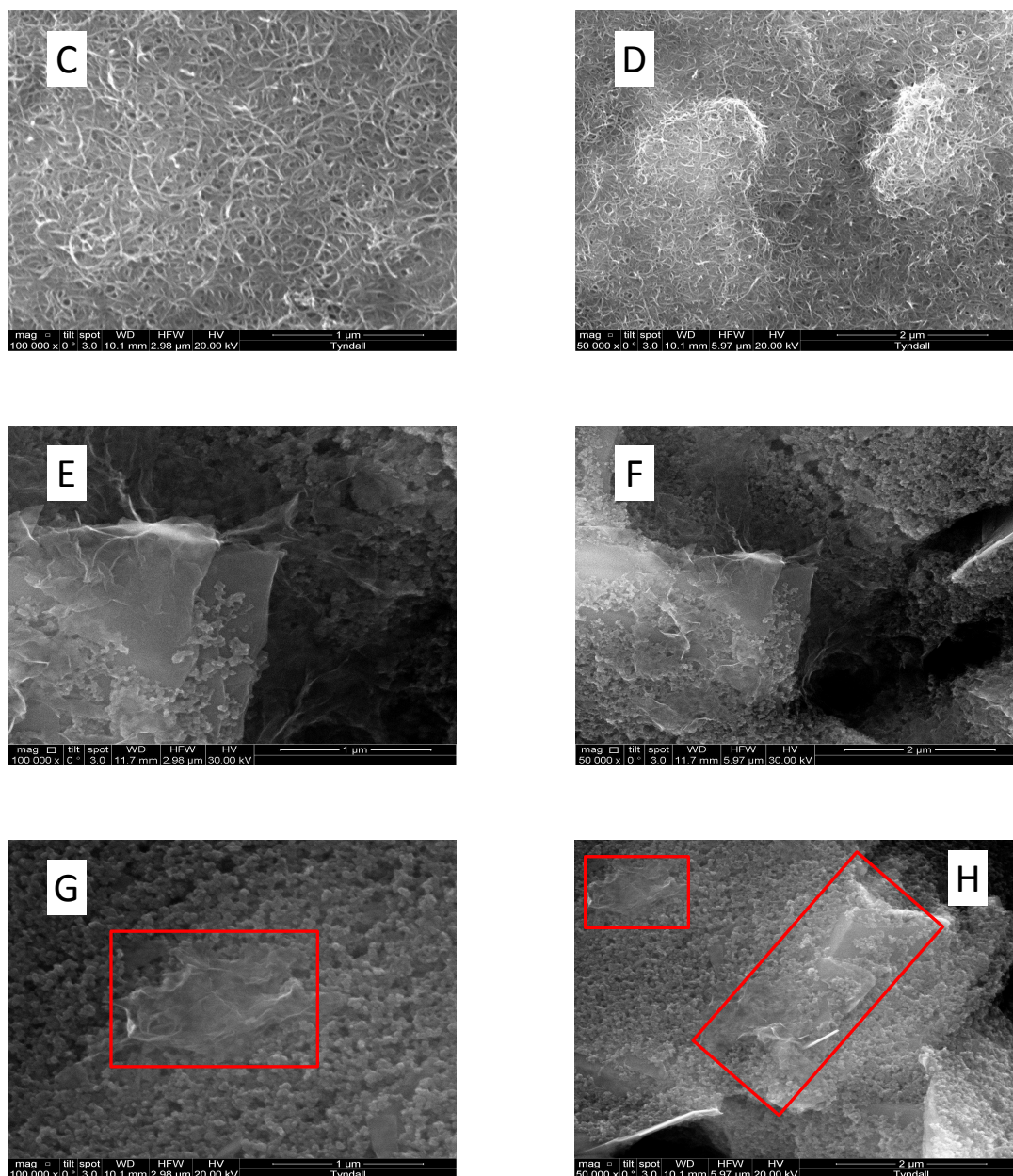


Figure 2.40: SEM of modified electrodes at nanocarbon modified electrodes. MWCNT (A,B) MWCNT/Nafion (C,D) RGO (E,F) RGO/Nafion (G,H)

2.7.3 Contact Angle

In order to further investigate the nature of the surface of these electrodes, contact angle measurements were again carried out. As expected, the carbon nanotube modified electrodes displayed a very hydrophobic surface [34, 35]. Contact angles of around 134° were observed at both MWCNT and MWCNT/Nafion electrodes in comparison to 102.1° and 107.2° at RGO and RGO/Nafion electrodes. These results are summarised in table 2.9.

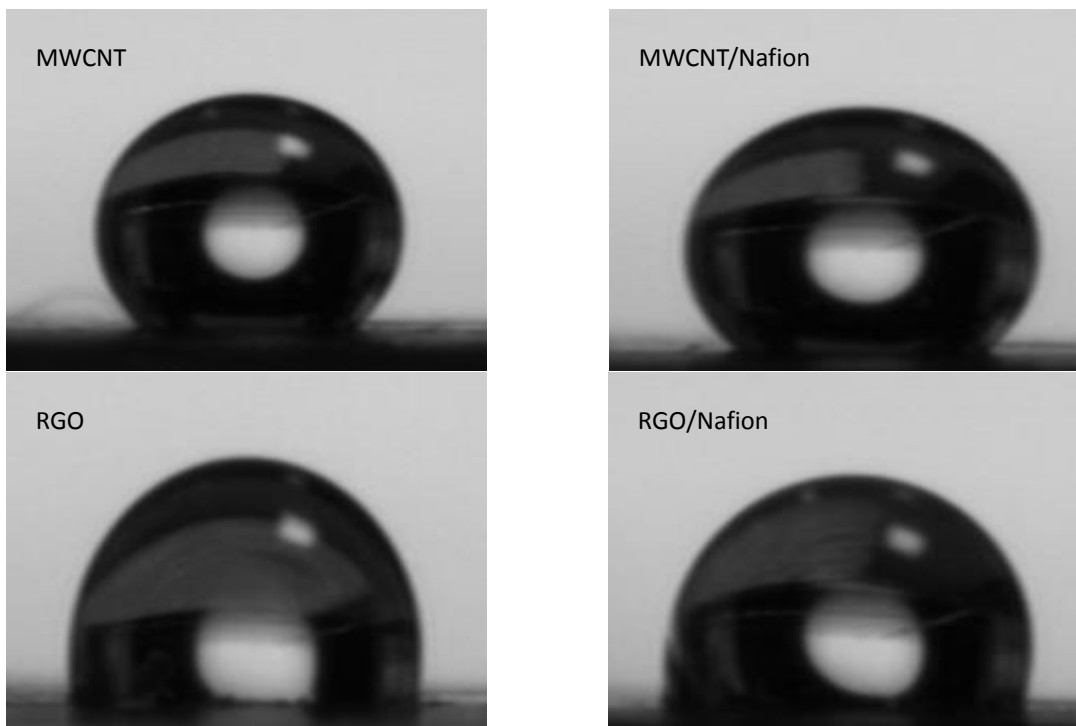


Figure 2.41: Contact angle droplets at nanocarbon modified electrodes

Table 2.9: Contact Angle (degrees) for pretreated electrodes

Electrode Pretreatment	Contact Angle
MWCNT	134.3 ± 2.42
MWCNT/Nafion	134.85 ± 2.78
RGO	102.1 ± 3.64
RGO/Nafion	107.25 ± 6.23

2.7.4 Thin Layer Effects

An investigation into the possibility of thin layer effects at the nanocarbon modified electrodes revealed that there was no evidence of any effect on the electrode's electrochemical signal. As seen from Table 2.10, none of the electrodes displayed slopes approaching 1 which one would expect in the case of thin layer effects. This is most likely due to the fact that only a small amount of solution was dropcast onto the working electrode surface ($0.5 \mu\text{L}$ of RGO/Nafion and RGO; and $2 \mu\text{L}$ of RGO and MWCNT). Hence, a thicker

layer of material wasn't formed on the surface which would contribute to thin layer effects. Similarly to the electrochemically pretreated electrodes, more ideal slopes close to 0.5 were observed when using the hexaamine ruthenium (III) chloride redox probe. Values were closest to 0.5 at the MWCNT, MWCNT and RGO/Nafion electrodes and therefore the Randles Sevcik equation could be used for these electrodes to compute accurate electrode areas.

Table 2.10: Slopes of $\text{Log } I_p$ vs $\text{Log } \nu$

	Slope ($\text{Log } I_p$ vs $\text{Log } \nu$)	R^2
<u>MWCNT</u>		
Ferri/ferrocyanide	0.358	0.9835
Hexaamine ruthenium (III) chloride	0.4455	0.998
<u>MWCNT/Nafion</u>		
Ferri/ferrocyanide	0.3574	0.9987
Hexaamine ruthenium (III) chloride	0.4817	0.9906
<u>RGO</u>		
Ferri/ferrocyanide	0.2554	0.9863
Hexaamine ruthenium (III) chloride	0.3735	0.9937
<u>RGO/Nafion</u>		
Ferri/ferrocyanide	<i>N/A</i>	<i>N/A</i>
Hexaamine ruthenium (III) chloride	0.4457	0.9799

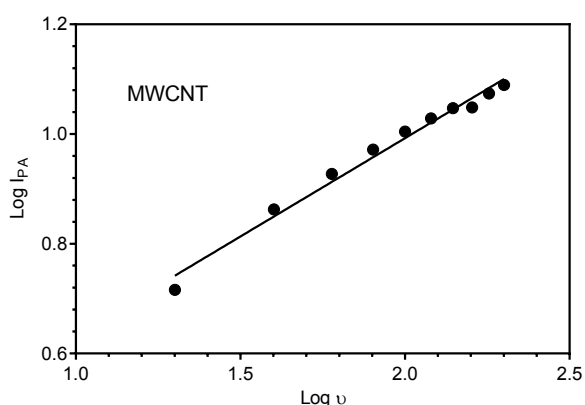


Figure 2.42: $\text{Log } I_A$ vs $\text{Log } \nu$ at a MWCNT modified electrode. The graphs for the other electrodes are contained in the appendix

2.7.5 Electrochemical Characterisation - Ferri/Ferrocyanide

Cyclic voltammograms were then carried in 1 mM $[\text{Fe}(\text{CN})_6]^{3-/4-}$ at a scan rate of 100 mV/s at the four different nanocarbon modifications. The results are displayed in Fig. 2.43 in comparison to an unmodified graphite electrode. Both the MWCNT and MWCNT/Nafion electrodes lead to an increase in anodic peak current compared to the unmodified electrode. However, this increase is accompanied with an increase in background non-Faradaic current so that the net peak currents are in fact similar to the graphite electrode. In contrast, there is a significant decrease in both anodic peak current and peak potential at the RGO and RGO/Nafion modified electrodes. This indicates that both the nafion and RGO have a negative influence on electron transfer kinetics.

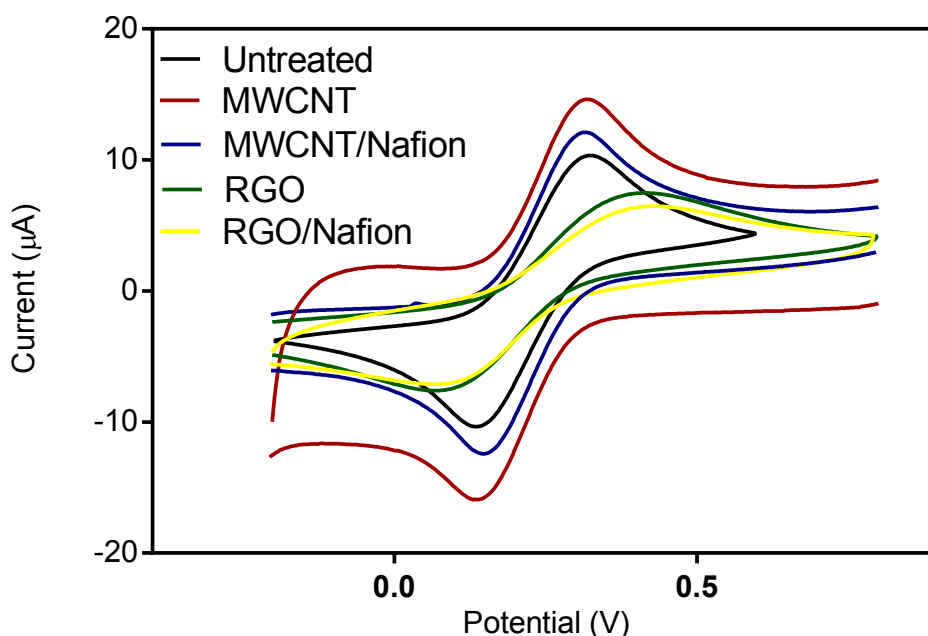


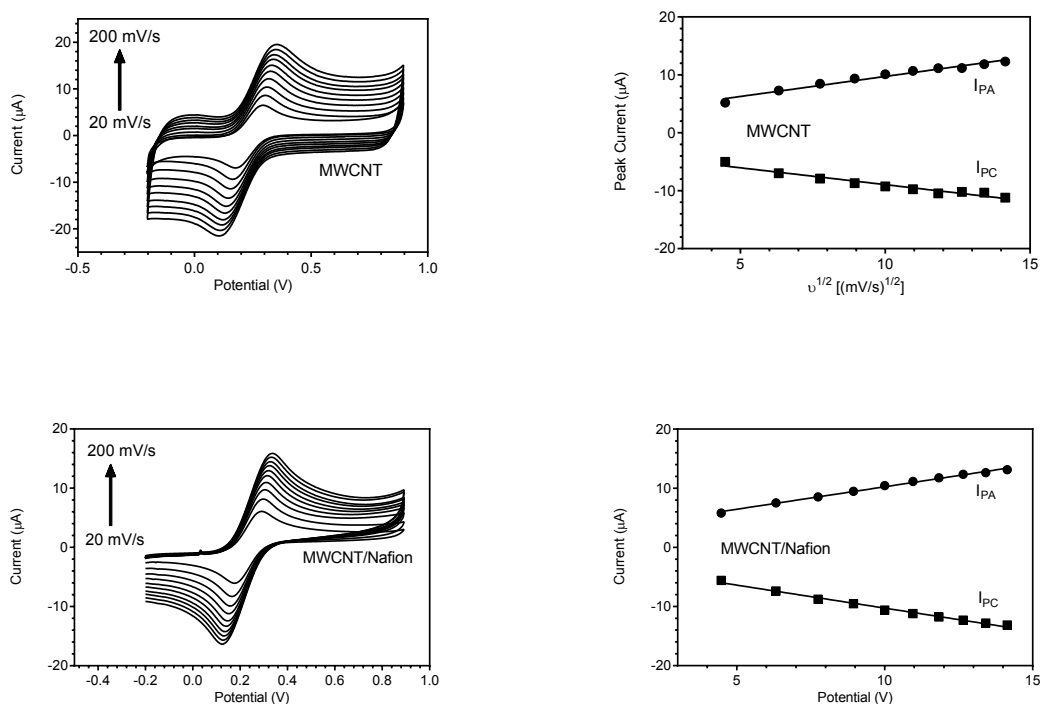
Figure 2.43: CVs of nanocarbon modified electrodes in 100 μM $[\text{Fe}(\text{CN})_6]^{3-/4-}$ in 1 M KCl at a scan rate of 100 mV/s.

Table 2.11: Peak potential separation and peak anodic current from CV measurements for different nanocarbon modified electrodes

Electrode	ΔE (mV)	I_{PA}
MWCNT	176 (± 4)	10.2 (± 0.2)
MWCNT/Nafion	155 (± 2)	10.6 (± 0.2)
RGO	269 (± 50)	7 (± 2)
RGO/Nafion	279 (± 42)	1.6 (± 0.5)

2.7.5.1 Scan Rate Studies - Ferri/Ferrocyanide

Varying the scan rate at 20 mV/s intervals from 20-200 mV/s revealed diffusion limited processes at the MWCNT, MWCNT/Nafion and RGO modified electrodes as can be seen in the linear relationship observed between peak current and the square root of square of scan rate in Fig. 2.44. However, this linear relationship is not observed at the RGO/Nafion electrode where electrochemical activity was inhibited significantly. Although it is clear that the peak current increases with increasing scan rate (bottom left graph in Fig. 2.41), there is also a shift in background current which negates the increasing Faradaic current.



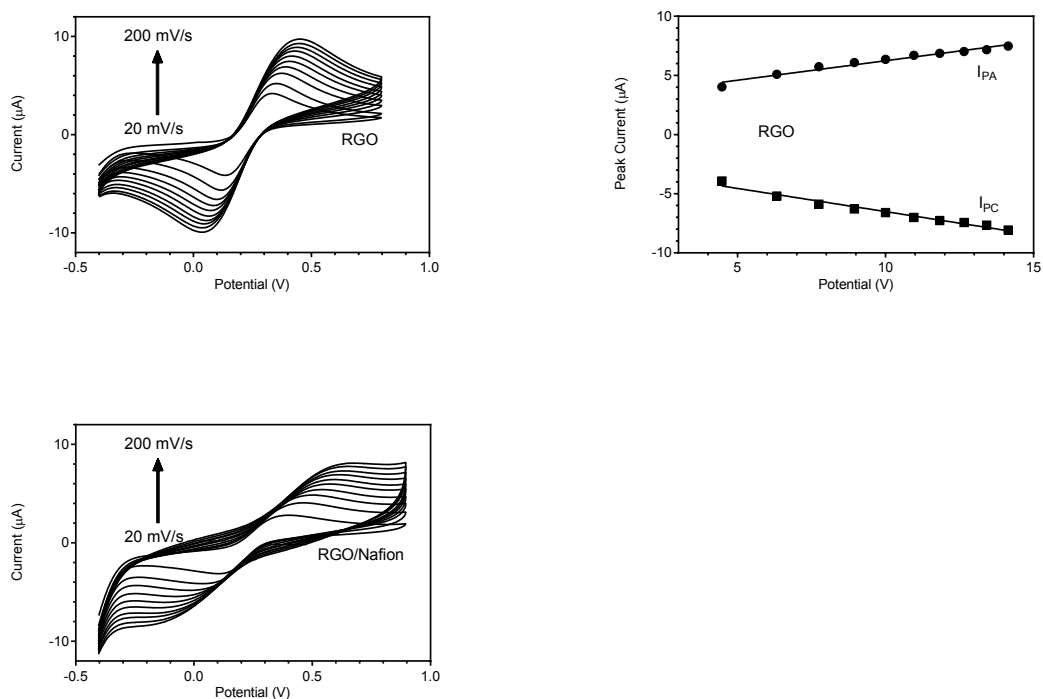


Figure 2.44: CVs at scan rates of 20 - 200 mV/s in 1 mM $[\text{Fe}(\text{CN})_6]^{3-/4-}$ (1 M KCl supporting electrolyte) at nanocarbon modified electrodes.

2.7.6 Electrochemical Characterisation - Hexamine Ruthenium (III) Chloride

Cyclic voltammograms were then carried out in ruthenium (III) chloride at each modified electrode. Interestingly, at each electrode, a narrowing of the potential window occurred. This was most noticeable at the MWCNT/Nafion modified electrode as can be seen in Fig. 2.45. All modifications resulted in a greater anodic peak current but the net peak current was only greater at the MWCNT electrodes. Corresponding electrode areas were calculated for both MWCNT and for the RGO/Nafion electrodes with the results shown in Table. 2.12. An electrode area for the RGO electrode was not calculated due to the fact that a graph of log scan rate vs log peak didn't produce a graph of slope near to 0.5 (the exact value was 0.3735).

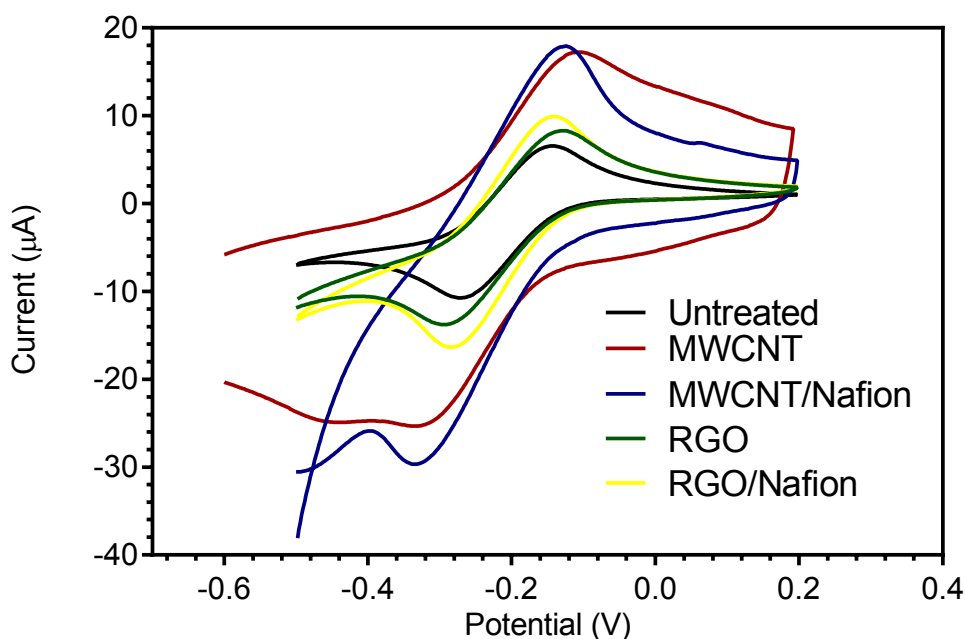


Figure 2.45: CVs of 1 mM Hexamine Ruthenium (III) Chloride in 50 mM PBS pH 7.4 at nanocarbon modified electrodes.

Table 2.12: Peak potential separation and peak anodic current from CV measurements for different nanocarbon modified electrodes

Electrode	ΔE (mV)	I_{PA}	A_{R-S} (cm ²)	% Roughness Factor
MWCNT	211 (\pm 9)	14.2 (\pm 0.3)	0.1573	221.6
MWCNT/Nafion	160 (\pm 22)	8 (\pm 1)	0.0839	181.1
RGO	154 (\pm 11)	5.1 (\pm 0.1)	N/A	N/A
RGO/Nafion	130 (\pm 16)	6.3 (\pm 0.1)	0.0559	78.7

2.7.6.1 Scan rate studies - Hexamine Ruthenium (III) Chloride

Varying the scan rate at 20 mV/s intervals from 20-200 mV/s revealed diffusion limited processes at the MWCNT, MWCNT/Nafion, RGO and RGO/Nafion modified electrodes as can be seen in the linear relationship observed between peak current and the square root of scan rate in Fig. 2.46.

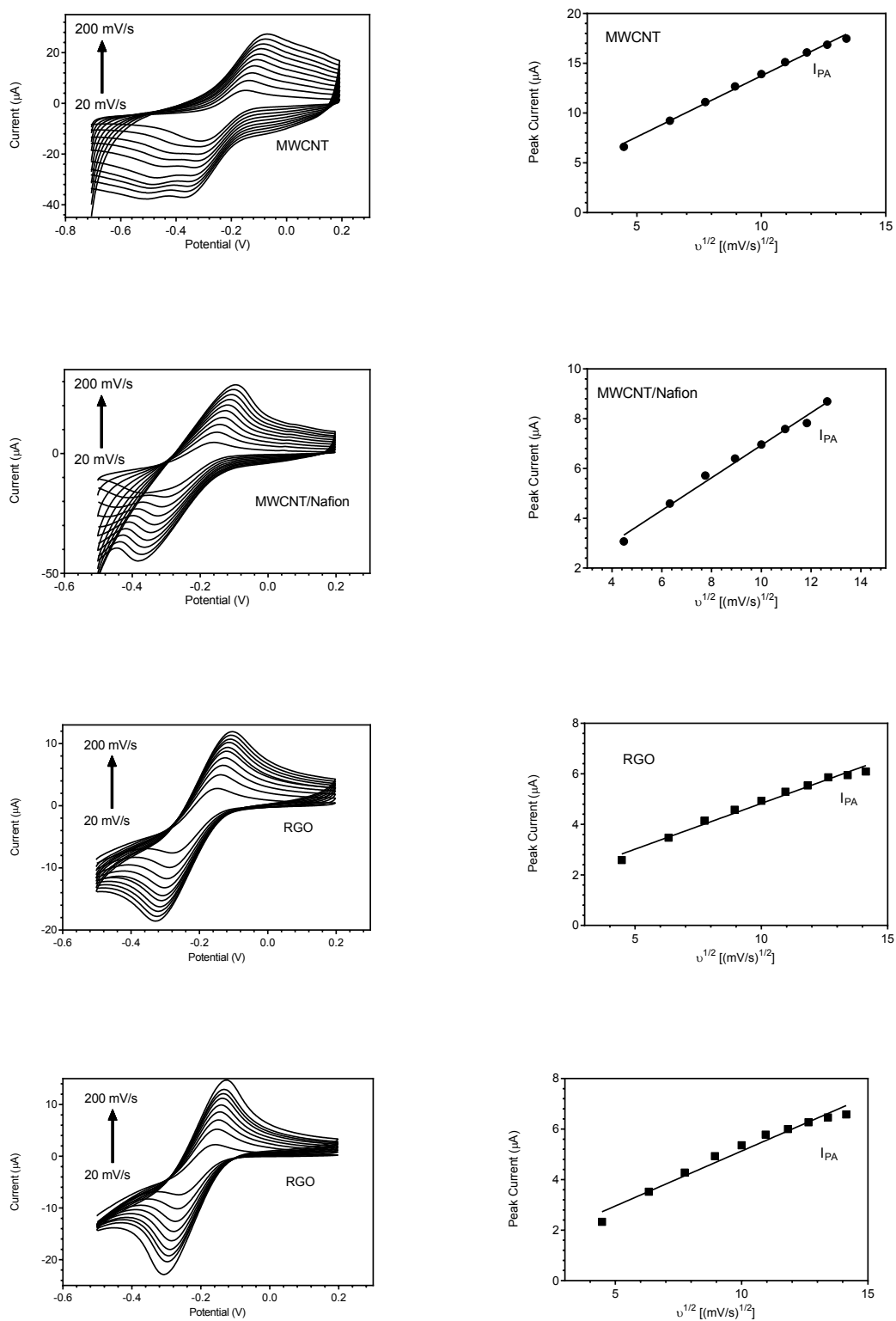


Figure 2.46: CVs at scan rates of 20 - 200 mV/s in 1 mM Hexamine Ruthenium (III) Chloride

2.7.7 Amperometric p-aminophenol detection

Next, each electrode was compared for the amperometric detection of p-aminophenol as described previously for the electrochemically pretreated electrodes. From Fig. 2.47 it would appear that the MWCNT/Nafion modified electrode has the largest analytical signal. ANOVA analysis of the slopes of the calibration curves (Fig. 2.48) for p-aminophenol result in a P value of 0.00037 which indicates that the sensitivities are statistically different. However, an unpaired t test between the MWCNT/Nafion and RGO electrodes reveals a P value of 0.0673 which means there is no statistically significant difference between these two electrodes.

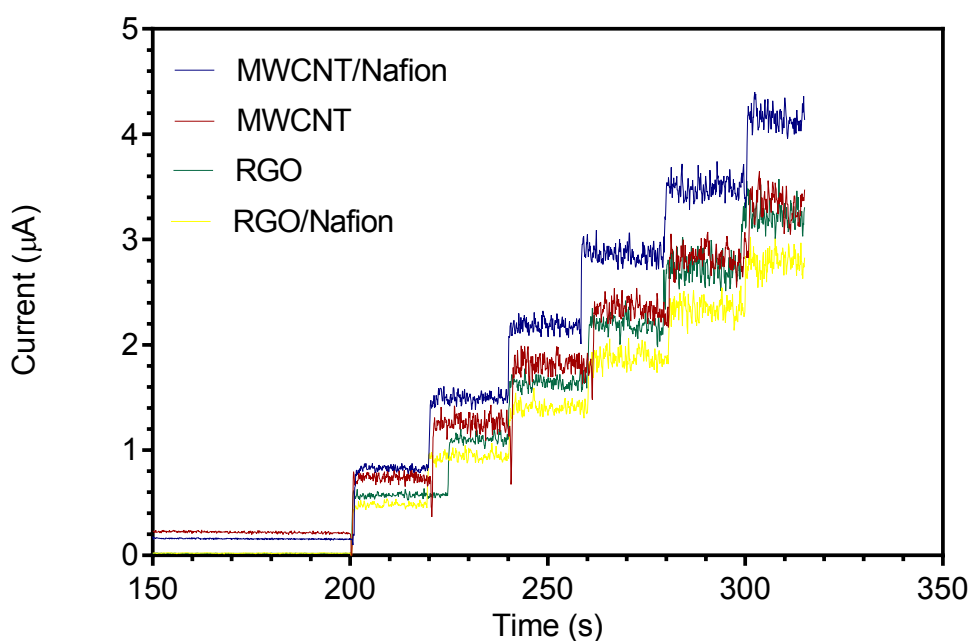


Figure 2.47: Standard addition of 10 μL of 5 mM stock solution of pAP to DEA buffer pH 9.5 under stirred conditions at bare and nanocarbon modified electrodes

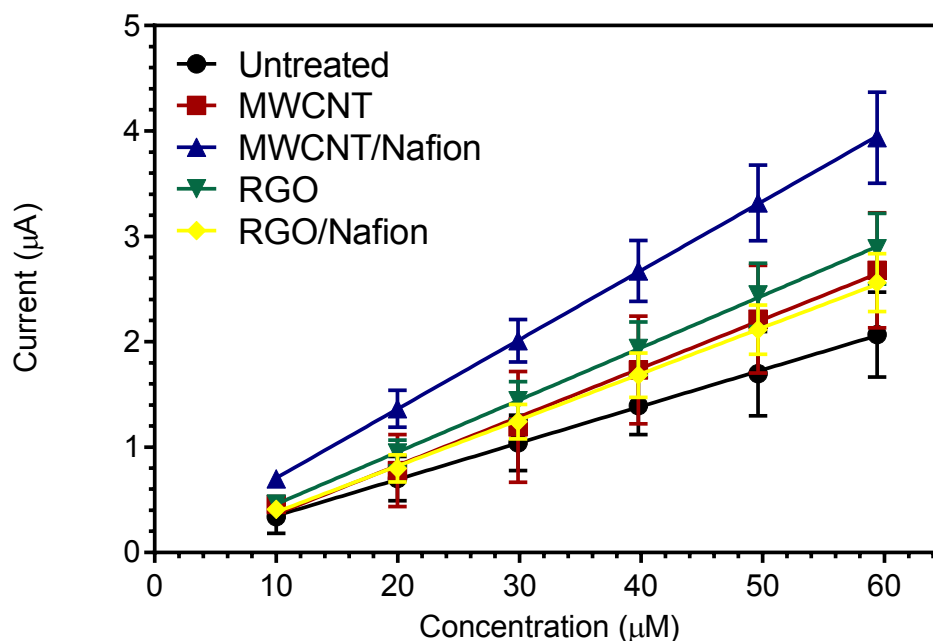


Figure 2.48: Calibration curve for p-aminophenol detection at nanocarbon modified electrodes - concentrations of 10, 20, 30, 40, 50, 60 μM

Table 2.13: Sensitivity for amperometric p-aminophenol detection at nanocarbon modified electrodes

	Slope/Sensitivity ($\mu\text{A}/\mu\text{M}$)	R^2
MWCNT	0.0461	0.8130
MWCNT/Nafion	0.0657	0.9583
RGO	0.0495	0.9510
RGO/Nafion	0.0436	0.9556

However, as was observed in the SEM measurements, the RGO didn't fully cover the working electrode surface.

2.7.8 Electrochemical Immunoassay at MWCNT/Nafion electrode

A competitive electrochemical immunoassay was then carried out at the MWCNT/Nafion electrode. The same parameters were used as those optimised

at the electrochemically pretreated electrode with the results displayed in Fig. 2.50 and the results outlined in Table 2.14.

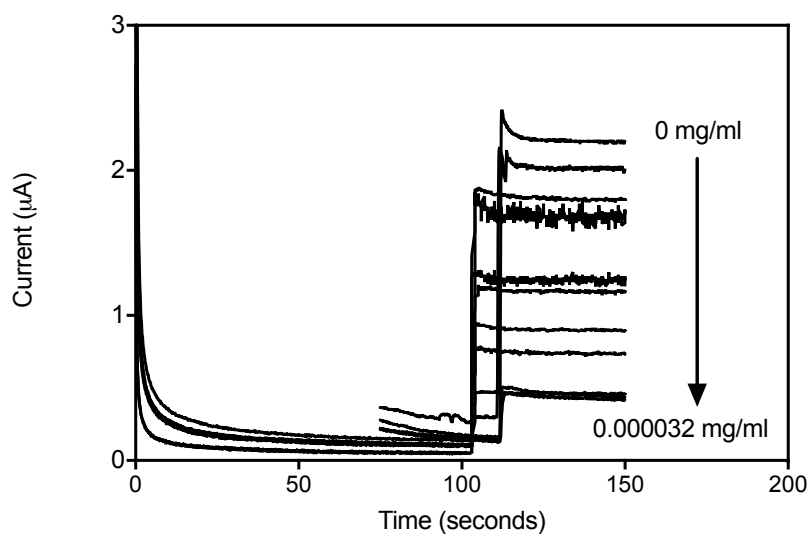


Figure 2.49: Hydrodynamic amperograms for a range of mouse IgG concentrations at a MWCNT/Nafion electrode. After a period of 200 seconds 50 μL of pAPP (25 mg/mL) was added to a stirred solution of 4950 μL DEA buffer, pH 9.5. A fixed potential of 0.28 mV was used.

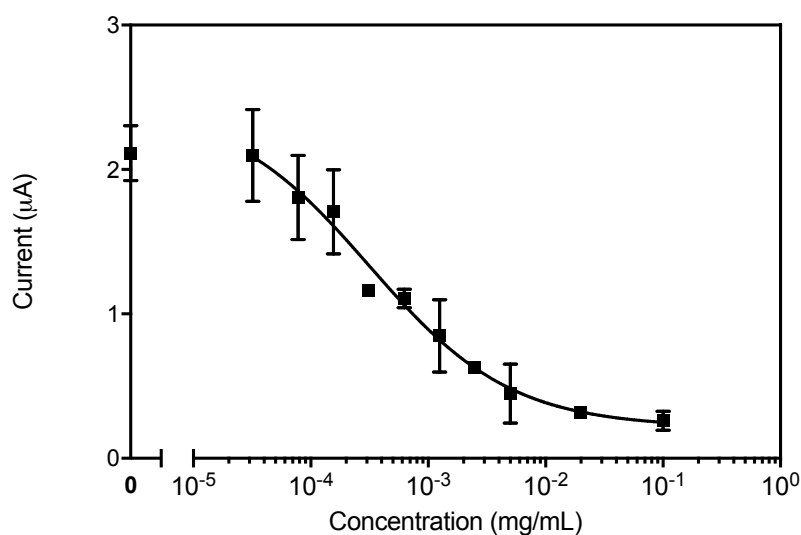


Figure 2.50: Competitive electrochemical immunoassay for mouse IgG at a MWCNT/Nafion electrode with parameters optimised in section 2 of this chapter for a pre-anodised electrode - coating antibody concentration: 0.04 mg/mL, competition incubation time: 90 mins, $R^2 = 0.9286$ and $n = 3$.

Table 2.14: Electrochemical Immunoassay results at MWCNT/Nafion electrode

Electrode	LOD (ppm)	IC50 (ppm)	LR (ppm)	R ²
MWCNT/Nafion	0.2	0.3	0.04 - 2.7	0.9286

2.7.9 Summary of Results and Control Assays

Finally, the electrochemical immunosensors developed previously in this chapter were compared to immunosensors at a bare graphite electrode (Fig. 2.51) and an electrochemically pretreated electrode with covalent attachment (Fig. 2.52). Again, the same assay conditions were employed as those optimised for the pretreated electrode earlier in this chapter.

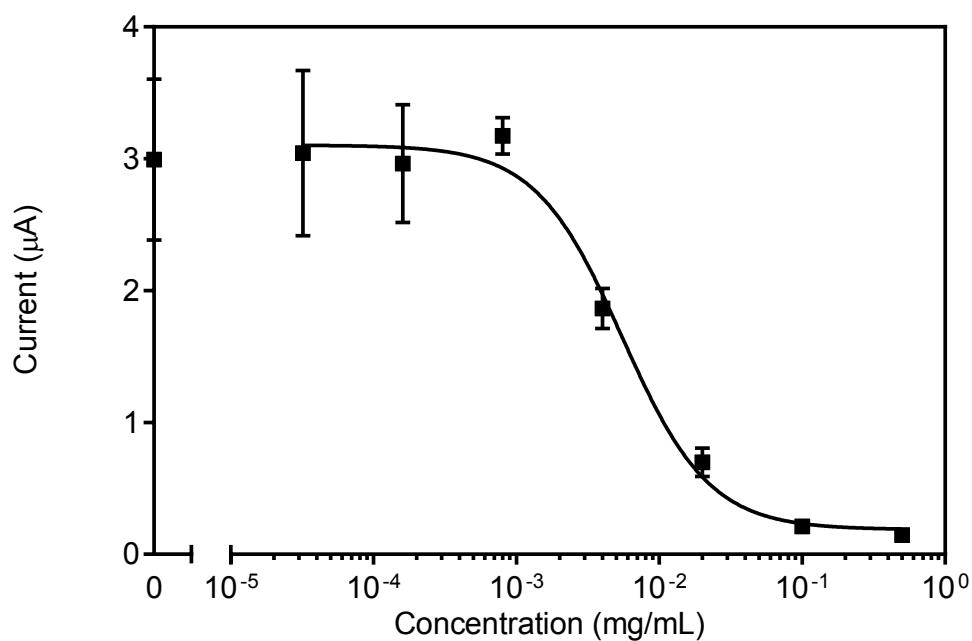


Figure 2.51: Competitive electrochemical immunoassay at untreated electrode.
R² = 0.954, n = 3

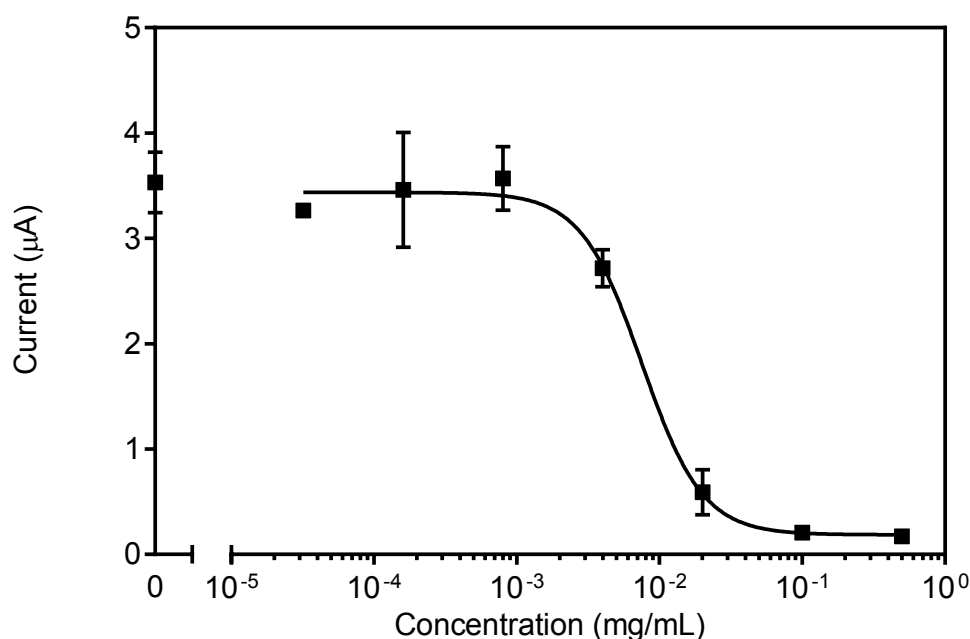


Figure 2.52: Competitive electrochemical immunoassay at pre-anodised electrode using covalent attachment. $R^2 = 0.976$, $n = 3$

In the comparison of results as shown in Table 2.15 it is clear that the MWCNT/Nafion electrode has the most promising analytical characteristics with the lowest LOD and IC50 values. However, it must be noted that the linear range for this electrode is smaller than for the other electrodes investigated in this chapter. Despite this it was decided that the MWCNT/Nafion would be used for future immunosensor applications in this thesis.

Table 2.15: Summary of Electrochemical Immunoassay results for mouse IgG detection

Electrode	LOD (ppm)	IC50 (ppm)	LR (ppm)	R^2
Na ₂ CO ₃ (passive adsorption)	0.9	2.6	1.4 - 4.9 ppm	0.9608
MWCNT/Nafion	0.2	0.3	0.04 - 2.7	0.9286
Na ₂ CO ₃ (covalent attachment)	4.3	7.5	3.5 - 16	0.976
Untreated	8.9	5.5	1.9 - 16.2	0.954

2.8 Conclusions and Future Prospects

In this chapter a range of electrochemical pretreatments and nanocarbon electrodes were characterised physically and electrochemically as well as being compared for mouse IgG detection. It was shown that electrochemical pretreatments can improve electron transfer kinetics and also be used for electrochemical immunosensor applications. However, it was found a MWCNT/Nafion modified had the most promising analytical characteristics with a LOD of 0.2 ppm compared to 8.9 ppm at a bare electrode. It was then used for the detection of deoxynivalenol in chapter 3. Although the LOD at the MWCNT/Nafion electrode was lower it also displayed a significantly reduced linear range. This would have to be taken into account when applying the sensor to real world scenarios. Significant electrochemical and physical characterisation of each electrode was also carried out at each electrode giving an insight into their fundamental properties.

Future work could investigate other pretreatments. For example, mechanical polishing of both carbon and platinum screen printed electrodes have recently been investigated as a means of improving electrochemical performance [36, 37]. Of particular significance is that mechanical polishing has been used to improved IgG adsorption [38]. However, this approach for IgG hasn't been extensively used. A possible further study could compare electrochemically pretreated electrodes with mechanically polished ones using the competitive immunoassay system used in this chapter. There is also a possibility to investigate new carbon nanomaterials such as carbon nanohorns amongst others. A comprehensive comparison could also be investigated of nanomaterial/polymer composites for electrochemical immunosensor applications.

References

- [1] Wenrong Yang, Kyle R. Ratinac, Simon P. Ringer, Pall Thordarson, J. Justin Gooding, and Filip Braet. Carbon Nanomaterials in Biosensors: Should You Use Nanotubes or Graphene? *Angewandte Chemie International Edition*, 49(12):2114–2138, March 2010.
- [2] Meng Li, Yuan-Ting Li, Da-Wei Li, and Yi-Tao Long. Recent developments and applications of screen-printed electrodes in environmental assays—A review. *Analytica Chimica Acta*, 734:31–44, July 2012.
- [3] Mónica Moreno, Alberto Sánchez Arribas, Esperanza Bermejo, Manuel Chicharro, Antonio Zapardiel, Marcela C. Rodríguez, Yamile Jalit, and Gustavo A. Rivas. Selective detection of dopamine in the presence of ascorbic acid using carbon nanotube modified screen-printed electrodes. *Talanta*, 80(5):2149–2156, March 2010.
- [4] I. Palchetti, A. Cagnini, M. Mascini, and A. P. F. Turner. Characterisation of Screen-Printed Electrodes for Detection of Heavy Metals. *Microchimica Acta*, 131(1-2):65–73, June 1999.
- [5] Miquel Albareda-Sirvent, Arben Merkoçi, and Salvador Alegret. Configurations used in the design of screen-printed enzymatic biosensors. A review. *Sensors and Actuators B: Chemical*, 69(1–2):153–163, September 2000.
- [6] Vanessa Escamilla-Gómez, David Hernández-Santos, María Begoña González-García, José Manuel Pingarrón-Carrazón, and Agustín Costa-García. Simultaneous detection of free and total prostate specific antigen on a screen-printed electrochemical dual sensor. *Biosensors and Bioelectronics*, 24(8):2678–2683, April 2009.
- [7] Joseph Wang, Maria Pedrero, Henning Sakslund, Ole Hammerich, and Jose Pingarron. Electrochemical activation of screen-printed carbon strips. *The Analyst*, 121(3):345, 1996.
- [8] Eva Dock and Tautgirdas Ruzgas. Screen-Printed Carbon Electrodes Modified with Cellobiose Dehydrogenase: Amplification Factor for Catechol vs. Reversibility of Ferricyanide. *Electroanalysis*, 15(5-6):492–498, April 2003.
- [9] Gang Cui, Jae Hyun Yoo, Joung Su Lee, Jina Yoo, Jung Hee Uhm, Geun Sig

- Cha, and Hakhyun Nam. Effect of pre-treatment on the surface and electrochemical properties of screen-printed carbon paste electrodes. *The Analyst*, 126(8):1399–1403, 2001.
- [10] Aoife Morrin, Anthony J. Killard, and Malcolm R. Smyth. Electrochemical Characterization of Commercial and Home-Made Screen-Printed Carbon Electrodes. *Analytical Letters*, 36(9):2021–2039, January 2003.
- [11] Rashid O. Kadara, Norman Jenkinson, and Craig E. Banks. Characterisation of commercially available electrochemical sensing platforms. *Sensors and Actuators B: Chemical*, 138(2):556–562, May 2009.
- [12] T. J. Davies, M. E. Hyde, and R. G. Compton. Nanotrench arrays reveal insight into graphite electrochemistry. *Angewandte Chemie-International Edition*, 44(32):5121–5126, 2005. WOS:000231367300030.
- [13] Anisha N. Patel, Manon Guille Collignon, Michael A. O’Connell, Wendy O. Y. Hung, Kim McKelvey, Julie V. Macpherson, and Patrick R. Unwin. A New View of Electrochemistry at Highly Oriented Pyrolytic Graphite. *Journal of the American Chemical Society*, 134(49):20117–20130, December 2012.
- [14] E. J. Moore, M. P. Kreuzer, M. Pravda, and G. G. Guilbault. Development of a rapid single-drop analysis biosensor for screening of phenanthrene in water samples. *Electroanalysis*, 16(20):1653–1659, October 2004. WOS:000224940300001.
- [15] Farzana Darain, Sang-Un Park, and Yoon-Bo Shim. Disposable amperometric immunosensor system for rabbit IgG using a conducting polymer modified screen-printed electrode. *Biosensors & Bioelectronics*, 18(5-6):773–780, May 2003.
- [16] María Díaz-González, David Hernández-Santos, María Begoña González-García, and Agustín Costa-García. Development of an immunosensor for the determination of rabbit IgG using streptavidin modified screen-printed carbon electrodes. *Talanta*, 65(2):565–573, January 2005.
- [17] Md Abdul Aziz, Sangjin Park, Sangyong Jon, and Haesik Yang. Amperometric immunosensing using an indium tin oxide electrode modified with multi-walled carbon nanotube and poly(ethylene

- glycol)-silane copolymer. *Chemical Communications*, (25):2610–2612, 2007. WOS:000247397400024.
- [18] Adeline Huiling Loo, Alessandra Bonanni, Adriano Ambrosi, Hwee Ling Poh, and Martin Pumera. Impedimetric immunoglobulin G immunosensor based on chemically modified graphenes. *Nanoscale*, 4(3):921–925, 2012. WOS:000299292600034.
- [19] Marcus J. Sims, Neil V. Rees, Edmund J. F. Dickinson, and Richard G. Compton. Effects of thin-layer diffusion in the electrochemical detection of nicotine on basal plane pyrolytic graphite (BPPG) electrodes modified with layers of multi-walled carbon nanotubes (MWCNT-BPPG). *Sensors and Actuators B: Chemical*, 144(1):153–158, January 2010.
- [20] Ian Streeter, Gregory G. Wildgoose, Lidong Shao, and Richard G. Compton. Cyclic voltammetry on electrode surfaces covered with porous layers: An analysis of electron transfer kinetics at single-walled carbon nanotube modified electrodes. *Sensors and Actuators B-Chemical*, 133(2):462–466, August 2008. WOS:000259268600017.
- [21] Gareth P. Keeley and Michael E. G. Lyons. The Effects of Thin Layer Diffusion at Glassy Carbon Electrodes Modified with Porous Films of Single-Walled Carbon Nanotubes. *International Journal of Electrochemical Science*, 4(6):794–809, June 2009. WOS:000267341400005.
- [22] Edward P. Randviir, Dale A. C. Brownson, Jonathan P. Metters, Rashid O. Kadara, and Craig E. Banks. The fabrication, characterisation and electrochemical investigation of screen-printed graphene electrodes. *Physical Chemistry Chemical Physics*, 16(10):4598–4611, 2014. WOS:000332393200020.
- [23] Jonathan Moldenhauer, Madeline Meier, and David W. Paul. Rapid and Direct Determination of Diffusion Coefficients Using Microelectrode Arrays. *Journal of The Electrochemical Society*, 163(8):H672–H678, January 2016.
- [24] K. Sudhakara Prasad, Govindan Muthuraman, and Jyh-Myng Zen. The role of oxygen functionalities and edge plane sites on screen-printed carbon electrodes for simultaneous determination of dopamine, uric acid and ascorbic acid. *Electrochemistry Communications*, 10(4):559–563, April 2008.

- [25] Maria Gómez-Mingot, Jesús Iniesta, Vicente Montiel, Rashid O. Kadara, and Craig E. Banks. Screen printed graphite macroelectrodes for the direct electron transfer of cytochrome c. *Analyst*, 136(10):2146–2150, April 2011.
- [26] Andrew Kozbial, Zhiting Li, Jianing Sun, Xiao Gong, Feng Zhou, Yongjin Wang, Haochen Xu, Haitao Liu, and Lei Li. Understanding the intrinsic water wettability of graphite. *Carbon*, 74:218–225, August 2014.
- [27] Rishi Raj, Shalabh C. Maroo, and Evelyn N. Wang. Wettability of Graphene. *Nano Letters*, 13(4):1509–1515, April 2013. WOS:000317549300024.
- [28] Young Jun Shin, Yingying Wang, Han Huang, Gopinadhan Kalon, Andrew Thye Shen Wee, Zexiang Shen, Charanjit Singh Bhatia, and Hyunsoo Yang. Surface-Energy Engineering of Graphene. *Langmuir*, 26(6):3798–3802, March 2010.
- [29] M. P. Kreuzer, C. K. O’Sullivan, M. Pravda, and G. G. Guilbault. Development of an immunosensor for the determination of allergy antibody (IgE) in blood samples. *Analytica Chimica Acta*, 442(1):45–53, August 2001. WOS:000170709700005.
- [30] Sa Fernando, Jr Sportsman, and Gs Wilson. Studies of the Low-Dose Hook Effect in a Competitive Homogeneous Immunoassay. *Journal of Immunological Methods*, 151(1-2):27–46, July 1992. WOS:A1992JD60400004.
- [31] Y. F. Xu, M. Velasco-Garcia, and T. T. Mottram. Quantitative analysis of the response of an electrochemical biosensor for progesterone in milk. *Biosensors & Bioelectronics*, 20(10):2061–2070, April 2005. WOS:000227845700022.
- [32] Pedro José Lamas-Ardisana, Paula Queipo, Pablo Fanjul-Bolado, and Agustín Costa-García. Multiwalled carbon nanotube modified screen-printed electrodes for the detection of p-aminophenol: Optimisation and application in alkaline phosphatase-based assays. *Analytica Chimica Acta*, 615(1):30–38, May 2008.
- [33] Joseph Wang, Mustafa Musameh, and Yuehe Lin. Solubilization of Carbon Nanotubes by Nafion toward the Preparation of Amperometric Biosensors.

- Journal of the American Chemical Society*, 125(9):2408–2409, March 2003.
- [34] Shuhong Li, Huanjun Li, Xianbao Wang, Yanlin Song, Yunqi Liu, Lei Jiang, and Daoben Zhu. Super-Hydrophobicity of Large-Area Honeycomb-Like Aligned Carbon Nanotubes. *The Journal of Physical Chemistry B*, 106(36):9274–9276, September 2002.
- [35] Asa H. Barber, Sidney R. Cohen, and H. Daniel Wagner. Static and Dynamic Wetting Measurements of Single Carbon Nanotubes. *Physical Review Letters*, 92(18):186103, May 2004.
- [36] Loanda R. Cumba, Christopher W. Foster, Dale A. C. Brownson, Jamie P. Smith, Jesus Iniesta, Bhawana Thakur, Devaney R. do Carmo, and Craig E. Banks. Can the mechanical activation (polishing) of screen-printed electrodes enhance their electroanalytical response? *Analyst*, 141(9):2791–2799, April 2016.
- [37] Junqiao Lee, Damien W. M. Arrigan, and Debbie S. Silvester. Mechanical polishing as an improved surface treatment for platinum screen-printed electrodes. *Sensing and Bio-Sensing Research*, 9:38–44, July 2016.
- [38] Miloslav Pravda, Catriona O’Meara, and George G. Guilbault. Polishing of screen-printed electrodes improves IgG adsorption. *Talanta*, 54(5):887–892, June 2001.

Chapter 3

Electrochemical Immunosensor for Deoxynivalenol Detection

3.1 Objectives and Novelty

The aim of this chapter was to develop an electrochemical immunosensor for the mycotoxin, deoxynivalenol. Firstly, an indirect competitive ELISA method was developed. This method was then transferred onto a MWCNT/Nafion modified electrode which had been established in the previous chapter as the most promising electrode studied in this thesis for electrochemical immunosensor applications. Both ELISA and immunosensor methods were developed with EU limits for wheat samples in mind which would allow the developed sensor to be used for this application in future work.

This is the first example of an electrochemical immunosensor for deoxynivalenol detection based on a carboxylic acid functionalised MWCNT/Nafion modified screen printed electrode. Recently, an immunosensor based on single walled carbon nanotubes and chitosan has been developed for DON detection with a very low LOD of 5 pg/mL and a linear range of 0.01 ng/mL - 1000 ng/mL [1]. This LOD is lower than that achieved by the sensor developed in this chapter (0.95×10^{-3} mg/mL). However, considering that EU regulations set a maximum level of 1.75×10^{-3} mg/mL for DON in raw grain samples, the sensor developed by Qing et. al doesn't have the sufficiently wide linear range to provide accurate quantitative around this maximum level. In contrast, the sensor developed in this work has a linear range that extends to 6.3×10^{-3} mg/mL which makes it a practical solution for DON detection in raw grain samples at the appropriate regulatory levels.

3.2 Introduction

Deoxynivalenol (DON) (Fig. 3.1) is a trichothecene mycotoxin that is produced from fungi of wheat, cereal and grains. As was previously discussed in Chapter 1 mycotoxins are secondary metabolites produced by molds and fungi. More specifically, DON is a non-macrocylic B trichothecene characterised by a ketone group in the C-8 position as seen in Fig. 3.1. In contrast, the type A trichothecenes such as T-2 toxin, H-2 toxin, neosolaniol and diacetoxyscirpenol contain a hydrogen or an ester group in this position.

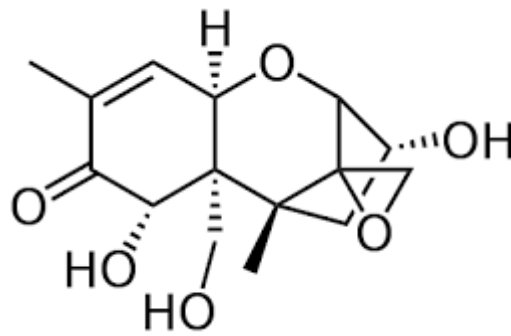


Figure 3.1: Chemical Structure of Deoxynivalenol

In animal studies, low doses of trichothecenes can cause growth and immune issues, and at larger doses, diarrhea, emesis, leukocytosis, hemorrhage, endotoxemia and even death [2]. Although only discovered in the 1970s, there is historical evidence that DON caused outbreaks of human gastroenteritis in Japan as far back as the 1940s [3]. With these risks in the mind, the EU has set maximum levels on DON in a range of food stuffs as seen in Table 3.1.

Table 3.1: EU limits for Deoxynivalenol in common grains and products

Product	EU limit ($\mu\text{g}/\text{kg}$)
Wheat	1750
Corn	1750
Baby Food	250
Cereal	750



Figure 3.2: Healthy (left) and fusarium infected maize (right) [4]

The fusarium fungi which leads to be mycotoxin development can be seen visually in certain cases as shown in the case of an infected corn sample in

Fig. 3.2 above. However, this isn't necessarily apparent in processed products and the extent of degradation isn't always that extreme. Hence, the need for analytical technology.

3.3 Methods of Deoxynivalenol Detection

Methods for the detection of DON can be generally described by two different approaches. The first are rapid screening techniques which are generally qualitative, low cost methods which should indicate the presence of DON in samples prior to further more expensive quantitative assessment being carried out. The aim of these screening techniques is to reduce costs by limiting the number of samples that require the more expensive techniques.

3.3.1 Fast Screening methodologies

The majority of fast screening techniques are based on immunochemical methods including ELISA, lateral flow dipsticks (LFDs), fluorescence polarization immunoassay (FPIA) as well as biosensor methods such as SPR and electrochemical immunoassay [5]. However, the Association of Analytical Communities (AOAC) have only approved two commercially available immunochemical kits for reliable DON detection. These are the Ridascreen Fast DON and Agra Quant DON ELISA kits which have limits of detection of < 0.2 mg/kg and 0.2 mg/kg respectively. Both of these kits are based on competitive assays. This assay format is considered the most suitable for DON detection as DON is a small molecule and hence less suitable for a sandwich assay which requires an analyte that has multiple antibody binding sites.

3.3.1.1 Optical Biosensor techniques

There have been a number of reports of the detection of DON using SPR in the literature. As mentioned in chapter 1, this technique has the advantage of being label free and reusable. The use of this technique for the detection of DON was first reported in 2003 [6]. A commercial Biacore Q system and CM5 sensor chip were used in conjunction with a range of DON antibodies. In this inhibition

assay a DON-casein conjugate and free DON in the sample solution competed for binding to a free DON antibody. A significant advantage of this technique was the ability of the sensor to be reused more than 500 times. No LOD was reported for this sensor but it was able to detect DON in contaminated wheat samples below the EU limit of 1750 $\mu\text{g}/\text{kg}$. However, in comparison to LC/MS system used to benchmark the system, there was considerable differences in the results achieved by the sensor method particularly for dry-ground samples.

Similar work has been carried out more recently again with use of a commercial Biacore SPR system and inhibition assay [7]. However, in this report the antibody used cross-reacted with DON and nivalenol (NIV) allowing detection of both these mycotoxins in wheat samples. This system achieved better comparison to LC/MS results than the work of Tudos et. al discussed above.

3.3.1.2 Immunoassay techniques

Ji et. al have reported an indirect competitive ELISA for DON detection in wheat samples [8]. This assay uses a 3-O-Hemisuccinyl-DON-Ovalbumin coating conjugate which competes with DON for binding to anti-DON IgG. Goat anti-rabbit IgG was used as the secondary antibody (presumably peroxidase linked) and an ABTS substrate was used.

Compared to other mycotoxins, there have been relatively few reports of the detection of deoxynivalenol using electrochemical immunosensors, as a number of recently published reviews have shown [9, 10, 11]. However, some examples do exist in the literature. Romanazzo et. al reported the use an Enzyme-Linked-Immuno-magnetic- Electrochemical (ELIME) assay using a DON antibody fragment and external magnetic system which could accommodate 8 separate screen printed electrodes as shown Fig 3.3. As is often the case for the detection of trichothecenes, the sensor showed large cross reactivities to 3AcDON but was insensitive to 15AcDON, HT-2, T-2 and Nivalenol.

More recently, there have been more sensitive sensors developed for DON detection. A SWCNT/Chitosan modified glassy carbon electrode again using the indirect competitive format with a DON-BSA coating conjugate was able to achieve a LOD of 5 pg/mL [1]. Differential pulse voltammetry was used which contributed to the low LOD achieved and didn't require a stirred solution.

A less sensitive, but label free impedimetric sensor was developed for DON

detection by Sunday et. al [12]. A gold nanoparticles-dotted 4-nitrophenylazo functionalised graphene modified glassy carbon electrode was used with a LOD of 0.3 $\mu\text{g}/\text{mL}$. This LOD was below EU regulatory limits and had the advantage of being label free in comparison to the other electrochemical immunosensors.

3.3.2 Chromatography based methods

After rapid screening techniques have been used to identify contaminated batches, chromatography reference methods are then used to accurately and reliably quantify DON concentrations in samples. Due to the polar nature of the DON molecule, HPLC is a popular technique for DON detection [13, 14, 15, 16]. A limit of detection of 14 $\mu\text{g}/\text{kg}$ was achieved using a UV detector in conjunction with HPLC. However, this approach has the disadvantage of requiring the samples to be derivatized in order to reduce the boiling point to allow vaporisation [17]. Hence, LC-MS and LC-MS/MS are more attractive solution as derivatization is not required. Using this technique without any sample clean-up, LODs of 10 $\mu\text{g}/\text{kg}$ and 8 $\mu\text{g}/\text{kg}$ were achieved for DON detection in corn and rice samples respectively [18].

3.3.3 Screen Printed Electrodes for Mycotoxin Detection

There have been a number of reports in the literature of the use of screen printed electrodes for mycotoxin detection. These include two approaches for the detection aflatoxin M1 (AFM1) in milk samples. AFM1 is found in milk samples due to metabolism by the cow of aflatoxin B1 which is extremely carcinogenic and is structurally similar to AFM1 [19]. Micheli et. al used a direct competitive assay in which free AFM1 and AFM1 conjugated with HRP compete to bind with anti-AFM1 antibodies immobilised onto an untreated screen printed graphite electrode . A LOD of 25 ppt and working range of 30 - 160 ppt were achieved [20]. Parker et. al also utilised a bare screen printed electrode for AFM1 detection but with a significantly higher LOD of 39,000 ppt [21]. In this assay an anti-rat capture antibody was first immobilised onto the electrode surface to allow the oriented capture of the anti-AFM1 antibodies onto the surface. HRP labelled antigen was utilised in a similar fashion to Micheli's paper. The main advantage of this approach was the sample pre-treatment incorporating 18mM calcium chloride into the washing buffer which stabilised

the whey proteins in the milk and eliminated the interference associated with these proteins.

3.4 Materials and Methods

3.4.1 Instrumentation

The instrumentation used was the same as described in chapter 2.

3.4.2 Reagents

DON-BSA coating conjugate was purchased from BioTeZ Berlin Buch GmbH (Germany). Anti-DON antibodies were purchased from antibodies-online.com (Aachen, Germany). Deoxynivalenol, PBS tablets, sodium carbonate, sodium bicarbonate, trizma base, hydrochloric acid, sodium hydroxide, diethanolamine, alkaline phosphatase labelled anti-mouse IgG, tween 20 was purchased from Sigma Aldrich (Wicklow, Ireland)

3.4.3 Electrode preparation

Screen printed electrodes were modified with MWCNT/Nafion as described in chapter 2.

3.4.4 Anti-DON IgG/Anti-mouse IgG binding study (Direct Capture Assay)

- A 1/5 dilution of Anti-DON IgG was carried out from an initial concentration of 1 mg/mL in carbonate/bicarbonate buffer. 50 μ L of each concentration was added to a well of a 96 well plate (x3).
- The plate was incubated at 37° for 1 hour.
- The plate was washed with 200 μ L of pH 7.4 Tris-Tween solution (x3) and 200 μ L of 1 % BSA was then added to each well. The plate was incubated at 37 degrees for one hour.

- The plate was washed with 200 μL of pH 7.4 Tris-Tween solution (x3) to remove excess BSA solution.
- 50 μL of AP labelled anti-mouse IgG was then added to each well and the plate was incubated at 37° for 1 hour.
- After a further washing step, 100 μL of pNPP, diluted in DEA buffer was added to each well and again a 1 hour incubation was carried out at 37°.
- The plate was measured at 405nm using the plate reader.

3.4.5 Chessboard ELISA

- 50 μL of 1/100, 1/500 and 1/1000 were added to their section on the 96 well plate as described in Fig 3.4. The plate was then incubated at 37 degrees for 1 hour
- The plate was washed with 200 μL of pH 7.4 Tris-Tween solution (x3) and 200 μL of 1 % BSA was then added to each well. The plate was incubated at 37 degrees for one hour.
- The plate was washed with 200 μL of pH 7.4 Tris-Tween solution (x3) to remove excess BSA solution
- A 1/5 serial dilution of anti-DON IgG was carried from an initial concentration of 0.04 mg/mL and 50 μL was added to the appropriate section of the plate as outlined in Fig. 3.4. The plate was incubated at 37 degrees for 1 hour.
- The plate was washed with 200 μL of pH 7.4 Tris-Tween to remove excess and loosely bound anti-DON antibodies and 50 μL AP labelled anti-mouse IgG was added to each well. The plate was incubated for a further hour at 37 degrees celcius.
- After a further washing step, 100 μL of pNPP, diluted in DEA buffer was added to each well and again a 1 hour incubation was carried out at 37 degrees celcius.
- The plate was measured at 405 nm using the plate reader.

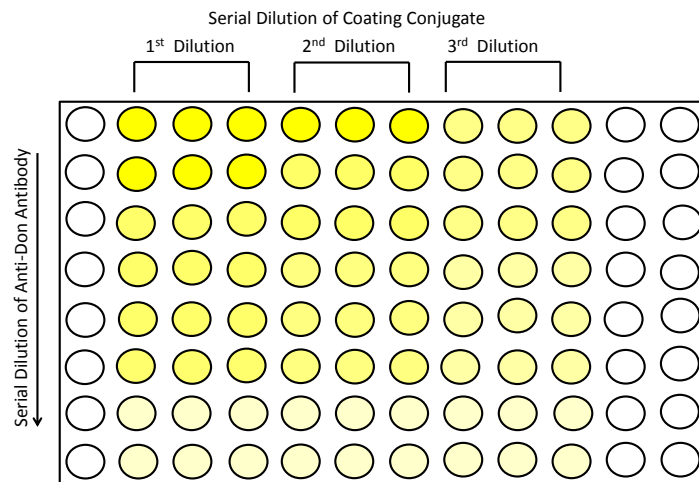


Figure 3.3: Schematic of chessboard titration

3.4.6 AP Labelled Anti-mouse IgG Optimisation (Indirect Capture Assay)

- A 1/100 dilution of DON-BSA was prepared in carbonate/bicarbonate buffer pH 9.5. 50 μL was added to each well of a 96 well plate. The plate was incubated at 37° for 1 hour.
- The plate was washed with 200 μL of pH 7.4 Tris-Tween solution (x3) and 200 μL of 1 % BSA was then added to each well. The plate was incubated at 37 degrees for one hour.
- The plate was washed with 200 μL of pH 7.4 Tris-Tween solution (x3) to remove excess BSA solution.
- 50 μL of 0.04 mg/mL anti-DON IgG was added to added to each well and the plate was incubated at 37 degrees for 1 hour followed by a further washing step.
- A 1/2 serial dilution of anti-mouse IgG was carried out and 50 μL of each concentration (in triplicate) was added to the appropriate wells.
- Measurement was then carried out for incubation times of 15, 30, 45, 60 and 75 minutes.

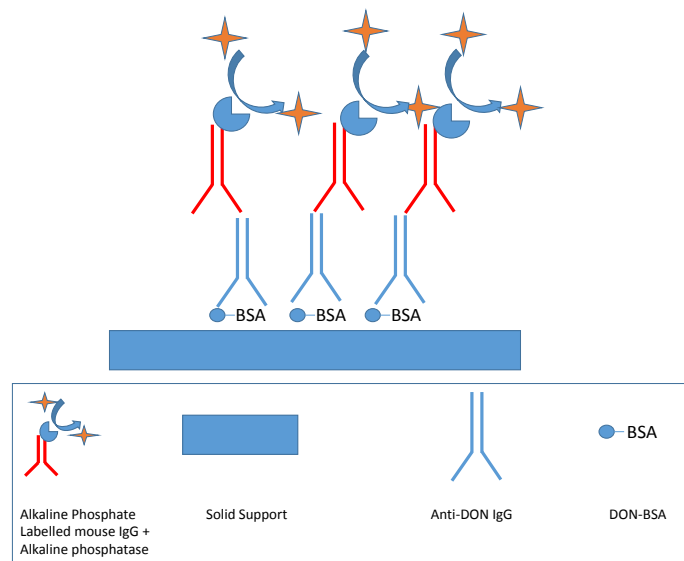


Figure 3.4: Schematic of indirect capture assay showing binding DON-BSA immobilised onto a surface with a anti-DON antibody and subsequent binding to anti-mouse AP labelled.

3.4.7 Indirect Competitive ELISA

- 50 μL of 1/100 DON-BSA in pH 9.5 carbonate/bicarbonate buffer was added to each well. The plate was then incubated at 37 degrees for 1 hour
- The plate was washed with 200 μL of pH 7.4 Tris-Tween solution (x3) and 200 μL of 1 % BSA was then added to each well. The plate was incubated at 37 degrees for one hour.
- The plate was washed with 200 μL of pH 7.4 Tris-Tween solution (x3) to remove excess BSA solution.
- 25 μL each of 0.008 mg/mL anti-DON IgG was mixed to 25 μL of AP labelled anti-mouse IgG (1/16,000 dilution) prior to addition to each well. The plate was incubated at 37 degrees for 90 minutes.
- The plate was washed with 200 μL of pH 7.4 Tris-Tween to remove excess and loosely bound antibodies and 100 μL
- After a further washing step, 100 μL of pNPP, diluted in pH 9.5 DEA buffer was added to each well and again a 1 hour incubation was carried out at 37 degrees celcius.

- The plate was measured at 405nm using the plate reader.

3.4.8 Coating Conjugate Optimisation - Indirect Capture Assay

- 8 μL 0.4M/0.1M EDC/NHS solution was added to each electrode and left to incubate at room temperature for 1 hour
- A 1/5 dilution was carried of DON-BSA and 8 μL of each concentration was added to the working electrode surface (x3) and left to incubate at room temperature for 2 hours.
- The electrodes were washed with 500 μL of 1 % Tris (0.05 % Tween) (x2) and 800 μL of nanopure water (x1).
- 60 μL of 1 % BSA was added to each electrode and allowed to incubate for 1 hour at room temperature.
- 10 μL of 1/100 concentration of anti-DON Ab (diluted in tris buffer) was added to each electrode and incubated for 1 hour at room temperature and washed with washing buffer and water again.
- 10 μL of AP labelled anti-mouse was then added to each electrode and allowed to incubate at room temperature for 1 hours
- The electrodes were stored in Tris buffer or nanopure water at 4 degrees
- For measurement, each electrode was placed in a 5 mL glass beaker containing 4900 μL of DEA buffer pH 9.5. After a period of 200 seconds, 100 μL of pAPP (25 mg/mL) was added manually. A fixed potential of 0.28 mV was used for these amperometric measurements.

3.4.9 Detecting Antibody Optimisation - Indirect Capture Assay

In order to optimise the DON Ab concentration, an indirect capture assay was again carried out. A DON-BSA concentration of 0.04 mg/mL was used (optimised from the previous section). A 1/5 serial dilution of DON Ab was carried out establish an optimum concentration and all other steps were the same as outlined from section 3.4.8.

3.4.10 Blocking Study - Indirect Capture Assay

An indirect capture assay was carried out using the concentrations optimised in sections 3.4.7 and 3.4.8. At the blocking step stage, 60 μL of 1 % BSA, 2 % BSA, 1 % casein and 2 % casein respectively were added to the electrodes (x3). The assay was completed as described in sections 3.4.8.

3.4.11 Indirect Competitive Electrochemical Immunoassay

The assay outlined in this section is for optimised parameters and is outlined graphically in Fig. 3.5.

- 8 μL 0.4 M/0.1 M EDC/NHS solution was added to each electrode and left to incubate at room temperature for 1 hour
- A 0.04 mg/mL concentration of DON-BSA and 8 μL of each concentration was added to the working electrode surface (x3) and left to incubate at room temperature for 2 hours.
- The electrodes were washed with 500 μL of 1 % Tris (0.05 % Tween) (x2) and 800 μL of nanopure water (x1).
- 60 μL of 1 % casein was added to each electrode and allowed to incubate for 1 hour at room temperature.
- A 1/5 dilution of DON antigen was carried out from an initial concentration of 5 mg/mL. Each respective concentration was mixed with an equal amount of 0.016 mg/mL anti-DON Ab and mixed gently. 10 μL of each mixture was then added to the working electrode surface and incubated at room temperature for 90 minutes followed by a washing step.
- 10 μL of AP labelled anti-mouse was then added to each electrode and allowed to incubate at room temperature for 1 hours
- The electrodes were stored in Tris buffer or nanopure water at 4 degrees.
- For measurement, each electrode was placed in a 5 mL glass beaker containing 4900 μL of DEA buffer pH 9.5. After a period of 200 seconds, 100 μL of pAPP (25 mg/mL) was added manually. A fixed potential of 0.28 mV was used for these amperometric measurements.

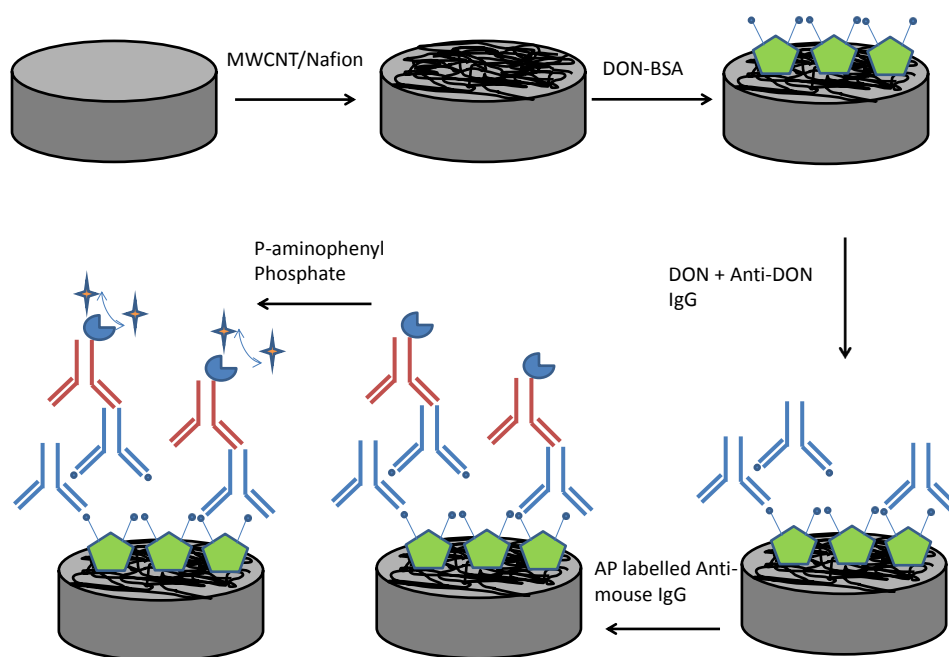


Figure 3.5: Steps involved in the preparation of immunosensor for DON detection

3.5 Results and Discussion Part 1 - ELISA

3.5.1 Anti-DON/Anti-mouse IgG binding - Direct Capture Assay

Prior to the development of the electrochemical immunosensor, initial ELISA experiments were carried out in order to examine the viability of the proposed assay and to ascertain the affinities of the assay components towards each other. The first of these experiments investigated the binding of the anti-DON monoclonal antibody (produced in mouse) to the alkaline phosphatase labelled secondary antibody used in chapter 2. A simple capture assay was employed in which a serial dilution of anti-DON antibody was immobilised onto the surface of the plate and a fixed amount of labelled antibody was introduced. From Fig 3.6. it is clear that successful binding of the anti-DON and anti-mouse antibodies occurred. Saturation of the anti-DON occurred at a concentration of 0.2 mg/mL.

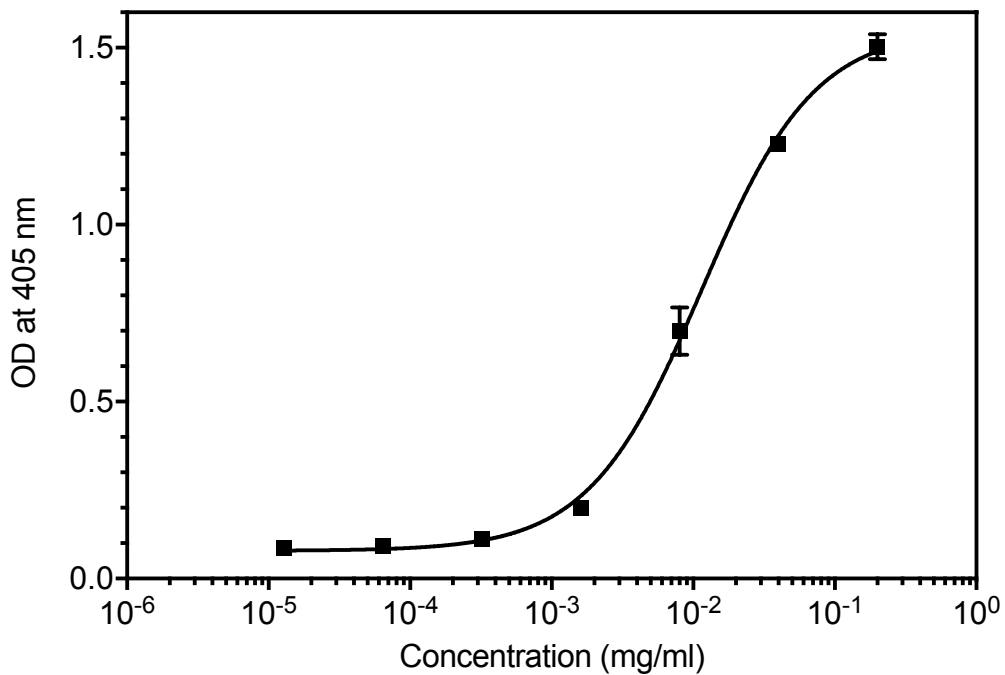


Figure 3.6: Direct capture assay for anti-DON/anti-mouse IgG revealing saturation at an anti-DON IgG concentration of 0.2 mg/mL. An AP labelled anti-mouse IgG dilution of 1/30,000 was used.

3.5.2 Chessboard Titration

Chessboard titrations provide a relatively quick and effective way of simultaneously optimising two separate assay components. In this case, an indirect capture assay was used in which DON-BSA and anti-DON antibodies were titrated against each other as outlined in the previous section again with a 1/30,000 dilution of AP labelled anti-mouse used. Fig 3.7 shows a 3D representation of the obtained data with different colours representing different absorbance regions. The absorbance increases with both Don-BSA and anti-DON antibody concentration, reaching a maximum for concentrations of 1/10 dilution and 0.04 mg/mL respectively. However, in order to conserve reagents and produce a cost effective assay a DON-BSA concentration of 1/100 was used in conjunction with the 0.04 mg/mL concentration of anti-DON antibody.

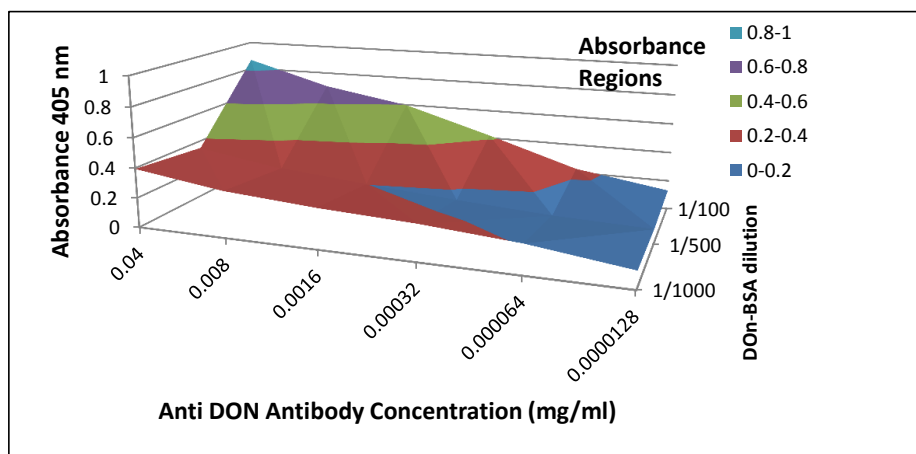


Figure 3.7: Chessboard titration results in which DON-BSA and anti-DON IgG concentrations were varied simultaneously with a maximum absorbance at a DON-BSA concentration of 1/10 and an anti-DON IgG concentration of 0.04 mg/mL.

3.5.3 Anti-mouse IgG Optimisation

Next, using the optimised concentrations of DON-BSA and anti-DON antibody determined from the previous section, the AP labelled anti-mouse IgG concentration was optimised. This was again done using the indirect capture assay format. A 1/2 serial dilution was carried out (from an initial 1/1000 dilution of the stock solution). For each dilution, the plate was measured at 15 minute intervals. From Fig. 3.8, 1/16,000 was chosen as the optimal secondary antibody dilution with an incubation time of 1 hour. There was comparatively little variation between OD values for different incubation times at this concentration. This should lead to less inter assay variability and also negates the need for a stop solution. Also, an OD value of around 1 is obtained at these parameters. OD values above 2 are not suitable, as they are outside the linear range of the instrument.

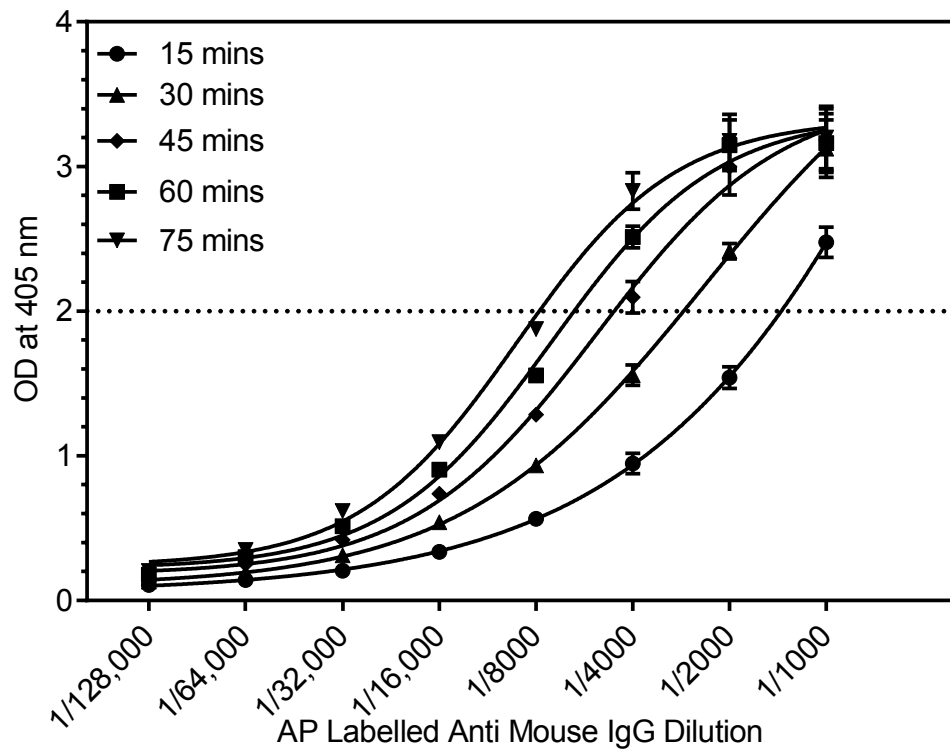


Figure 3.8: Indirect capture assay where AP labelled anti-mouse IgG concentration is varied with DON-BSA and anti-DON IgG concentrations of 1/100 and 0.04 mg/mL respectively. $n = 3$.

3.5.4 Competitive ELISA

An indirect competitive assay was then carried using the parameters optimised in the previous sections. A competition time of 90 minutes was used as this had been shown to help negate the low dose effect in Chapter 2. The calibration curve is shown in Fig. 3.9 and the assay parameters are summarised in table 3.2. The linear range and LOD were calculated as outlined in the statistical analysis section at the end of chapter 1.

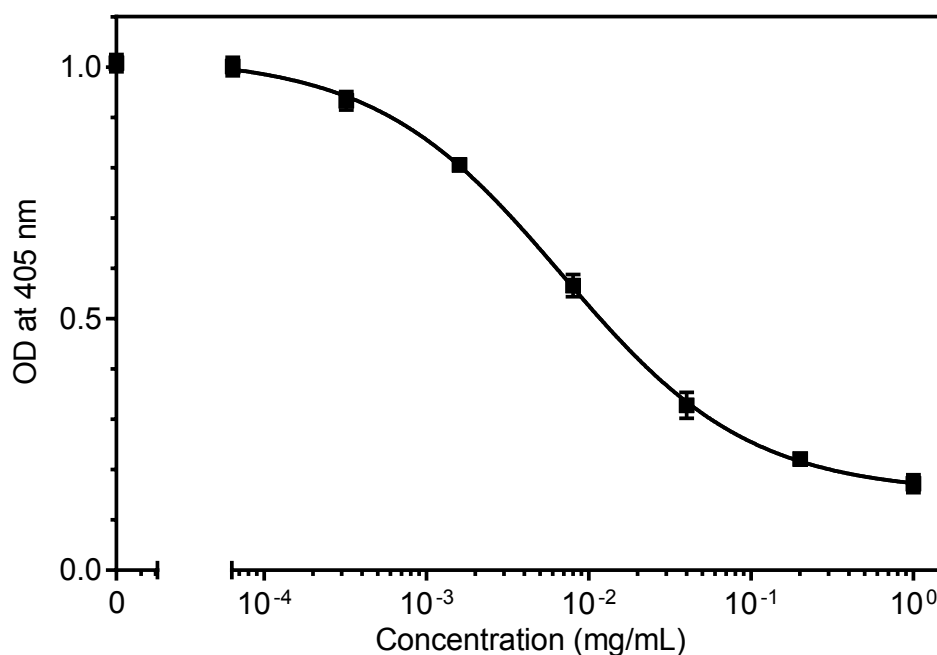


Figure 3.9: Indirect Competitive ELISA for DON with optimised DON-BSA, anti-DON IgG and AP labelled anti-mouse IgG of 1/100, 0.04 mg/mL and 1/16,000 respectively. $R^2 = 0.9975$, $n = 3$.

Table 3.2:

IC50	LOD	Linear Range	Inhibition	R^2 %
6.856 ppm	0.534 ppm	0.9 - 53 ppm	87 %	0.9975

Importantly, the limit of detection (blank - $3 \times \text{std}_{\text{blank}}$) of 0.534 ppm is below the EU regulation limit of 1.75 ppm for DON in wheat samples. However, it is above the 0.2 ppm limit for baby food meaning that this assay would not be suitable for that particular application.

3.6 Results and Discussion Part 2 - Electrochemical Immunoassay

In this section the assay developed in part 1 was then transferred onto the MWCNT/Nafion modified screen printed electrode for the development of an electrochemical immunosensor.

3.6.1 Assay component solution

Initial assay development experiments which attempted to optimise the DON-BSA concentration on the electrode surface resulted in very high levels of non-specific binding in which there was little to no difference between varying concentrations of DON-BSA and the blank control. In these experiments, both anti-DON IgG and anti-mouse IgG were diluted in Tris solution only. In order to rectify the issue, it was decided to vary the solution that each assay component was diluted in. Fig 3.10 shows that complete blocking of the electrode surface occurred when both anti-DON IgG and anti-mouse IgG were diluted in 2 % casein blocking solution (the decision was taken to change from BSA to casein as a blocking agent due to its better performance on carbon nanotube electrodes). However, a clear difference in signal could be achieved if either the anti-DON IgG or anti-mouse IgG were diluted in casein with the other in Tris solution. Diluting anti-DON in casein was carried out for subsequent experiments.

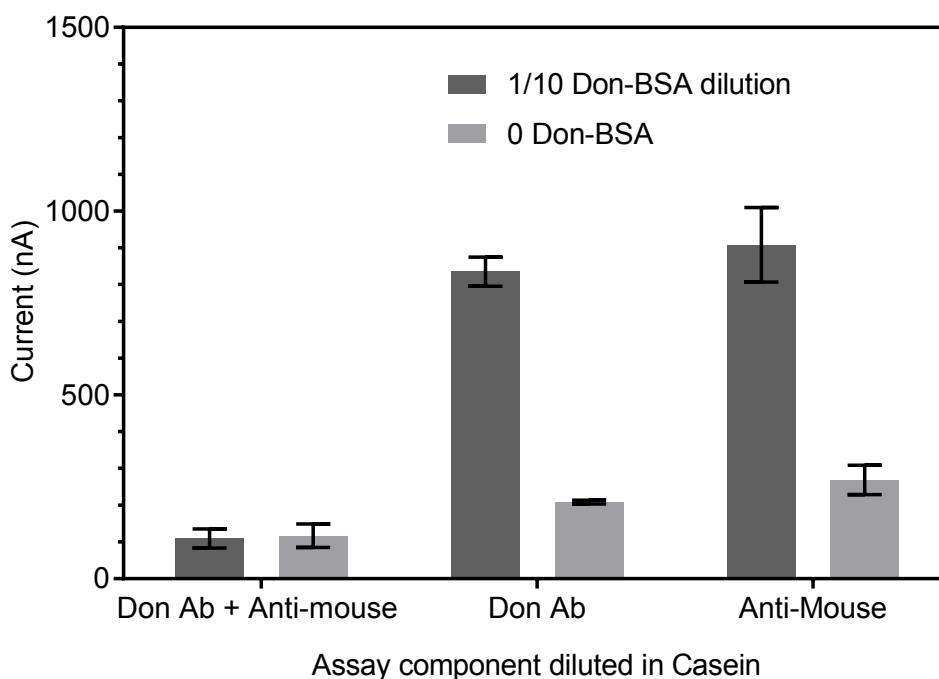


Figure 3.10: Optimisation of assay component solution

3.6.2 Coating Conjugate Optimisation

Having obtained an optimal assay component dilution, attention was returned to optimising DON-BSA concentration on the electrode surface. A fixed 0.04 mg/mL dilution of anti-DON IgG was chosen to conduct the experiment as the high concentration was guaranteed to give an adequate electrochemical signal. Similarly to the ELISA assay, saturation was achieved at 0.04 mg/mL DON-BSA concentration as seen in Fig. 3.11 and hence this concentration was used for all further experiments.

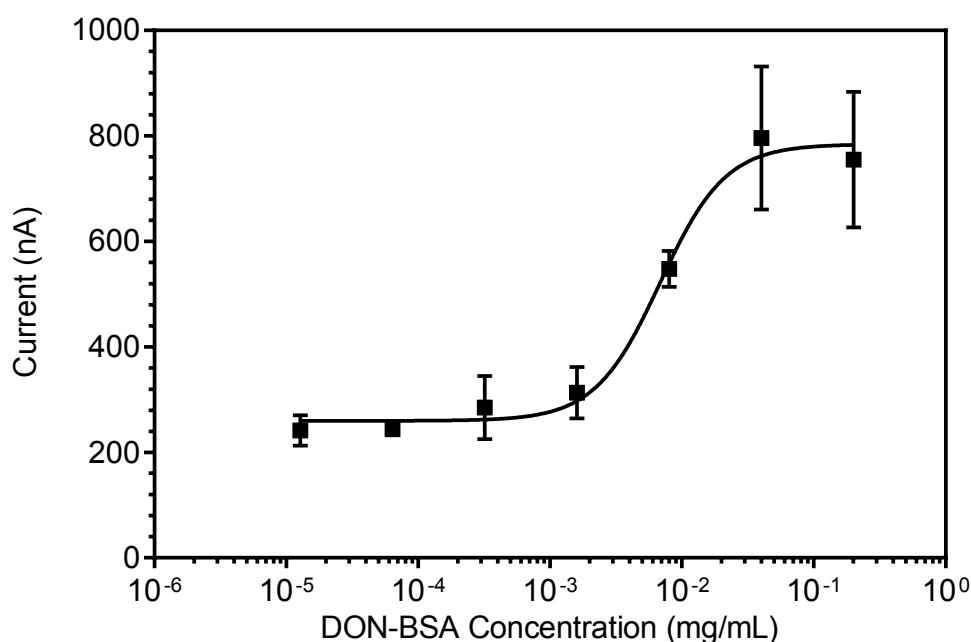


Figure 3.11: Optimisation of DON-BSA coating conjugate using an indirect capture capture assay with a fixed anti-DON IgG concentration of 0.04 mg/mL and a 1/1000 dilution of AP labelled anti-mouse IgG. Saturation was achieved at a DON-BSA concentration of 0.04 mg/mL. $n = 3$.

3.6.3 Detecting Antibody Optimisation

Using the optimised DON-BSA concentration, a 1/5 serial dilution of anti-DON IgG was carried out (Fig 3.12). A levelling off of current signal occurred at 0.008 mg/mL and this concentration was used for all further experiments.

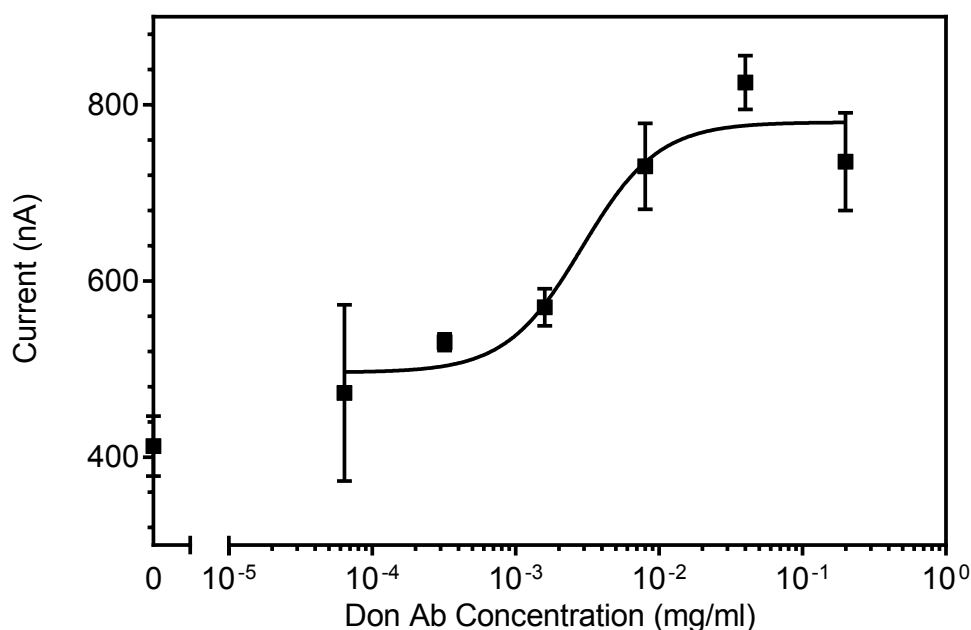


Figure 3.12: Optimisation of anti-DON IgG concentration using an indirect capture assay with DON-BSA concentration of 0.04 mg/mL, AP labelled anti-mouse IgG dilution of 1/1000. Current saturation occurred at 0.008 mg/mL. $n = 3$.

3.6.4 Blocking Study

It was stated in section 4.6.1 that the decision was made to change from BSA from casein solution as it had proved to be a more blocking buffer. This is possibly due to the fact that BSA doesn't bind as strongly to hydrophobic surfaces such as carbon nanotubes[22]. A further investigation into the blocking buffer to use for this assay was carried out by comparing non-specific binding in an indirect capture assay. 1 % and 2 % BSA and casein solutions were compared. Fig 3.13 shows that both casein solutions proved superior to BSA in preventing non-specific binding. Hence, 1 % casein was used for future experiments.

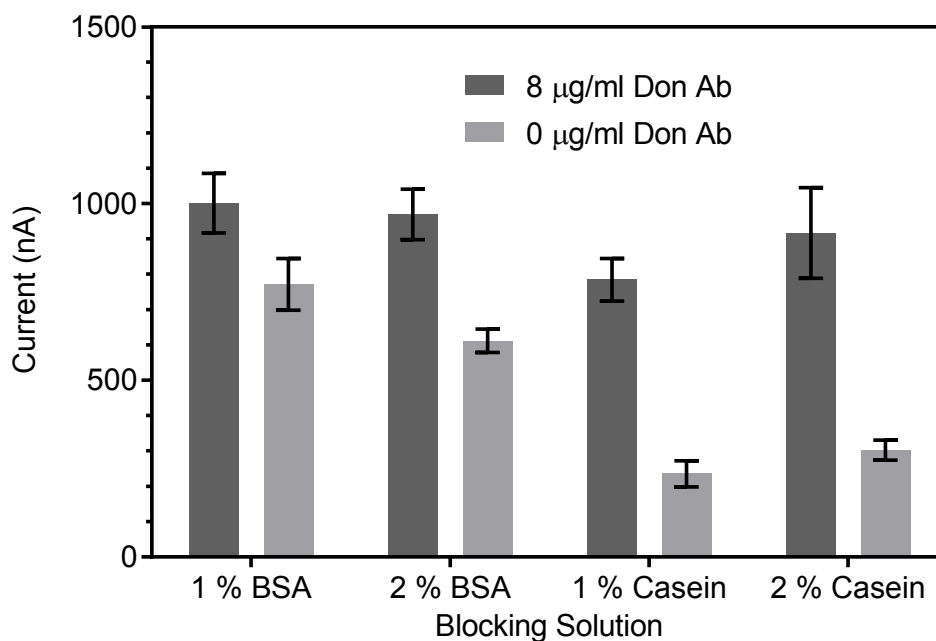


Figure 3.13: An indirect capture assay with DON-BSA concentration of 0.04 mg/mL, AP labelled anti-mouse IgG dilution of 1/1000 and anti-DON IgG concentration of 0.008 mg/mL. 4 different blocking solutions were compared - 1 % BSA, 2 % BSA, 1 % BSA and 2 % BSA. $n = 3$.

3.6.5 AP labelled anti-mouse optimisation

The assay parameters established thus far were used to construct an indirect competitive assay for DON. However, there were significant repeatability issues as well as there being little variation in electrochemical signal between high and low DON concentrations. Up to this point in the development of the assay a concentration of 1/1000 AP labelled anti-mouse IgG had been used. However, 3 other dilutions (1/750, 1/500 and 1/100) were analysed using an indirect capture assay with optimised DON-BSA and anti-DON IgG concentrations. Fig 3.14 shows that the largest current to background signal was achieved with the 1/100 concentration and this dilution factor was used in subsequent experiments.

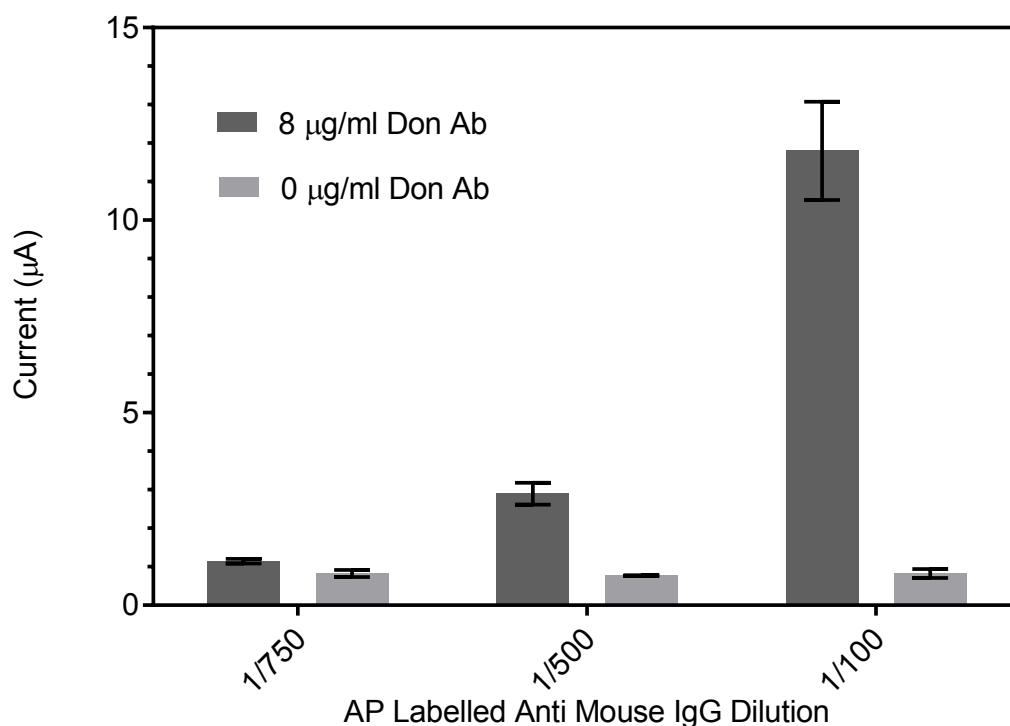


Figure 3.14: An indirect capture assay with DON-BSA concentration of 0.04 mg/mL and anti-DON IgG concentration of 0.008 mg/mL. 3 different concentrations of AP labelled anti-mouse were compared - 1/750, 1/500 and 1/100. $n = 3$.

3.6.6 Indirect Competitive Immunosensor

Finally, using the parameters optimised in the previous sections of this chapter an indirect competitive assay was carried out as described in section 3.4.12. The analytical parameters are outlined in Table 3.3. The IC₅₀ value of 2 ppm is particularly interesting considering MRL of DON in wheat samples in 1.75 ppm. Although more sensitive electrochemical immunosensors for DON have been outlined (discussed in the introduction to this chapter), this approach appears particularly promising as the assay developed is sensitive to changes around the relevant concentrations of DON concentrations in grain samples from regulatory point of view.

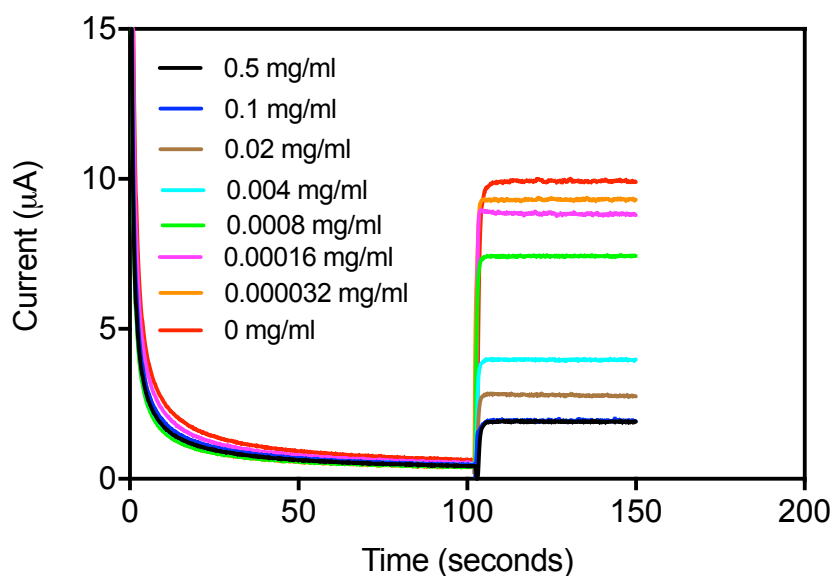


Figure 3.15: Hydrodynamic amperograms for a range of DON concentrations at a MWCNT/Nafion electrode. After a period of 200 seconds 100 μL of pAPP (25 mg/mL) was added to a stirred solution of 4900 μL DEA buffer, pH 9.5. A fixed potential of 0.28 mV was used.

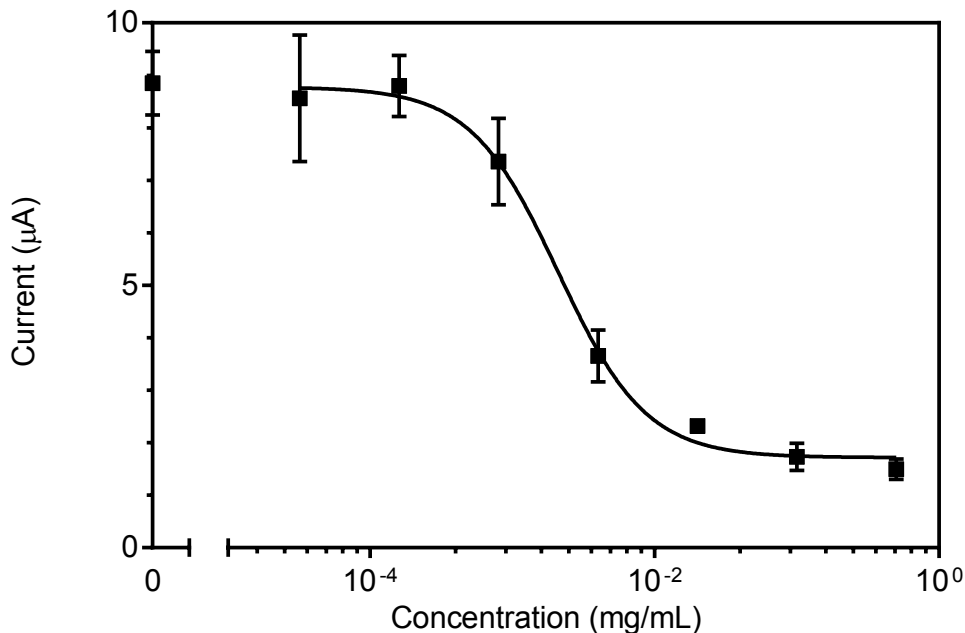


Figure 3.16: Indirect competitive electrochemical immunoassay for DON with optimised experimental conditions of DON-BSA concentration of 0.04 mg/mL, AP labelled anti-mouse IgG dilution of 1/100 and anti-DON IgG concentration of 0.008 mg/mL. 1 % casein was used as a blocking solution. $R^2 = 0.9679$, $n = 3$.

Table 3.3: Summary of results for an optimised electrochemical immunosensor for DON detection at a MWCNT/Nafion modified electrode.

IC50	LOD	Linear Range	R ²
2 ppm	0.95 ppm	0.7 - 6.3 ppm	0.9679

3.7 Conclusions and Future Work

In this chapter a MWCNT/Nafion modified screen printed electrode was developed for the detection of the mycotoxin deoxynivalenol with a LOD of 0.95 ppm, linear range of 0.7 - 6.3 ppm and R² value of 0.9769. This compared to an LOD of 0.534 ppm and linear range of 0.9 - 53 ppm for a customised ELISA. The LODs achieved should allow detection in wheat and grain samples that is in line with the sensitivity required by EU regulations (1.75 ppm). Various assay parameters (assay component concentration, blocking solution etc. were optimised using indirect capture assays for both the ELISA and electrochemical immunosensor.

The developed sensor is based on an indirect competitive assay. Future work could also investigate the use of a displacement assay which could decrease end user steps. Another approach could be to use a direct competitive assay which could use a enzyme labelled DON antibody which would decrease overall assay development time by negating the need for an enzyme labelled secondary antibody. Furthermore, the development of a label free sensor could be investigated using the MWCNT/Nafion electrode optimised in this study. Clearly, further work is needed to allow the sensor developed to be used in real samples. One such approach could be the use of an immunoaffinity column in order to isolate the analyte from the real sample. It will also be necessary to investigate how the sensor performs in the presence of other mycotoxins, in particular 3-Ac-DON which tends to have a strong cross reactivity towards anti-DON antibodies. Future work would also require comparison of the sensor with a standardised reference method of DON detection such as a commercially available ELISA kit.

References

- [1] Ying Qing, ChaoRui Li, XianXian Yang, XiPeng Zhou, Jian Xue, Mei Luo, Xuan Xu, Shuai Chen, and JingFu Qiu. Electrochemical immunosensor using single-walled carbon nanotubes/chitosan for ultrasensitive detection of deoxynivalenol in food samples. *Journal of Applied Electrochemistry*, pages 1–9, June 2016.
- [2] James J. Pestka. Deoxynivalenol: mechanisms of action, human exposure, and toxicological relevance. *Archives of Toxicology*, 84(9):663–679, August 2010.
- [3] T. Yoshizawa and N. Morooka. Deoxynivalenol and Its Monoacetate - New Mycotoxins from *Fusarium-Roseum* and Moldy Barley. *Agricultural and Biological Chemistry*, 37(12):2933–2934, 1973. WOS:A1973R893700040.
- [4] P. Fandohan, K. Hell, W. F. O. Marasas, and M. J. Wingfield. Infection of maize by *Fusarium* species and contamination with fumonisin in Africa. *African Journal of Biotechnology*, 2(12):570–579, January 2003.
- [5] Julie P. Meneely, Francesco Ricci, Hans P. van Egmond, and Christopher T. Elliott. Current methods of analysis for the determination of trichothecene mycotoxins in food. *TrAC Trends in Analytical Chemistry*, 30(2):192–203, February 2011.
- [6] A. J. Tudos, E. R. Lucas-van den Bos, and E. C. A. Stigter. Rapid surface plasmon resonance-based inhibition assay of deoxynivalenol. *Journal of Agricultural and Food Chemistry*, 51(20):5843–5848, September 2003. WOS:000185403200003.
- [7] Tomoyuki Kadota, Yoko Takezawa, Satoshi Hirano, Osamu Tajima, Chris M. Maragos, Takashi Nakajima, Toshitsugu Tanaka, Yoichi Kamata, and Yoshiko Sugita-Konishi. Rapid detection of nivalenol and deoxynivalenol in wheat using surface plasmon resonance immunoassay. *Analytica Chimica Acta*, 673(2):173–178, July 2010. WOS:000280213500010.
- [8] Fang Ji, Hua Li, Jianhong Xu, and Jianrong Shi. Enzyme-Linked Immunosorbent-Assay for Deoxynivalenol (DON). *Toxins*, 3(8):968–978, August 2011.

- [9] Xu Wang, Reinhard Niessner, Dianping Tang, and Dietmar Knopp. Nanoparticle-based immunosensors and immunoassays for aflatoxins. *Analytica Chimica Acta*, 912:10–23, March 2016.
- [10] Gaelle Catanante, Amina Rhouati, Akhtar Hayat, and Jean Louis Marty. An Overview of Recent Electrochemical Immunosensing Strategies for Mycotoxins Detection. *Electroanalysis*, 28(8):1750–1763, August 2016.
- [11] Ruchika Chauhan, Jay Singh, Tushar Sachdev, T. Basu, and B. D. Malhotra. Recent advances in mycotoxins detection. *Biosensors and Bioelectronics*, 81:532–545, July 2016.
- [12] Christopher Edozie Sunday, Milua Masikini, Lindsay Wilson, Candice Rassie, Tesfaye Waryo, Pricilla G. L. Baker, and Emmanuel I. Iwuoha. Application on Gold Nanoparticles-Dotted 4-Nitrophenylazo Graphene in a Label-Free Impedimetric Deoxynivalenol Immunosensor. *Sensors*, 15(2):3854–3871, February 2015.
- [13] S. Daenicke, H. Valenta, and S. Matthes. On the interactions between Fusarium toxin-contaminated wheat and nonstarch polysaccharide hydrolyzing enzymes in diets of broilers on performance, intestinal viscosity, and carryover of deoxynivalenol. *Poultry Science*, 86(2):291–298, February 2007. WOS:000243841800012.
- [14] S. Danicke, K. P. Brussow, H. Valenta, K. H. Ueberschar, U. Tiemann, and M. Schollenberger. On the effects of graded levels of Fusarium toxin contaminated wheat in diets for gilts on feed intake, growth performance and metabolism of deoxynivalenol and zearalenone. *Molecular Nutrition & Food Research*, 49(10):932–943, October 2005. WOS:000233039300005.
- [15] E. Razzazi-Fazeli, J. Bohm, K. Jarukamjorn, and J. Zentek. Simultaneous determination of major B-trichothecenes and the de-epoxy-metabolite of deoxynivalenol in pig urine and maize using high-performance liquid chromatography-mass spectrometry. *Journal of Chromatography B-Analytical Technologies in the Biomedical and Life Sciences*, 796(1):21–33, October 2003. WOS:000185955700003.
- [16] Michael Sulyok, Franz Berthiller, Rudolf Krska, and Rainer Schuhmacher. Development and validation of a liquid chromatography/tandem mass spectrometric method for the determination of 39 mycotoxins in

- wheat and maize. *Rapid Communications in Mass Spectrometry*, 20(18):2649–2659, 2006. WOS:000240951100003.
- [17] Ran Ran, Canhua Wang, Zheng Han, Aibo Wu, Dabing Zhang, and Jianxin Shi. Determination of deoxynivalenol (DON) and its derivatives: Current status of analytical methods. *Food Control*, 34(1):138–148, November 2013.
- [18] F. Soleimany, S. Jinap, and F. Abas. Determination of mycotoxins in cereals by liquid chromatography tandem mass spectrometry. *Food Chemistry*, 130(4):1055–1060, February 2012. WOS:000296124600040.
- [19] U. Konietzny and R. Greiner. The application of PCR in the detection of mycotoxigenic fungi in foods. *Brazilian Journal of Microbiology*, 34(4):283–300, December 2003. WOS:000234802400001.
- [20] L. Micheli, R. Grecco, M. Badea, D. Moscone, and G. Palleschi. An electrochemical immunosensor for aflatoxin M1 determination in milk using screen-printed electrodes. *Biosensors & Bioelectronics*, 21(4):588–596, October 2005.
- [21] Charlie O. Parker and Ibtisam E. Tohill. Development of an electrochemical immunosensor for aflatoxin M1 in milk with focus on matrix interference. *Biosensors and Bioelectronics*, 24(8):2452–2457, April 2009.
- [22] Y. L. Jeyachandran, E. Mielczarski, B. Rai, and J. A. Mielczarski. Quantitative and Qualitative Evaluation of Adsorption/Desorption of Bovine Serum Albumin on Hydrophilic and Hydrophobic Surfaces. *Langmuir*, 25(19):11614–11620, October 2009.

Chapter 4

Electrochemical Detection of Caffeine

4.1 Objectives and Novelty

The central objective of this chapter was to develop a low cost sensor for caffeine detection. In part one, Nafion modified screen printed graphite electrodes and electrochemically pretreated screen printed graphite electrodes were compared and the advantages and disadvantages of each approach were investigated. It was found that the electrochemically pretreated electrode could be used as a re-usable sensor for up to 9 consecutive measurements. In contrast, the Nafion modified electrode was more suitable as a disposable sensor but lower limits of detection could be achieved. It was also the case that the Nafion modified electrode performed significantly better in the real samples.

In part 2, a commercial screen printed graphene electrode was investigated for its use in caffeine detection. Particular attention was paid to the characterisation of this electrode towards an appraisal of its graphene type qualities. It was found that this electrode offered no discernable improvement compared to the screen printed graphite electrodes used in part 1. Furthermore, it was found that the electrode was in fact graphite in nature and displayed no graphene characteristics.

This chapter presents a new electrochemical pretreatment technique which allows for a significant improvement in electrochemical signal for caffeine oxidation compared to bare screen printed electrodes. This is the first reported re-usable, low cost caffeine sensor based on screen printed electrodes. The only previously published report using SPEs was based on a disposable reduced graphene modified electrode [1]. Without the need for a nanomaterial modifier and also the fact that the sensor could be used up to 9 times means that it provides a significantly more cost effective solution than those previously presented in the literature. Furthermore, this chapter also provides the first physical and electrochemical characterisation of commercial screen printed graphene electrodes based on graphene ink. It was concluded that these commercial sensors had the characteristics of graphite as opposed to graphene.

4.2 Introduction

Caffeine (1,3,7-trimethylxanthine) (Fig. 4.1) is a ubiquitous modern drug, being a constituent of tea, coffee as well as a range of soft drinks. It has been

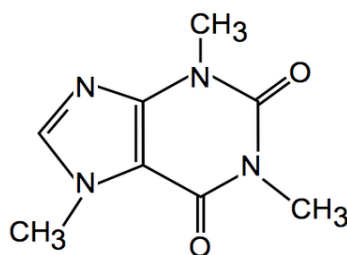


Figure 4.1: Chemical structure of caffeine

associated with both positive health effects such as increased cognitive function [2] as well negative effects such as the increased occurrence of headaches particularly when users suddenly stop taking the substance [3]. Hence, it is of paramount importance that food companies are able to perform analytical tests for caffeine in their products. This is particularly the case for so called energy drinks have a very high caffeine content. Any drinks in the EU now containing more than 150 mg of caffeine per litre must have a label indicating high caffeine content. Also where caffeine is added to foods for physiological effect, the packaging must contain the phrase - 'High caffeine content. Not recommended for children or pregnant or breast-feeding women'.

For these reasons there has been a significant amount of research into techniques enabling the detection of caffeine. Many of these studies were based on techniques such as gas chromatography/mass spectroscopy [4], ion chromatography [5] and high performance liquid chromatography [6]. These techniques, whilst providing good reproducibility and sensitivity, are expensive to carry out and require highly skilled personnel. For these reasons electrochemical detection of caffeine provides a low cost, easy to use alternative. The major difficulty in attempting to detect caffeine electrochemically, results from the fact that its oxidation occurs at a high potential (1.2-1.4 V) [7]. Hence, any electrode material used must have a wide potential range, in order for the oxidation peak to be distinguished from the background buffer.

A 2013 review of these techniques has been carried out by Svorc [8]. This review paper indicates that the majority of research on the area is focused on the detection of caffeine by voltammetric methods using carbon based electrodes. This trend has continued to the present day. For example, Torres et al. have developed a simple electrochemical sensor based on a Nafion modified glassy carbon electrode [9]. Interestingly, they showed that the

Nafion modified sensor was more sensitive than a multiwalled carbon nanotube modified electrode or a poly(3,4-ethylenedioxy-thiophene) (PEDOT) modified electrode achieving a limit of detection of 0.04 μM .

Boron doped diamond is another carbon based electrode material that has been used for the electrochemical detection of caffeine in both pharmaceutical formulations [10],[11] and beverage samples [12].

Alizadeh et al. developed a caffeine sensor utilising a molecularly imprinted polymer synthesised specifically for caffeine and embedded onto a carbon paste electrode [13]. A limit of detection of $1.5 \times 10^{-8} \text{ mol L}^{-1}$ was achieved. A carbon paste electrode was also used by Sanghavi et al. to achieve a limit of detection of $8.83 \times 10^{-8} \text{ M}$. In their case the electrode was modified with in situ surfactant modified multiwalled carbon nanotubes [14]. A recently published account compared caffeine detection at a boron doped diamond electrode and a batch injection analysis system [15]. Slightly better % RSD of 3.1 % vs 4.1 % was found for the batch injection analysis system but the electrochemical cell was able to achieve a lower LOD. Considering that LOD is not a particularly significant parameter in food samples with high caffeine content, this automated system shows promise for high throughput analysis. Another important consideration in caffeine sensor development is the ability of the sensor to detect caffeine in potentially interfering compounds. With that in mind, Jesny et. al developed a sensor that could detect caffeine the presence of xanthine, theophylline and uric acid using square wave voltammetry [16]. Well defined oxidation peaks were observed for each analyte.

4.2.1 Nafion modified electrodes

Nafion is a perfluorinated polymer first synthesised in the 1960s by DuPont. As an excellent conductor of protons, it has been used extensively in the development of fuel cell applications [17]. However, Nafion has also been useful in the construction of electrochemical sensors. This can be attributed to its unique ion-exchange, discriminative and biocompatibility properties. It has also been used as a stable solvent for carbon nanotubes, in the construction of hydrogen peroxide based biosensors and the detection of NADH [18]. Nafion can also improve graphene based sensors by re-orienting graphene layers to expose their edge planes, hence improving electron transfer rates [19]. In the case of caffeine detection, Nafion has proved to be a very useful electrode

modification allowing a dramatic increase in peak current densities.

4.2.2 Screen Printed Graphene Electrodes

In the previous chapters of this thesis the use of nanomaterials has been facilitated through the use of the drop cast method. However, this process of pipetting a small amount material that has been dispersed in a solvent onto an electrode surface has a number of limitations. Firstly, the need to modify electrode surfaces is a time consuming process that also incurs the extra cost of the modifier. Also, the drop-cast method tends to produce electrode surfaces that are less reproducible. Hence, it is advantageous to consider materials that contain the inherent characteristics of the nanomaterial without the need for any electrode modification. One approach is through the use of graphene inks for the production of screen printed graphene electrodes.

Despite the potential advantages of this approach, only two reports exist in the literature on the use of graphene screen printed electrodes for electrochemical sensing applications. The first, by Ping et al. reported the use of a home made chemically reduced graphene oxide ink for the detection of ascorbic acid, dopamine and uric acid [20]. The fabricated graphene sensor had an improved electrochemical response towards the ferri/ferrocyanide redox couple, ascorbic acid, dopamine acid and uric acid, in particular the latter three analytes were detected at different potentials simultaneously. However, Randviir et al. presented a number of criticisms to this approach [21]. As the graphene used was produced using the modified Hummers method the electrocatalytic effect was mostly likely due to the large number of defects on the basal plane surface of the electrode and also from metal ions which are a byproduct from the strong acids used in this graphene synthesis method. It was argued that the electrode was in fact more electrochemically graphite like than graphene like with respect to edge plane content.

With these criticisms in mind Randviir et. al claimed the first reported use of what they describe as a 'true screen-printable graphene ink' [21]. Two commercially available graphene inks were used from Gwent Materials Ltd. However, only one appeared to exhibit graphene like behaviour with the other displaying graphite properties as determined by Raman Spectroscopy, XPS and SEM. Ascorbic acid, uric acid and dopamine were investigated electrochemically although only at fixed concentrations and a single scan rate

(100 mV/s). The oxidation potentials for ascorbic acid and dopamine were noticeably different, but UA and AA had similar peak potentials. So, although a true screen printable graphene electrode was reported its actual analytical characteristics were inferior to those reported by Ping et al.

In this chapter, the only currently available commercial screen printed graphene electrode (Kanichi Research Limited) is analysed for the voltammetric detection of caffeine and more broadly for its use in other electroanalytical applications. It becomes clear that this commercially available graphene electrode displays characteristics very similar to that of a graphite electrode.

4.3 Materials and Methods

4.3.1 Reagents

Caffeine, phosphoric acid, boric acid, acetic acid, sodium chloride, potassium chloride and Nafion perfluorinated solution were purchased from Sigma Aldrich (Wicklow, Ireland). All solutions were made up using de-ionised water of resistivity no less than 18.2 m Ω cm. 10 mM stock solutions of caffeine were made up daily and diluted with supporting electrolyte to the appropriate molarity. Stock solutions were then sonicated in a water bath for around 20 minutes or until the caffeine had fully dissolved. All chemicals were of analytical grade.

4.3.2 Electrochemical measurements

All electrochemical measurements were carried out in a 5 mL beaker in a Faraday cage. The solution was agitated using a magnetic stirrer between measurements. All electrochemical measurements were carried out on a PalmSens potentiostat (PalmSens BV, The Netherlands) or CHI Potentiostat 660B (CH Instruments Inc., Austin, Texas). Screen printed graphite and screen printed graphene electrodes were purchased from Kanichi Research Ltd. (Manchester, UK).

4.3.3 Modification of Electrodes with Nafion

Prior to modification, the electrodes were pre-anodised in Na_2CO_3 as described earlier in the thesis producing an electrochemically activated, hydrophilic surface. Next, 5 % nafion was diluted to different concentrations using de-ionised water. 4 μl of the diluted Nafion samples were then drop cast onto the working electrode. The solution was allowed to evaporate from the surface of the electrode for at least 1 hour and stored at 4 degrees celcius.

4.3.4 Effect of pH and Supporting Electrolyte

Britton-Robinson Buffer was prepared by mixing equal volumes 0.04 M concentrations of boric acid, phosphoric acid and acetic acid. Different buffer pHs from 2 to 8 were prepared by adjusting the solution using 0.2 M sodium hydroxide. Cyclic voltammograms were then carried out in 200 μM caffeine solution.

4.3.5 Real Sample Analysis

Red Bull energy drink was purchased from a local store. The sample was poured into a glass beaker and allowed to de-gas for around an hour. Then, a 1/10 dilution was carried out with phosphoric acid prior to analysis.

4.3.6 Raman Spectroscopy

Raman Spectroscopy measurements were carried out using an Invia Reflex MicroRaman Renishaw. The laser wavelength used was 514.5 nm. The grating used was 2400 lines/mm and the laser power on sample was 2mW.

4.3.7 SEM

SEM measurements were carried out as described in Chapter 2.

4.3.8 Contact Angle

Contact angle measurements were carried out as described in Chapter 2.

4.4 Results and Discussion

4.4.1 Influence of pH and Supporting Electrolyte

In order to investigate the influence of pH in caffeine oxidation, cyclic voltammetry measurements of 200 μM caffeine were carried in 0.1 M Britton-Robinson buffer from pH 2-7 at a bare graphite SPE. This “universal buffer” is a combination of boric, phosphoric and acetic acid, titrated to the desired pH with sodium hydroxide. Each of these acids has a different dissociation constant allowing a wide range of pHs to be established.

In Fig 4.2 it is seen that peak potential decreases linearly with increasing pH with a slope of 19 mV/pH with an R^2 value of 0.8485. Similarly, Svorc et. al [22] and Spataru [7] showed a linear decrease in potential with increasing pH, in their case at boron doped diamond electrodes. However, both papers reported a “Nernstian” response of ca 60 mV/pH which was deemed to indicate that an equal number of protons and electrons were involved in the reaction. These results were reported without consideration towards the electrochemical reversibility of the reaction - the only case in which the Nernst equation applies. One method to determine electrochemical reversibility is through investigation of scan rate. Scan rate studies for caffeine oxidation as seen in this thesis (section 4.48) and throughout the literature show a shift in peak potential with increasing scan rate [22, 23] . This is indicative of a quasi or irreversible process and hence the Nernst equation should not be applied. Caution is therefore needed in the analysis of pH variance and a “non-Nernstian” response as seen in this work should not be viewed as indicative of a different reaction mechanism at work. Nevertheless, the variation of peak potential with pH does indicate that protons are involved in the reaction.

The relationship between peak current and pH is of more value when considering the design of an electrochemical sensor. Fig 4.3 shows that peak current is maximal at pH 2 and reaches a minimum at pH 4. Also of note is the poor reproducibility at pH 7. At higher pH values it was difficult to

establish a peak current as it became masked by the background discharge of the supporting electrolyte. Hence, it was established that acidic conditions were more favourable for caffeine oxidation owing to the large and clearly defined peak current.

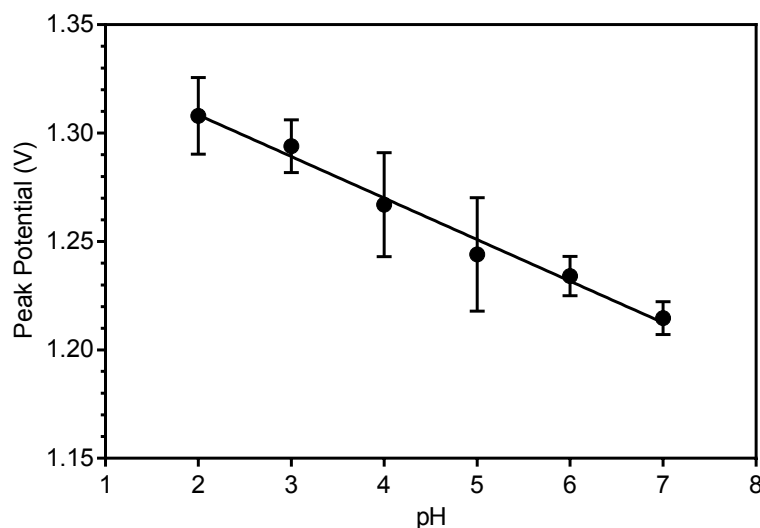


Figure 4.2: Variation of pH as a function of peak potential of cyclic voltammetry measurements with a scan rate of 100 mV/s in 200 μ M caffeine (Britton-Robinson supporting electrolyte. $R^2 = 0.8485$, $n = 3$.)

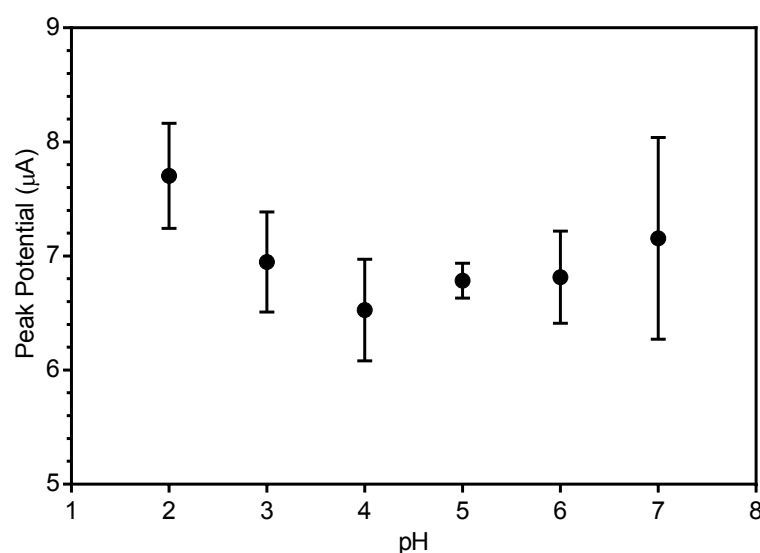


Figure 4.3: Variation of pH as a function of peak current of cyclic voltammetry measurements with a scan rate of 100 mV/s in 200 μ M caffeine (Britton-Robinson supporting electrolyte).

Hence, cyclic voltammograms of 200 μM caffeine in four different acids, sulphuric acid, phosphoric acid, nitric acid and hydrochloric acid (all 0.1 M), were compared in order to choose an appropriate supporting electrolyte.

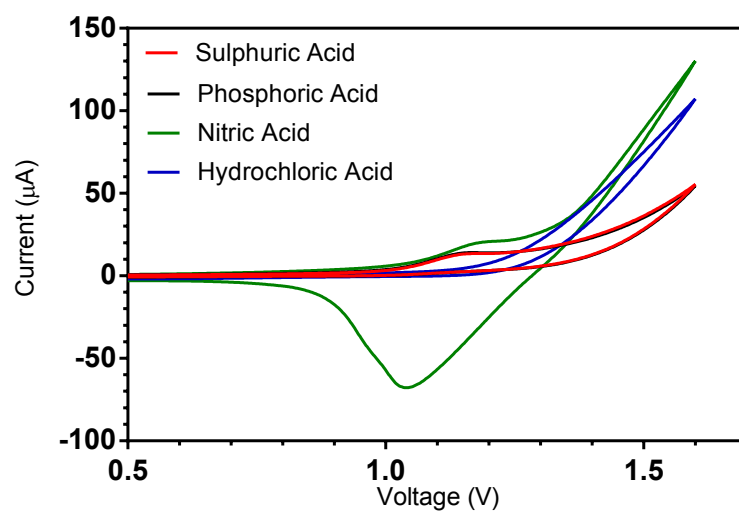


Figure 4.4: Cyclic voltammograms of 200 μM caffeine in different acidic media at a scan rate of 100 mV/s with a bare graphite SPE.

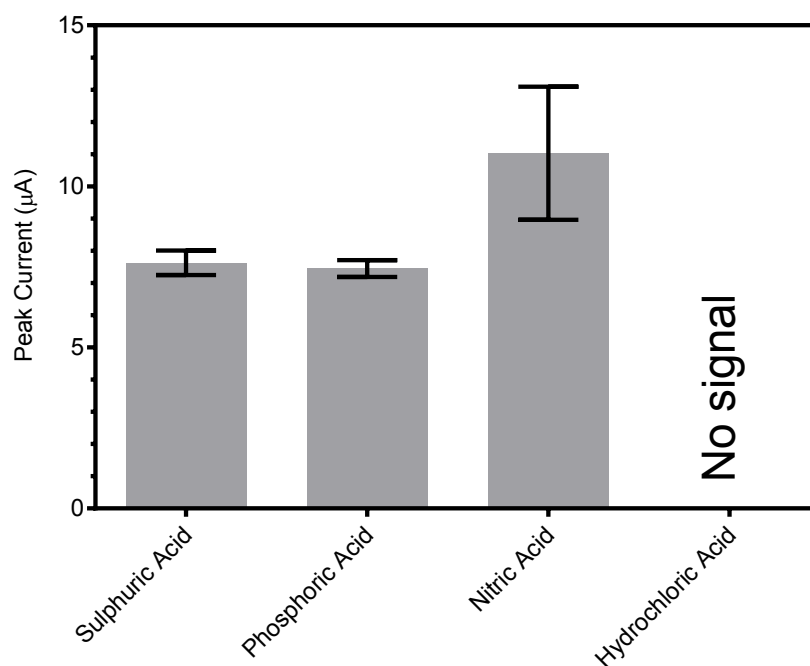


Figure 4.5: Comparison of peak current from cyclic voltammetry measurements of 200 μM caffeine in a 0.1 M solutions of a range of acidic media.

From Fig.4.4 it is immediately obvious that nitric acid has a large background

reduction peak and no oxidation peak is present in hydrochloric acid. Hence these two acids were deemed unsuitable for further use. Phosphoric acid and sulphuric acid both display similar results with peaks occurring at $1.163 \text{ V} \pm 0.002 \text{ V}$ and $1.165 \text{ V} \pm 0.007 \text{ V}$ respectively. The peak currents were also similar with values of $7.4 \mu\text{A} \pm 0.3$ and $7.6 \mu\text{A} \pm 0.4$ in phosphoric acid and sulphuric acid. Both acids could be used equally well but it was decided to use phosphoric acid for all further experiments.

4.4.2 Nafion Modified electrodes

A number of different strategies were employed in order to improve the electrochemical response of the electrodes towards the oxidation of caffeine. Firstly, modifying the electrodes with Nafion was investigated as it has been shown that Nafion modification can improve caffeine sensor performance for both glassy carbon [24, 25] and boron doped diamond [26]

0.1 %, 0.2 % and 0.3 % concentrations of Nafion were using analysed by cyclic voltammetry for caffeine detection as well as detection of 1 mM ferri/ferrocyanide in 1 M KCl. The CVs in ferri/ferrocyanide in Fig 4.6 reveal that as Nafion concentration increases the electrode behaves more as an insulator. At a concentration of 0.1 % redox peaks are clearly visible with peak separation of $123 \text{ mV} \pm 5 \text{ mV}$. At 0.2 % the peak separation increases to $155 \text{ mV} \pm 23 \text{ mV}$ and at 0.3 % no oxidation or reduction peaks are visible reflecting the insulating nature of Nafion.

For caffeine detection (Fig 4.7), a Nafion concentration of 0.2 % was deemed to be optimal as a peak current of $24.5 \mu\text{A} \pm 3.5 \mu\text{A}$ is observed at this concentration, compared to peak currents of $21.2 \mu\text{A} \pm$ at 0.1 % Nafion and $11.0 \mu\text{A} \pm 3.3 \mu\text{A}$ at 0.3 % Nafion. This reflects the fact that caffeine oxidation involves both protons and electrons and hence a material which balances these two considerations is needed.

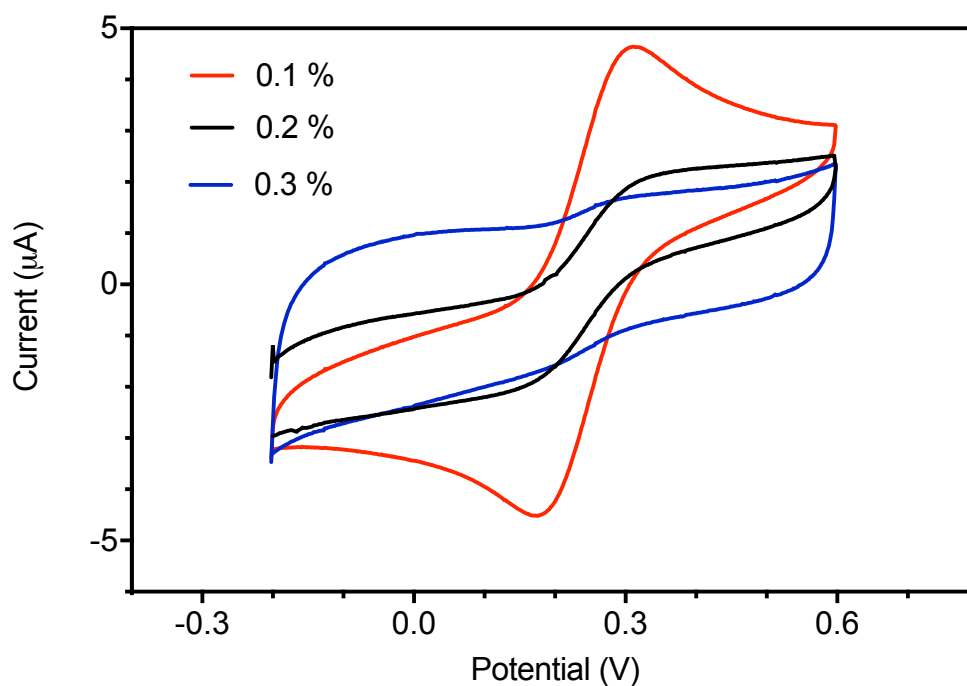


Figure 4.6: Cyclic Voltammograms of 1 mM ferri/ferrocyanide in 1M KCl at electrodes modified with 0.1 %, 0.2 % and 0.3 % Nafion concentrations.

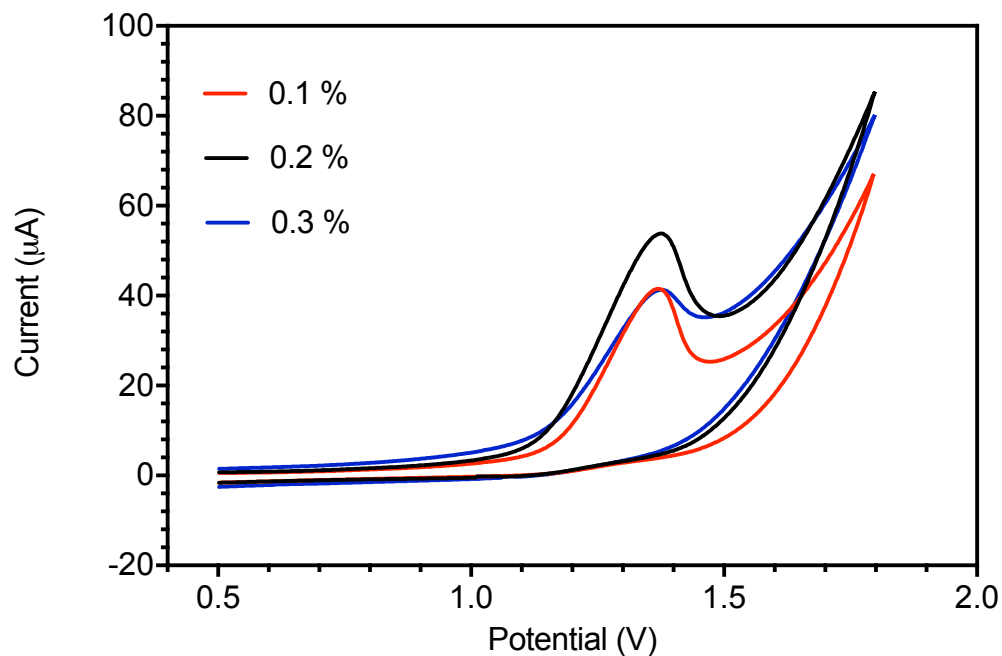


Figure 4.7: Cyclic Voltammograms of 200 μM caffeine at electrodes with 0.1 %, 0.2 % and 0.3 % Nafion concentrations

4.4.3 Electrochemically Pretreated Electrodes

It was seen in Chapter 1 that pretreating these graphite screen printed electrodes can have a positive impact on their electrochemical characteristics. The result of those pretreatments was to remove the electrode's insulating polymer binder and also to introduce oxygen functionalities onto the electrode surface which promotes electron transfer particularly in the case of inner sphere redox probes. In the case of caffeine two different pretreatment methods are compared - pre anodisation of the electrodes in saturated Na_2CO_3 at 1.2 V for 5 minutes and also performing 30 CV scans on the electrode in 0.1 phosphoric acid (supporting electrolyte). Fig 4.8 shows that the treatment of the electrodes in 0.1 M phosphoric acid greatly enhances the electrochemical signal with a peak current of $22 \mu\text{A} \pm 1 \mu\text{A}$ compared to $7.7 \mu\text{A} \pm 0.2$ at the bare electrode. In contrast, the pre-anodisation technique produces no improved electroanalytical characteristics (in fact a slight decrease in peak current is observed - $7 \mu\text{A} \pm 1 \mu\text{A}$). This indicates that oxygen functionalities on the electrode surface don't play a major role in the oxidation of caffeine. However, removing the insulating binder can improve sensor performance.

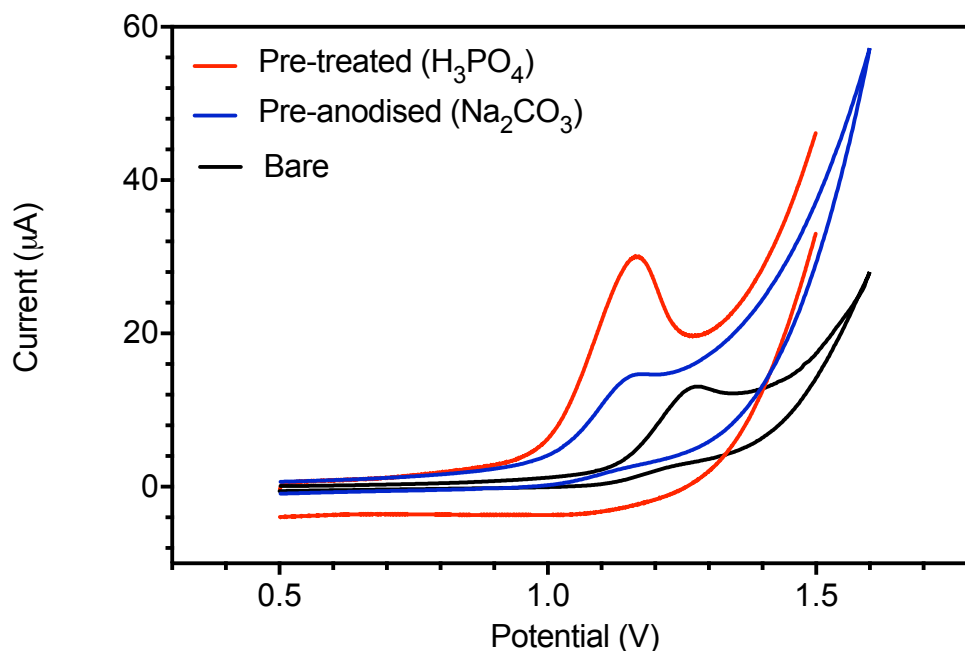


Figure 4.8: Cyclic Voltammograms of 200 μM caffeine in 0.1 M H_3PO_4 at bare graphite and electrochemically pretreated graphite electrodes

4.4.4 SEM

4.4.4.1 Pretreated Electrode

SEM images were taken at electrodes pretreated in H_3PO_4 . Similarly to the electrochemical pretreatments used in Chapter 2, there was no discernable change in the composition of the electrode surface compared to an untreated electrode.

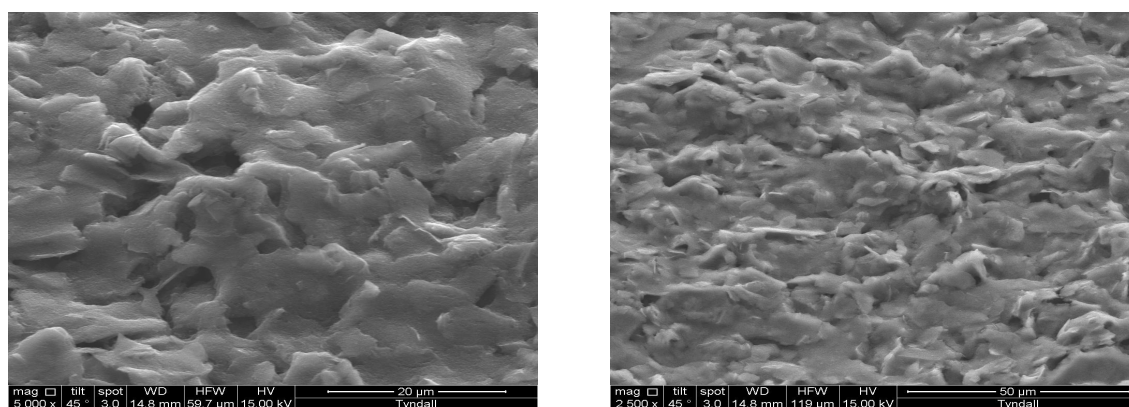
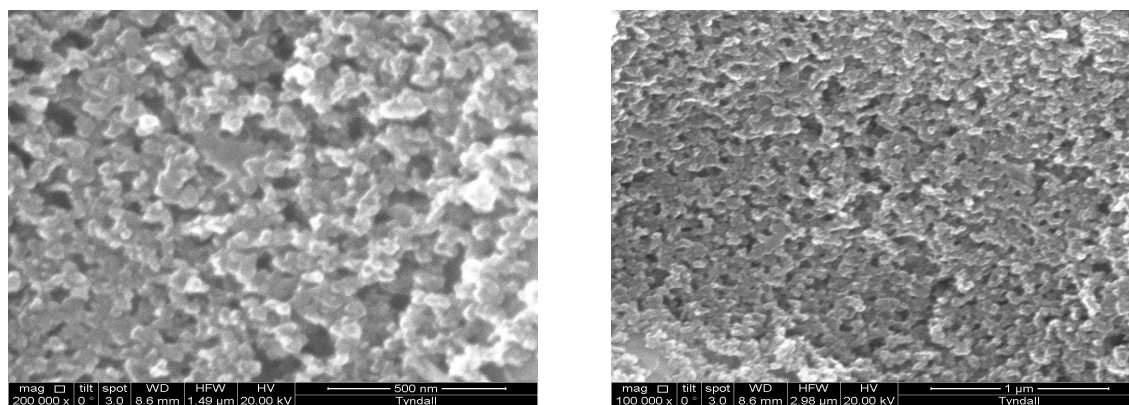


Figure 4.9: Scanning Electron Micrographs of electrochemically pretreated electrodes

4.4.4.2 Nafion modified electrode

SEM images were also taken at nafion modified electrodes. Fig 4.10 shows how the Nafion fully covered the electrode surface (bottom images) compared to the bare electrode (upper two images). Hence, the electrochemical behaviour at the modified electrode can be confidently ascribed to the Nafion modification.



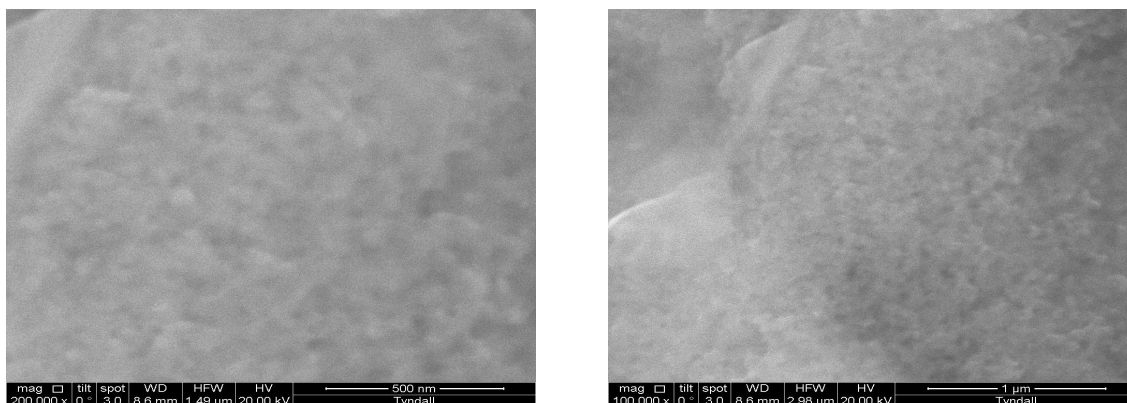


Figure 4.10: Scanning Electron Micrographs of Untreated (above) and Nafion modified (below) graphite working electrodes

4.4.5 Contact Angle

Contact angle measurements were also carried out at both electrodes. At the pretreated and Nafion modified electrodes contact angles of 117 ± 4 and 74 ± 4 degrees were observed respectively. The electrochemical pretreatment caused a decrease in the contact angle due to the introduction of oxygen functional groups and roughening of the electrode surface.

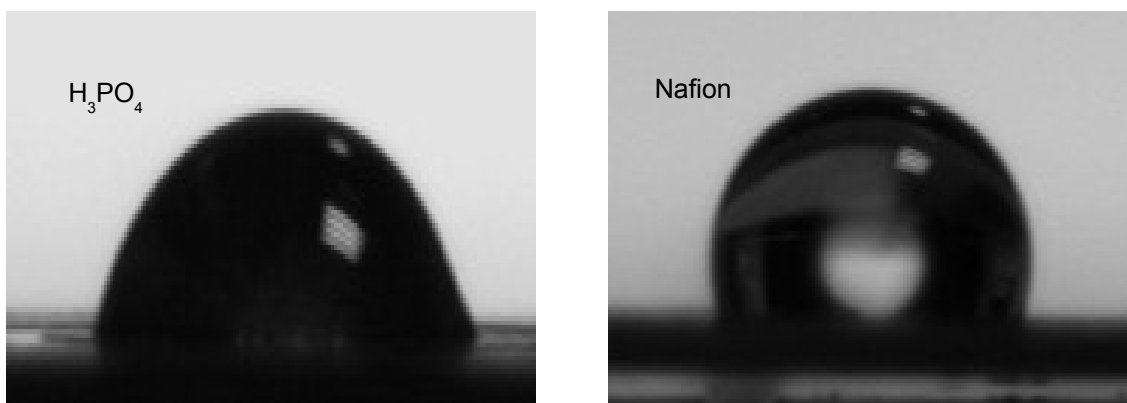


Figure 4.11: Contact angle droplets at both Nafion modified and pretreated electrodes showing the hydrophilic nature of the pretreated electrode in comparison to the bare SPE.

4.4.6 Electrochemical Characterisation

Electrochemical characterisation was then carried out at both electrodes, again using both ferri/ferrocyanide and hexamine ruthenium (III) chloride as outlined in the following sections.

4.4.6.1 Ferri/ferrocyanide

In 1 mM ferri/ferrocyanide both electrodes displayed diffusion limited behaviour (Fig 4.12 - 4.15). As expected the peak currents were noticeably decreased at the Nafion modified electrode as Nafion is known to inhibit electron transfer kinetics (discussed earlier). The electrochemically pretreated electrode had a peak current at 100 mV/s of $11.9 \mu\text{A} \pm 0.1$ which is a similar value as those achieved for the different pretreatments in Chapter 2. In the analysis of graphs of $\log v$ vs \log peak current (see Thin Layer section of the appendix for graph) a slope of 0.4334 was obtained. This isn't considered close enough to the ideal value of 0.5 to then calculate the electrochemical surface area. A slope of 0.2327 was obtained at the Nafion modified electrode.

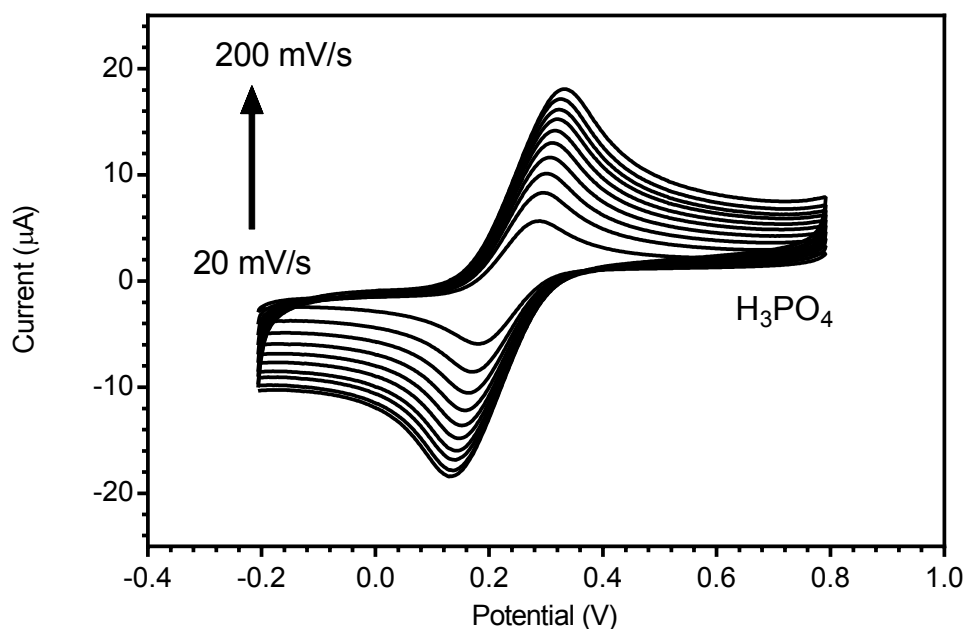


Figure 4.12: Cyclic voltammograms at an electrochemically pretreated electrode at scan rates of 20, 40, 60, 80, 100, 120, 140, 160, 180 and 200 mV/s in 1 mM $[\text{Fe}(\text{CN})_6]^{3-/4-}$ in 1M KCl

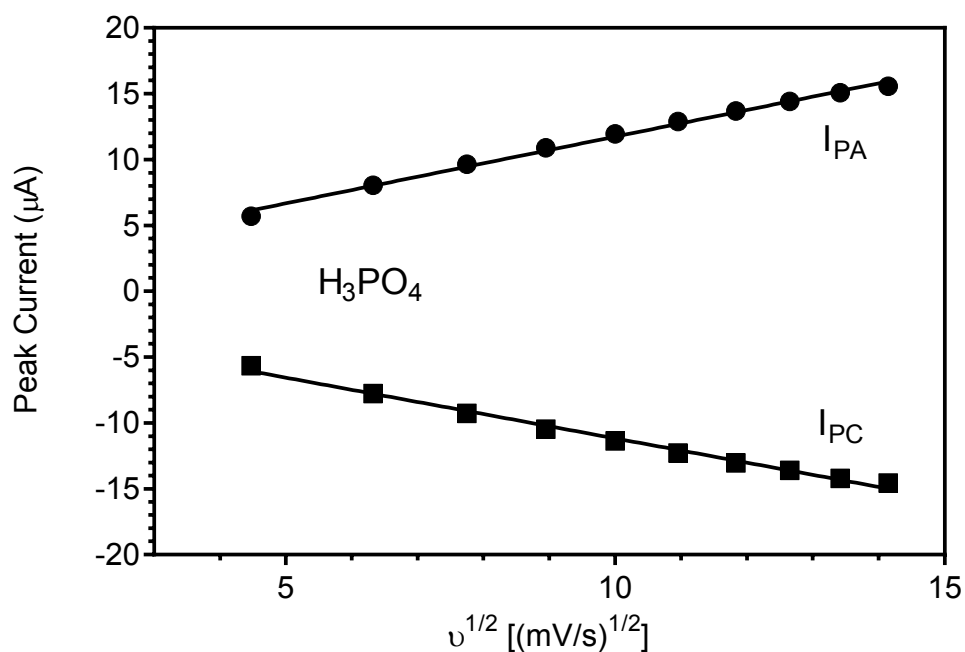


Figure 4.13: Graph of peak anodic and cathodic peak current vs square root of scan rate from the electrochemically pretreated electrode

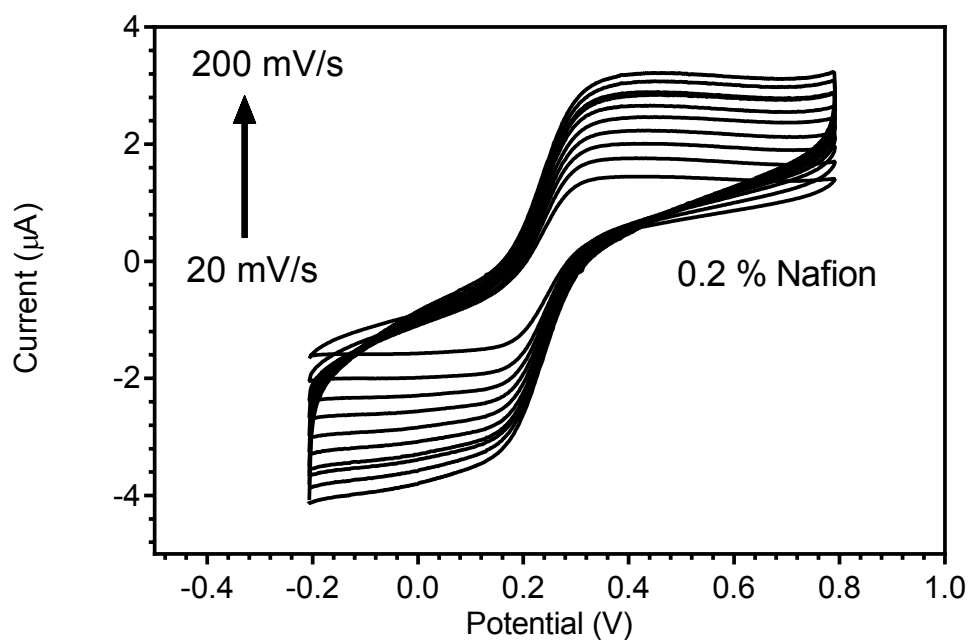


Figure 4.14: Cyclic voltammograms at a Nafion modified electrode at scan rates of 20, 40, 60, 80, 100, 120, 140, 160, 180 and 200 mV/s in 1 mM $[\text{Fe}(\text{CN})_6]^{3-/4-}$ in 1M KCl

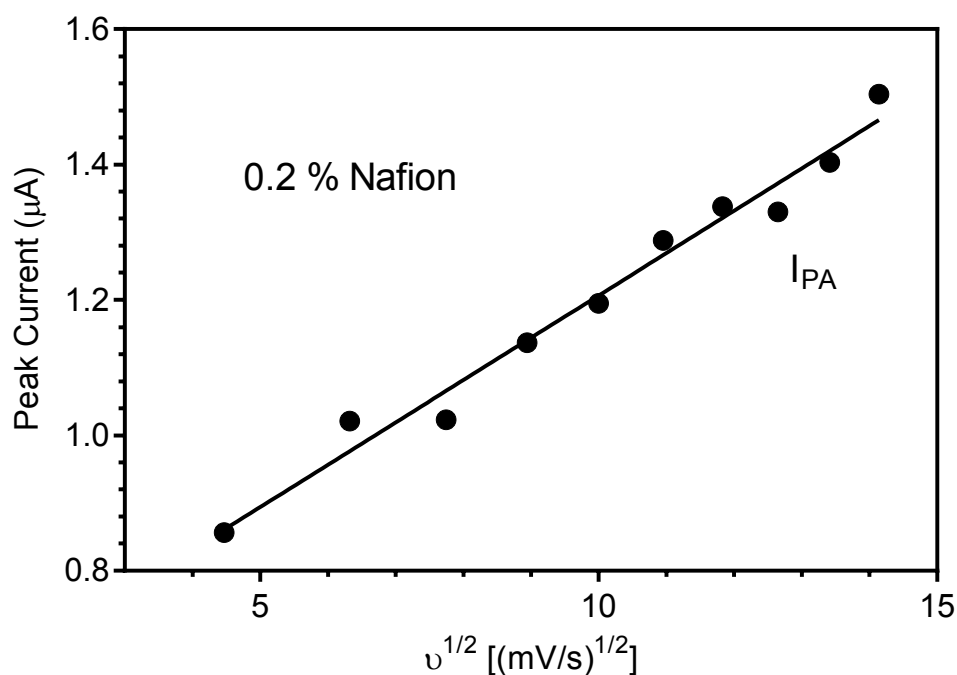


Figure 4.15: Graph of peak anodic and cathodic peak current vs square root of scan rate from the Nafion modified electrode

4.4.6.2 Hexamine Ruthenium (III) Chloride

Interestingly the opposite behaviour is observed for hexamine ruthenium (III) chloride. Remarkably, a significant increase in peak current is observed at the Nafion modified electrode at 100 mV/s - $21.9 \mu\text{A} \pm 0.2 \mu\text{A}$. An explanation is unknown as to why there is this significant increase in electrochemical activity at the Nafion modified electrode. At the electrochemically pretreated electrode in contrast the peak current at 100 mV/s is a mere $6.0 \mu\text{A} \pm 0.3 \mu\text{A}$. The slopes to determine thin layer effects were 0.4471 and 0.6506 at the pretreated and Nafion modified electrode. Hence an electrode area of 0.067 cm^2 and roughness factor of 94 % could be established.

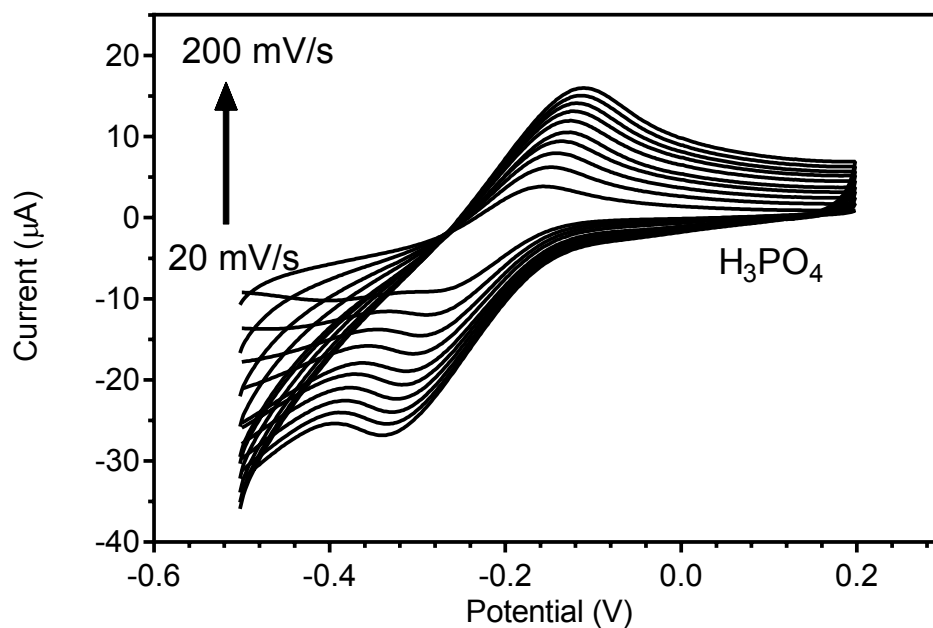


Figure 4.16: Cyclic voltammograms at an electrochemically pretreated electrode at scan rates of 20, 40, 60, 80, 100, 120, 140, 160, 180 and 200 mV/s in 1 mM hexamine ruthenium (III) chloride in 0.1 M PBS

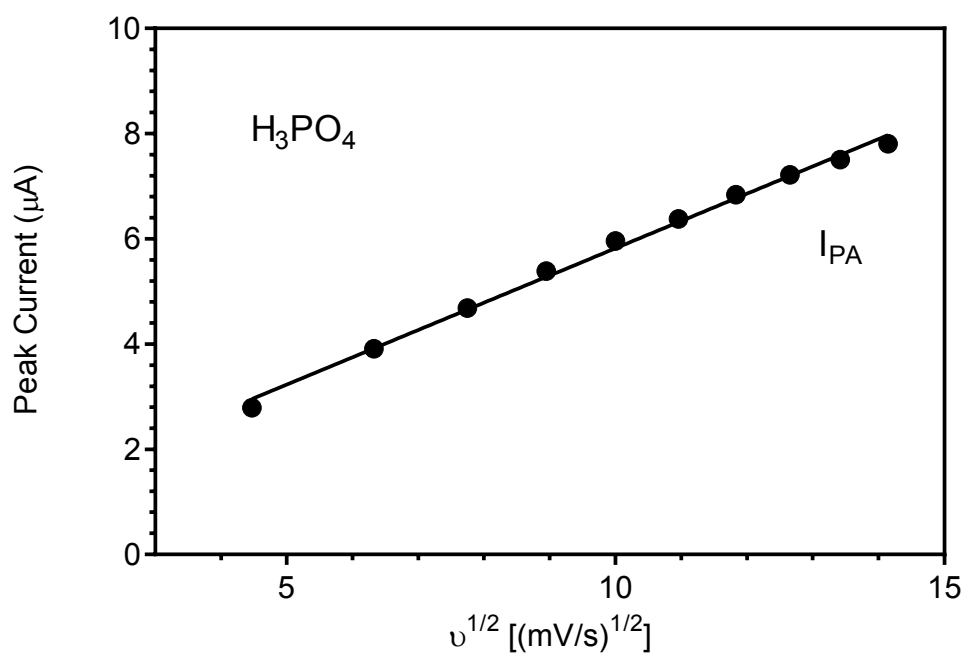


Figure 4.17: Graph of peak anodic and cathodic peak current vs square root of scan rate from the electrochemically pretreated electrode

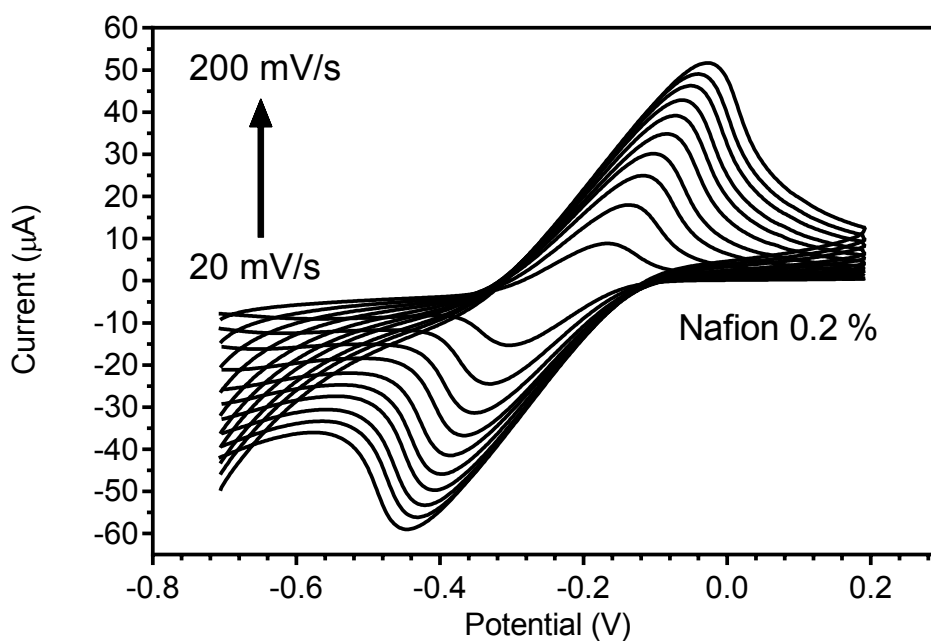


Figure 4.18: Cyclic voltammograms at a Nafion modified electrode at scan rates of 20, 40, 60, 80, 100, 120, 140, 160, 180 and 200 mV/s in 1 mM hexamine ruthenium (III) chloride in 0.1 M PBS

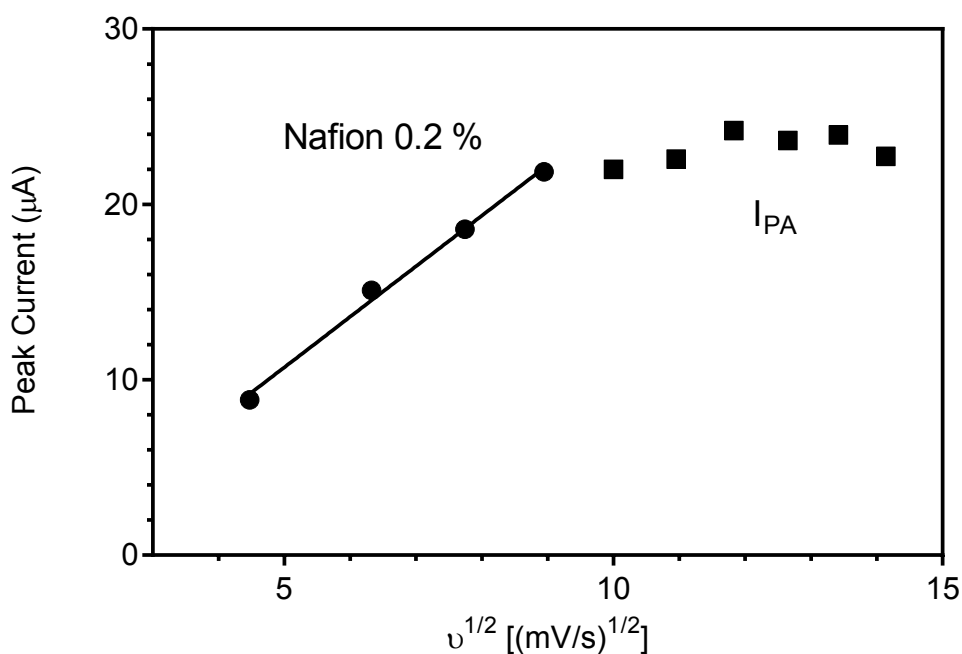


Figure 4.19: Graph of peak anodic and cathodic peak current vs square root of scan rate from the Nafion modified electrode

4.4.7 Cleaning Study

As mentioned in the introduction to this chapter, the electrochemical sensors for caffeine detection as described in the literature fall into two camps - disposable sensors using screen printed electrodes and re-usable boron doped diamond or glassy carbon sensors. In this study the feasibility of developing a re-usable, low cost sensor with screen printed electrodes is investigated. During the process of performing an electrochemical measurement, a certain amount of caffeine (or possibly some of products of the caffeine oxidation reaction) remain on the surface of the electrode after the completion of the measurement. This is not a limiting process as can be seen in the scan rate studies in the following section. However, if the sensor is to be re-usable, then this residue needs to be removed, otherwise false positive results would be possible in the subsequent measurements. The cleaning step used here is to perform scans in 0.1 M phosphoric acid between measurements. This has the effect of stripping the outer layer of the electrode and hence removing the contaminating caffeine.

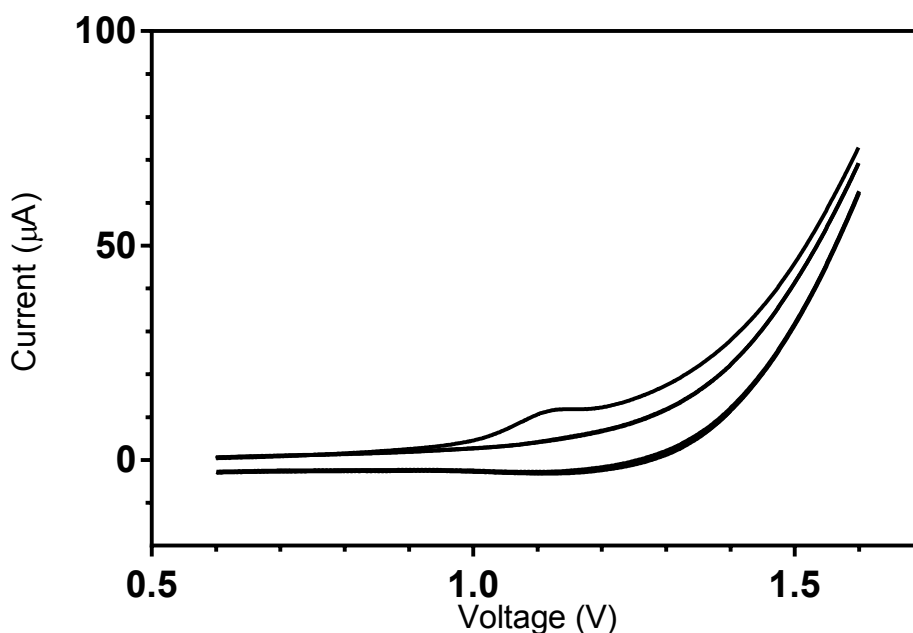


Figure 4.20: Cyclic Voltammogram in blank 0.1 M phosphoric acid subsequent to measurement in 200 μM caffeine solution

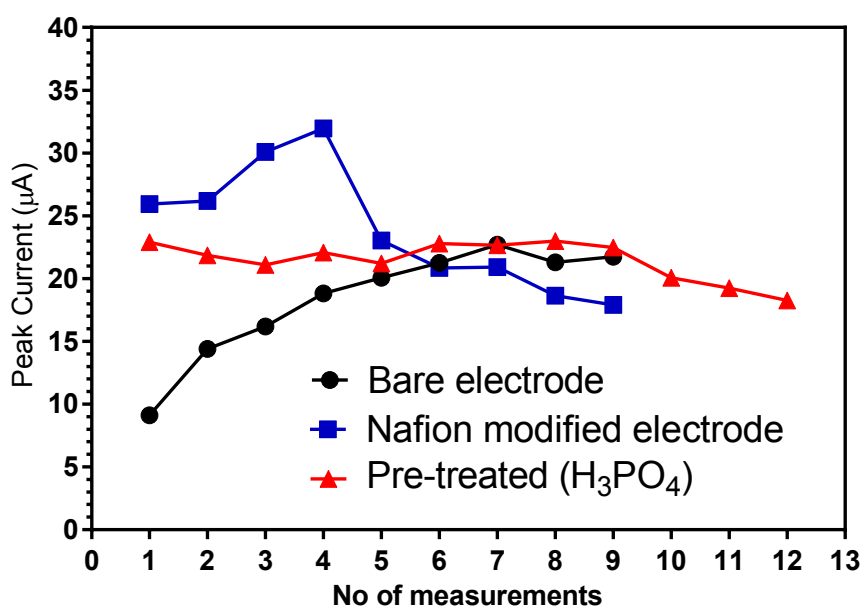


Figure 4.21: Consecutive CV measurements in 200 μM caffeine solution with cleaning step between each measurement

The cleaning process was carried out at bare, pretreated and Nafion modified electrodes. It was found that the electrochemical signal of the bare electrode actually increased after successive cleaning steps up to the 10th and 11th measurements. This was likely due to the removal of the polymer binder with successive cleaning steps. In contrast, the signal at the Nafion modified electrodes decreased with successive measurements as Nafion was removed during the successive cleaning steps. However, at the pretreated electrode the signal remained stable for 9 measurements which could bring considerable cost reduction in commercial applications.

Table 4.1: Relative Standard deviation percentages for consecutive 9 measurements of 200 μM caffeine in 0.1 NH_3PO_4

Electrode	% RSD - 9 consecutive measurements
Bare Electrode	24.02
Nafion modified Electrode	20.61
Pretreated (H ₃ PO ₄)	3.21

4.4.8 Effect of scan rate

In order to further understand the nature of the caffeine oxidation mechanism, scan rate studies were undertaken at both pretreated and Nafion modified electrodes. Both electrodes showed a linear relationship between peak current and square root of scan rate indicating a diffusion limited process (Fig 4.22 - 4.25). Adsorption has some role to play in the reaction as shown in the previous section, however scan rate doesn't scale linearly with peak current as would be expected for an adsorption limited process. Also, there is a drift in peak potential with an increase in scan rate which is expected for irreversible reaction such as this [27].

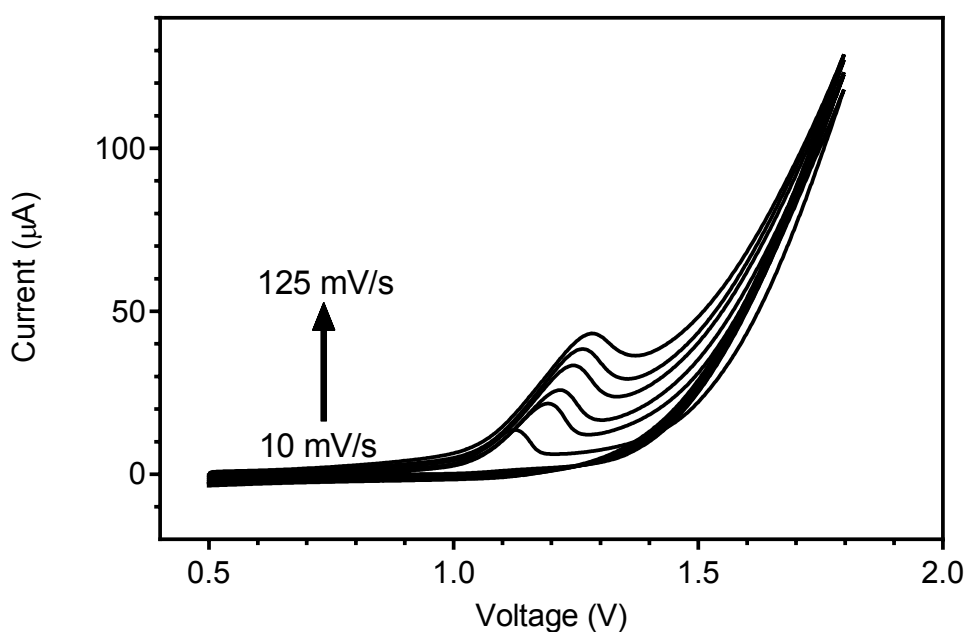


Figure 4.22: CVs at a Nafion modified electrode in the presence of 200 μM caffeine at a range of scan rates

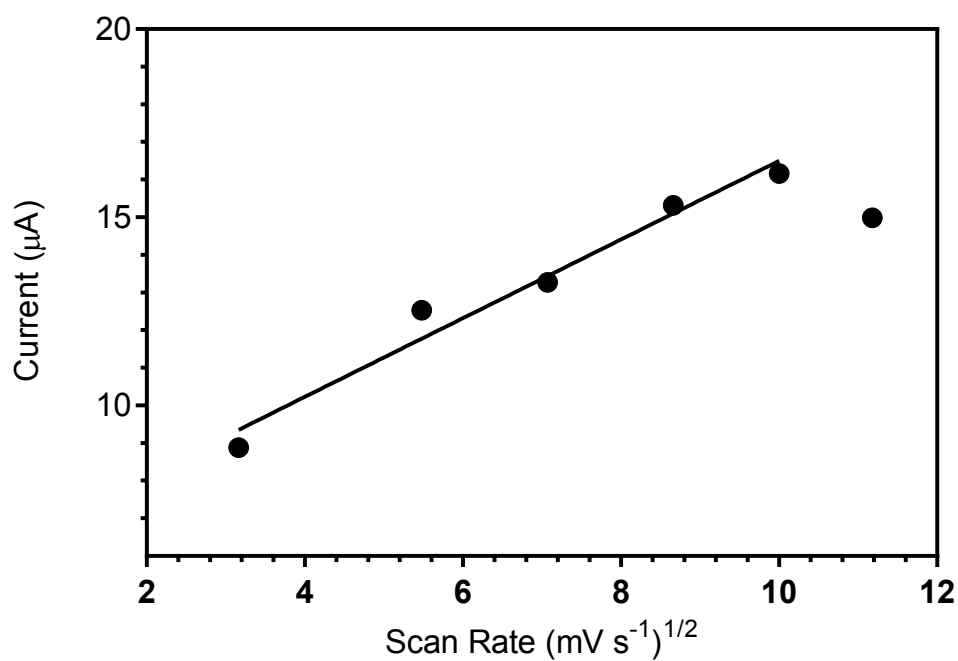


Figure 4.23: Variation of peak current with square root of scan rate at Nafion modified electrode in 200 μM caffeine

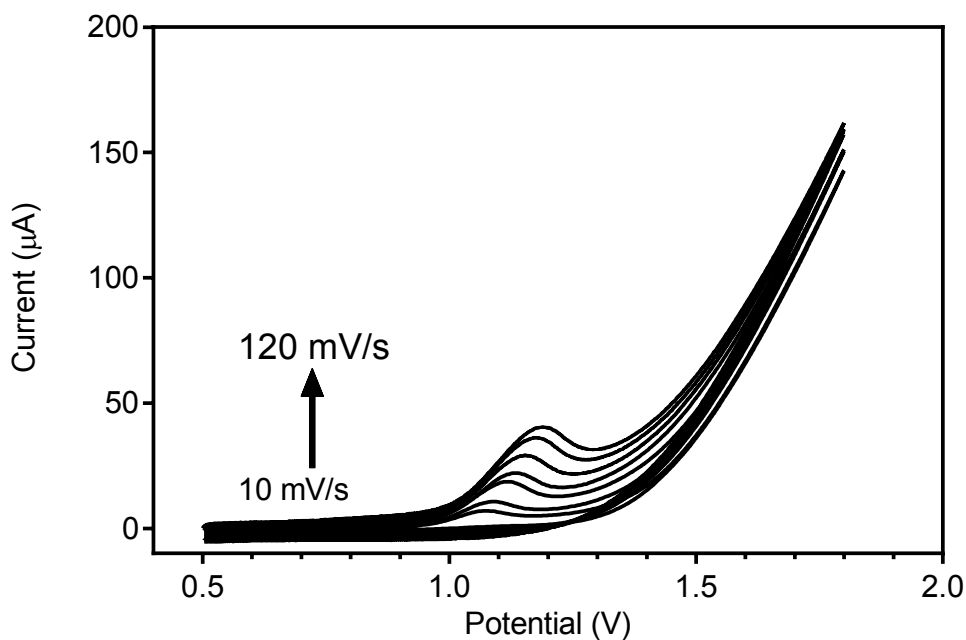


Figure 4.24: Variation of peak current with square root of scan rate at n=Nafion modified electrode in 200 μM caffeine

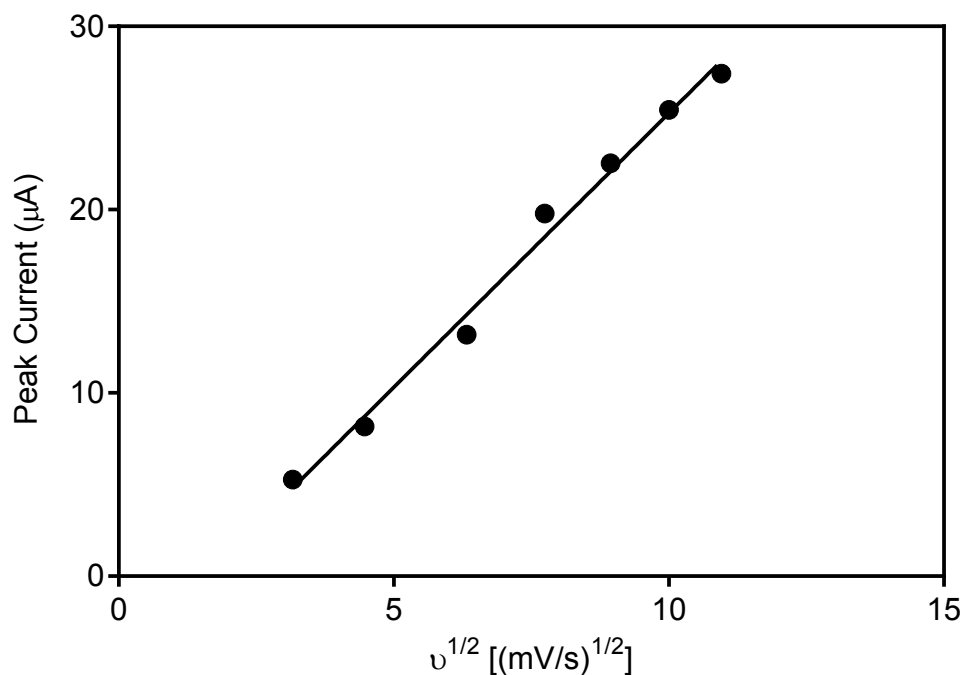


Figure 4.25: Variation of peak current with square root of scan rate at Nafion modified electrode in 200 μM caffeine

4.5 Optimisation of SVW parameters

Square wave voltammetry is typically a more sensitive technique than cyclic voltammetry and hence was used with the Nafion modified electrode. Re-producible results could not be achieved at the pretreated electrode and so it was decided that linear sweep voltammetry would be used to construct a calibration in that case (see next section).

Optimisation of the experimental parameters is a key factor in SWV measurements as they can have a considerable influence on the peak current. Initially, an amplitude of 30 mV was fixed and the frequency was varied between 10 mV and 60 Hz (Fig 4.26). Peak current was at a maximum for 20 Hz and hence this frequency was chosen for all further measurements. Then, at a frequency of 20 Hz, the amplitude was varied between 10 mV and 110 mV (Fig 4.27). The peak current increased with increasing amplitude up until 100 mV, after which a plateau appeared. Similar results were found by Mersal at a pseudo carbon paste electrode [28].

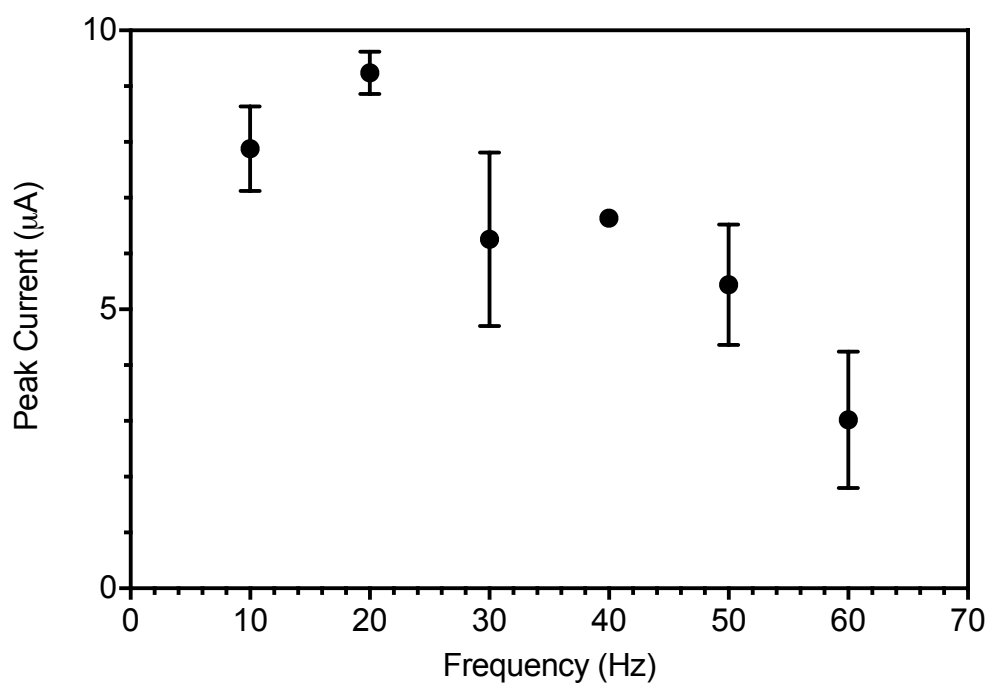


Figure 4.26: Variation of SWV frequency at fixed amplitude of 30 mV in 200 μM caffeine solution (diluted in 0.1 M H_3PO_4).

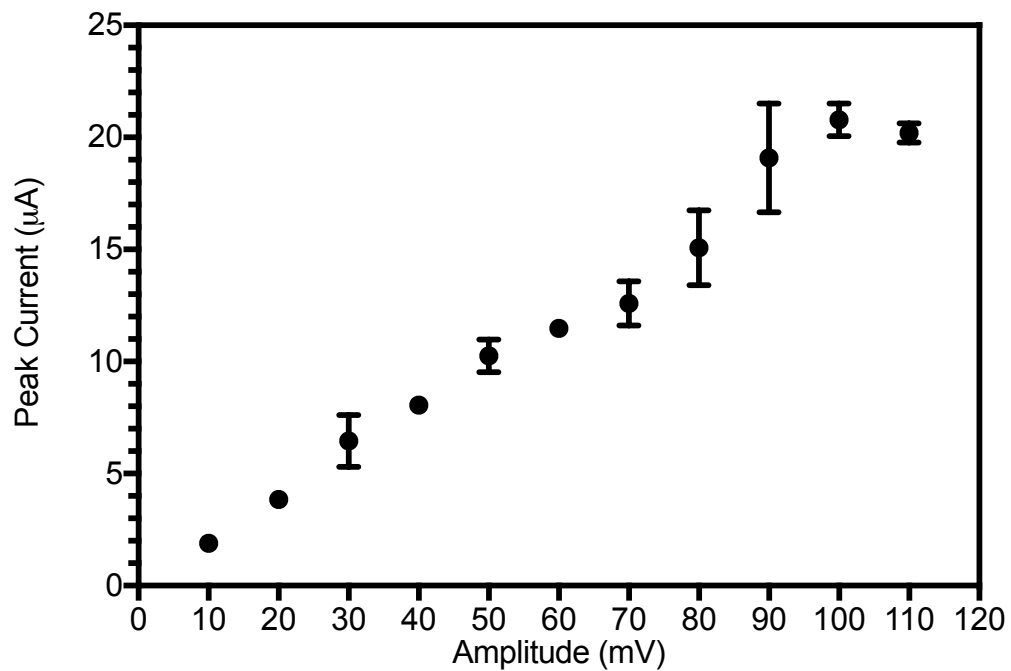


Figure 4.27: Variation of SWV amplitude at fixed frequency of 20 Hz in 200 μM caffeine solution (diluted in 0.1 M H_3PO_4).

4.6 Analytical Characteristics of Developed Sensors

Calibration curves were then constructed at both electrodes as outlined in the following two sections.

4.6.1 Pretreated Electrode

Successive additions of 5 mM stock solution to 4995 μL of H_3PO_4 led to an increase in oxidation peak current as shown in Fig 4.28. From Fig 4.29 it can be seen that there are two separate linear regions. The upper region is described by the equation $y = 0.08247x + 3.816$ with an R^2 value of 0.9839 whilst the lower region is described by the equation $y = 0.2473x - 0.5527$ with an R^2 value of 0.9648. Extrapolating the lower region to estimate the zero value, a limit of detection of 9 μM was found with a linear range of 10-20 μM .

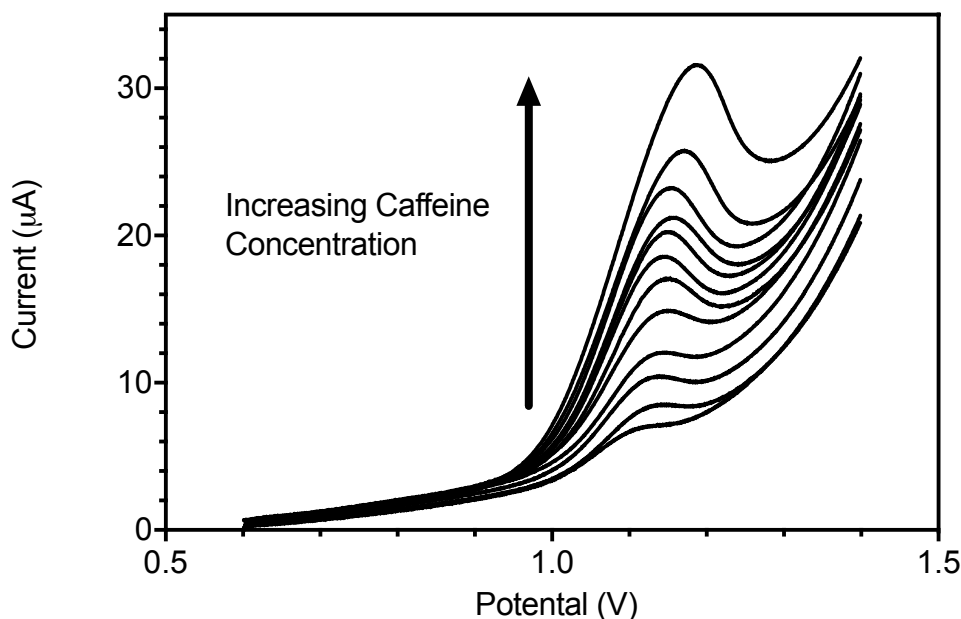


Figure 4.28: Linear sweep voltammograms at electrochemically pretreated screen printed electrode at varying caffeine concentrations - 10 μM , 14 μM , 20 μM , 30 μM , 50 μM , 70 μM , 89 μM , 109 μM , 128 μM , 148 μM

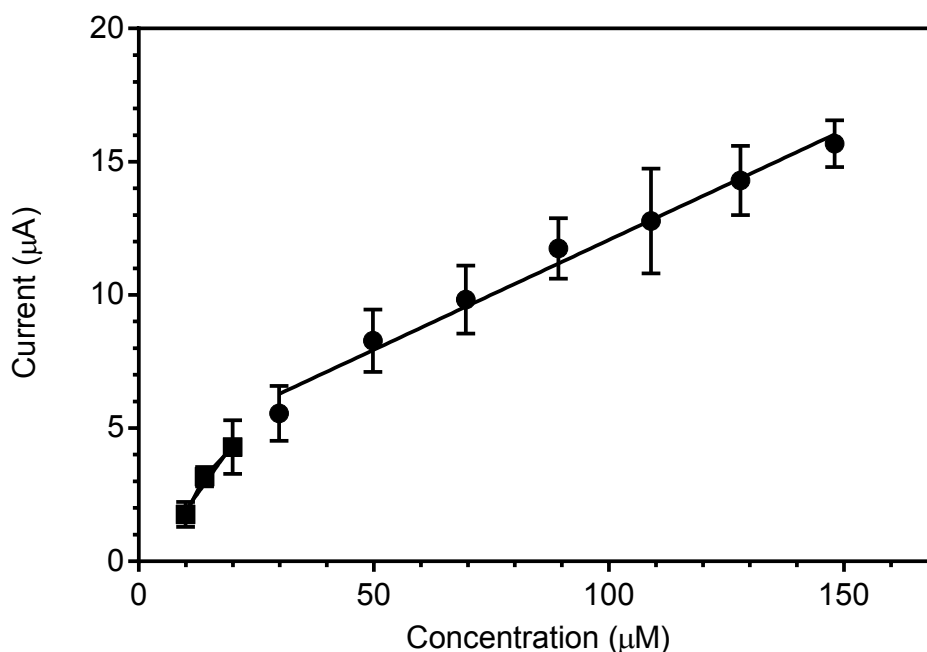


Figure 4.29: Calibration curve of electrochemically pretreated electrode for caffeine detection showing two linear regions. The lower region has an R^2 value of 0.9648 while the upper region has an R^2 value of 0.9839. $n = 3$.

4.6.2 Nafion modified electrode

Using the optimised SWV parameters determined in section 4.5 a calibration curve at the Nafion modified electrode was constructed (Fig 4.31) described by the equation $y = 0.1362x - 0.0406$ after measurement of the SWV response at multiple concentrations (Fig. 4.30). The linear range for this sensor was 10-128 μM and the LOD was 8 μM . This LOD was very similar to the result achieved at the pretreated electrode but the pretreated electrode had the advantage of a lower cost of modification. Lower limits of detection have been achieved in the literature (see introduction to this chapter) but this isn't necessarily a key consideration in food analysis as the caffeine content in energy drinks, coffee etc. is relatively high.

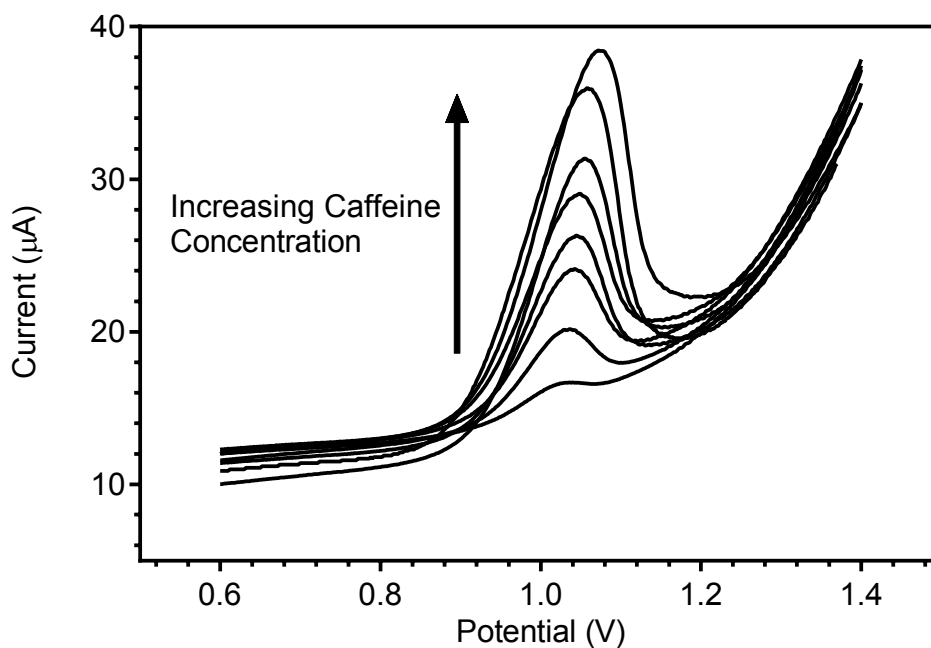


Figure 4.30: Square voltammograms at Nafion modified screen printed electrode at varying caffeine concentrations - $10 \mu\text{M}$, $30 \mu\text{M}$, $50 \mu\text{M}$, $70 \mu\text{M}$, $89 \mu\text{M}$, $109 \mu\text{M}$, $128 \mu\text{M}$ and $148 \mu\text{M}$

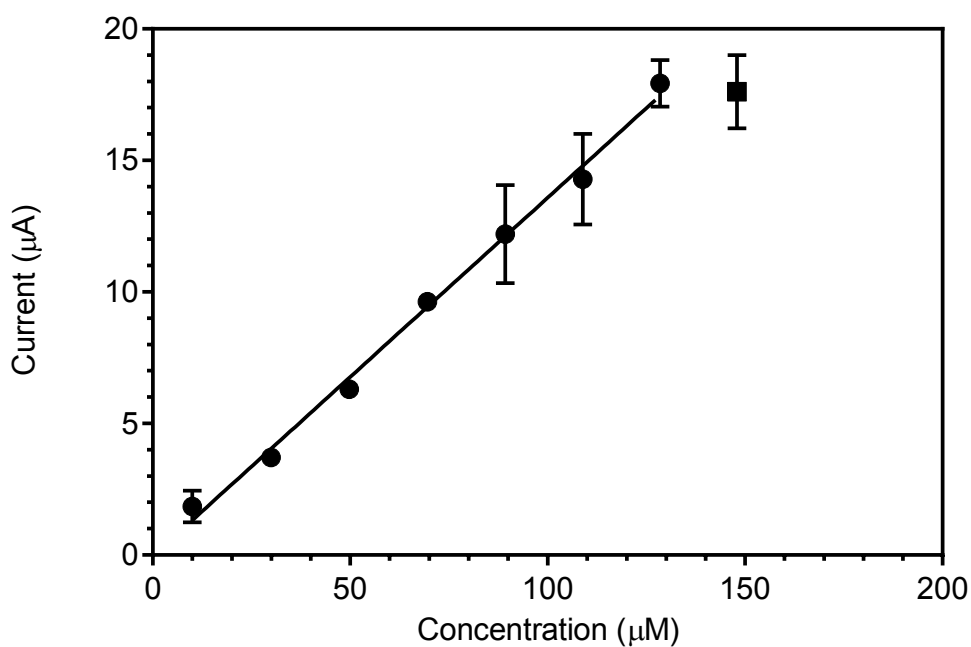


Figure 4.31: Calibration curve of Nafion modified electrode for caffeine detection at a Nafion modified electrode in a $0.1 \text{ M H}_3\text{PO}_4$ supporting electrolyte.

4.7 Sensor Storage

An important characteristic of any electrochemical sensor is its ability to perform even after storage in various conditions. Hence, the storage conditions of both sensors was compared at both room temperature as well as 4 degrees celcius. It can be seen from Fig. 4.32 that in both storage conditions no loss of signal is observed at the Nafion modified electrode. However, there is a significant loss of signal at the pretreated electrode. This suggests that surface contamination occurs at the pretreated electrode possibly through oxidation from the ambient air.

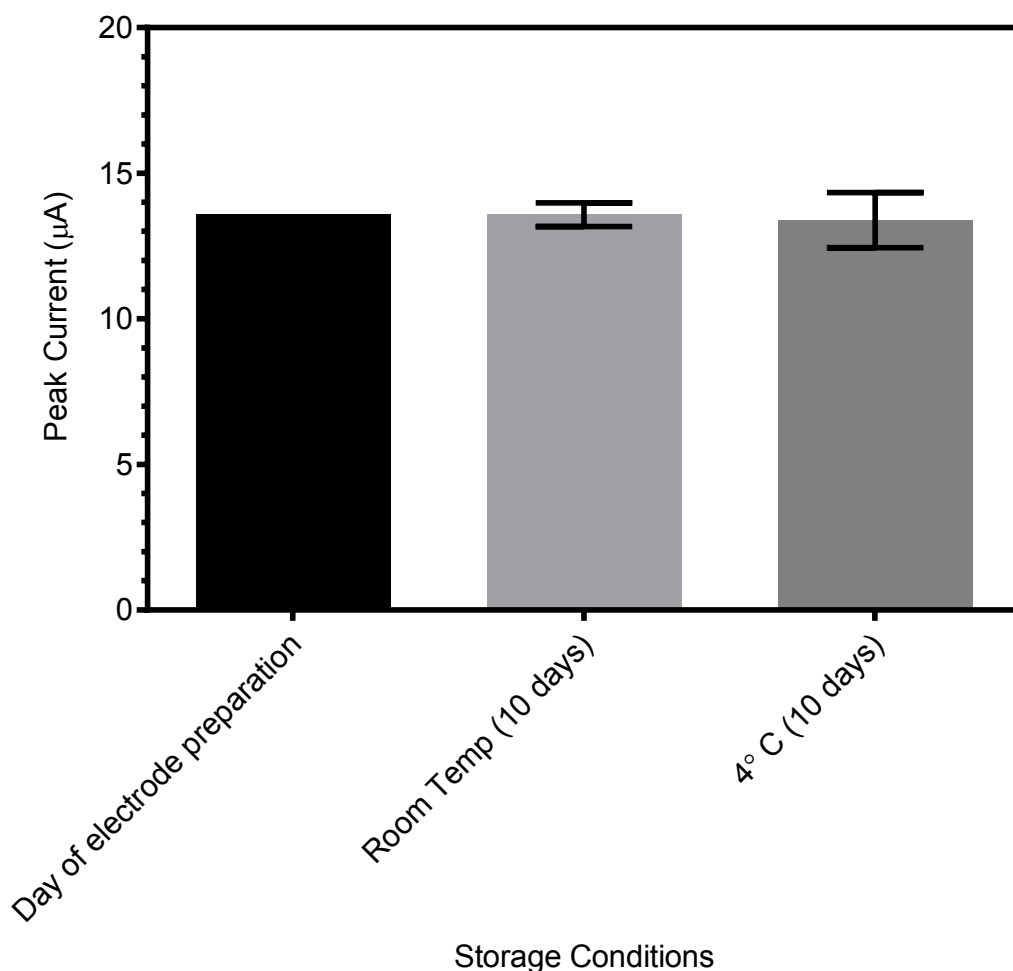


Figure 4.32: Nafion sensor signal for 100 μM caffeine at 4 degrees celcius and room temperature

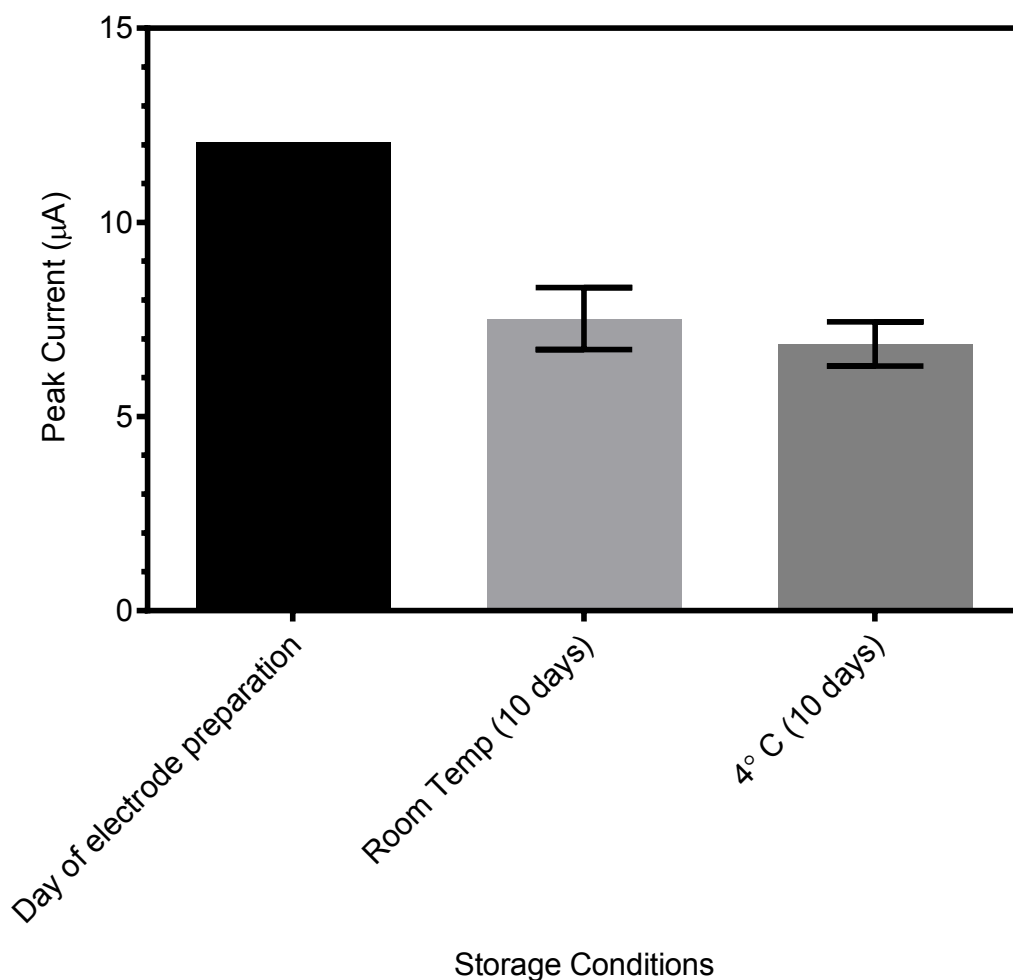


Figure 4.33: Pretreated sensor signal for 100 μM caffeine at 4 degrees celcius and room temperature

4.8 Interference Analysis

Interference analysis was carried out by investigating the influence of both sucrose and glucose on caffeine oxidation at both sensors. 100 μM of both sugars were added to 1 M phosphoric acid containing 100 μM of caffeine. The LSV peak current (for the pretreated electrode) and SWV peak current (for the Nafion modified electrode) are outlined in the table below. It can be seen that there is a significant interference in the caffeine oxidation signal. This type of interference wasn't observed by Torres et al. at bare and Nafion modified glassy carbon electrodes in the presence of fructose, sucrose, glucose, ascorbic acid and citric acid [9]. This could suggest that the interference is more prevalent at

screen printed electrodes. Unfortunately, interference studies were not carried out by Vasilescu et. al using the developed screen printed sensor [1].

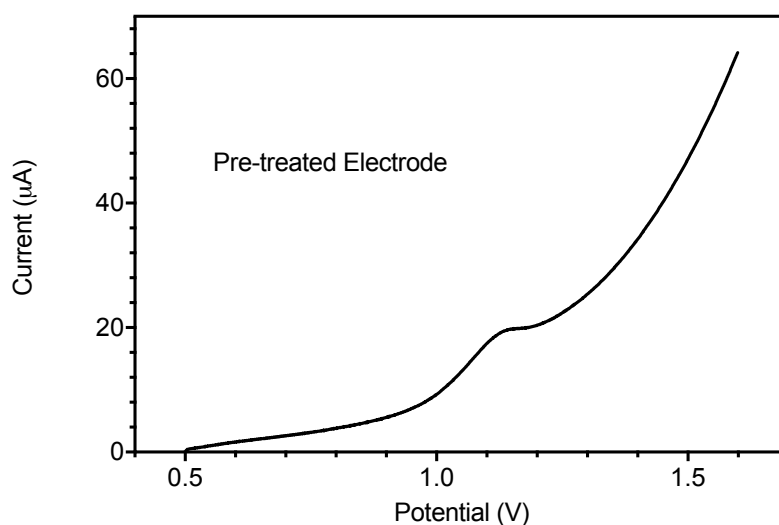


Figure 4.34: Linear sweep voltammogram of 100 μM caffeine in the presence of 100 μM glucose and 100 μM sucrose at electrochemically pretreated electrode

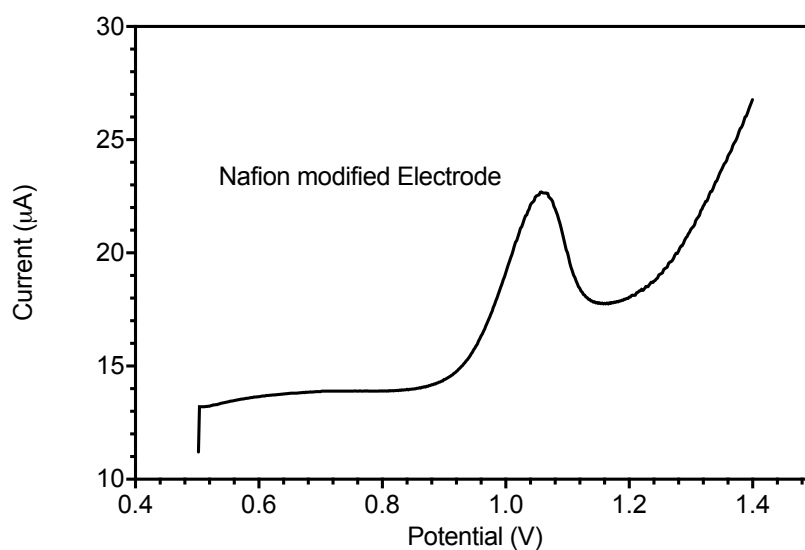


Figure 4.35: Square voltammogram of 100 μM caffeine in the presence of 100 μM glucose and 100 μM sucrose at Nafion modified electrode

Table 4.2:

Electrode	% Signal in presence of interfering compound
Nafion modified Electrode	60 %
Pretreated (H_3PO_4)	55 %

4.9 Real Sample Analysis

Next, both sensors were used to detect caffeine in a commercially available energy drink sample. Although both sucrose and fructose appeared to have significant impact on sensor signal, these ingredients within the energy drinks didn't influence the sensor to same degree in the case of the Nafion modified sensor. However, in the case of the pretreated electrode sufficient recovery percentages were unable to be established. This shows that further work is required prior to the pretreated electrode before it could be used in real world applications. The recovery percentages are outlined in Table 4.3.

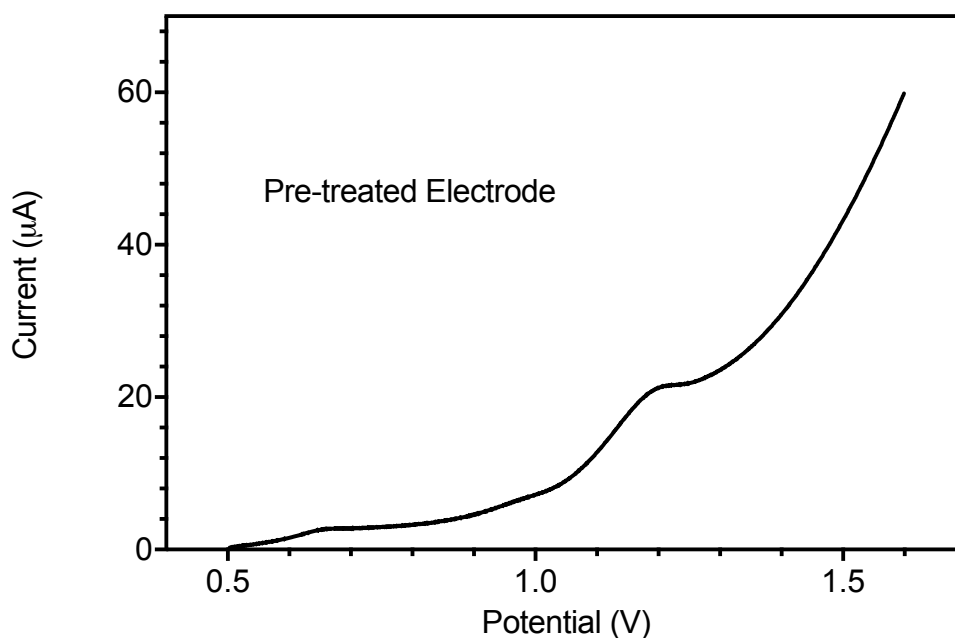


Figure 4.36: Linear Sweep voltammogram in 1/10 dilution of Red Bull at an electrochemically pretreated electrode

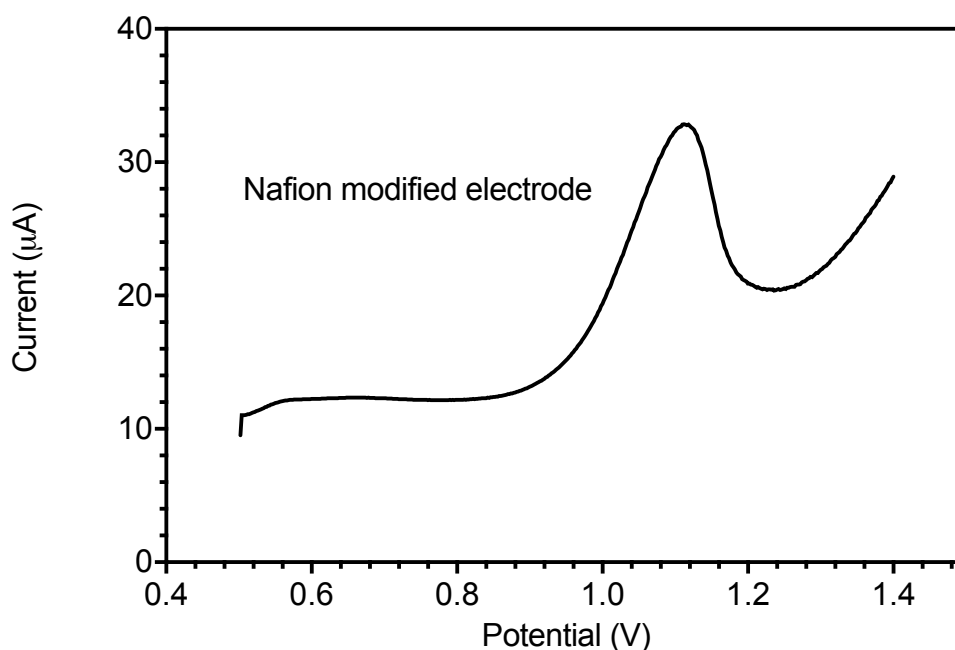


Figure 4.37: Square voltammogram in 1/10 dilution of Red Bull at a Nafion modified electrode

Table 4.3: Recovery percentages of the caffeine detection in Red Bull samples

Electrode	% Recovery
Nafion modified Electrode	87 %
Pretreated (H ₃ PO ₄)	65 %

4.10 Part 2 - Caffeine Detection at Screen Printed Graphene

4.10.1 Electrochemical Characterisation

Electrochemical characterisation of the screen printed graphene electrodes was carried out using the ferri/ferrocyanide and hexamine ruthenium (III) chloride redox couples. In the case of hexamine ruthenium (III) chloride, at a scan rate of 100 mV/s, screen printed graphene displays a peak potential separation of 129 mV, in comparison to 133.33 mV at the graphite electrode. These similar values indicate a structurally similar surface in contrast to the different voltammetric response achieved by Randviir et al. [21].

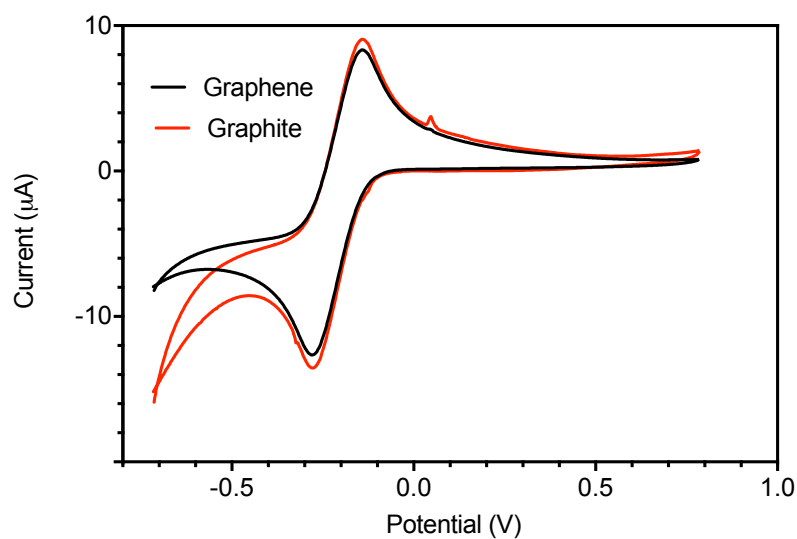


Figure 4.38: Cyclic voltammograms at bare SPE and GSPE in 1 mM hexaammine ruthenium (III) chloride with a supporting electrolyte of 0.1 M PBS buffer at a scan rate of 100 mV/s.

In contrast, for ferri/ferrocyanide significantly different CVs are observed as can be seen in Fig. 4.39 with graphene electrode displaying a reduced peak current of $6.0 \mu\text{A} \pm 0.3 \mu\text{A}$ and increased peak potential separation of $270 \text{ mV} \pm 39 \text{ mV}$.

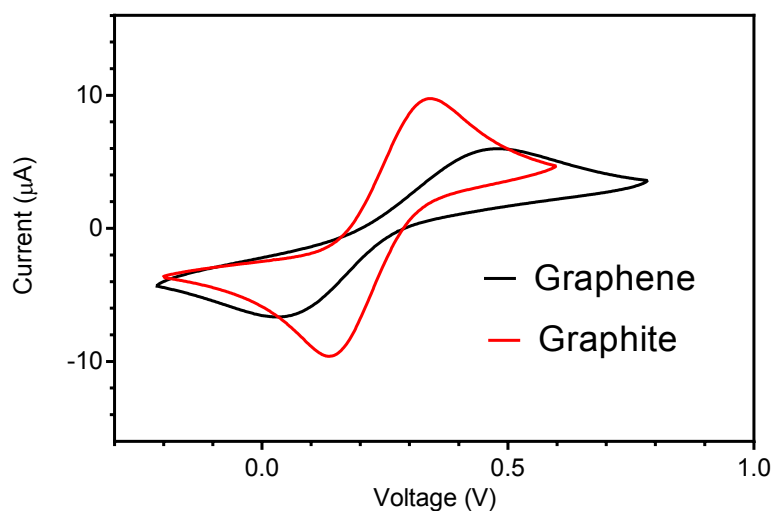


Figure 4.39: Cyclic voltammograms at bare SPE and GSPE in 1 mM ferri/ferrocyanide with a supporting electrolyte of 1 M KCl at a scan rate of 100 mV/s.

4.10.1.1 Scan Rate Studies

Thin layer effects were also investigated at the graphene electrode (graphs shown in the appendix) which revealed slopes of 0.3936 and 0.4734 for the plot of log scan rate vs log of peak current at ferri/ferrocyanide and ruthenium (III) chloride respectively. As was the case at the pretreated graphite electrodes, more ideal behaviour was observed for hexamine ruthenium (III) chloride oxidation. The following four graphs, (Fig 4.40 - 4.43) of square root of scan vs peak current at the two redox probes show linear straight line correlation indicating diffusion limited process'. The graph for hexamine ruthenium (III) was then used to calculate the electrochemical surface area and % surface roughness with values of 0.143 cm² and 202 % respectively.

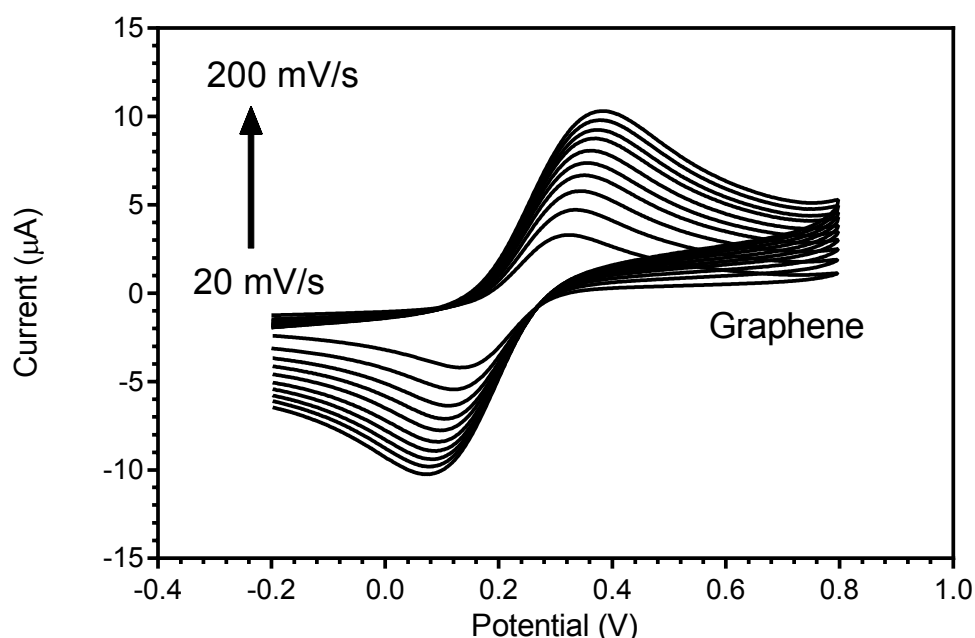


Figure 4.40: Cyclic voltammograms at a screen printed graphene electrode at scan rates of 20, 40, 60, 80, 100, 120, 140, 160, 180 and 200 mV/s in 1 mM [Fe(CN)₆]^{3-/4-} in 1M KCl

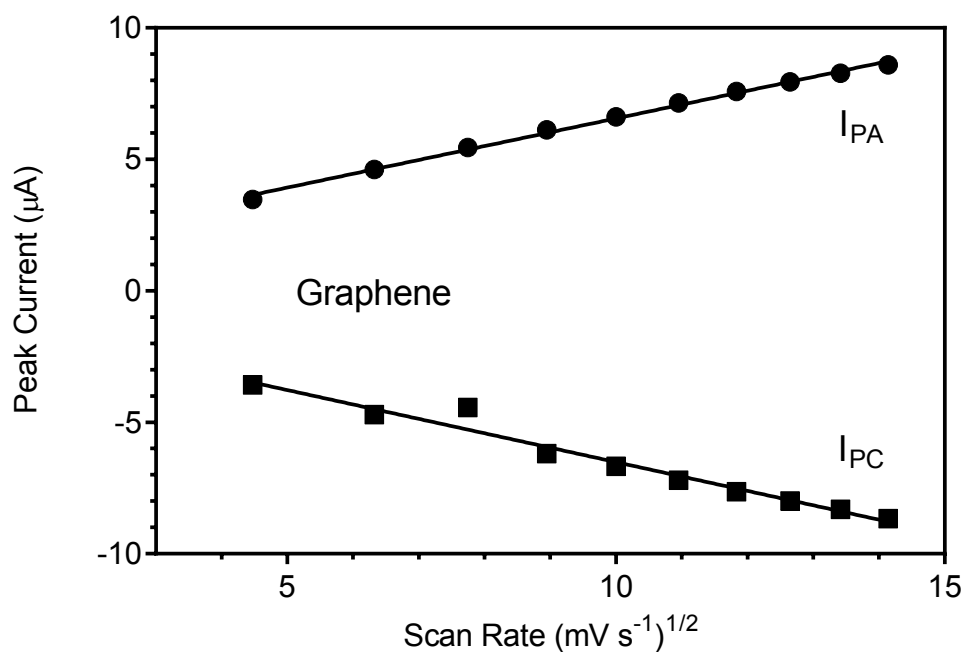


Figure 4.41: Graph of peak anodic and cathodic peak current vs square root of scan rate from a screen printed graphene electrode

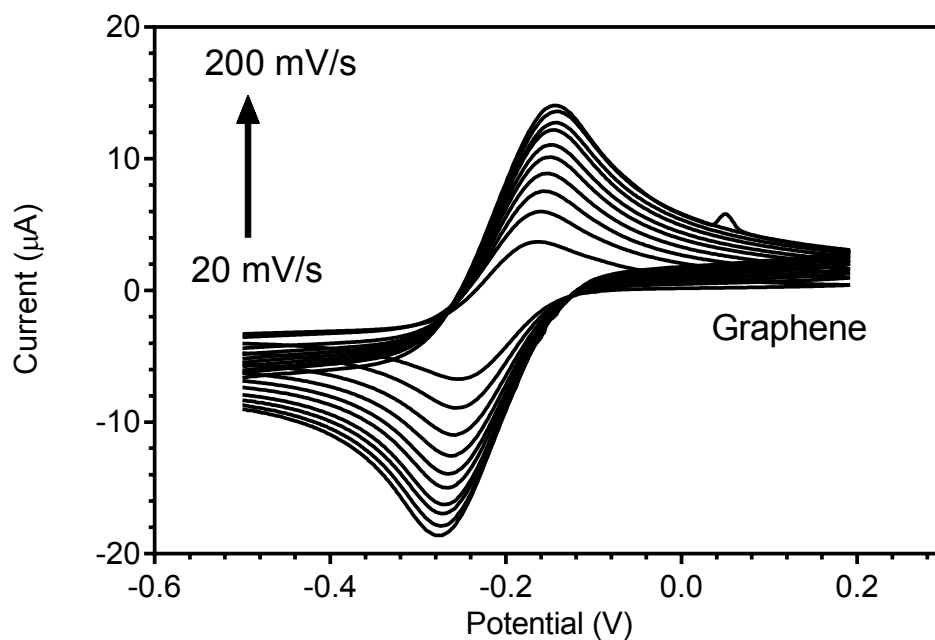


Figure 4.42: Cyclic voltammograms at a screen printed graphene electrode at scan rates of 20, 40, 60, 80, 100, 120, 140, 160, 180 and 200 mV/s in 1 mM hexamine ruthenium (III) chloride in 0.1M PBS

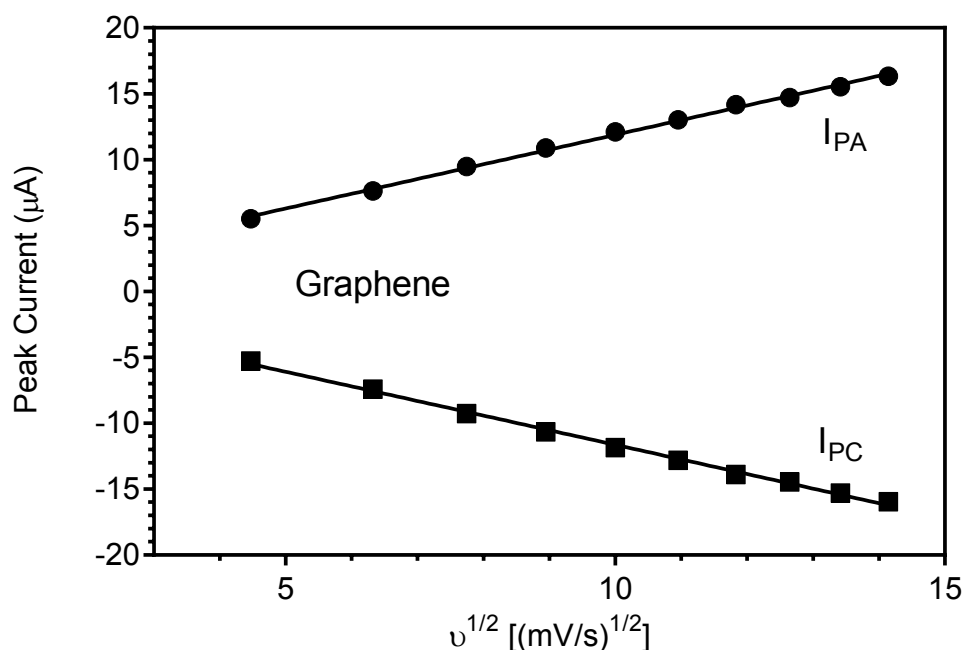


Figure 4.43: Graph of peak anodic and cathodic peak current vs square root of scan rate from a screen printed graphene electrode

4.10.2 SEM

SEM was used in order to characterise the surface morphology of the GSPE. SEM images were taken at four different magnifications (500x, 1000x, 2,500x and 5000x) - Fig 4.44. At magnifications of 2500x and 5000x it appears that the surface is similar to that of screen printed graphite electrodes [29, 30, 31] and that graphite flakes are clearly visible. The significant surface roughness suggests a high curing temperature during the production of the electrodes. At lower curing temperatures a smoother surface is obtained as the polymer binder and solvents haven't been evaporated [29] The relatively large graphene domains observed by Randviir [21] are not seen indicating that the electrodes have a graphite type structure.

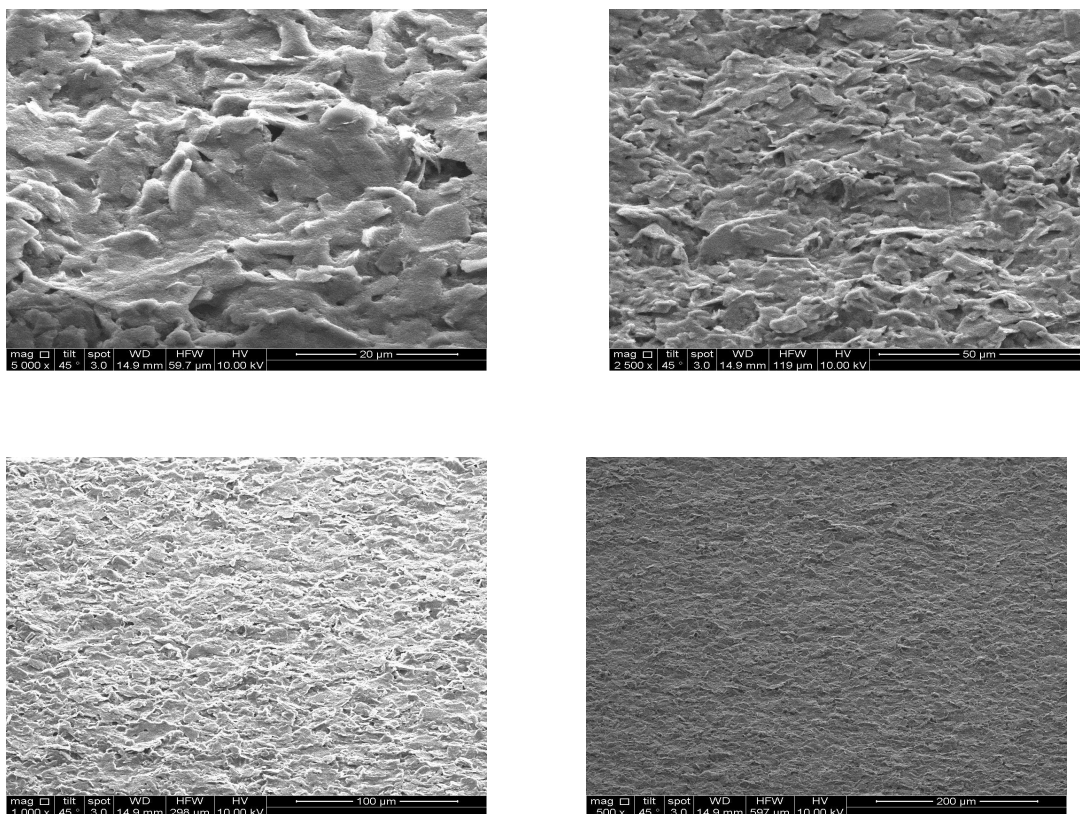


Figure 4.44: Scanning Electron Micrographs of screen printed graphene working electrodes at magnifications of 5000x (top left), 2500 (top right) 1000x (bottom left) and 500x (bottom right)

4.10.3 Raman Spectroscopy

Raman Spectroscopy is a spectroscopy technique based on the inelastic scattering of photons that has been used extensively for the characterisation of graphitic materials [32, 33, 34]. For this work it is particularly useful in distinguishing graphite and graphene. In Fig 4.45 the Raman spectra for unmodified screen printed graphite and and graphene electrodes is shown. Peaks are seen in both electrodes at 1375 cm^{-1} , 1570 cm^{-1} and 2710 cm^{-1} . The first of these peaks is referred to as the D band and is associated with defects in the material surface. The ratios of the intensity of the D band to the G band (due to bond stretching of sp^2 carbon pairs) is then used as a way of quantifying that disorder. In the case of graphite $I(\text{D})/I(\text{G})$ is ≈ 0.2 , whilst for graphene this ratio increases to ≈ 0.33 . This higher level of disorder can be attributed to the higher oxygen content in the graphene electrode. The position of the G peak can also be used to differentiate between graphite and graphene. In the case of single layer graphene, this peak upshifts but this is not seen for the graphene

screen printed electrode [35]. However, this shift is not seen for two graphene layers and it is not expected that screen printed graphene would actually have single layer graphene.

The 2D peak is associated with second order of the zone boundary phonons arising from double resonance Raman scattering with 2 phonon emission. Its position and shape can also be used to characterise the number of graphene layers in a material [36]. Both the screen printed graphite and graphene electrodes have an asymmetric 2D band peak at 2710 cm^{-1} . The shape of the peak (more easily seen in Fig 4.46) indicates that at least 10 graphene layers are present in both samples [35]. For single layer graphene a symmetric peak is observed at less than 2700 cm^{-1} [35]. Randviir et. al were able to observe 6-8 layer graphene [21] in their screen printed graphene electrode but the Raman analysis in this study indicates graphite behaviour for both the graphite and graphene electrodes.

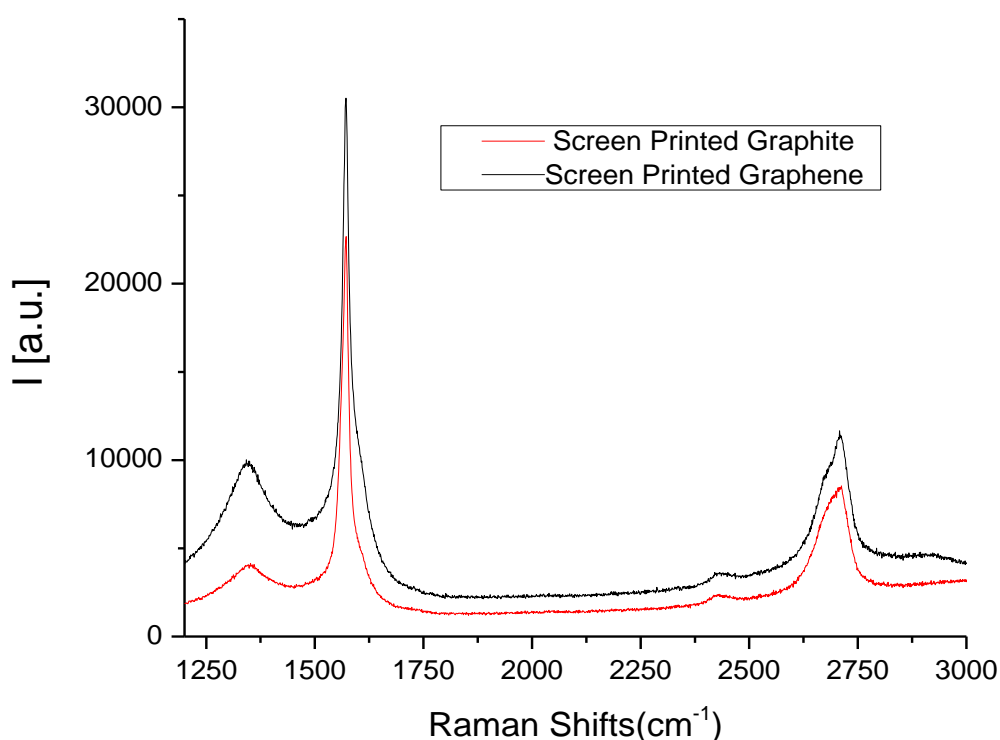


Figure 4.45: Raman spectra for bare SPE and GSPEs

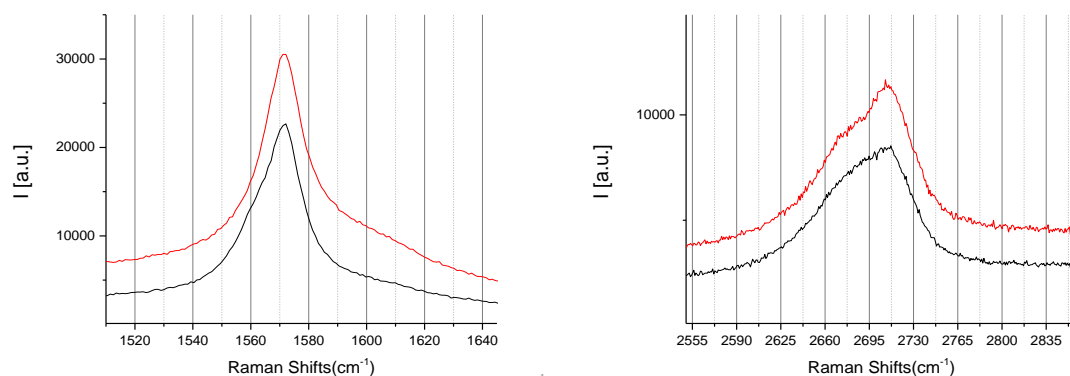


Figure 4.46: D and G bands at bare SPE and GSPEs

4.10.4 Caffeine Detection at Screen Printed Graphene

4.10.5 Influence of pH

Analysis of the variation of CV oxidation peak current with pH in Britton-Robinson showed similar results to those achieved at bare graphite electrodes (Fig. 4.1 and 4.2). A linear relationship was observed between peak potential (Fig. 4.47) and pH and peak current was at a maximum for pH 2 and pH 8 (Fig. 4.48).

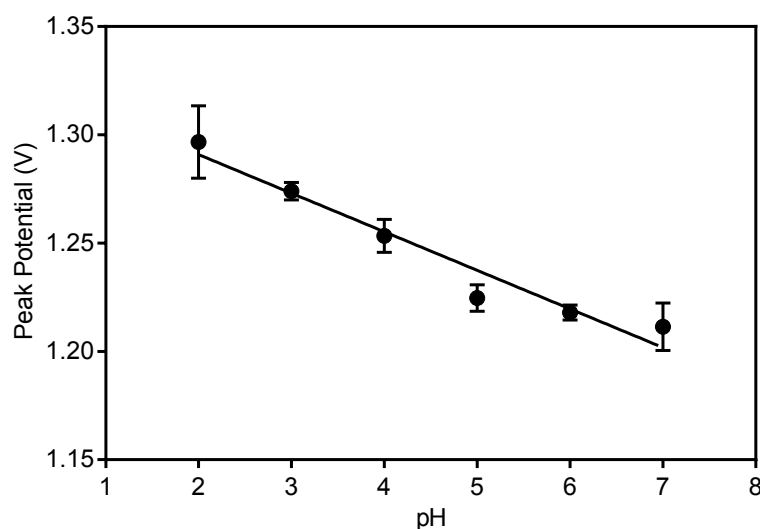


Figure 4.47: Variation of pH as a function of peak potential of cyclic voltammetry measurements with a scan rate of 100 mV/s in 200 μ M caffeine (Britton-Robinson supporting electrolyte) at a graphene SPE. $R^2 = 0.8959$, $n = 3$.

However, at higher pHs, the peaks were masked by the background buffer and hence consistent and reliable values couldn't be determined. Complete disappearance of the peak current occurred at pHs greater than 8.

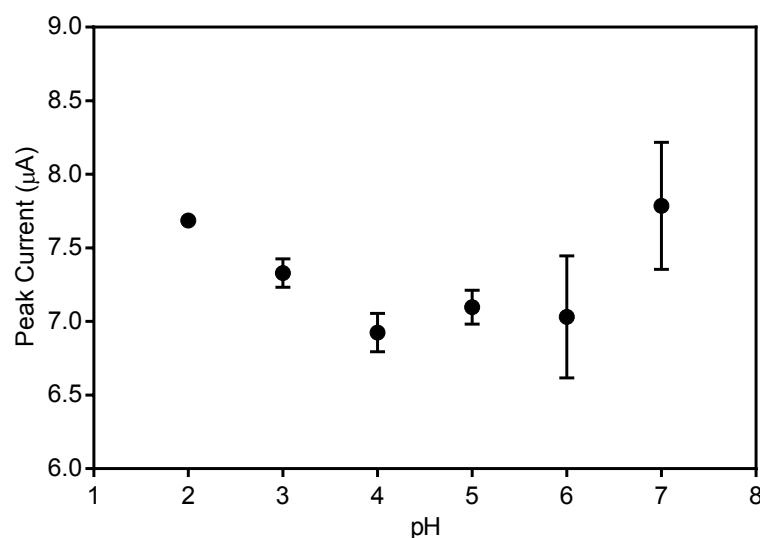


Figure 4.48: Variation of pH as a function of peak current of cyclic voltammetry measurements with a scan rate of 100 mV/s in 200 μM caffeine (Britton-Robinson supporting electrolyte) at a graphene SPE.

4.10.6 Electrochemical Detection of Caffeine

It has been shown in the previous sections of this chapter that behaviour of both commercial graphite and graphene SPEs was similar enough to suggest that graphene behaviour was not observed. Similarly this is observed for caffeine oxidation with similar CVs observed as shown in Fig. 4.39. A peak current for the graphene electrode of $8.41 \mu\text{A} \pm 0.07 \mu\text{A}$

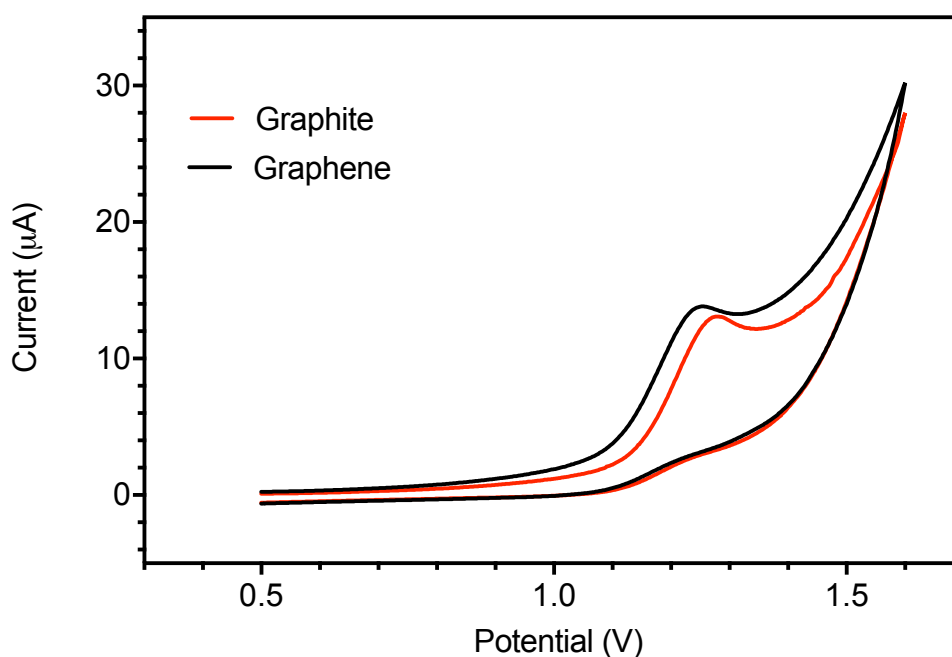


Figure 4.49: CVs at bare SPE and GSPE in the presence of 200 μM caffeine

It was decided not to continue with any further analysis of this electrode for caffeine oxidation as its behaviour was so closely aligned to the previously analysed graphite SPE.

4.11 Conclusions

In this chapter, electrochemical sensors for caffeine were developed at electrochemically pretreated, Nafion modified and graphene screen printed electrodes. Interestingly, it was observed through rigorous characterisation that the commercial screen printed graphene electrodes were in fact graphitic in nature. Hence, extensive analysis of these electrodes towards caffeine oxidation wasn't carried out. Both the Nafion and pretreated electrodes displayed similar LODs of 8 μM and 9 μM respectively. However, in the investigation of practical uses of the sensor, the Nafion modified electrode had better % recoveries in real sample analysis and also wasn't adversely affected after storage in different conditions for 10 days. Future work will focus on improving the recoverabilities achievable in real samples.

A summary is given below of the different materials and modifications explored for caffeine detection in this chapter.

Table 4.4: Summary of results of the different electrode materials and modifications used for caffeine detection.

Electrode modification	LOD	Linear Range	Electrochemical Technique
Nafion modified SPE	8 μM	10 - 148 μM	SWV
Electrochemically Pretreated	9 μM	10 - 20 μM	LSV
Graphene SPE	N/A	N/A	CV

Future work following on from this thesis could focus on the development of a micro total analysis system that would allow continuous, automated caffeine detection. This is of particular interest to food companies that need to monitor caffeine concentrations in their products at regular intervals. It would also be advantageous to combine a caffeine sensor with other parameters of interest such as pH or dissolved oxygen content into a single system. These type of lab on a chip systems incorporating a caffeine sensor promise to be an important area of research in years to come.

References

- [1] Ioana Vasilescu, Sandra A. V. Eremia, Ramona Penu, Camelia Albu, Antonio Radoi, Simona C. Litescu, and Gabriel-Lucian Radu. Disposable dual sensor array for simultaneous determination of chlorogenic acid and caffeine from coffee. *RSC Advances*, 5(1):261–268, 2015.
- [2] Andrew P. Smith. Caffeine, cognitive failures and health in a non-working community sample. *Human Psychopharmacology: Clinical & Experimental*, 24(1):29–34, January 2009.
- [3] J. E. James. Acute and chronic effects of caffeine on performance, mood, headache, and sleep. *Neuropsychobiology*, 38(1):32–41, 1998. WOS:000075472400006.
- [4] Kamlesh Shrivastava and Hui-Fen Wu. Rapid determination of caffeine in one drop of beverages and foods using drop-to-drop solvent microextraction with gas chromatography/mass spectrometry. *Journal of Chromatography A*, 1170(1–2):9–14, November 2007.
- [5] Qing-chuan Chen, Shi-fen Mou, Xiao-ping Hou, and Zhe-ming Ni. Simultaneous determination of caffeine, theobromine and theophylline in foods and pharmaceutical preparations by using ion chromatography. *Analytica Chimica Acta*, 371(2–3):287–296, October 1998.
- [6] Feng Zhao, He-Tong Lin, Shen Zhang, Yi-Fen Lin, Jiang-Fan Yang, and Nai-Xing Ye. Simultaneous Determination of Caffeine and Some Selected Polyphenols in Wuyi Rock Tea by High-Performance Liquid Chromatography. *Journal of Agricultural and Food Chemistry*, 62(13):2772–2781, April 2014.
- [7] Nicolae Spătaru, Bulusu V. Sarada, Donald A. Tryk, and Akira Fujishima. Anodic Voltammetry of Xanthine, Theophylline, Theobromine and Caffeine at Conductive Diamond Electrodes and Its Analytical Application. *Electroanalysis*, 14(11):721–728, 2002.
- [8] Lubomir Svorc. Determination of Caffeine: A Comprehensive Review on Electrochemical Methods. *International Journal of Electrochemical Science*, 8(4):5755–5773, April 2013. WOS:000318217200115.
- [9] A. Carolina Torres, Madalina M. Barsan, and Christopher M. A. Brett. Simple electrochemical sensor for caffeine based on carbon and

- Nafion-modified carbon electrodes. *Food Chemistry*, 149:215–220, April 2014.
- [10] Bruna Cláudia Lourenção, Roberta Antigo Medeiros, Romeu C. Rocha-Filho, Luiz Henrique Mazo, and Orlando Fatibello-Filho. Simultaneous voltammetric determination of paracetamol and caffeine in pharmaceutical formulations using a boron-doped diamond electrode. *Talanta*, 78(3):748–752, May 2009.
- [11] Bruna Cláudia Lourenção, Roberta Antigo Medeiros, Romeu C. Rocha-Filho, and Orlando Fatibello-Filho. Simultaneous Differential Pulse Voltammetric Determination of Ascorbic Acid and Caffeine in Pharmaceutical Formulations Using a Boron-Doped Diamond Electrode. *Electroanalysis*, 22(15):1717–1723, August 2010.
- [12] Yavuz Yardım, Ertugrul Keskin, and Zühre Şentürk. Voltammetric determination of mixtures of caffeine and chlorogenic acid in beverage samples using a boron-doped diamond electrode. *Talanta*, 116:1010–1017, November 2013.
- [13] Taher Alizadeh, Mohamad Reza Ganjali, Mashaalah Zare, and Parviz Norouzi. Development of a voltammetric sensor based on a molecularly imprinted polymer (MIP) for caffeine measurement. *Electrochimica Acta*, 55(5):1568–1574, February 2010.
- [14] Bankim J. Sanghavi and Ashwini K. Srivastava. Simultaneous voltammetric determination of acetaminophen, aspirin and caffeine using an in situ surfactant-modified multiwalled carbon nanotube paste electrode. *Electrochimica Acta*, 55(28):8638–8648, December 2010.
- [15] Weberson P. Silva, Luiz A. J. Silva, Clarice H. França, Raquel M. F. Sousa, Rodrigo A. A. Muñoz, and Eduardo M. Richter. Square-wave Voltammetric Determination of Propyphenazone, Paracetamol, and Caffeine: Comparative Study between Batch Injection Analysis and Conventional Electrochemical Systems. *Electroanalysis*, pages n/a–n/a.
- [16] S. Jesny and K. Girish Kumar. Non-Enzymatic Electrochemical Sensor for the Simultaneous Determination of Xanthine, its Methyl Derivatives Theophylline and Caffeine as well as its Metabolite Uric Acid. *Electroanalysis*, pages n/a–n/a.
- [17] S. J. Peighambaroust, S. Rowshanzamir, and M. Amjadi. Review of

- the proton exchange membranes for fuel cell applications. *International Journal of Hydrogen Energy*, 35(17):9349–9384, September 2010.
- [18] Joseph Wang, Mustafa Musameh, and Yuehe Lin. Solubilization of Carbon Nanotubes by Nafion toward the Preparation of Amperometric Biosensors. *Journal of the American Chemical Society*, 125(9):2408–2409, March 2003.
- [19] Dale A. C. Brownson and Craig E. Banks. Graphene electrochemistry: Fabricating amperometric biosensors. *Analyst*, 136(10):2084–2089, April 2011.
- [20] Jianfeng Ping, Jian Wu, Yixian Wang, and Yibin Ying. Simultaneous determination of ascorbic acid, dopamine and uric acid using high-performance screen-printed graphene electrode. *Biosensors and Bioelectronics*, 34(1):70–76, April 2012.
- [21] Edward P. Randviir, Dale A. C. Brownson, Jonathan P. Metters, Rashid O. Kadara, and Craig E. Banks. The fabrication, characterisation and electrochemical investigation of screen-printed graphene electrodes. *Physical Chemistry Chemical Physics*, 16(10):4598–4611, February 2014.
- [22] L'ubomir S'vorc, Peter Tomcik, Jana Svitkova, Miroslav Rievaj, and Dusan Bustin. Voltammetric determination of caffeine in beverage samples on bare boron-doped diamond electrode. *Food Chemistry*, 135(3):1198–1204, December 2012. WOS:000310396700047.
- [23] Jun-Yong Sun, Ke-Jing Huang, Shuai-Yun Wei, Zhi-Wei Wu, and Fang-Ping Ren. A graphene-based electrochemical sensor for sensitive determination of caffeine. *Colloids and Surfaces B: Biointerfaces*, 84(2):421–426, June 2011.
- [24] Barbara Brunetti, Elio Desimoni, and Paolo Casati. Determination of Caffeine at a Nafion-Covered Glassy Carbon Electrode. *Electroanalysis*, 19(2-3):385–388, January 2007.
- [25] Suling Yang, Ran Yang, Gang Li, Lingbo Qu, Jianjun Li, and Lanlan Yu. Nafion/multi-wall carbon nanotubes composite film coated glassy carbon electrode for sensitive determination of caffeine. *Journal of Electroanalytical Chemistry*, 639(1–2):77–82, February 2010.
- [26] C. A. Martínez-Huitle, N. Suely Fernandes, S. Ferro, A. De Battisti, and M. A. Quiroz. Fabrication and application of Nafion®-modified

- boron-doped diamond electrode as sensor for detecting caffeine. *Diamond and Related Materials*, 19(10):1188–1193, October 2010.
- [27] R. G. Compton and C. E. Banks. *Understanding Voltammetry, 2nd Edition*. Imperial Coll Press, Covent Garden, 2011. WOS:000342743700014.
- [28] Gaber A. M. Mersal. Experimental and Computational Studies on the Electrochemical Oxidation of Caffeine at Pseudo Carbon Paste Electrode and Its Voltammetric Determination in Different Real Samples. *Food Analytical Methods*, 5(3):520–529, June 2012.
- [29] Pablo Fanjul-Bolado, David Hernández-Santos, Pedro José Lamas-Ardisana, Alberto Martín-Pernía, and Agustín Costa-García. Electrochemical characterization of screen-printed and conventional carbon paste electrodes. *Electrochimica Acta*, 53(10):3635–3642, April 2008.
- [30] Aoife Morrin, Anthony J. Killard, and Malcolm R. Smyth. Electrochemical Characterization of Commercial and Home-Made Screen-Printed Carbon Electrodes. *Analytical Letters*, 36(9):2021–2039, January 2003.
- [31] Rashid O. Kadara, Norman Jenkinson, and Craig E. Banks. Characterisation of commercially available electrochemical sensing platforms. *Sensors and Actuators B: Chemical*, 138(2):556–562, May 2009.
- [32] Stephanie Reich and Christian Thomsen. Raman spectroscopy of graphite. *Philosophical Transactions of the Royal Society of London A: Mathematical, Physical and Engineering Sciences*, 362(1824):2271–2288, November 2004.
- [33] M. S. Dresselhaus, G. Dresselhaus, R. Saito, and A. Jorio. Raman spectroscopy of carbon nanotubes. *Physics Reports*, 409(2):47–99, March 2005.
- [34] L. M. Malard, M. A. Pimenta, G. Dresselhaus, and M. S. Dresselhaus. Raman spectroscopy in graphene. *Physics Reports*, 473(5–6):51–87, April 2009.
- [35] Andrea C. Ferrari. Raman spectroscopy of graphene and graphite: Disorder, electron–phonon coupling, doping and nonadiabatic effects. *Solid State Communications*, 143(1–2):47–57, July 2007.

- [36] A. Gupta, G. Chen, P. Joshi, S. Tadigadapa, and Eklund. Raman Scattering from High-Frequency Phonons in Supported n-Graphene Layer Films. *Nano Letters*, 6(12):2667–2673, December 2006.

Chapter 5

Conclusions and Future Prospects

5.1 Conclusions and Future Prospects

At the end of each experimental chapter in this thesis specific suggestions for future work were given with a view of further developing the work. In the following sections a broader viewpoint is given towards future work. This is discussed from the viewpoint of both new materials and more importantly how the assays developed in this thesis could be integrated into a lab on chip device. A number of different approaches are discussed below.

5.1.1 New Carbon Nanostructures

In this thesis, graphite, reduced graphene oxide, multiwalled carbon nanotubes and graphene electrodes were all investigated for chemical sensing and immuonsensing applications. These materials have generally proved to be the most popular carbon based materials for sensing applications. However, new forms of carbon materials are beginning to emerge [1] such as carbon nanohorns (Fig. 5.1) which could potentially offer improvements compared to the above mentioned materials.

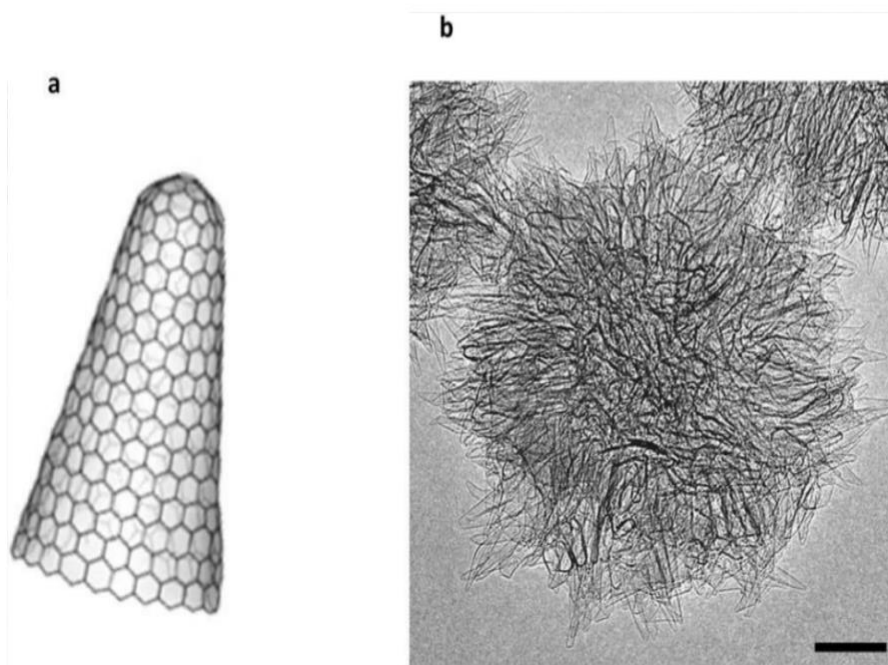


Figure 5.1: Structure of carbon nanohorns (a) and TEM image (b) [1]

5.1.2 Paper Based Analytical Devices

An promising new area is the use of paper based analytical devices (PADs) for analytical measurements. The advantages of paper include its ubiquity, low cost (typical device cost is < \$0.01), ability to transport fluids without the need of pumps and compatibility with exciting analytical techniques [2]. There exist a range of patterning techniques for feature construction including photolithography, plotting, inkjet printing, plasma etching, cutting and wax printing. The basis of these techniques is to pattern hydrophilic channels surrounded by hydrophobic barriers allowing the flow of small volumes of liquid. Many of the early devices were based on colorimetric detection such as paper based ELISA [3]. However, electrochemical detection was soon introduced in order to alleviate the issues traditionally associated with colorimetric assays such as interferences in real samples. The first example of this type of sensor was used to detect glucose, lactate and uric acid [4] by incorporating screen printed electrodes into the hydrophilic region of photolithography patterned device and immobilising oxidase enzymes onto the electrode surface. The vast majority of these devices have used screen printed carbon electrodes, however there are also examples of the use of gold [5] and pencil drawn graphite [6]. In an analogous fashion to their incorporation with conventional electrodes, nanomaterials and polymers have also been used in paper based analytical devices. Examples include the use of gold nanoparticles [7], graphene [8], carbon nanotubes [9] and chitosan [10].

5.1.3 Advanced Instrumentation

One of the promises of electrochemical biosensor technology is its ability to provide portable handheld devices that can replace lab based techniques. However, the vast majority of research (this thesis included) is still carried out on bench top electrochemical cells which are used in conjunction with bulky potentiostats, faraday cages and desktop computers or laptops. Smaller potentiostats with a more limited range of electrochemical techniques are currently available from countries such as PalmSens and Ivium Technologies which could potentially provide a portable system. This could be suitable for at-line testing but for in-line testing and hand held devices there is a requirement for truly miniaturised instrumentation. DropSens now provide a handheld potentiostat that is compatible with their screen printed electrodes

and can be configured for one LSV, CV, SWV, DPV and amperometry. It also incorporates an LCD screen which can automatically display analyte concentration and provides a promising solution. There have been a small number of 'home-made' approaches towards potentiostat development but point of care devices again are driving this research [11, 12]

Another developing area in instrumentation is the use of smartphones in conjunction with electrochemical sensors. Smartphones offer an excellent option for portable electrochemical analysis because the technology required to analyse and communicate results is already embedded within the device [13]. Typically a customised attachment is then added to the phone which allows the electrochemical detection to take place [14]. An immunosensor for the detection has already been developed for the detection of the malaria biomarker *plasmodium falciparum* histidine-rich protein 2 [15].

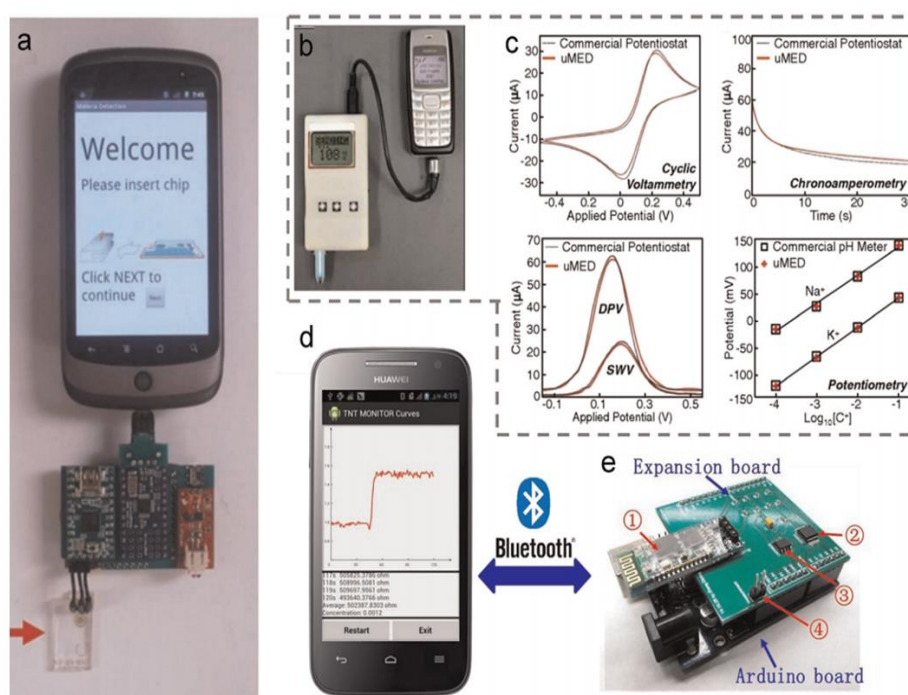


Figure 5.2: Integrated smart phone/electrochemical sensors [13]

5.1.4 Lab on a Chip/MicroTotal Analysis Systems

Lab on a chip technology aims to combine all the aspects of the analytical experiment onto a single device. Microfluidics, which allows the movement of liquids in small channels, is a key enabling technology in the development of

these types of devices. A common approach is the use of polydimethylsiloxane (PDMS) to construct channels through which small volumes of liquids can flow with the aid of external pumps. Ultraviolet curable dielectric inks can also be used for the patterning of microfluidic channels using screen printing technology. This type of easily fabricated technology has been used for the detection of mouse IgG as a model analyte [17]. Each step of the assay from antibody immobilisation through to electrochemical detection can be done on the device in sealed microfluidic channels. In relation to applications within the food industry, a commercially available microfluidic chip has been used for the detection of zearalenone in baby food samples with a limit of detection of 20 ppb [18]. The same group again used a commercial microchip for electrokinetic injection and pumping in the detection of zearalenone, with this approach making use of magnetic beads and an external magnetic [19].

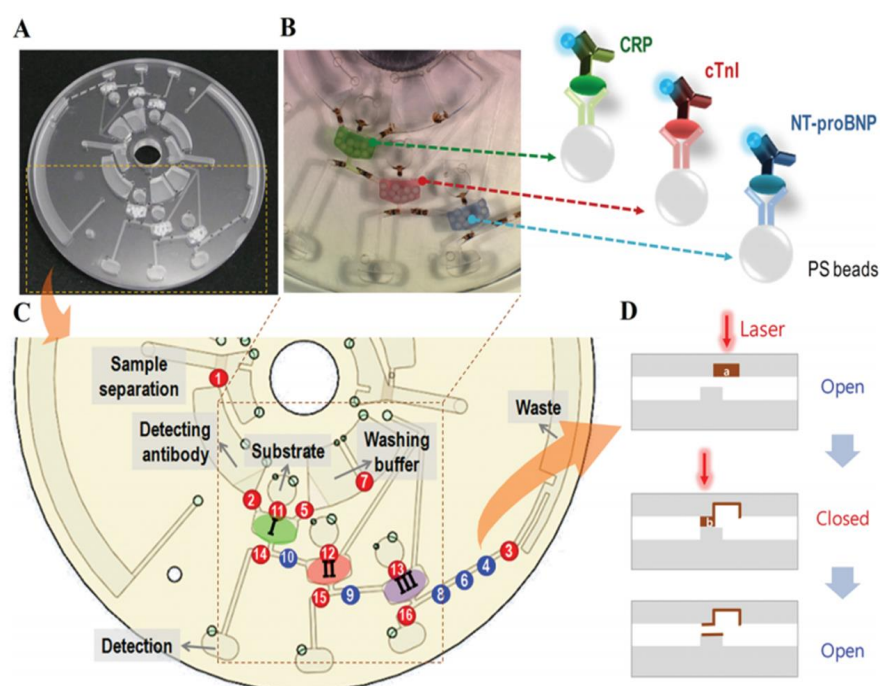


Figure 5.3: Lab on a Chip for Integrated Multiplex Immunoassay [16]

In order for electrochemical sensors to become commercially viable in real world food analysis applications it is this type of integrated thinking that will be needed in future studies.

References

- [1] Paloma Yáñez-Sedeño, Araceli González-Cortés, Lourdes Agüí, and José M. Pingarrón. Uncommon Carbon Nanostructures for the Preparation of Electrochemical Immunosensors. *Electroanalysis*, 28(8):1679–1691, 2016.
- [2] Andres W. Martinez, Scott T. Phillips, George M. Whitesides, and Emanuel Carrilho. Diagnostics for the Developing World: Microfluidic Paper-Based Analytical Devices. *Analytical Chemistry*, 82(1):3–10, 2010.
- [3] Chao-Min Cheng, Andres W. Martinez, Jinlong Gong, Charles R. Mace, Scott T. Phillips, Emanuel Carrilho, Katherine A. Mirica, and George M. Whitesides. Paper-Based ELISA. *Angewandte Chemie-International Edition*, 49(28):4771–4774, 2010.
- [4] Wijitar Dungchai, Orawon Chailapakul, and Charles S. Henry. Electrochemical Detection for Paper-Based Microfluidics. *Analytical Chemistry*, 81(14):5821–5826, 2009.
- [5] Rafaela Fernanda Carvalhal, Marta Simao Kfourri, Maria Helena de Oliveira Piazzetta, Angelo Luiz Gobbi, and Lauro Tatsuo Kubota. Electrochemical Detection in a Paper-Based Separation Device. *Analytical Chemistry*, 82(3):1162–1165, 2010.
- [6] Nicolo Dossi, Rosanna Toniolo, Andrea Pizzariello, Flavia Impellizzieri, Evandro Piccin, and Gino Bontempelli. Pencil-drawn paper supported electrodes as simple electrochemical detectors for paper-based fluidic devices. *Electrophoresis*, 34(14):2085–2091, 2013.
- [7] Xiaoxiao Ge, Abdullah Mohamed Asiri, Dan Du, Wei Wen, Shengfu Wang, and Yuehe Lin. Nanomaterial-enhanced paper-based biosensors. *Trac-Trends in Analytical Chemistry*, 58:31–39, 2014.
- [8] Pratima Labroo and Yue Cui. Graphene nano-ink biosensor arrays on a microfluidic paper for multiplexed detection of metabolites. *Analytica Chimica Acta*, 813:90–96, 2014.
- [9] Panpan Wang, Lei Ge, Mei Yan, Xianrang Song, Shenguang Ge, and Jinghua Yu. Paper-based three-dimensional electrochemical immunodevice based on multi-walled carbon nanotubes functionalized

- paper for sensitive point-of-care testing. *Biosensors & Bioelectronics*, 32(1):238–243, 2012.
- [10] Weiping Li, Li Li, Shenguang Ge, Xianrang Song, Lei Ge, Mei Yan, and Jinghua Yu. Multiplex electrochemical origami immunodevice based on cuboid silver-paper electrode and metal ions tagged nanoporous silver-chitosan. *Biosensors & Bioelectronics*, 56:167–173, 2014.
- [11] Carlyn Loncaric, Yiting Tang, Cassie Ho, M. Ash Parameswaran, and Hua-Zhong Yu. A USB-based electrochemical biosensor prototype for point-of-care diagnosis. *Sensors and Actuators B-Chemical*, 161(1):908–913, 2012.
- [12] Andres Felipe Diaz Cruz, Nicolas Norena, Ajeet Kaushik, and Shekhar Bhansali. A low-cost miniaturized potentiostat for point-of-care diagnosis. *Biosensors & Bioelectronics*, 62:249–254, December 2014.
- [13] David Erickson, Dakota O'Dell, Li Jiang, Vlad Oncescu, Abdurrahman Gumus, Seoho Lee, Matthew Mancuso, and Saurabh Mehta. Smartphone technology can be transformative to the deployment of lab-on-chip diagnostics. *Lab on a Chip*, 14(17):3159–3164, 2014.
- [14] Diming Zhang and Qingjun Liu. Biosensors and bioelectronics on smartphone for portable biochemical detection. *Biosensors & Bioelectronics*, 75:273–284, 2016.
- [15] Peter B. Lillehoj, Ming-Chun Huang, Newton Truong, and Chih-Ming Ho. Rapid electrochemical detection on a mobile phone. *Lab on a Chip*, 13(15):2950–2955, 2013.
- [16] Jiwoon Park, Vijaya Sunkara, Tae-Hyeong Kim, Hyundoo Hwang, and Yoon-Kyoung Cho. Lab-on-a-Disc for Fully Integrated Multiplex Immunoassays. *Analytical Chemistry*, 84(5):2133–2140, 2012.
- [17] Hua Dong, Chang-Ming Li, Yi-Fan Zhang, Xiao-Dong Cao, and Ye Gan. Screen-printed microfluidic device for electrochemical immunoassay. *Lab on a Chip*, 7(12):1752–1758, 2007.
- [18] Miriam Hervas, Miguel Angel Lopez, and Alberto Escarpa. Electrochemical microfluidic chips coupled to magnetic bead-based ELISA to control allowable levels of zearalenone in baby foods using simplified calibration. *Analyst*, 134(12):2405–2411, 2009.

- [19] Mirian Hervas, Miguel A. Lopez, and Alberto Escarpa. Integrated electrokinetic magnetic bead-based electrochemical immunoassay on microfluidic chips for reliable control of permitted levels of zearalenone in infant foods. *Analyst*, 136(10):2131–2138, 2011.

Appendix A

XPS

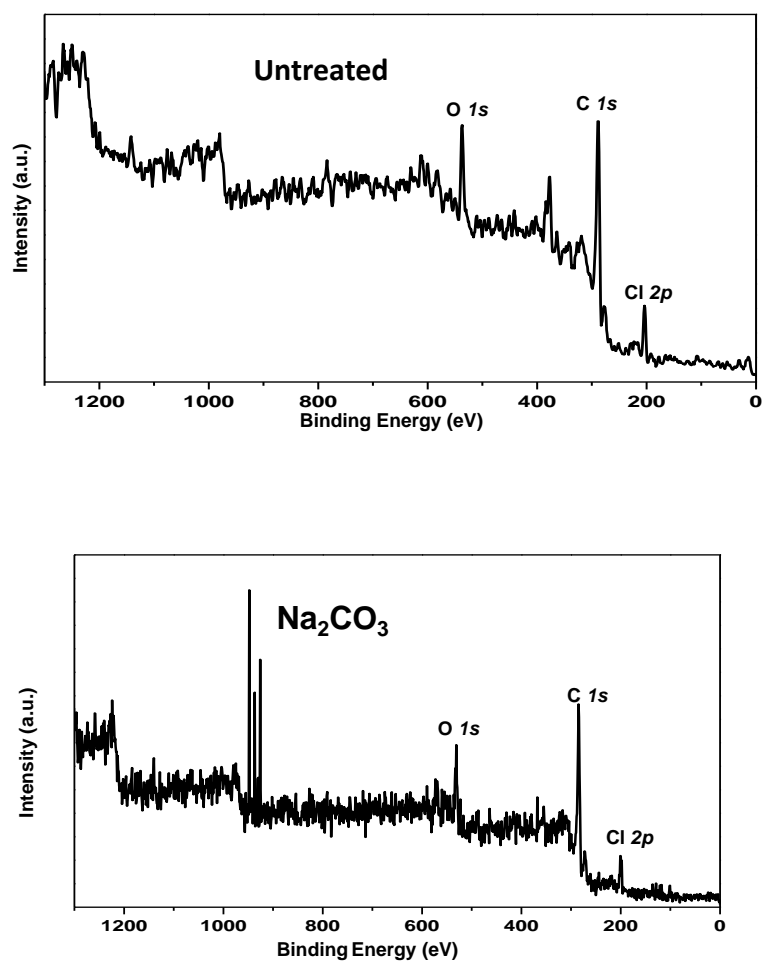


Figure A.1: XPS spectra of untreated and electrochemically pretreated electrodes.

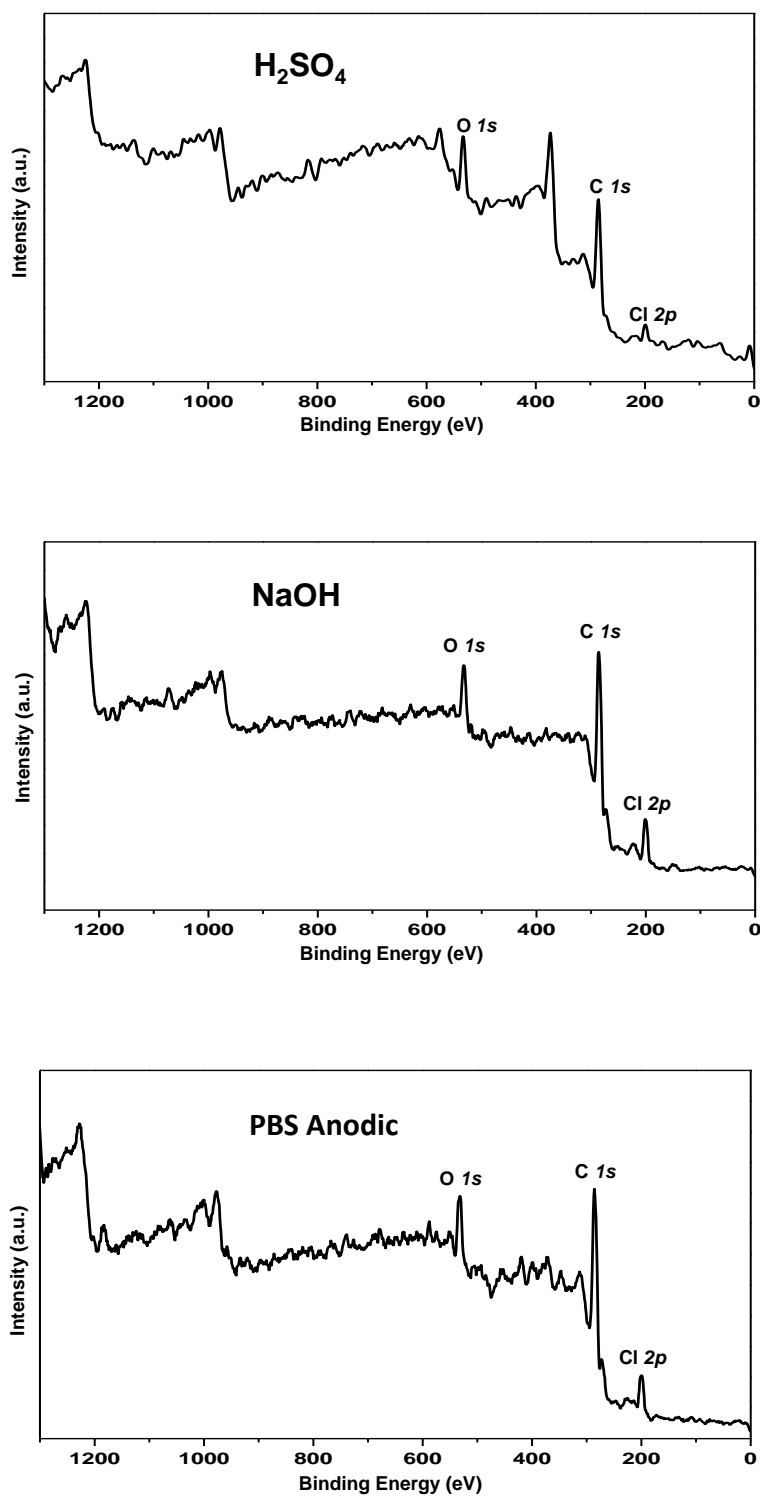


Figure A.2: XPS spectra for bare and pre-treated electrodes

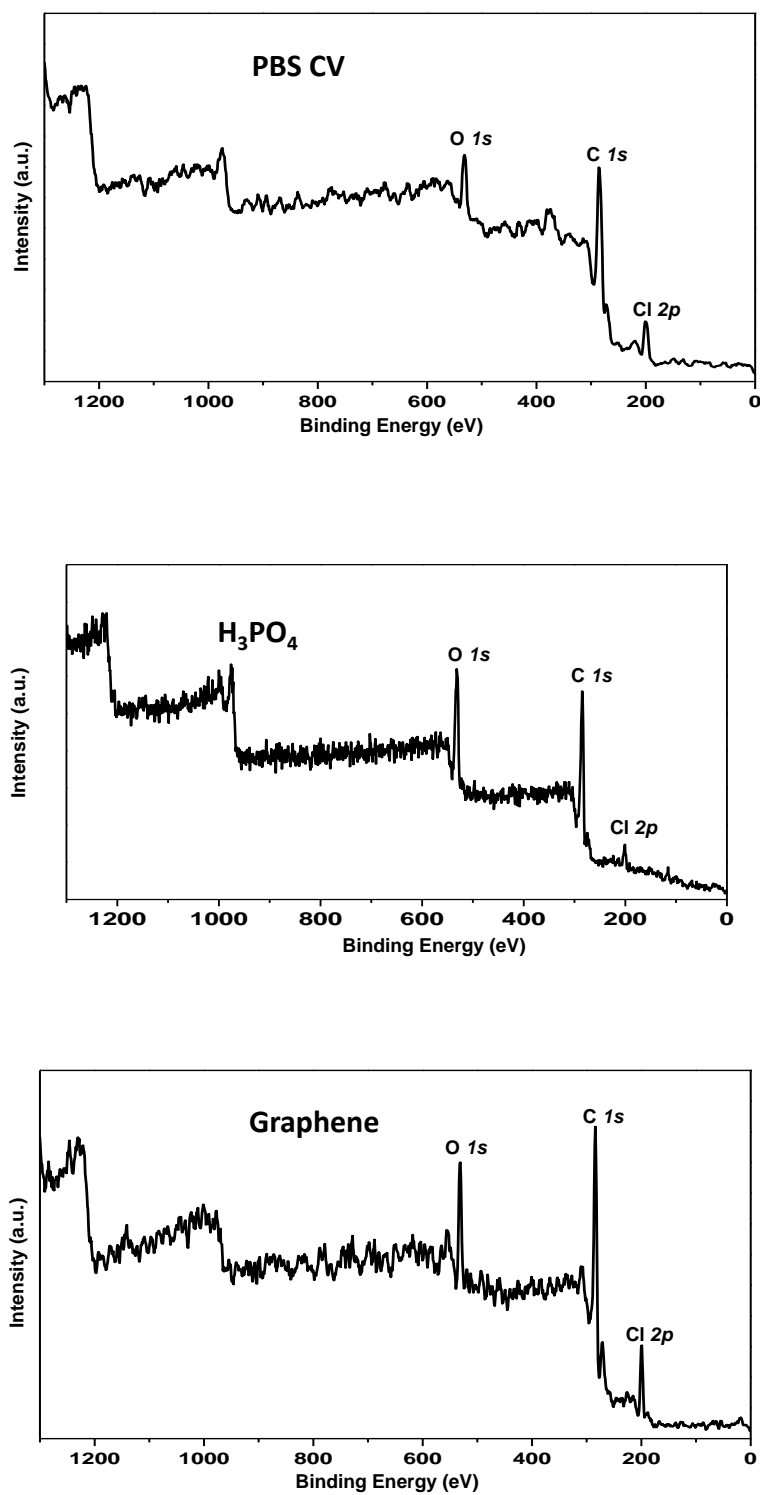
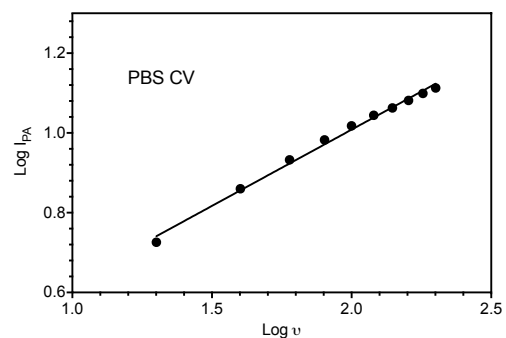
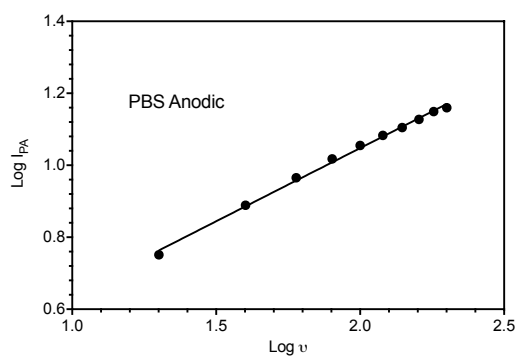
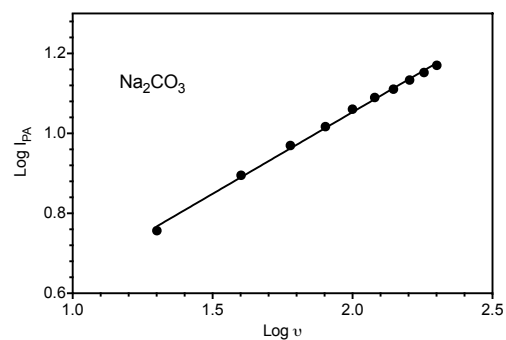
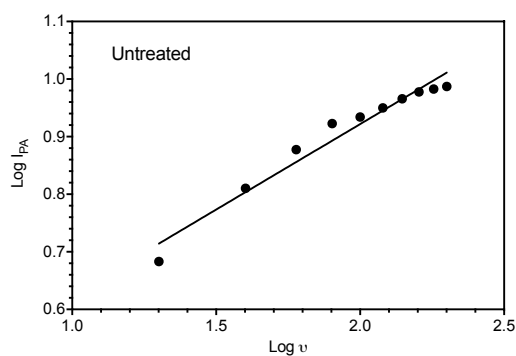


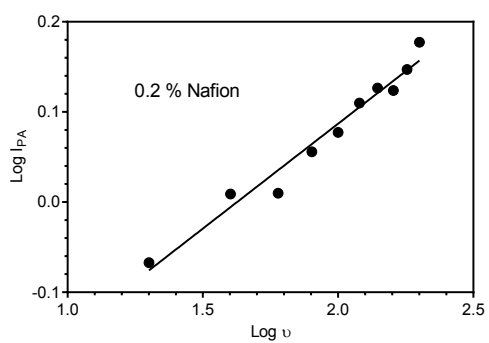
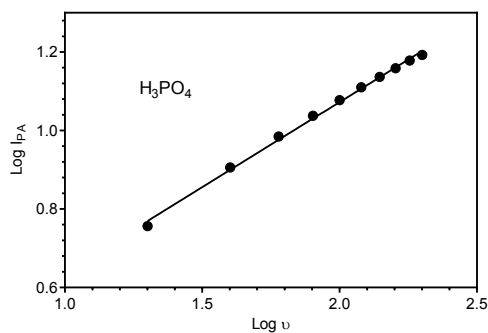
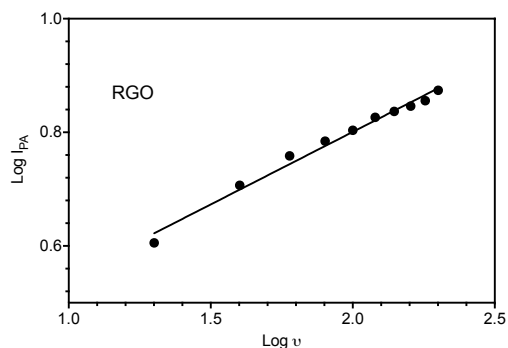
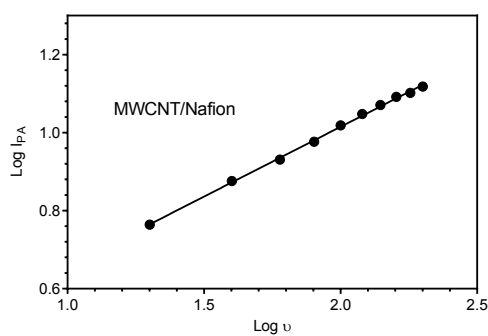
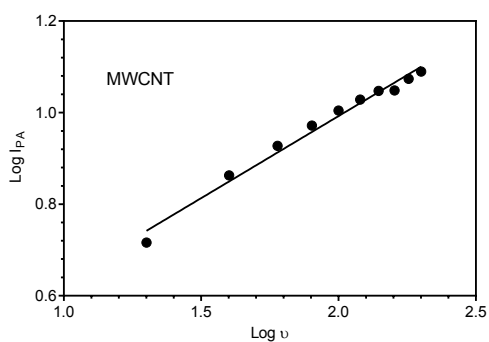
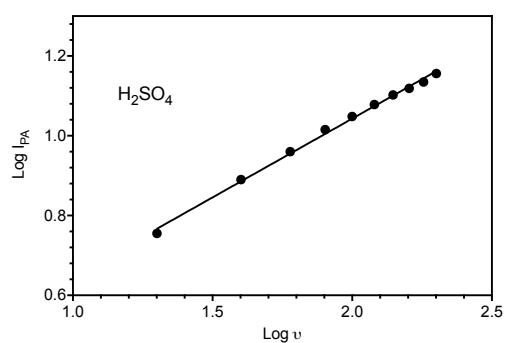
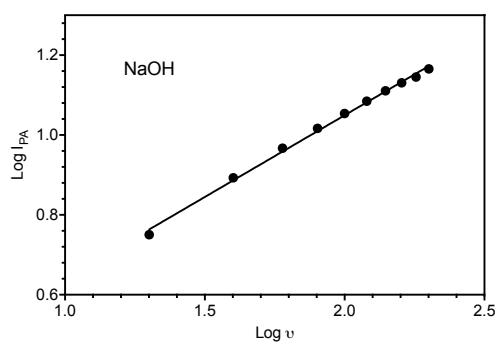
Figure A.3: XPS spectra for electrochemically pretreated graphite electrodes and graphene SPEs.

Appendix B

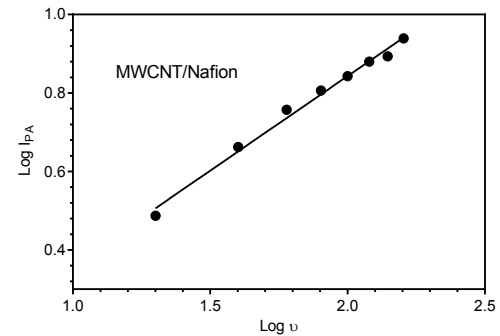
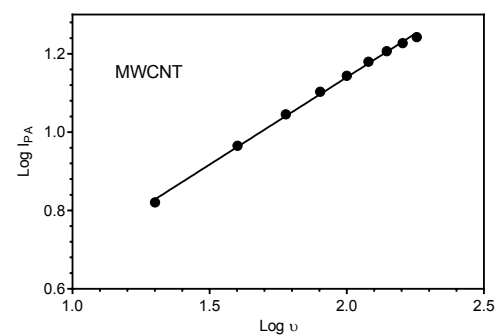
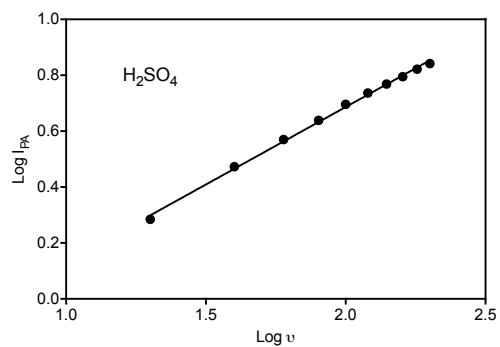
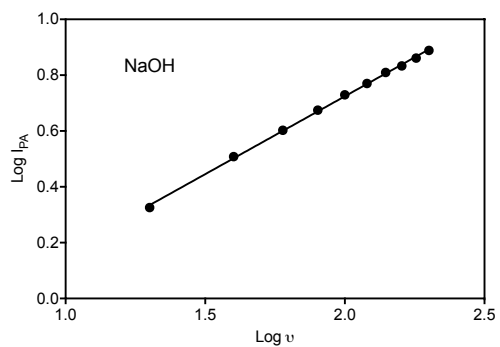
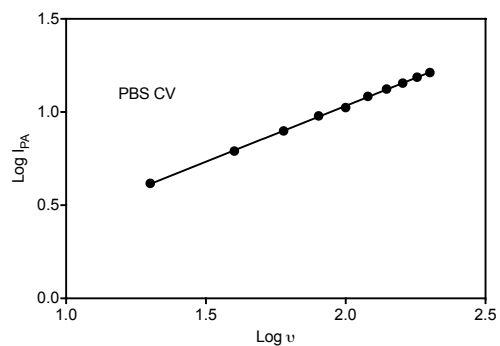
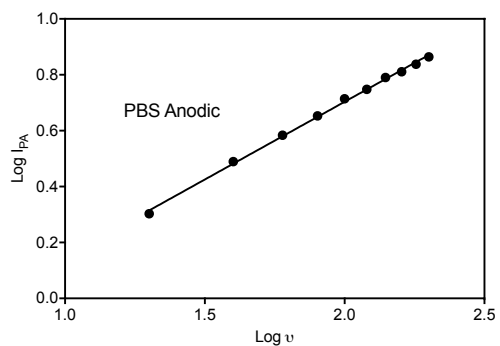
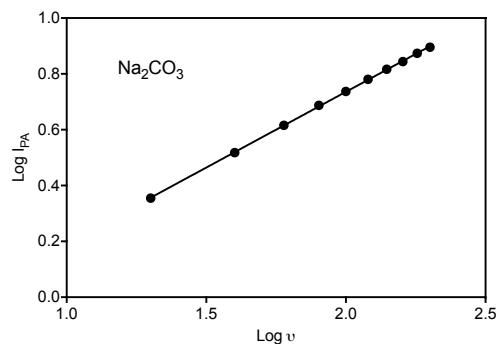
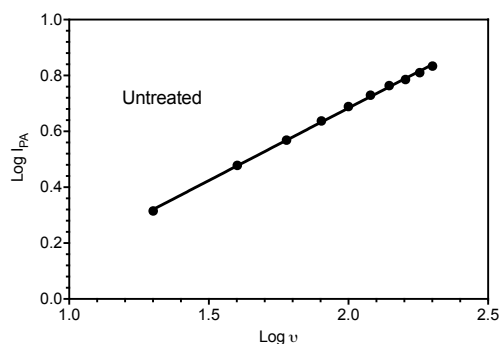
Thin Layer Effects

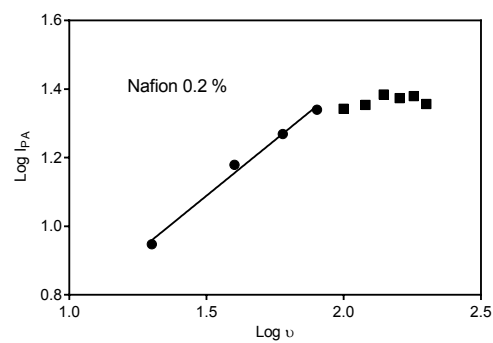
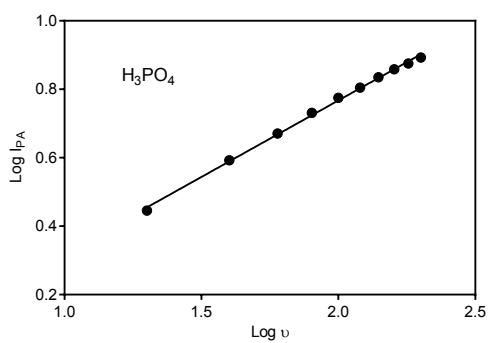
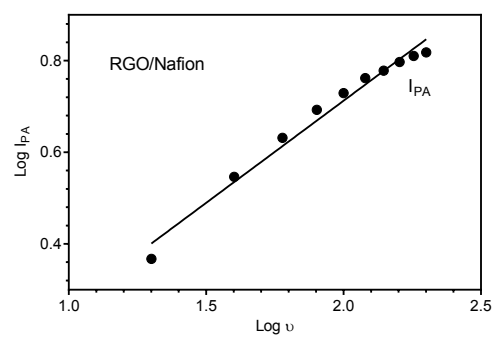
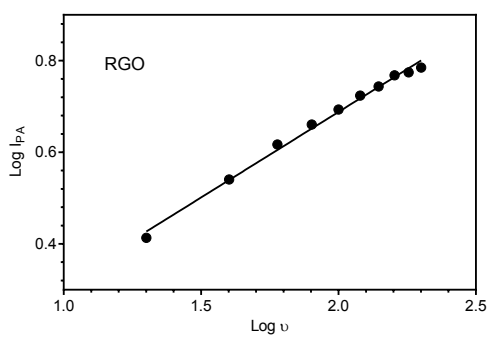
B.1 Ferri/Ferrocyanide





B.2 Ruthenium (III) Chloride





Appendix C

Publications

C.1 Journal Publications

1. G.F. Duffy and E.J. Moore, *Electrochemical Immunosensors for Food Analysis: A Review of Recent Developments*, Analytical Letters.
In press and available online
2. G.F. Duffy, C Cummins, M.A. Morris and E.J. Moore, *Comparison of electrochemically pretreated and nafion modified screen printed electrodes for caffeine detection in energy drink samples*
In Preparation.
3. G.F. Duffy and E.J. Moore *Electrochemically pretreated and nanocarbon modified screen printed electrodes for the development of alkaline phosphatase based electrochemical immunosensors*
In Preparation.

C.2 Oral Presentations

1. Development of chemically modified screen printed carbon electrodes for caffeine and mouse IgG detection
Chemistry Colloquium, NUI Maynooth, June 25th, 2015
2. Development of chemically modified screen printed carbon electrodes for caffeine and mouse IgG detection

IMA 2015, Kalamata, 22nd September 2015

3. Nanostructure Modified Screen Printed Electrodes for Caffeine detection and Alkaline Phosphatase based Electrochemical Immunoassay
ChemCys (Chemistry Conference for Young Scientists), March 17th 2016, Blankenberge, Belgium

C.3 Poster Presentations

1. Development and Characterisation of Miniaturised Electrochemical Arrays for use as Immuno and Chemical sensors in the Food and Health Industries
Gerard Duffy, Una Crowley, Gerard McGlacken, Eric Moore
Conference in Analytical Sciences Ireland (CASI) (University College Cork) 1st July 2013
2. Development of Multi-parameter Sensing Devices with applications in the Food and Health Industries
Gerard Duffy, Gerard McGlacken, Eric Moore
Tyndall Industry Health Day (Oriel House, Ballincollig) 17-19th September 2013
3. Development of Electrochemical Sensors for the Detection of Toxins and Chemical Contaminants in Food
Gerard Duffy, Gerard McGlacken, Eric Moore
MNBS/EPoSS joint event (Tyndall National Institute) 24-26th September 2013
4. Development of Electrochemical Sensors for the Detection of Toxins and Chemical Contaminants in Food
Gerard Duffy, Gerard McGlacken, Eric Moore
Recent Advances in Food Analysis (Prague, Czech Republic) November 5-8th 2013